

AD-A087 737

DAYTON UNIV OH SCHOOL OF ENGINEERING
ANALYSIS AND MEASUREMENT OF HELMETED AIRCREWMAN RESPONSE RESULT--ETC(U)
JAN 80 N S PHILLIPS F33615-77-C-0534

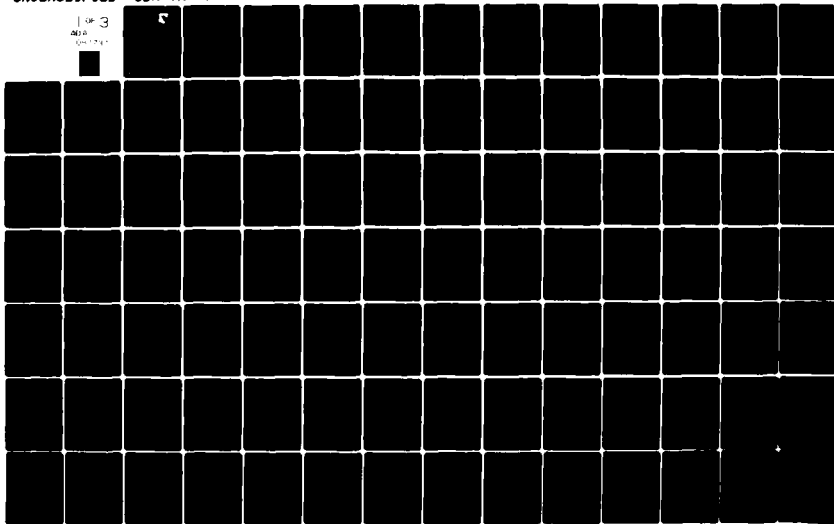
UNCLASSIFIED

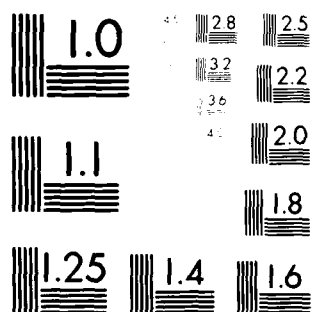
UDR-TR-79-56

AMRL-TR-79-75

NL

1 of 3
ADA
101-174





MICROCOPY RESOLUTION TEST CHART
 NATIONAL BUREAU OF STANDARDS-1963-A

54
AMRL-TR-79-75

LEVEL II



12

ADA 087737

ANALYSIS AND MEASUREMENT OF HELMETED AIRCREWMAN RESPONSE RESULTING FROM BIRDSTRIKE

*NORMAN S. PHILLIPS
UNIVERSITY OF DAYTON
SCHOOL OF ENGINEERING
DAYTON, OHIO 45469*

JANUARY 1980

**DTIC
ELECTE**
AUG 8 1980

Approved for public release; distribution unlimited.

**AIR FORCE AEROSPACE MEDICAL RESEARCH LABORATORY
AEROSPACE MEDICAL DIVISION
AIR FORCE SYSTEMS COMMAND
WRIGHT-PATTERSON AIR FORCE BASE, OHIO 45433**

DDC FILE COPY

80 8 7 058

NOTICES

When US Government drawings, specifications, or other data are used for any purpose other than a definitely related Government procurement operation, the Government thereby incurs no responsibility nor any obligation whatsoever, and the fact that the Government may have formulated, furnished, or in any way supplied the said drawings, specifications, or other data, is not to be regarded by implication or otherwise, as in any manner licensing the holder or any other person or corporation, or conveying any rights or permission to manufacture, use, or sell any patented invention that may in any way be related thereto.

Please do not request copies of this report from Air Force Aerospace Medical Research Laboratory. Additional copies may be purchased from:

National Technical Information Service
5285 Port Royal Road
Springfield, Virginia 22161

Federal Government agencies and their contractors registered with Defense Documentation Center should direct requests for copies of this report to:

Defense Documentation Center
Cameron Station
Alexandria, Virginia 22314

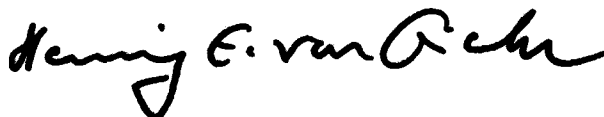
TECHNICAL REVIEW AND APPROVAL

AMRL-TR-79-75

This report has been reviewed by the Office of Public Affairs (PA) and is releasable to the National Technical Information Service (NTIS). At NTIS, it will be available to the general public, including foreign nations.

This technical report has been reviewed and is approved for publication.

FOR THE COMMANDER



HENNING E. VON GIERKE
Director
Biodynamics and Bioengineering Division
Air Force Aerospace Medical Research Laboratory

SECURITY CLASSIFICATION OF THIS PAGE (When Data Entered)

19 REPORT DOCUMENTATION PAGE		READ INSTRUCTIONS BEFORE COMPLETING FORM	
1. REPORT NUMBER AMRL-TR-79-75	2. GOVT ACCESSION NO. AD-A087737	3. RECIPIENT'S CATALOG NUMBER	
4. TITLE (and Subtitle) ANALYSIS AND MEASUREMENT OF HELMETED AIRCREWMAN RESPONSE RESULTING FROM BIRDSTRIKE		5. TYPE OF REPORT & PERIOD COVERED Final Rept. 1 Mar 1977-31 Mar 1979	
7. AUTHOR(s) Norman S. Phillips		6. PERFORMING ORG. REPORT NUMBER UDR-TR-79-56	
9. PERFORMING ORGANIZATION NAME AND ADDRESS University of Dayton School of Engineering Dayton, Ohio 45469		8. CONTRACT OR GRANT NUMBER(s) F33615-77-C-0534	
11. CONTROLLING OFFICE NAME AND ADDRESS Air Force Aerospace Medical Research Laboratory, Aerospace Medical Division, Air Force Systems Command Wright-Patterson Air Force Base, Ohio 45433		10. PROGRAM ELEMENT, PROJECT, TASK AREA & WORK UNIT NUMBERS 62202F, 7231-16-09	
14. MONITORING AGENCY NAME & ADDRESS (if different from Controlling Office)		12. REPORT DATE Jan 1980	
		13. NUMBER OF PAGES 234	
		15. SECURITY CLASS. (of this report) UNCLASSIFIED	
		15a. DECLASSIFICATION/DOWNGRADING SCHEDULE	
16. DISTRIBUTION STATEMENT (of this Report) Approved for public release; distribution unlimited.			
17. DISTRIBUTION STATEMENT (of the abstract entered in Block 20, if different from Report)			
18. SUPPLEMENTARY NOTES			
19. KEY WORDS (Continue on reverse side if necessary and identify by block number) Head Injury Z90 Standard Injury Criteria, Helmets Birdstrikes ATBM Model			
20. ABSTRACT (Continue on reverse side if necessary and identify by block number) The purpose of the research was to investigate and evaluate the bird-strike phenomena in terms of injury potential. Data collected during canopy testing indicated that significant deflection could occur and cause deformation into the space occupied by the helmeted aircrewman. The traveling wave and its interaction with the helmeted head created an unusual impact environment for which evaluation criteria did not exist. In order to generate new criteria it was necessary to utilize the Articulated Total Body Model (ATBM)			

DD FORM 1 JAN 73 1473

EDITION OF 1 NOV 65 IS OBSOLETE

SECURITY CLASSIFICATION OF THIS PAGE (When Data Entered)

Block 20. Continued.

and incorporate within the model characteristics of the canopy, the helmet and human head and neck system. With a configuration representative of the impact phenomena, the kinetic response of the system to selected impacts could be compared with biomechanical data to infer injury.

The deformation characteristics of the canopy were established by analysis of F-16 film data collected during birdstrike tests. The data indicate that the canopy deformation depth is proportional to bird kinetic energy but that canopy deformation wave speed does not increase with bird speed.

The helmet stiffness characteristics were established from available drop test data. Force-displacement curves were idealized for incorporation into the ATBM. These, along with canopy compliance data, were used to construct the stiffness at the canopy-helmet interference.

Data from the canopy, helmet, and aircrewman position studies were incorporated, with current biomechanical coefficients for the idealized human, into the ATBM. Analyses were conducted for several variations of bird position and velocity at impact. The results indicate the helmeted head/neck system is a low frequency system relative to the bird impact and that the head cannot rotate out of the path of the canopy deformation wave. The helmet is crushed upon the skull with injurious force and motions at helmet liner deformations of about one inch.

The injury criteria for the head and neck were established by compiling and collating existing information and relating the parameter magnitudes to nonconcussive response. The data, when plotted on acceleration-time coordinates, led to the selection of the maximum strain criteria model as a means of predicting injury.

A simplified model of the canopy/helmet/head and neck system was found. A helmeted head represented by a rigid body pivoted at the occipital condyles with only damping, can reasonably approximate the kinematics of the head center of gravity and resulting strain. Parameter studies conducted using the simplified model indicate that an increase of one-half inch in liner crush above a tolerable depth causes a greater change in head acceleration and strain than any realistic change in wave speed, angle of impact, surface friction, neck damping coefficient, or bird radius.

Additional tests were conducted on standard Air Force helmets to better evaluate their strength characteristics. Static force-displacement tests indicate that the standard helmet and liner is more similar to a liner and "rigid" shell than to a liner only. Comparisons of static with dynamic test data imply that the initial crush force may be due to viscoelastic liner response. The results indicate that future testing will require impact velocities three times greater than currently used.

The results of the research efforts were used to develop a proposed standard. The current 290 standard was modified to reflect changes in the impact test conditions and in the calculation of injury potential as a function of orientation. The modifications reflect the fact that testing conditions for a birdstrike environment are dictated by the configuration of the currently acceptable helmets.

SUMMARY

Several U.S. Air Force aircraft have been lost because of birdstrikes onto the canopy. With aircraft flying at higher airspeeds and lower altitudes, the probability of a more severe birdstrike has increased. One means of defeating the bird impact is to provide a canopy that does not fracture but absorbs the energy of impact by deforming. If the deformation is too great, the canopy can hit the helmeted aircrewman. If this does occur, how is the effect of the impact evaluated? Is the blow to the head sufficient to cause loss of control of the aircraft? Can the helmet be modified to improve its injury protection capability?

High speed birdstrike film data were analyzed to better understand the birdstrike phenomenon. Impacts of two and four pound birds onto an F-16 canopy at velocities of from 123 to 363 knots were examined. Canopy deformations of up to 9 inches were observed. The wave motion of the deformation was found to travel along the canopy at a velocity of equal to, or less than the velocity of the bird depending upon the impulsive nature of the impact. A slower bird slides along the canopy while the faster bird is disintegrated and the canopy responds freely afterwards.

A study of the F-16 cockpit configuration using anthropometric templates and layout drawings was conducted. With the head located at the design eye position, the deformations observed would be potentially dangerous.

A computer analog of the helmeted aircrewman was used to calculate the response of the aircrewman to a series of simulated birdstrike impacts. The analyses indicated that the head and neck are low frequency systems relative to the impulsive nature of the birdstrike. Hence, the canopy deformation crosses over the head essentially crushing the liner onto the skull. Approximately one inch of crush is sufficient to exceed many of the head injury tolerance criteria available.

Accession For	<input checked="" type="checkbox"/> DTIC <input type="checkbox"/> GPO <input type="checkbox"/> NTIS	<input type="checkbox"/> DDC TAB <input type="checkbox"/> Unannounced <input type="checkbox"/> Justification	By	Distribution	Availability Codes
					A. all in/or Hist special

As one portion of the research, injury criteria for the head and neck were reviewed to create parameter values that could be compared with the curves of constant strain for the maximum strain criteria model and a strain value of 0.00329 was established as the limit for nonconcussive blows to the head.

A simplified model of the head, a rigid body pivoted at a point to duplicate the location of the skull-neck point, was found to adequately duplicate head motion and hence strain. Hence, the complex response of the computer analog was replaced by an analysis which can be accomplished by hand. The simplified model was used to study variations of crush depth, incidence angle, bird radius, surface friction, and neck frictional coefficient. The results indicated the dominance of the change of crush depth over all other variations studied.

An instrumented test device was designed, fabricated, and calibrated for future birdstrike tests. The device is essentially a strain-gaged tube. The measurements from the device can be used to calculate moments at the tube mounting surface. These, with acceleration output at an attached anthropometric head and tube base plate, will permit calculation of the forces at the point of impact between canopy and helmet.

Limited testing was conducted with a standard Air Force helmet using a unique test device. The results indicated that there is significant difference between the crushing force generated by a "soft" and "hard" shell. Additionally, the difference between static and dynamic data indicate the liner is sensitive to velocity across its thickness. Tests should be conducted at impact velocities for higher than currently used.

A revised ANSI-Z90 helmet test standard was generated to reflect changes required due to the birdstrike environment. The revision pointed out the difficulty in attempting to force one standard to reflect two different requirements. Acceptability of current helmets under Z90 creates the test environment for the birdstrike phenomena.

PREFACE

The initial impetus for this research was created by the results of F-16 canopy tests. Birdstrikes created large deformations or failures. Once failure by penetration or cracking had been eliminated, large deformations were still present. If a large deformation passed through the space occupied by the helmet aircrewman, the effect was unknown. Questions arose as to the effect of the presence of the head, the stiffness of the canopy, the nature of the injury, and the forces generated. Hence, this effort was an attempt to use existing analytical models and some experimental data to better understand the birdstrike head impact phenomenon. The determination of allowable canopy deformation and adequate helmet clearances was a problem not only in the design of canopies and crewstations, but in the establishment of protective equipment criteria.

The program effort was greatly assisted by the participation of the program monitor, Mr. James W. Brinkley of the Biomechanics Protection Branch, Biodynamics and Bioengineering Division of the Aerospace Medical Research Laboratory. Mr. Larry J. Specker, also of the Biomechanical Protection Branch, provided assistance in obtaining data in the early phases of the effort. Mr. Ints Kaleps of the Mathematical Analysis Branch, Biodynamics and Bioengineering Division of the Aerospace Medical Research Laboratory, and Mr. William Bowman of Systems Research Laboratories, Dayton, Ohio, provided invaluable assistance in generating necessary output from the Articulated Total Body Model (ATBM) routine available at Wright-Patterson Air Force Base.

A research program is never conducted by one individual and the accomplishments reflect the efforts of many. Members of the University of Dayton Research Institute whose participation was required and appreciated are: Mr. Robert Dominic, Mrs. Louise Farren, Mr. Ira Fiscus, Mr. Dart Peterson, Mr. George Roth, and Mr. Blaine West.

TABLE OF CONTENTS

<u>Section</u>	<u>Page</u>
1 INTRODUCTION	22
2 ANALYSIS OF CANOPY TEST DATA	26
Introduction	26
Data Available	26
Data Reduction	27
Data Results	33
Data Interpretation	39
3 CREW POSITION STUDY	41
Introduction	41
Data Available	41
Data Compilation	41
Data Results	46
4 SELECTION AND USE OF ANALYTICAL CREWMAN SIMULATOR	50
Introduction	50
Simulations Available	50
Generation of Birdstrike Model	52
Bird/Canopy Configuration	53
Helmet Configuration	60
Anthropometric Data and Seat Configuration	65
Calculation of Selected Impacts	66
Computer Analysis of Visor Effect	77
Computer Analysis of Headrest Response	83
Crewman Simulation Results	87
5 ESTABLISHMENT OF INJURY CRITERIA	90
Introduction	90
Data Search	90
Angular Displacements	91
Angular Velocity	92
Angular Acceleration	94
Translational Displacement	96
Translational Velocity	96
Translational Acceleration	99
Joint Forces	102
Joint Torques	103
Contact Forces	103
Summary of Injury Criteria	104
Data Correlation and Compilation	104
Selection of Criteria	112
Summary	114

TABLE OF CONTENTS (Continued)

<u>Section</u>		<u>Page</u>
6	DEVELOPMENT OF A SIMPLIFIED ANALOG MODEL	115
	Introduction	115
	Model Development	115
	Parameter Variation Study	128
7	DEVELOPMENT OF AIRCREWMAN SIMULATION FOR TESTING	141
	Introduction	141
	Preliminary Test Hardware Designs	142
	Test Results Using First Generation Device	145
	Additional Measurement Technique	149
	Development of Design Criteria	154
	Test Device Preliminary Design	155
	Finalized Device Design	166
	Test Device Calibration	168
	Summary	172
8	FLIGHT HELMET STUDY	173
	Introduction	173
	Selection of Protocol and Test Procedures	174
	Fabrication of Test Hardware	177
	Test Program	178
	Data Interpretation	184
	Test Data Summary	188
9	PROPOSED STANDARD	191
	Introduction	191
	Review of Current Standards	193
	Development of New Criteria	196
	Development of Impact Testing Requirements	200
	Development of Proposed Standard	206
	Scope, Purpose, and Requirements	208
	Definitions	208
	Construction	208
	Materials and Labeling	209
	Extent of Protection and Sample for Testing	209
	Conditions for Testing	209
	Tests for Protective Headgear	209
	Low Level Impact Condition	209
	Acceptable High Level Performance	210
	Calculation of MSC	210
10	SUMMARY, CONCLUSIONS, AND RECOMMENDATIONS	213
	Summary	213
	Conclusions	214
	Recommendations	216

TABLE OF CONTENTS (Concluded)

<u>Section</u>	<u>Page</u>
APPENDIX	218
REFERENCES	226

LIST OF ILLUSTRATIONS

<u>Figure</u>		<u>Page</u>
1	Distortion of Canopy at 0.00008 Seconds after Reference Frame.	29
2	Distortion of Canopy at 0.00024 Seconds after Reference Frame.	29
3	Normals to Observed External Mold Line Constructed to Allow Determination of Maximum Normal Displacement.	30
4	Maximum Normal Amplitude of Deflection Wave, Showing its Approximation to a Half Sine Wave.	31
5	Waveform Prior to Maximum Deformation.	32
6	Waveform During Decay.	33
7	Typical Data Plot Redrawn from AEDC Calcomp Plot. This plot indicates that the maximum displacement was not read.	36
8	Estimated Curve of Maximum Vertical Displacement at Station 140.0, Plotted with Estimated Curve of Maximum Normal Displacement for 0.50-inch Thickness.	37
9	Estimated Curve of Maximum Vertical Displacement at Station 140.0, Plotted with Estimated Curve of Maximum Normal Displacement for 0.625-inch Thickness.	38
10	Wave Speed versus Kinetic Energy.	38
11	Canopy Clearance Layout for 5th Percentile Aircrewman in F-16.	42
12	Canopy Clearance Layout for 95th Percentile Aircrewman in F-16.	43
13	Envelope of Possible Helmet Positions for 5th Percentile Aircrewman Seated in Upper Seat Position with Eye along Upper Eye Axis.	45
14	Locations of Probable Positions of Eye Analysis Point for Eye Located along Upper, Design, and Lower Eye Axes, with Seat at Upper, Middle and Lower Positions (5th Percentile Aircrewman).	46

LIST OF ILLUSTRATIONS (Continued)

<u>Figure</u>		<u>Page</u>
15	Locations of Probable Positions of Eye Analysis Point for Eye Located along Upper, Design, and Lower Eye Axes, with Seat at Middle and Lower Positions (95th Percentile Aircrewman).	47
16	Portion of Layout Showing Eye Analysis Points and Skull Locations.	48
17	Force-Time Profile from UDRI-TR-77-17.	54
18	Generalized Triangular Kinematics.	55
19	Model Fit of Experimental Data.	56
20	Force-Time Profile of Local Deforming Canopy.	57
21	Canopy Stiffness Model.	58
22	Bird/Helmet Impact Points for Mid-Eye Analysis Point.	59
23	Schematic of "Suspension" System Used in CAL3D Model to Support Helmet and Liner on Skull.	61
24	Force-Deformation Curve from Drop Test Data on HGU-22/P Styrofoam, Insolite, and Foam Helmets at Impact Velocities of 16.23 and 16.9 ft/sec Against Hemispherical Anvil.	63
25	Force-Deformation Curves from Drop Tests on HGU-22/P Helmet with Fitting Pads, at Impact Velocity of 13.08 ft/sec Against Flat Anvil.	64
26	Force-Displacement Curves for Canopy-Helmet Interference.	67
27	Theoretical Displacement δ versus Computed Displacement δ_H .	68
28	Fore-and-Aft Head Acceleration versus Time with Other Tabulated Output Variables.	70
29	Injury Parameters versus Displacement for Head Fore-and-Aft Translational Acceleration \ddot{X} , Head Translational Velocity \dot{X} , and Head Angular Acceleration, $\ddot{\theta}$.	71

LIST OF ILLUSTRATIONS (Continued)

<u>Figure</u>		<u>Page</u>
30	Injury Parameters versus Displacement for Head Angular Velocity $\dot{\theta}$, Skull Force, and Neck Axial Force.	71
31	Injury Parameters versus Displacement for Neck Shear Force and Neck Moment.	72
32	Number of Injury Criteria Exceeded versus Displacement.	73
33	Theoretical Displacement δ versus Computed Displacement δ_H with Comparison of "Stiff" and "Soft" Canopy.	75
34	Comparison of Injury Parameters versus Displacement for Stiff and Soft Canopies for Head Fore-and-Aft Translational Acceleration \ddot{X} , and Head Angular Acceleration $\ddot{\theta}$.	75
35	Comparison of Injury Parameters versus Displacement for Stiff and Soft Canopies for Head Angular Velocity $\dot{\theta}$, Skull Force and Neck Angular Force.	76
36	Comparison of Injury Parameters versus Displacement for Stiff and Soft Canopies for Neck Shear Force and Neck Moment.	76
37	Deformation Patterns for Helmet Visor with Both Shades in the Up Position.	78
38	Visor Force-Displacement Curves.	79
39	Head Acceleration Generated With and Without Visor.	79
40	Neck Forces as Functions of Helmet Shell Without Visor.	80
41	Head Angular Motion Due to Shell With and Without Visor.	81
42	Visor Impact Area.	82
43	Helmet and Headrest Stiffness.	84
44	Head Acceleration and Strain for Birdstrike and Headrest Impact.	84

LIST OF ILLUSTRATIONS (Continued)

<u>Figure</u>		<u>Page</u>
45	Head Response with Headrest Located at Point of Maximum Velocity.	85
46	Head Response with Headrest Touching Helmet Shell at Impact.	86
47	Maximum Angular Rotation of Head and Neck in the Sagittal Plane about the Base of the Skull.	92
48	Theoretical Threshold of Concussion; Man.	94
49	Head Angular Velocity $\dot{\theta}$ versus Angular Acceleration $\ddot{\theta}$.	95
50	Compilation of Translational Velocity Data.	98
51	Compilation of Acceleration Data.	101
52	Compilation of Translational Data with Approximate Boundaries for Tolerable Response.	105
53	Translational Acceleration Data with Maximum Strain Criteria Variations.	106
54	Translational Data with Maximum Strain Criteria of 0.00329.	106
55	Maximum Strain Criterion Head Model.	107
56	Maximum Strain Criterion Curves for Human Lateral Head Impact.	110
57	Vertical Impact Tolerance Curve Based Upon 1000-Pound Skull Force and 440-Pound Neck Axial Force Limits.	111
58	Deformation Configuration for Two Intersecting Spheres.	116
59	Applied Force and Moment versus Time for 2-Inch Interference of 10-Inch Radius Bird (Bump) and Extra-Large Helmet Shell at 1400 Inches per Second; Impact Path 19° from Horizontal.	118

LIST OF ILLUSTRATIONS (Continued)

<u>Figure</u>		<u>Page</u>
60	Approximation of Moment Curve for Intersection of Helmet with a 10-Inch Radius Bird for Interference of 1.05 Inches.	121
61	Dimensional Data Necessary for Simplified Model.	123
62	Waveforms for Low-Level Birdstrikes.	125
63	Waveforms for High-Level Birdstrikes.	126
64	Variations in Acceleration Due to Different Angles of Incidence for 1.05-Inch Interference.	131
65	Variations in Acceleration Due to Different Wave Speeds for 1.05-Inch Interference.	131
66	Effects of Wave Speed Upon Maximum Strain for 1.05-Inch Interference.	132
67	Variations in Acceleration Due to Different Angles of Incidence for 1.55-Inch Interference.	133
68	Variations in Acceleration Due to Different Wave Speeds for 1.55-Inch Interference.	134
69	Variations in Acceleration Due to Different Friction Coefficients for 1.05-Inch Interference.	135
70	Variations in Acceleration Due to Different Friction Coefficients for 1.55-Inch Interference.	136
71	Effect on Duration of Acceleration Pulse and on Peak Acceleration of Increasing Bird Radius by a Factor of Two.	137
72	Effect of Changing Neck Damping Coefficient on Peak Acceleration.	139
73	Schematic of Head-Neck Test Device.	143
74	Calculated Head Response to 6000-Pound Impact Normal to Surface of Helmet.	143

LIST OF ILLUSTRATIONS (Continued)

<u>Figure</u>		<u>Page</u>
75	Test Apparatus for Measurement of Birdstrike Impact.	144
76	Motion of Fixed Points Due to Translational and Rotational Motion of the Head.	150
77	Facsimile of Typical Output of Dummy Head Motion Program.	153
78	Schematic Showing Three Design Conditions Applied to Rigid Plate.	156
79	Assumed Beam Elements for Condition 2.	157
80	Strain Gage Locations on Tube Supporting Head and Neck Structures.	158
81	Supporting Tube Assembly for Test Device, Preliminary Design.	161
82	Base Assembly for Test Device, Preliminary Design.	163
83	Natural Frequency versus Static Strength of Ethafoam.	163
84	Assembly, Preliminary Design of Test Device.	165
85	Assembly, Finalized Design of Test Device.	167
86	Calibration Fixture for Test Device.	169
87	Closeup of Test Device Calibration Fixture, Showing Load Cell.	169
88	Typical Strain versus Calibration Force for Minus-X Loading.	171
89	Helmet Testing Device, Showing HCL-4 Head Form (Skull Cap) and Anvil Representing Bird.	178
90	Sites for Measurement of Liner Thickness, Standard Large-Size Air Force Helmet with HCL-4 Head Form.	180

LIST OF ILLUSTRATIONS (Continued)

<u>Figure</u>		<u>Page</u>
91	Force-Strain Curves for Standard Flight Helmet Tested with HCL-4 Head Form and 10-Inch Radius Loading Head Positioned 30° Forward of Crown.	181
92	Force-Strain Curves for Helmet Liners Alone.	182
93	Force Differences Between Shell with Liner and Liner Alone (or "No-Shell") Conditions.	183
94	Comparison of Static and Dynamic Force-Strain Curves for Similar Thickness Liner Locations.	184
95	Force-Strain Curves for Impact Sites 30° Forward and 30° Aft of Crown.	185
96	Force-Strain Curves for Standard Flight Helmet Configuration and "Rigid" Shell with Foamed-in-Place Liner.	185
97	Force-Strain Curves for Interaction Forces for Two Standard Air Force Flight Helmets and one "Rigid" Shell with Foamed-in-Place Liner.	186
98	Schematic Comparing Liner Crush Mechanisms for Common Maximum Crush, for Liner-Only and Liner with "Rigid" Shell Configurations.	187
99	Triangular Waveforms Satisfying Particular Criteria.	194
100	Location of Waveform Pulses from Figure 99 on MSC Plot.	195
101	Skull and Neck Forces Required to Generate Triangular Pulse.	198
102	Vertical Impact Tolerance Curve Based Upon 1000-Pound Skull Force and 440-Pound Neck Axial Force Limits.	200
103	Force-Displacement Curve for Drop No. 13 of HGU-22/P Helmet (Drop on Crown).	204
104	Frontal Acceleration and Strains as Functions of Impact Velocity.	207

LIST OF ILLUSTRATIONS (Concluded)

<u>Figure</u>		<u>Page</u>
105	Triangular Acceleration Pulse with Linear Approximations.	211
106	Calculated Strain for 50 g Triangular Pulse.	212

LIST OF TABLES

<u>Table</u>		<u>Page</u>
1	Results of Film Analysis	34
2	Limits of Injury Resulting in Concussion	69
3	Head Model Parameters	107
4	Suggested Reasonable Criteria for Non-concussive Impacts	112
5	Values Used in Parametric Study	130
6	Percent Change of Peak Acceleration Due to Variation in Parameters	138
7	Computation of Load Cell Force Magnitudes	146
8	Computation of Acceleration Magnitudes	146
9	Liner and Shell Thickness for Points Described in Figure 90	180

ACRONYMS AND ABBREVIATIONS

<u>Acronym</u>	<u>Identification</u>
AEDC	Arnold Engineering Development Center
AFFDL	Air Force Flight Dynamics Laboratory
SAT	Special Assistance Team
ASD	Aeronautical Systems Division, Air Force Systems Command
AMRL	Aerospace Medical Research Laboratory, Air Force Systems Command
AFSC	Air Force Systems Command
RTD	Research and Technology Division, Air Force Systems Command
CAL3D	Vehicle-occupant model by Calspan
UCIN	Vehicle-occupant by the University of Cincinnati
TTI	Vehicle-occupant by Texas Transportation Institute
HSRI3D	Vehicle-occupant model by the University of Michigan Highway Safety Research Institute
SAEJ3D	Vehicle-occupant model by the Society of Automotive Engineering of Japan
FAA3D	Vehicle-occupant model by Ultrasystems
ATBM	Articulated Total Body Model
NTIS	National Technical Information Service
COMPENDEX	Data File of Engineering Indexes Abstracts
DOT	United States Department of Transportation
SAE	Society of Automotive Engineers
HSRI	Highway Safety Research Institute of the University of Michigan
ASCE	American Society of Civil Engineers
MSC	Maximum Strain Criteria
WSC	Wayne State Curve

ACRONYMS AND ABBREVIATIONS (Concluded)

<u>Acronym</u>	<u>Identification</u>
UDRI	University of Dayton Research Institute
MTS	MTS Systems Corporation
ANSI	American Standards Institute
CFR	Coefficient of Friction

LIST OF SYMBOLS

<u>Symbol</u>	<u>Meaning</u>
A	area
(A)	aft, direction of -X
C	damping coefficient
(C)	compression
(D)	down, direction of +Z
F	force
F_{cc}	compressive crippling allowable
F_o	impulse
G	gravitational units
I	mass moment of inertia
I	planar moment of inertia
J	polar moment of inertia
L	length
L'	effective length
M	mass
M_p	moment at pivot point
\bar{M}	externally applied moment
(R)	right, direction of +Y
R_B	radius of bird or canopy deformation wave
R_H	radius of helmet
\ddot{R}	acceleration of absolute position vector
(T)	tension
(U)	up, direction of -Z
V	velocity
V	applied shear force

LIST OF SYMBOLS (continued)

<u>Symbol</u>	<u>Meaning</u>
V_o	impact velocity
V_p	velocity of impacted surface
W	weight
X	X-coordinate
X_{max}	maximum strain criteria model displacement
\dot{X}	velocity in X-direction
\ddot{X}	acceleration in X-direction
\ddot{X}_p	plate acceleration in X-direction
Y	Y-coordinate
\dot{Y}	velocity in Y-direction
\ddot{Y}	acceleration in Y-direction
Z	Z-coordinate
\dot{Z}	velocity in Z-direction
\ddot{Z}	acceleration in Z-direction
\ddot{Z}_p	plate acceleration in Z-direction
b	thickness
d	distance bird travels from impact point to maximum deformation of helmet
f_b	bending stress
f_s	shear stress
g	gravitational units
$\bar{I}, \bar{J}, \bar{K}$	coordinate vectors
$\bar{I}^1, \bar{J}^1, \bar{K}^1$	displaced coordinate vectors
l	length
l_o	reference length

LIST OF SYMBOLS (continued)

<u>Symbol</u>	<u>Meaning</u>
m	mass
m	applied bending moment
r	radius
\bar{r}	position vector
s/l	nondimensional consumed length
t	time
t	thickness
u	translational acceleration
y	distance from neutral axis to fiber of interest
$\Delta_x, \Delta_y, \Delta_z$	translations along original x,y,z coordinates
Σ	summation
α	angular acceleration
α	damping term
$\bar{\alpha}$	angular acceleration vector
β	damped natural frequency
β	angle between impact point and maximum deformation of helmet
δ	displacement; deformation
δ_H	interference; computed displacement
ϵ	strain
θ	Euler angle about Y-coordinate
θ	angle; angular dimension
$\dot{\theta}$	angular velocity
$\ddot{\theta}$	angular acceleration
μ	Poisson's ratio

LIST OF SYMBOLS (concluded)

<u>Symbol</u>	<u>Meaning</u>
v	dimensionless response spectrum parameter
ρ	density
ρ	radius of gyration
σ	normal stress
τ	pulse duration
τ	shearing stress
τ	time selected to establish slope
ϕ	angle between impact surface and horizontal
ϕ	Euler angle about Z-coordinate
ψ	Euler angle about X-coordinate
ω	natural frequency
$\dot{\omega}$	angular acceleration
ω_n	natural frequency for lateral or longitudinal response

SECTION 1

INTRODUCTION

Operating statistics compiled during the period of 1968 through 1972 indicate that there were over 3500 birdstrikes recorded by the United States Air Force. Of the many recorded impacts, about 12 percent involved the windshield/canopy area of the aircraft. Of these, six caused the loss of the aircraft. Low level mission requirements at high speeds increase the probability of more and more severe birdstrikes.

Many approaches have been studied to alleviate or eliminate the birdstrike problem. The most direct approach taken recently was to change the structural properties of the windshield canopy. Various materials were tried in monolithic or laminated configurations to defeat the bird with either increased strength or energy absorbing deformation. Unfortunately, although the deformation may prevent the bird from penetrating the windshield, the deformation may pass into the volume occupied by the aircrewman. If the canopy deformation should impact with the helmet of the aircrewman, would the impact be injurious? This was the primary question to be answered by the research effort. In order to answer the primary question, it was first necessary to find answers to several secondary questions that contributed to the complexity of the problem, such as:

- Given that an impact occurs, how can it be described quantitatively?
- What effect does the helmet shell have upon the kinetics of the head?
- How can the desired parameters be measured?
- How can the human head-neck system be simulated for impact testing?
- What constitutes "injury"?

The specific objectives of the research were:

- (1) To provide methods of assessing the biomedical effects of direct impact to an aircrewman's helmeted head;
- (2) To describe measurement techniques capable of measuring the forces transmitted to the aircrewman's head;
- (3) To determine the influence of the structural properties of the USAF pilot's helmet on the impact transmitted; and
- (4) To develop the best method to simulate the crewman during tests conducted on aircraft canopies.

The objectives could not be achieved without studying theoretical and experimental data available relative to both the mechanical properties of canopies and the biomechanical properties of the human. The data evaluation translates into several specific requirements.

Quantitative descriptions of the canopy response due to a birdstrike can be developed theoretically. Study results were available which could be used to infer the response of any canopy to any bird. However, there were also available test data collected on the F-16 canopy which could be utilized. Consequently, acceleration and displacement data for at least 24 bird impact tests were to be reduced in order to provide estimates of canopy deformations. From the data it was hoped that some parametric relations could be established between bird mass and velocity, and canopy configuration and observed deformation. Since all data were related to the F-16, a crew position study for the F-16 cockpit was to be conducted to examine design eye position requirements as they related to experimentally measured deformation.

Aircrewman simulation was to be studied along two paths. First, the simulation was to be analytical. Existing mathematical analogs of the human body were to be investigated to select a particular one. The one selected had to have the capability to permit a quantitative description of the human head, neck, and upper torso, as well as interacting constraints such as restraints

and cushions. Additionally, the model had to permit the impact of moving surfaces or bodies to duplicate the impact of the canopy deformation wave, referred to herein as the "bump", and helmet.

The second simulation was to be a test apparatus capable of duplicating the response of the helmeted head while simultaneously providing measured data. The ultimate goal was the fabrication, calibration, and delivery of a breadboard device that could be used in canopy impact testing. The device had to be able to provide a measurement of the forces of impact, whether directed symmetrically or asymmetrically to the helmeted head.

Another aspect of the analytical simulation was the requirement to investigate the feasibility of developing a simplified model of the impact phenomenon: Could the complex mathematical analog be reduced to a simple model, which could be easily used by aircraft designers, with adequate accuracy for generating those parameters which would be the best indicators of injury?

The injury criteria to be used were to be developed from existing biomechanical data. Levels of injury ranging from short term disruption of psychomotor performance to major injury had to be defined quantitatively and documented.

Other specific requirements were related to the protection provided by the helmet and human body and canopy response. Equally important is an understanding of the helmet characteristics and how they influence the system response.

The last requirement was that of investigating experimentally and theoretically the effects of the helmet shell during impact. Helmet shape and surface friction were to be investigated to better evaluate the interaction at the point of contact with the canopy bump. Additionally, the potential of the shell to transfer impact energy directly into the ejection seat headrest was to be investigated.

Helmet liner characteristics were also to be examined experimentally. The mechanical response characteristics over a range of

impact conditions was to be investigated. Following the examination of shell and liner response, experimental studies were then required to evaluate the response properties of the USAF pilot's helmet.

The results of the analytical and experimental effort were to be used in the development of recommendations for future experimental evaluations of flight helmets.

Finally, a proposed standard for the evaluation of the biological effects of direct impact of the helmeted head was required. Test methods, test equipment, data processing techniques, and acceptance criteria were to be included.

In summary, the specific requirements of the effort reflect the need to relate the broad objectives to specific data. There were theoretical approaches to all aspects of the effort, but by using available test data for a specific canopy and helmet, it was possible to quantitatively describe many of the parameters which might have been misunderstood intuitively. The effort was designed to make use of experimental data to achieve better understanding of theoretical models. This may create a problem in loss of generality, but the problem is outweighed by a greater appreciation of the complexity of the impact phenomenon.

SECTION 2

ANALYSIS OF CANOPY TEST DATA

INTRODUCTION

Prior to this effort a study was conducted to investigate in a preliminary manner, the nature of the response of a helmeted head to high velocity impact. It seemed reasonable to assume that the windshield depression could be approximated by an ellipsoid traveling at the speed of the bird. One data point from test information was available: the vertical displacement as a function of time at one point on the interior of an F-111 canopy was published.^[1] This, along with derived displacement and bird speed, could be used to select an ellipsoid, but not a unique ellipsoid. Consequently, even for a fixed point on the canopy, it was impossible to "fit" the data uniquely. Thus, knowing that the deformation configuration was an ellipsoid changing with time, made it imperative that experimental data be examined to establish some quantitative description of the bird/canopy response.

Further, there was reasonable doubt concerning the compliance of the canopy. During some of the initial tests, there were impacts between the canopy and a helmeted headform. Without sufficient instrumentation available, there were differences in opinion as to whether or not the canopy could generate significant forces at the helmet, or whether the canopy would be deflected by the presence of the head.

Fortunately, during the time of the preliminary study several test programs had been initiated to collect film data for test shots using different weight birds at selected velocities.

DATA AVAILABLE

As of 17 May 1977, 28 F-16 canopy tests had been completed by the Air Force Flight Dynamics Laboratory (AFFDL) at the Arnold Engineering Development Center (AEDC). These tests were with two- and four-pound chickens impacted at speeds of from 123 knots to

a maximum of 349 knots. Canopies constructed of 0.500 and 0.625-inch-thick coated Texstar transparencies were used.

Additional tests using uncoated transparencies were conducted at AEDC for General Dynamics and at General Dynamics, Fort Worth.^[2] Ten tests were made, but only eight provide useful information. A complete tabulation of all film data reduced is contained in Table 1, which appears later in this section.

DATA REDUCTION

All films for data reduction were mounted onto a stop-action projector which displayed the image upon a ground glass screen. Once the film had been reviewed to determine that readable information was available, the film was rewound and a specific film frame was established as the initial reference frame. A frame counter was set to zero and all subsequent frames were identified relative to the reference. The reference was not necessarily the initiation of impact, since there was really no way of knowing exactly when it occurred. However, there was no other parameter to be correlated to the film action, hence an arbitrary reference was acceptable, as long as it was prior to impact.

The films viewed the F-16 canopy laterally from the intended point of impact. The camera was placed directly abeam of fuselage station 115.0 and waterline 125.5. Other camera angles were available, but seldom were they used since this one provided a view of the impacted canopy from impact point through fuselage station 140.0, the location of the design eye.

A projected image of the 16 mm film was one-fifth life-size. A vellum overlay was placed over the projected image and reference lines were made to coincide with fiducial references on the image. A separate vellum overlay was made for each impact studied. The overlay provided sequential positions of the bird and canopy. By scaling the fiducial lines of the image, it was apparent that some distortion existed due to the focal length of the camera.

Additionally, it was apparent that even with the relatively small magnification used, fiducial lines were stripes with indistinct edges.

The initial films were rigorously examined to determine just how much information could be extracted from them. For example, could the films assist in determining the impulse transferred to the canopy? The primary purpose was to determine bump size and speed, but by examining as much data as possible, it was hoped a better understanding of the phenomenon would result.

An example of the processing is explained by referring to the analysis of Test I.D. 4607. A two-pound bird traveling at approximately 350 knots impacted a coated 0.5-inch-thick transparency. The film was mounted, a reference frame was selected, and the motion of canopy and bird were plotted for every four frames of film. Seventy-six frames, corresponding to 0.0152 seconds, provided a history of the impact and canopy response. Two frames are represented in Figures 1 and 2. In drawing the overlay it was difficult at times to accurately define the motion without cycling the film back and forth to view the action. The chicken starts out as a well defined shape, but at impact becomes a fuzzy multicolored spray of particles. The canopy curvature is initially easily seen but as the bird disintegrates and the canopy bends, the lower surface of the canopy becomes confused with fiducial lines painted on the canopy, reflections of the canopy surface, and discolorations due to the bird. However, it was possible to follow the interior surface of the transparency. This was verified by having several people read the same film after being told that they were to follow the curvature generated by the interior surface of the canopy.

Once the motion of the canopy was defined, it was necessary to quantitatively describe the motion. A third-degree polynomial was generated to fit the observed mold line and differentiated to obtain the slope, and hence the normal, at any point along the curve.

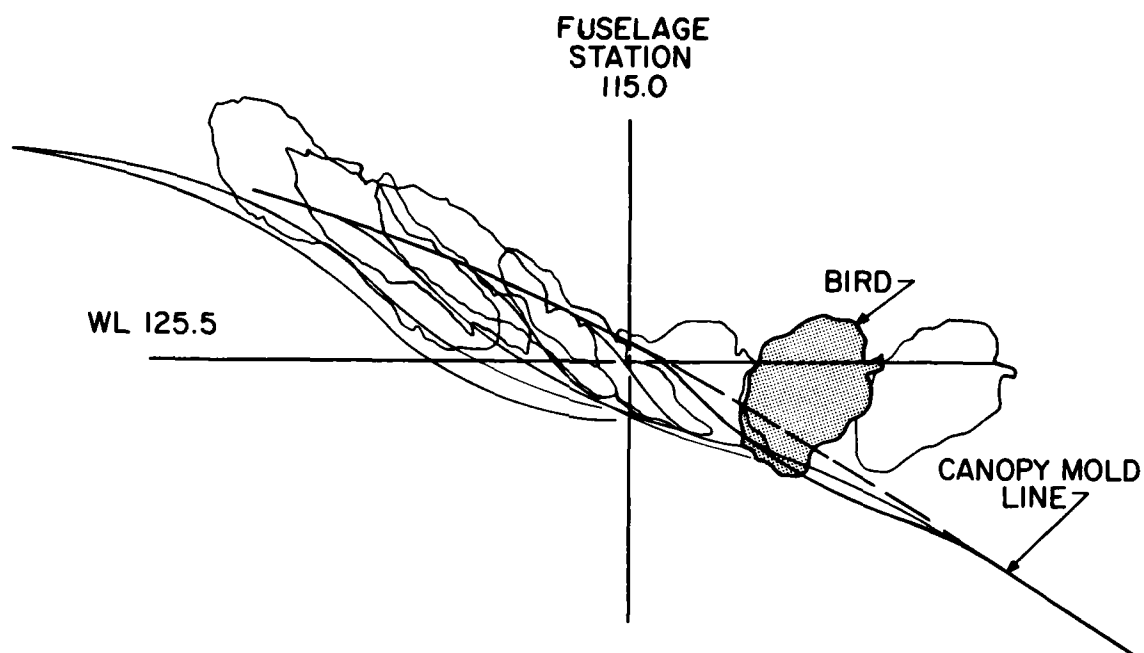


Figure 1. Distortion of Canopy at 0.00008 Seconds after Reference Frame (Test I.D. 4607).

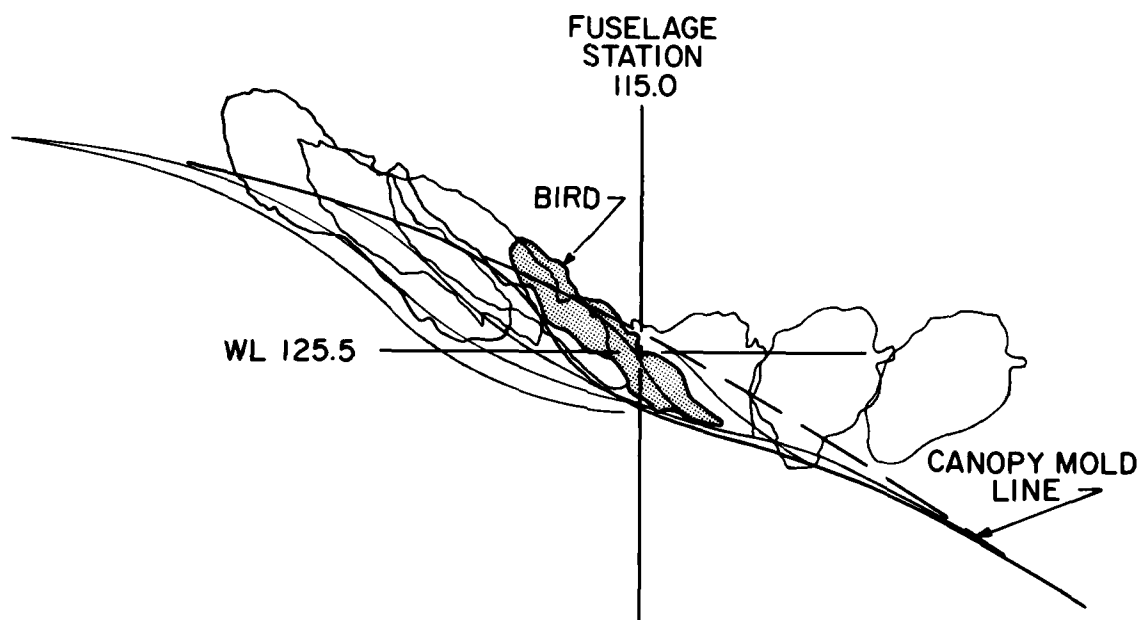


Figure 2. Distortion of Canopy at 0.00024 Seconds after Reference Frame (Test I.D. 4607).

Several points were selected and a family of normals were constructed. Using the overlay of the normals, every fourth film frame curvature was examined to determine the maximum normal displacement from the external mold line. Figure 3 shows the results of this procedure for Test I.D. 4607.

The process of examining the curvature relative to the normal to the surface generates a series of points which locates maximum normal deformation as a function of time. By examining Figure 3 it is apparent that if maximum normal deformation is used to define

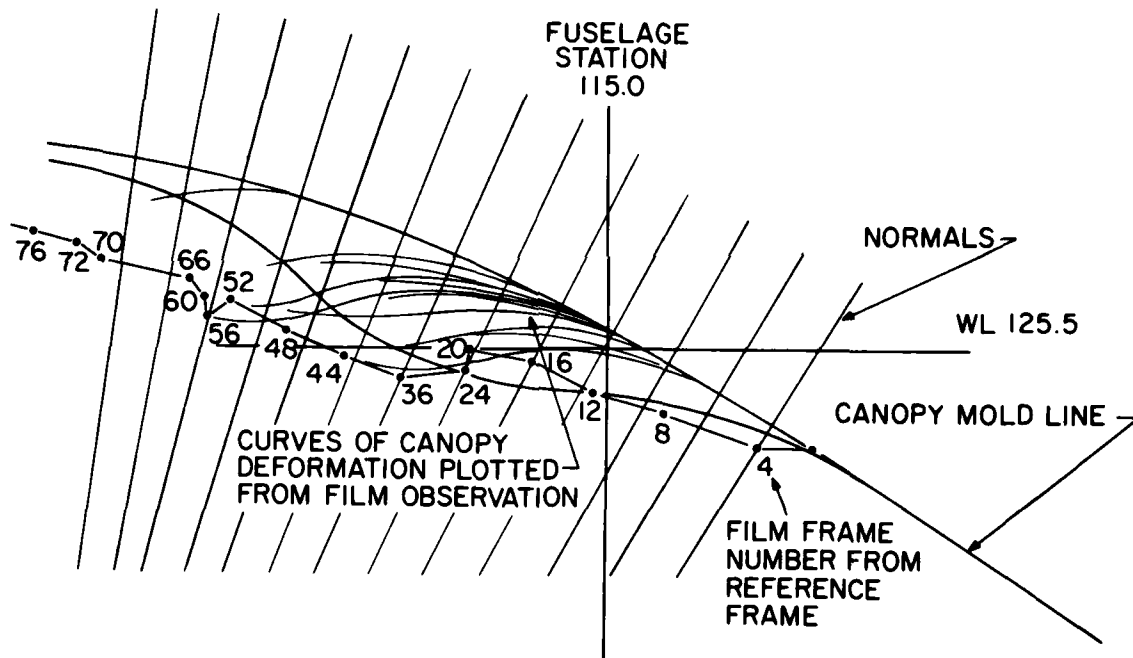


Figure 3. Normals to Observed External Mold Line Constructed to Allow Determination of Maximum Normal Displacement (Test I.D. 4607). Data points show point of maximum displacement for every fourth frame of film from reference frame to frame 76. This leads to the observation that the wave has periods of motion and periods of hesitation. Total elapsed time: 0.0152 seconds.

the motion, the wave increases in magnitude up to a maximum and then decreases. However, the fore and aft motion is not a continuously increasing and then decreasing function. The wave increases in magnitude, but its longitudinal motion seems to have periods of motion followed by periods of hesitation. This qualitatively agrees with the comments of others that the motion for the F-16 canopy has a wave and a cusp characteristic. Hence in defining the longitudinal velocity, it is necessary to specify where in the response the velocity is desired.

The maximum normal amplitude of the wave is plotted in Figure 4. The amplitude approximates a half sine pulse as is indicated by the approximation shown on the data. The velocity does not plot as well. This difference is to be expected in that while it is possible to reasonably well establish the magnitude of a shallow waveform, it is difficult to establish where the peak occurs.

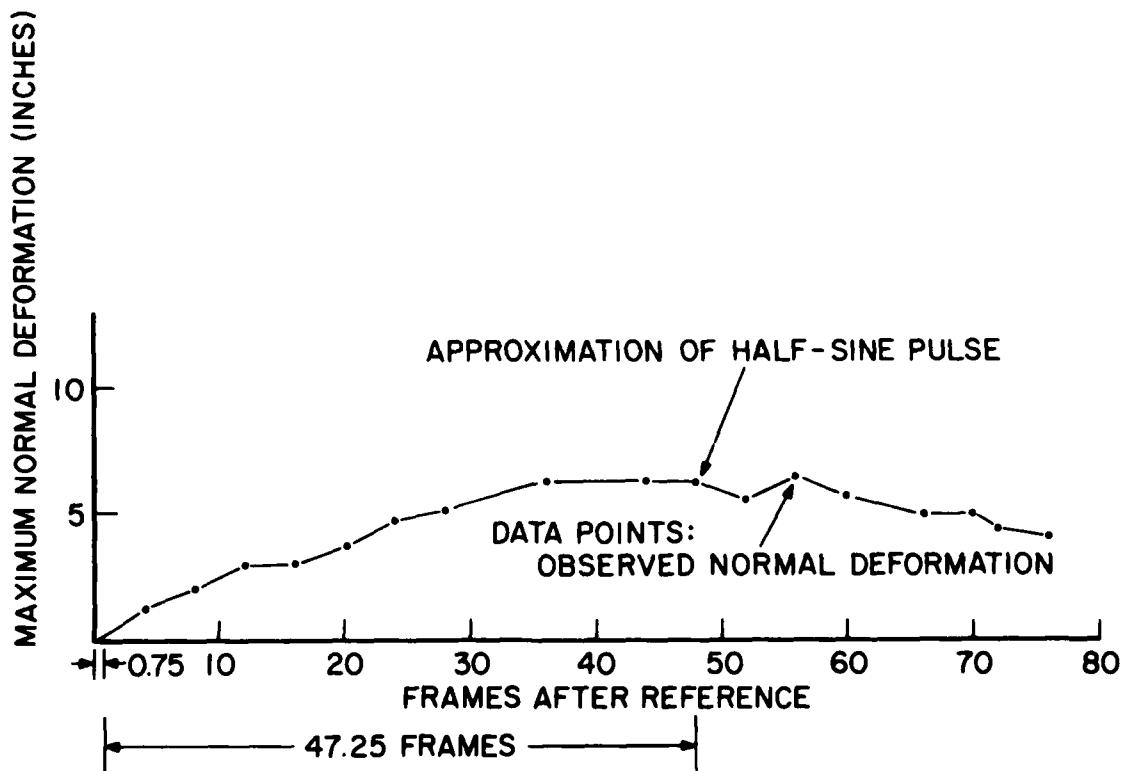


Figure 4. Maximum Normal Amplitude of Deflection Wave, Showing its Approximation to a Half Sine Wave (47.25 Frames = $T/4$; $T = 0.0380$ sec/cycle; $f = 26.3$ Hz).

After establishing the point of maximum deformation for every fourth frame, the curves were examined to obtain radius of curvature information. Plots as shown in Figures 5 and 6 are indicative of the curvature seen prior to maximum deformation and then during decay. The curves are all shown with the normal in the vertical position, the middle of the plot. Therefore, the waveforms shown depict a series of waveforms that could be seen if the observer were traveling with the wave and the normal to the exterior mold line. The curves indicate the change from large to small radii in the decay portion of the wave. In all cases, the leading edge, left side of the figure, could be seen. The trailing edge was not always as distinct because of bird disintegration. However, the curvature at maximum deformation was easily drawn. With these plots available, it was easy to overlay a scale drawing of arcs of many radii and determine the radii at selected points.

A second point required for further analysis was the wave speed. As mentioned, the wave in some instances seemed to have a hesitant motion which meant velocity determination would depend

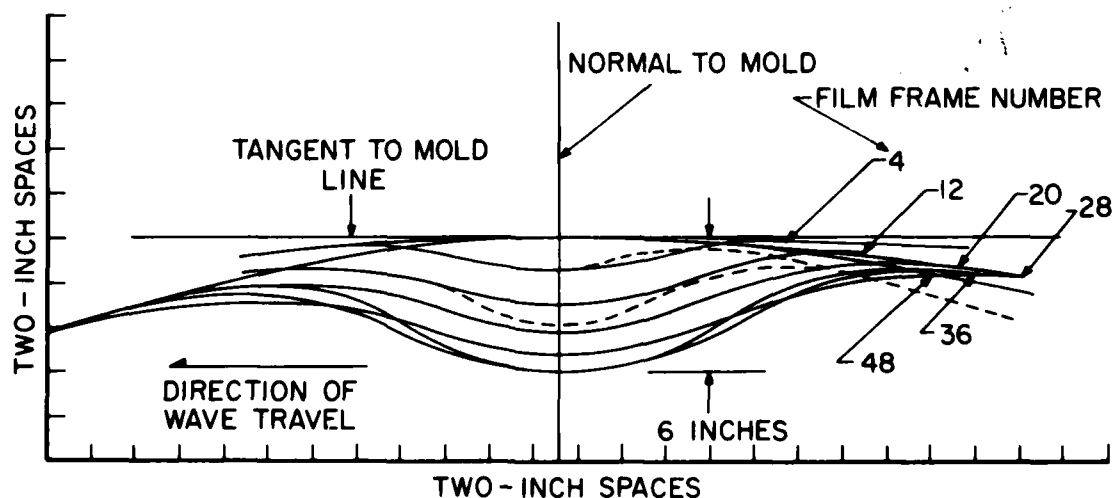


Figure 5. Waveform Prior to Maximum Deformation.

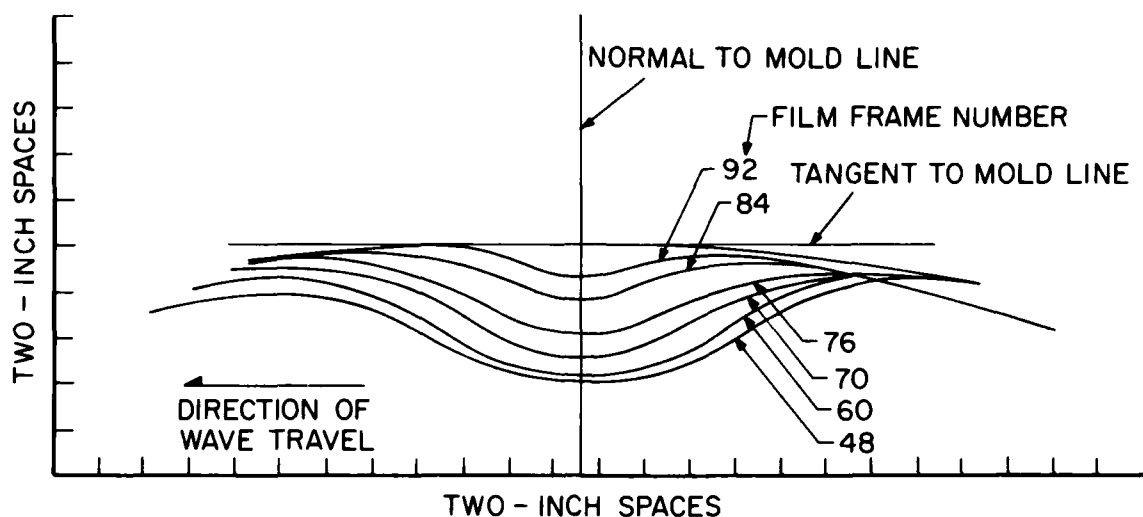


Figure 6. Waveform During Decay.

upon location along the path. Since it was necessary to have a specific value of wavespeed for computer modeling, the velocity of the wave was determined by calculating the average velocity from maximum deformation to fuselage station 140.0, the location of the design eye point.

Other sources of information were also available. Photographic data were processed both by General Dynamics and by the Arnold Engineering Development Center. The General Dynamics data provided maximum deformation information while the AEDC data was of the form of Figure 7. Figure 7 shows that the maximum displacement was not necessarily read. Instead, the maximum was omitted and the points on either side were connected by a straight line.

DATA RESULTS

The results of the film analysis are shown in Table 1 which represents the maximum normal displacement information for all test

TABLE 1. RESULTS OF FILM ANALYSIS

TEST IDENTIFICATION			TEST PARAMETER		MAXIMUM NORMAL DISPLACEMENT DATA								VERTICAL DISPLACEMENT DATA (STATION 140)			
1	2	3	4	5	6	7	8	9	10	11	12	13	14	15	16	
Test No.	Film I.D.	Canopy (C)No.	Temp. T (°F)	Thick-ness (inches) *	Bird Weight (lb)	Bird Speed (kt)	Kinetic Energy (lb-ft)	δ (inches)		Could Be Seen in AEDC Data?	Did Canopy Fail During Shot?	δ (inches)		Calculated Wave Speed (kt)		
								UD	AEDC			UD	AEDC			
004	4604	C1	75	0.50C	4.05	349	21,962		1.75		No	F	4.30		117	
006	4607	C4	75	0.50C	2.16	342	11,248	6.0	4.75	5.75	Maybe	F	4.30		117	
011	4605	C2	75	0.50C	4.07	176	5,613	2.75	1.50		No	F	1.0	2.00	182	
012	4606	C5	75	0.50C	2.10	191	3,411	1.50	1.00		No			0.50		
013	4612	C5	75	0.50C	4.06	123	2,735	1.75	0.75		No		0.75	0.50	208	
013A	4618	C5	75	0.50C	4.01	140	3,499	1.9	1.0		No		1.0	0.75	140	
014A	4619	C5	195	0.50C	4.14	159	4,660	2.6	1.25		No		1.75	0.60	132	
									1.0		No					
015A	4620	C5	-35	0.50C	4.04	164	4,838	1.5	0.75		No			0.75	156	
018	4626	C3	75	0.50C	4.07	149	4,022	2.6	1.0		No			0.75	142	
019	4627	C3	195	0.50C	4.10	150	4,107	2.3								
020	4627	C3	-35	0.50C	4.00	146	3,796								117	
020A	4638	C3	75	0.50C	4.18	157	4,587		0.75		No	F		0.50		
020B	4639	C3	75	0.50C	4.18	173	5,570	3.6	1.75		No	F	1.75	1.50	132	
									0.75		No					
015B	4640	C5	195	0.50C	4.10	170	5,277	2.6	3.0		Yes		1.75	1.50	184	
									2.0		Maybe					
015C	4641	C5	-35	0.50C	4.09	171	5,327	3.1								
015D	4659	C5	75	0.50C	4.01	154	4,236	3.4								
015E	4659	C5	75	0.50C	4.18	172	5,508	3.3	2.5		Yes	F	1.0	1.00		
									2.0		Yes					

*C-Coated
U-Uncoated

TABLE 1. RESULTS OF FILM ANALYSIS (Concluded)

TEST IDENTIFICATION			TEST PARAMETER		MAXIMUM NORMAL DISPLACEMENT DATA								VERTICAL DISPLACEMENT DATA (STATION 140)			
1	2	3	4	5	6	7	8	9	10	11	12	13	14	15	16	
Test No.	Film I.D.	Canopy (C) No.	Temp. T (°F)	Thick-ness (inches) *	Bird Weight (lb)	Bird Speed (kt)	Kinetic Energy (lb-ft)	δ (inches)		Could Be Seen in AEDC Data?	Did Canopy Fail During Shot?	δ (inches)		Calculated Wave Speed (kt)		
								UD	AEDC			UD	AEDC			
028	4650	C6	75	0.625C	4.02	157	4,414	1.20	0.75	No			0.50			
023	4650	C6	75	0.625C	4.05	187	6,308	1.40	2.25	Yes			1.00			
024	4651	C6	75	0.625C	4.20	250	11,691	3.35		No		F	1.75		98	
022	4653	C8	75	0.625C	4.11	199	7,249	2.20	2.25	Yes			1.00	0.75	200	
								2.25		No						
022A	4653	C8	195	0.625C	4.00	198	6,984	2.55	2.50	Yes			0.90		206	
022B	4654	C8	-35	0.625C	4.09	197	7,069	1.70								
022C	4655	C8	75	0.625C	4.01	201	7,215	1.65	1.00	No			0.75	0.50	262	
022D	4654	C8	75	0.625C	4.01	220	8,644	2.28	2.25	Yes			0.75	0.75	200	
022E	4656	C8	75	0.625C	4.12	231	9,792	2.90	2.75	Yes				0.50		
028A	4656	C7	75	0.625C	4.07	235	10,011	3.05	2.25	Yes	F			0.50		
								2.0								
022F	4657	C8	75	0.625C	4.02	363	23,592	5.40	5.50	Yes	F		3.0	3.00	65	
								4.50		No						
GD-1	4624		70	0.50U	2.16	344	11,384	5.6	5.25	Yes			3.5	3.50	101	
								5.5		Yes						
GD-2			75	0.50U	3.12	351	17,120		7.00	Yes				2.50		
								2.75		No						
GD-3			75	0.50U	4.02	340	20,697		8.50	Yes				6.50		
								8.0		Yes						
GD-4			75	0.50U	4.07	156	4,411			Yes						
								2.38	2.25	Yes			0.9	0.50		
								2.25		Yes						
GD-5	4660		75	0.50U	4.06	362	23,696	9.50	9.00	Yes		F	7.5	6.75		
1			AMB	0.625U	2.0	350	10,912									
								3.0								
2			AMB	0.625U	4.0	328	19,166					F				
3			AMB	0.625U	2.0	328	9,583					F				
4			AMB	0.625U	4.0	3.50	21,824									
5			AMB	0.500C								F				

*C- Coated
U- Uncoated

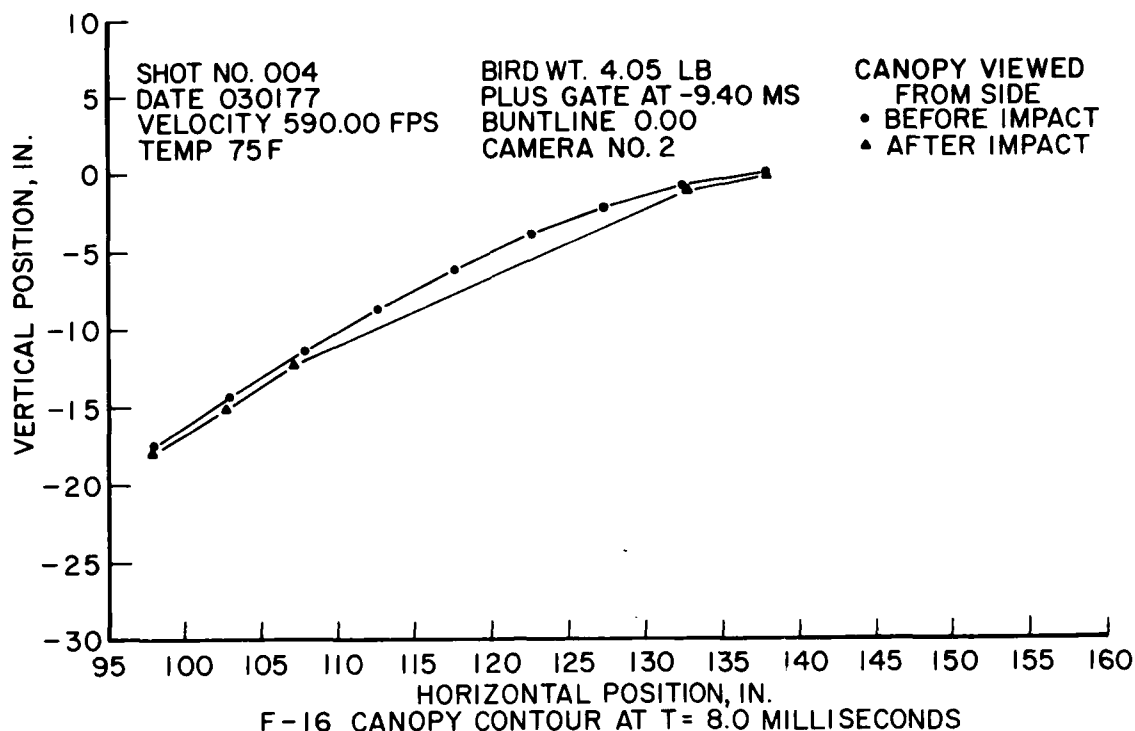


Figure 7. Typical Data Plot Redrawn from AEDC Calcomp Plot. This plot indicates that the maximum displacement was not read.

data available. The test number corresponds to the test number of the Special Assistance Team (SAT) memo entitled "Analysis of Bird Impact Tests of the F-16 Canopy."^[3] The second column is the film I.D. number and the third identifies the canopy used. It is important to realize that in some instances the same canopy was used for several shots. The subsequent columns provide the temperature of the canopy during the test, and the thickness of the canopy and whether or not the canopy was coated. Following these are the bird weight, the bird speed, and the kinetic energy in pound-feet. The next three columns indicate the deformation (δ) found by the present contract, AEDC, and General Dynamics. Not all films were available to all three contractors, nor did all agree on which were not capable of yielding usable results. Some films have multiple readings, indicating data taken from multiple cameras.

Column 12 indicates whether or not the peak value could be seen using the computer plotted data. Column 13 indicates whether or not a failure occurred during the shot. This could have been a perforation (I.D. 4604), a wave failure (I.D. 4607), or a crack (I.D. 4638).

During the development of Table 1 there was a desire to generate similar results from station 140.0 to better evaluate possible injury to the pilot. Consequently, the overlays were reexamined to determine the vertical displacement at station 140.0. Columns 14 and 15 present this information, and column 16 calculated average wave speed in knots for comparison with the bird speed for that particular shot. The data are plotted in Figures 8, 9, and 10.

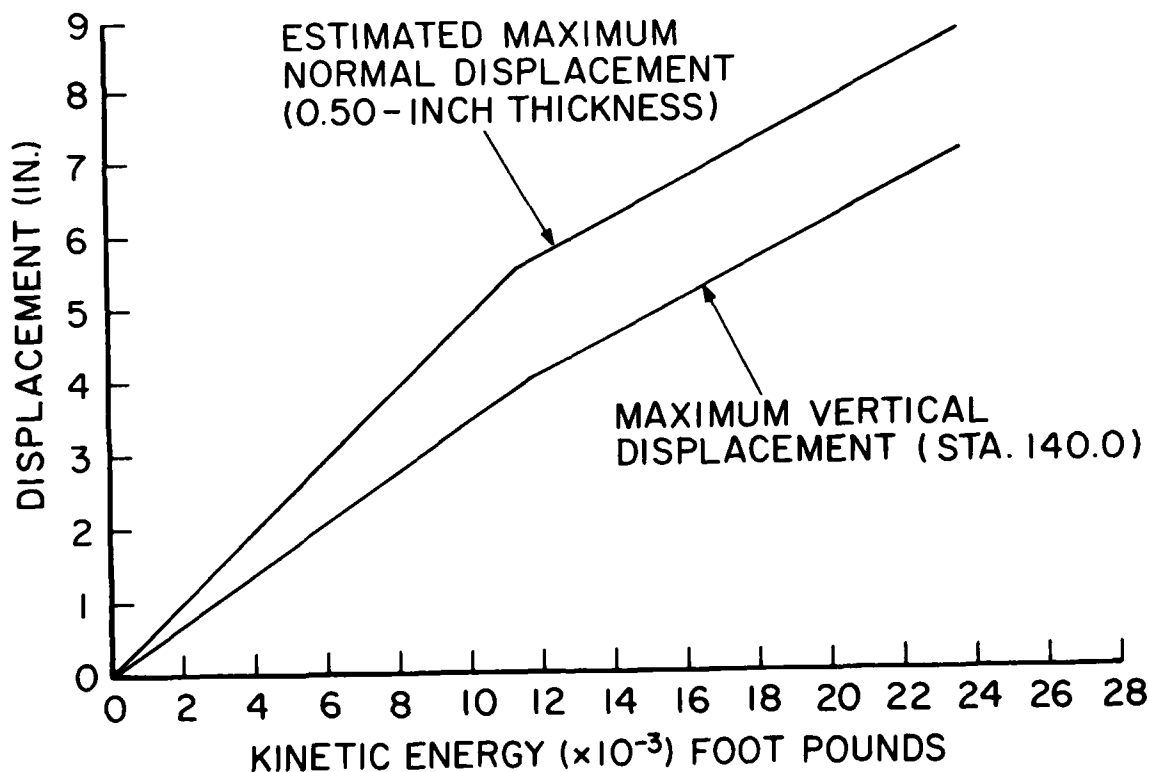


Figure 8. Estimated Curve of Maximum Vertical Displacement at Station 140.0, Plotted with Estimated Curve of Maximum Normal Displacement for 0.50-inch Thickness.

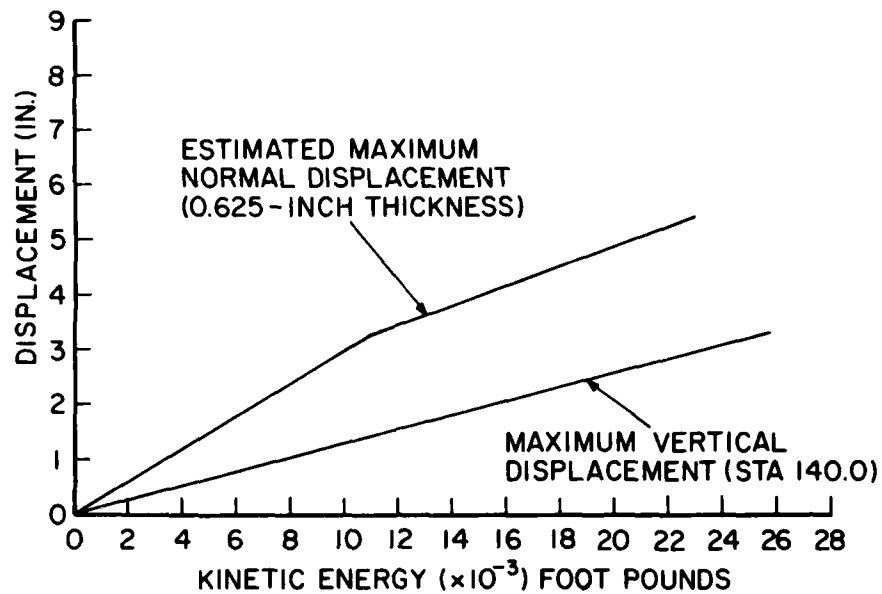


Figure 9. Estimated Curve of Maximum Vertical Displacement at Station 140.0, Plotted with Estimated Curve of Maximum Normal Displacement for 0.625-inch Thickness.

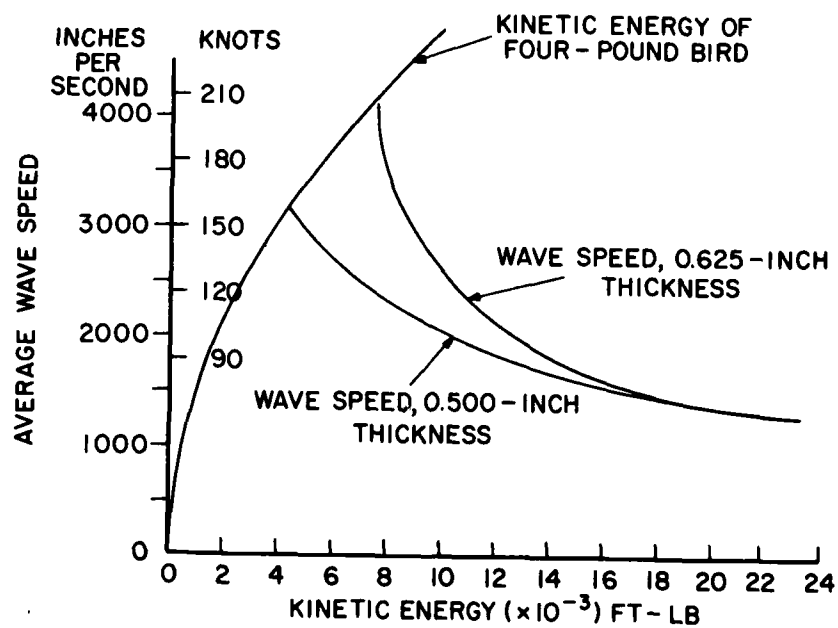


Figure 10. Wave Speed versus Kinetic Energy.

DATA INTERPRETATION

The deformation versus energy curves indicate that the canopy response can be represented by a bilinear curve. The displacement is a linear function up to a given value of energy and then becomes "stiffer," exhibiting proportionally less deformation with increased energy.

The wavespeed curves are interpreted as implying that the canopy responds in a manner similar to a low frequency elastic system. That is, at low bird velocities the bird impacts the canopy and takes a relatively long time to dissipate its energy into the canopy. However, at high impact velocities, the bird is consumed rapidly and the canopy reacts in the manner of a transient response. Hence, the speed of the input dictates the speed of the type of response.

All test data analyzed were for the F-16 configuration impacted at essentially one point. Therefore, it is not possible to relate deformation or wavespeed to bird impact velocity or energy for any other canopy configuration or impact point. From the curves available it does appear that the maximum deformation normal to canopy mold line is inversely proportional to the cube of the thickness and hence is related to the bending stiffness of the material. However, this is based only upon the two thicknesses available. Also, since canopy stiffness is a function of material thickness, curvature, and edge fixity, this relation may not apply to another configuration.

One aspect to be considered in the future is the location of the impact relative to the head location. The point of maximum normal deformation is well ahead of the head location. The wave is decaying in magnitude at the point of head impact. Specifically, for the test rigorously analyzed, the maximum deformation of 4.5 inches is reduced to 3.0 inches at the design eye point. This could be used to imply that by raising the impact point 3 inches vertically, the maximum deformation would occur at the head. However, this is not necessarily true since the higher impact point could provide a "stiffer" response which would negate the effect of a raised impact point.

In reviewing the data, it is apparent that only a limited amount are available. Given that we accept only one canopy configuration, there are insufficient data available to make quantitative predictions for all variations of material types, material thicknesses, and impact point. We do have some quantitative information available for the tests conducted, but cannot extrapolate because of the nonlinear multimodal nature of the response. Fortunately, other analytical efforts are being pursued^[4] to satisfy these requirements.

SECTION 3

CREW POSITION STUDY

INTRODUCTION

A specific requirement of the research was to study the variation of crew body position within the F-16 cockpit. This was required in order to relate the birdstrike phenomena to a specific configuration. The impact between canopy and helmet could be (and had been) examined as a relative position problem without even considering the true cockpit and seat requirements. However, a thorough examination of the effects of seat adjustment, aircrewman size, optics, and canopy mold line was certain to point out real world considerations for future studies.

DATA AVAILABLE

Several documents and drawings were used in analytically creating the F-16 environment. The F-16 cockpit dimensional data were available from the Aeronautical Systems Division (ASD) Crew Station Branch and were enlarged to obtain accurate one-half scale drawings. The enlargement was desirable so that one-half scale USAF drawing board manikins from the Aerospace Medical Research Laboratory (AMRL) Human Engineering Branch could be used directly. Two helmeted aircrewman manikins were available, a 5th percentile and a 95th percentile. The helmet shell dimensions were available from Air Force Systems Command (AFSC) RTD Drawing No. 65F-1578, Shell, Flying Helmet; and the helmet visor dimensions were from Sierra Drawing No. 561-628, Helmet Visor. Locations of the design eye positions were established by Elliot Bros. Drawing No. 229-005810 (optic). Seat adjustment information was available on the original layout drawing.

DATA COMPILATION

Figures 11 and 12 are layout drawings prepared for the 5th and 95th percentile aircrewmen using medium helmet shell size for

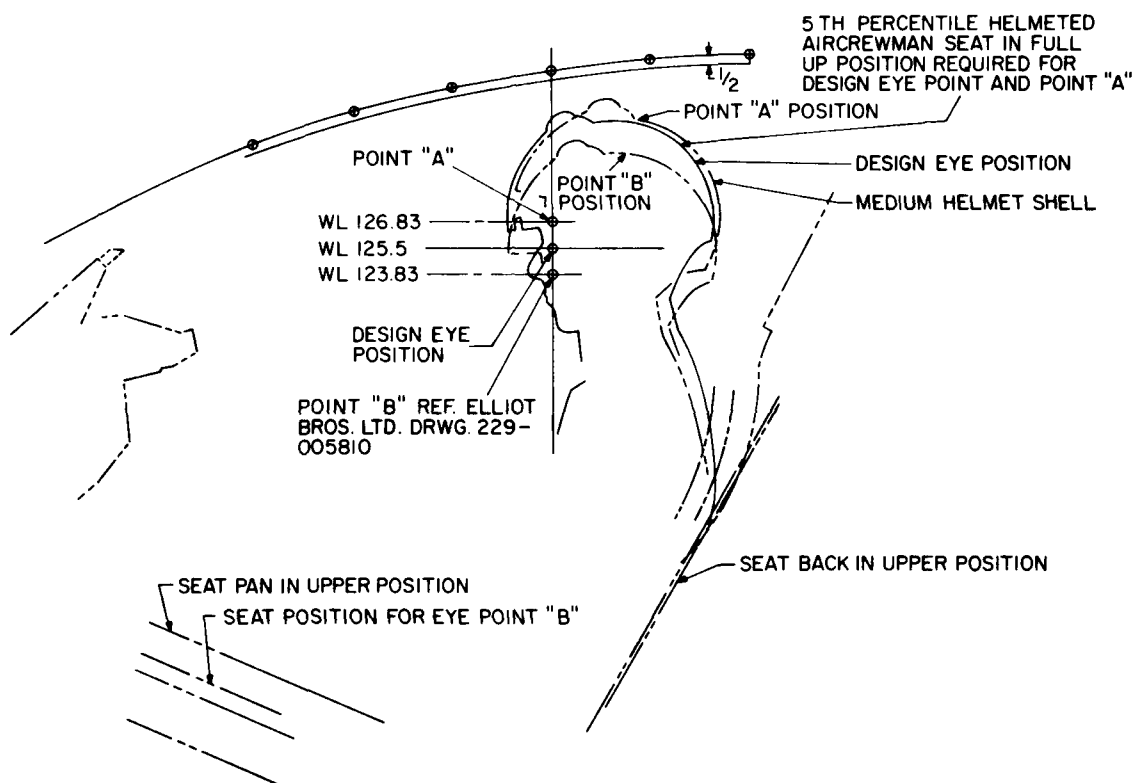


Figure 11. Canopy Clearance Layout for 5th Percentile Aircrewman in F-16. Eye Points "A" and "B" are the highest and lowest points, respectively, from which the head-up display optics can be observed by the pilot.

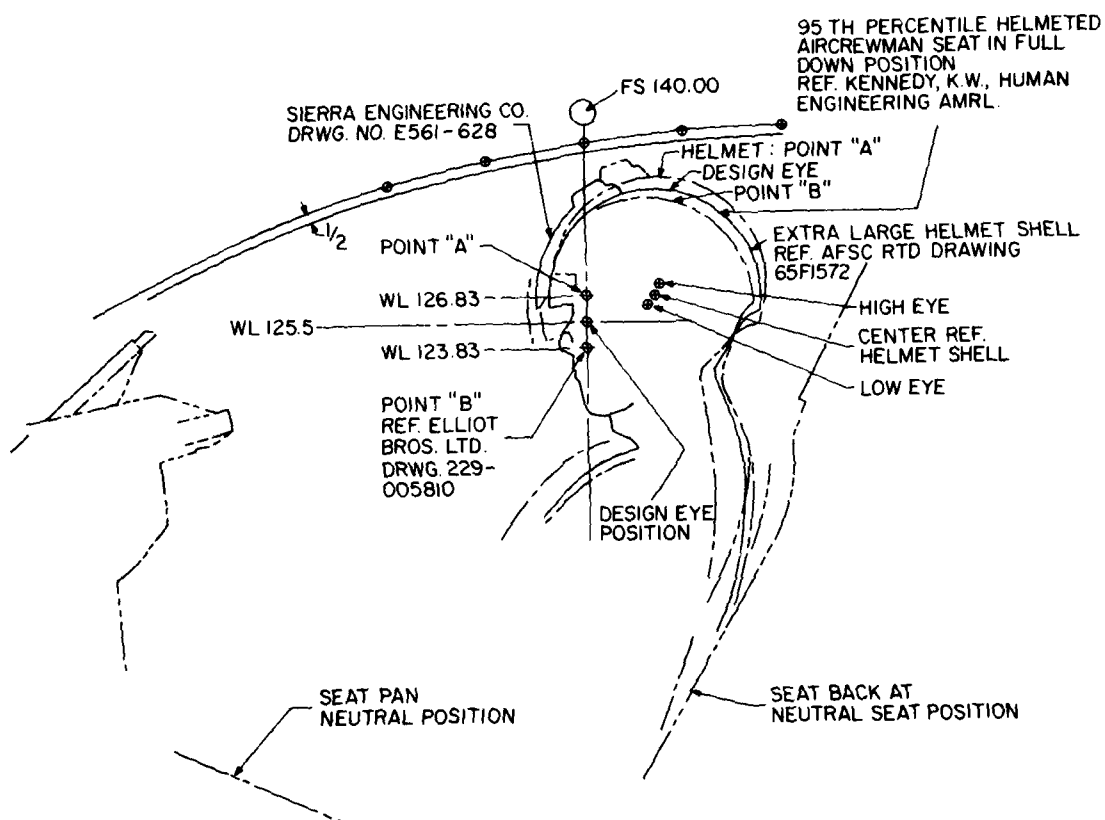


Figure 12. Canopy Clearance Layout for 95th Percentile Aircrewman in F-16. Eye Points "A" and "B" are the highest and lowest points, respectively, from which the head-up display optics can be observed by the pilot.

the 95th percentile man. Seat locations were established to satisfy the requirements for placing the eye at the "design eye" location.

During the development of first layouts it was apparent that certain positions would not be realistic flight positions. For the 5th percentile man, the upper eye position is nearly inaccessible. Using the plastic manikin, the aircrewman would have had to sit erect in the seat with no back support, have the seat adjusted to the highest position, and strain the neck with head tilted back in order to place his eye at the upper eye position. Equally improbable would be the likelihood of having the 95th percentile man at the upper seat adjustment since he would be "crushed" into the canopy. It was realized that not all combinations of eye positions, seat positions, and percentiles should be possible. The variations of each are provided so that each individual can place himself in an optimum position. The question to be answered is then, what are "optimum" positions?

In order to establish some additional means of locating the aircrewman other than "design" points, drawings were made in an attempt to establish envelopes of "probable" positions. This was done by placing a given-percentile manikin into the seat and then adjusting seat and manikin until the "eye" was along the axis of a particular design eye. The controlling parameter was then the optical axis through the design eye point and not the point itself. Both manikins were located at the three seat positions; upper, neutral, and lower, and the torso, head and neck were manipulated to place the eye along the selected axis. In placing the manikin, the torso was in a slumped position with maximum back support. The neck was then positioned by orienting the head vertically. In this manner it was hoped that a probable position, providing reasonable back support and head rotation, would result.

Envelopes of helmet position were developed by positioning the manikin as just discussed. A typical plot is shown in Figure 13. The figure indicates the canopy mold line and nominal thickness, as well as the locations of the optical axes. For this

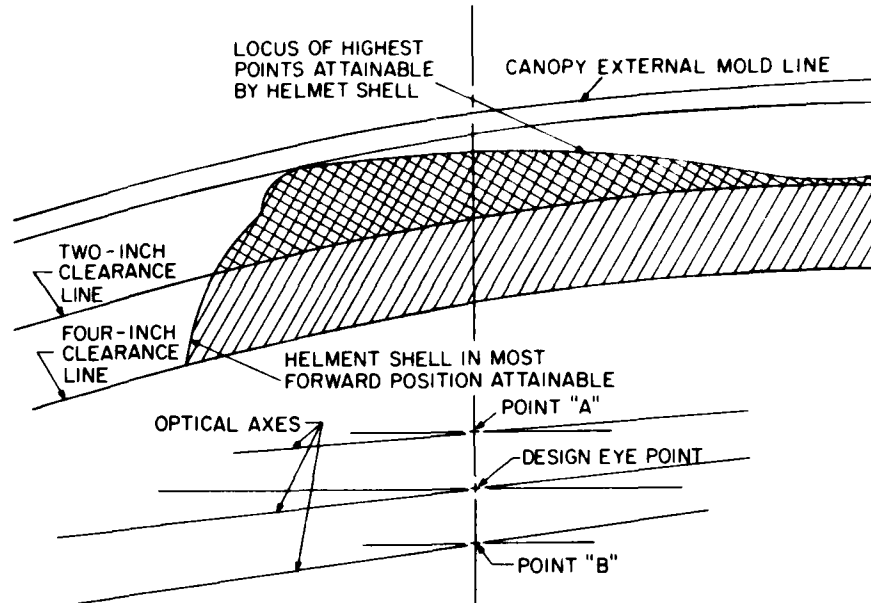


Figure 13. Envelope of Possible Helmet Positions for 5th Percentile Aircrewman Seated in Upper Seat Position With Eye along Upper Eye Axis (Axis through Point "A").

figure the shaded portion indicates the area between helmet shell external surface and a four-inch clearance line from the interior canopy surface. The helmet shell curve represents the locus of all possible shell positions with the manikin eye following the upper eye axis. Similar plots were made for all combinations of eye and seat position versus aircrewman percentile. It was discovered that some combinations of percentile, seat position, and eye position are unattainable. For example, a 5th percentile aircrewman with seat in the lowest position could not place his eye at the upper reference point; and a 95th percentile aircrewman with seat in the highest position could not place his eye at any eye reference point, nor could he place his eye at the lower eye reference point when the seat was in the mid (neutral) position. Thus it can be seen that eye position is the dominant parameter and is most indicative of where the helmet shell would be.

With eye position selected as the primary position indicator, the most probable position of the helmet was determined for both aircrewman percentiles. These are plotted in Figures 14 and 15. From these the mean values were established as eye analysis points as shown in Figure 16. The figure indicates that the manikin eye position is never at the design position although the eye is along the optical axis. Also, Figure 16 shows that for a given eye analysis position, the differences between the locations of the helmet shell due to changes in aircrewman percentile are small.

DATA RESULTS

At the beginning of the study there were many variables to be considered in establishing where an aircrewman might be sitting within the F-16 cockpit. It is easy to use a plastic model and

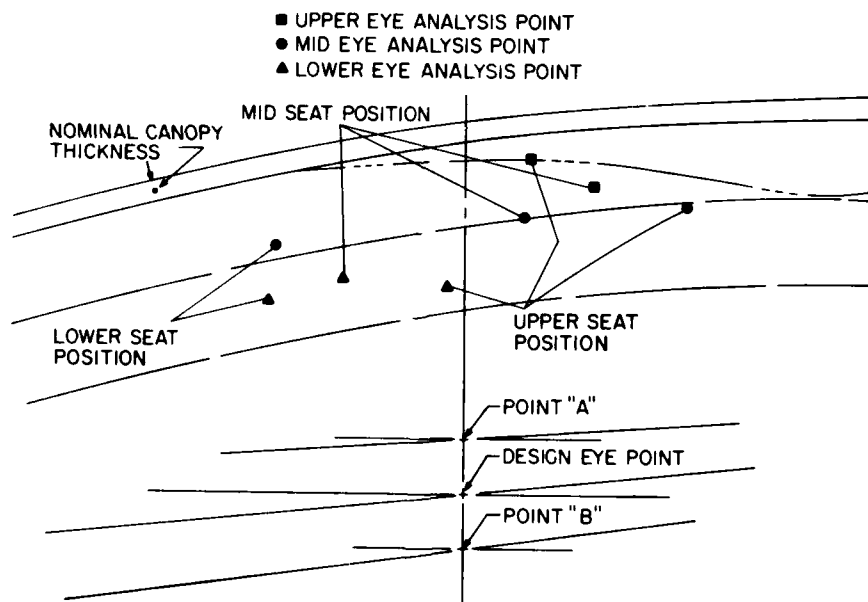


Figure 14. Locations of Probable Positions of Eye Analysis Point for Eye Located along Upper, Design, and Lower Eye Axes, with Seat at Upper, Middle and Lower Positions (5th Percentile Aircrewman). Note that when the seat is in the lower position, the upper eye position is not attainable.

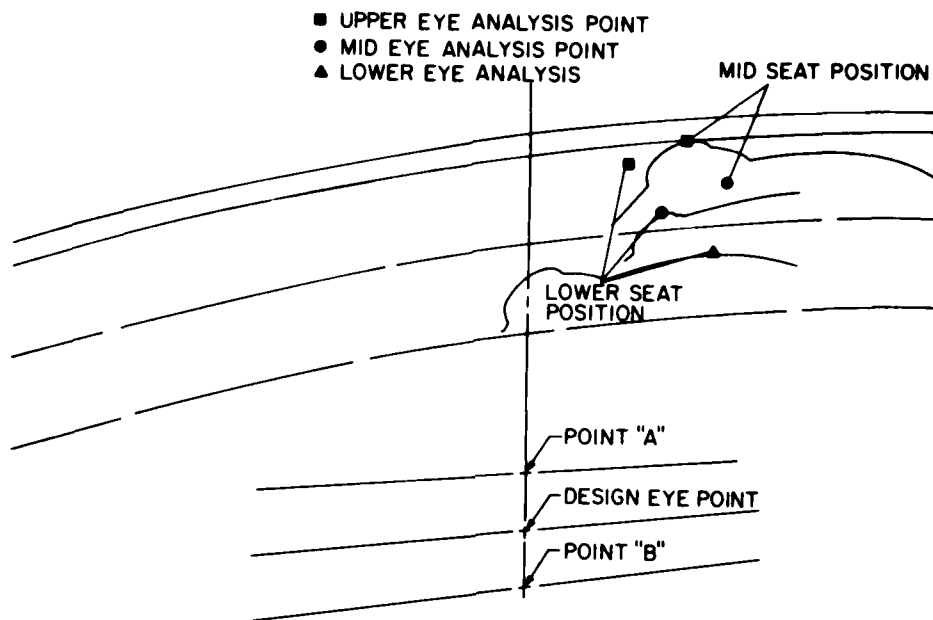


Figure 15. Locations of Probable Positions of Eye Analysis Point for Eye Located along Upper, Design, and Lower Eye Axes, with Seat at Middle and Lower Positions (95th Percentile Aircrewman). Note that when the seat is in the upper position, all eye positions are unattainable and when the seat is in the mid position, the lower eye position is unattainable.

scale layout drawing to position the helmet relative to the canopy interior surface. However, even with an articulated manikin there are some parameter variations which are inaccessible. This leads to an attempt to establish which parameters are dominant, and then how these can be used to infer probable helmet locations.

The approach used in this study established probable helmet position by first determining that eye position is most indicative of helmet position, and then used eye axes to locate the manikin in a "comfortable" position. The mean values of these locations were then used to establish eye analysis points for the F-16 configuration. From the figures shown, the clearances between canopy interior surface and helmet are:

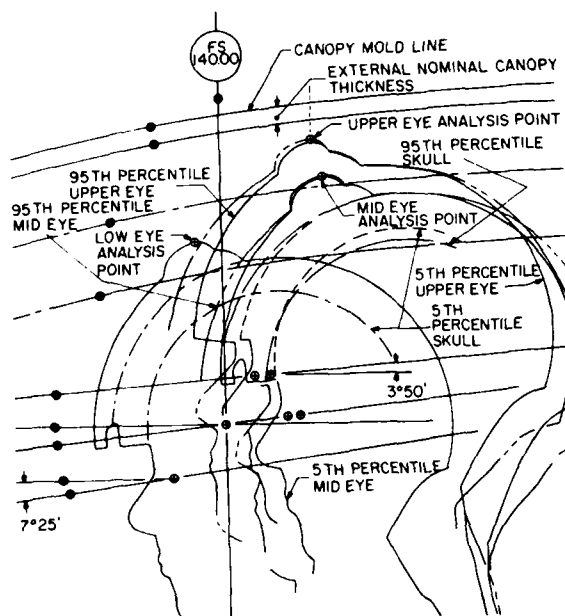


Figure 16. Portion of Layout Showing Eye Analysis Points and Skull Locations.

Upper eye position:	5/8 inch
Middle eye position:	1-3/4 inches
Lower eye position:	3 inches

These are all based upon the presence of a helmet visor as shown on the manikin. Many Air Force helmets currently used are of the "ram's horn" type having the visor adjustment on the side. For those types, the clearances would be increased by one-half inch.

From the previous section, canopy deformations of three inches were observed. This implies a 2-3/8 inch bump below the original interior surface for a 5/8-inch thick transparency. For that depth a man at the upper eye position would experience an interference between canopy and shell of 1-3/4 inches. At the middle eye point the interference would only be 5/8-inch. Assuming a "ram's horn" configuration, the shell would interfere 1-1/4 inches and 1/8 inch for the two eye positions. Since 1-1/4 inches is the thickness of a foamed-in-place liner according to the forming specifications, the "bump" would crush the shell and liner onto the skull and reach the maximum force capability of the liner if the head moves a small amount. Consequently, the study indicates that when any aircrewman in the F-16 cockpit is positioned at the upper eye analysis position with a birdstrike similar to the higher energy level tests conducted the impact is potentially dangerous. Additionally, since the optical path is at a smaller angle to the horizontal than that of the canopy mold line at station 140.0, moving the aircrewman forward to the design eye would create a more intolerable situation.

SECTION 4

SELECTION AND USE OF ANALYTICAL CREWMAN SIMULATOR

INTRODUCTION

The birdstrike phenomena, considering all aspects of bird and occupant response, had never been modeled. Other works had examined the bird's response to an impact, the canopy response to an impact, helmet response to a drop test, head and neck response to a blow, and torso response within a seat; but the total system response was never modeled. Therefore, it was necessary to find or construct a routine which would be capable of combining all of the aspects required.

The selected routine would have to permit a specified three-dimensional "bump" to impact a helmeted head. The relative velocity between helmet and bump would have to be variable as well as the mass, inertial characteristics, and compliance. The helmet model would have to reflect the size and inertial characteristics of the true helmet as well as the correct interface forces and moments between shell and head.

The model of the human would have to permit variable body segment geometry and point locations, with joint and surface stiffness and appropriate inertial characteristics. The man-model would then interface with seat characteristics such as seat and back cushions at arbitrary orientations in space, and restraint hardware. The model required is best described as a vehicle-occupant model which permits complex interaction between the occupant and his environment regardless of whether the environment is active or passive.

SIMULATIONS AVAILABLE

Ten distinct vehicle-occupant models were reported in a paper of King and Shou^[5] in early 1975. After that five other papers were available related to occupant-vehicle dynamics, but these were not the development of new models as much as the updating of

existing models. Several models were available, but the number was reduced by requiring three-dimensional response. The routines that were thought to be acceptable were:

1. CAL3D by Calspan^[6]
2. UCIN by the University of Cincinnati^[7]
3. TTI by Texas Transportation Institute^[8]
4. HSRI3D by the University of Michigan Highway Safety Research Institute^[9]
5. SAEJ3D by the Society of Automotive Engineering of Japan^[10]
6. FAA3D by Ultrasystems^[11]

Each will be discussed in terms of the data that was available at the initiation of this program.

The FAA3D model is not really an "occupant" oriented program. It was designed to be used by seat and restraint users with minimum consideration of the occupant. Eleven mass segments are available and are connected at ten joints. Joint resistances are specified by nonlinear torsional springs and viscous dampers, with the damping coefficient a constant value. External forces act at segment centers of gravity after the force deformation curves due to contact have been calculated. Contact planes are available to represent cabin surfaces which the occupant may travel into. The input to the model is a crush condition defined by the initial velocity, attitude, and acceleration as a function of time. Selected injury criteria are available as part of the output. In the discussion of the FAA3D model by Laananen^[11], it was stated that preliminary comparisons of predictions with test data were satisfactory, but that further validation study was required.

The SAEJ3D model was strictly a three-segment model similar to HSRI's original three-dimensional crash victim simulation of Robbins^[12]. These would not be acceptable because of their restricted capability.

The UCIN model consists of 12 rigid bodies to represent the human, and a cockpit and inertial reference. Cockpit impact planes are located relative to the vehicle frame and "hits" between occupant and aircraft are recorded. However, the model's developers concluded that options for a variable number of body elements were required, provisions for translation between members were needed, and further verification was required.

The routines remaining were the CAL3D and the HSRI3D. Both have an extensive history of development and both are sufficiently complex to enable modeling of the items listed at the beginning of this Section. Both have many areas of flexibility for describing the occupant and the vehicle. Contact surfaces and ellipsoids were available along with the capability to locate them as functions of time. Stiffness characteristics and damping characteristics were available not only for joints between elements but at contact surfaces. Both routines were sufficiently capable but the CAL3D had several more favorable features.

First, the CAL3D had been modified by AMRL several years previously and updated to include several requirements unique to the U.S. Air Force. In doing so, the routines were validated on the computer at Wright-Patterson Air Force Base and had been continually updated on the CDC 6000 system. Hence, the routine desired was being continually exercised, and several individuals were available with "hands-on" experience. Consequently, rather than beginning with a routine which may or may not have been "operational" and attempting to generate "hands-on" experience, the CAL3D as modified and identified in AMRL-TR-75-14^[13] was utilized for birdstrike modeling. The revised model is currently referred to as the Articulated Total Body Model (ATBM).

GENERATION OF THE BIRDSTRIKE MODEL

Several elements were quantitatively defined for the computer. These were the bird or canopy configuration, the helmet, the human, and the seat. Each was defined in terms of its compliance, motion, and location.

BIRD/CANOPY CONFIGURATION

The input to the ATBM has to provide an element of a particular size and inertial characteristics with a known compliance. The radius of curvature, speed, direction, and stiffness are all necessary if the canopy is to interact properly with the helmet in the model. From photographic data, curvature and speed were available, but compliance had to be evaluated. This was made possible by using UDRI-TR-77-17^[14] "Bird Impact Forces and Pressures on Rigid and Compliant Targets." With the procedures outlined, it was possible to relate the initial conditions of the bird to the force-time profile of the impact. Knowing this, it was then possible to estimate the nature of the system which created the output seen on the films.

From UDRI-TR-77-17 there are several equations for analysis. First, the average force generated is:

$$F = \frac{mV^2 \sin\phi}{\ell}$$

where m is the mass of the bird

V is the initial velocity of the bird

ℓ is the effective length of the bird, and

ϕ is the angle between the impact surface and the horizontal.

This is, of course, a relation between impulse and momentum normal to the surface.

For test 4607 the average force is:

$$F = \frac{2.1}{386} \times \frac{(7310)^2 \sin 30^\circ}{8.67}$$
$$= 16,800 \text{ pounds.}$$

This is the average force required to dissipate all of the momentum normal to the surface and assumes that the impact surface is rigid. Also, Test 4607 was chosen because of the impulsive response observed. According to the referenced work, the true force-time profile could therefore be:

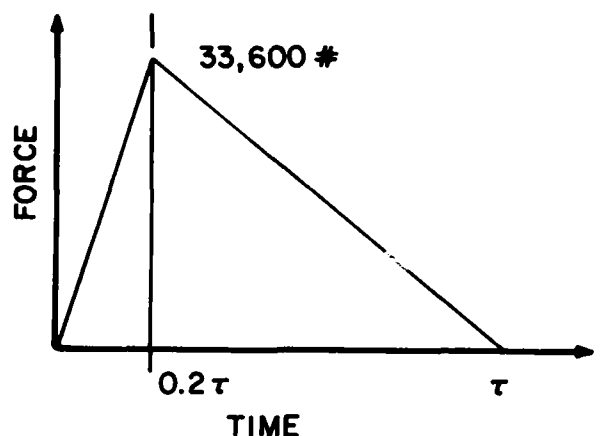


Figure 17. Force-Time Profile from UDRI-TR-77-17.

The peak force is double the average and occurs at two-tenths of the total pulse duration. This waveform is the first approximation in finding the nature of the force-time profile applied to the canopy. A better approximation is available from the equation:

$$F = \rho A (V \sin \phi - V_p)^2 \sin \phi$$

where ρ is the density of the bird

A is the area

V is the velocity

ϕ is the angle between the impact surface and the horizontal,
and

V_p is the velocity of the impacted surface.

In this equation area A is a function of s/l , a nondimensional consumed length, and s/l is a function of relative displacement between bird and impact surface. In order to use this relation it was apparent that some model of impact surface kinematics would be required.

It was assumed that at the impact point the kinematics of the canopy would be dictated by a triangular acceleration pulse of the same waveform as the force-time profile just discussed. Therefore, the kinematics could be as shown in Figure 18. The figure indicates

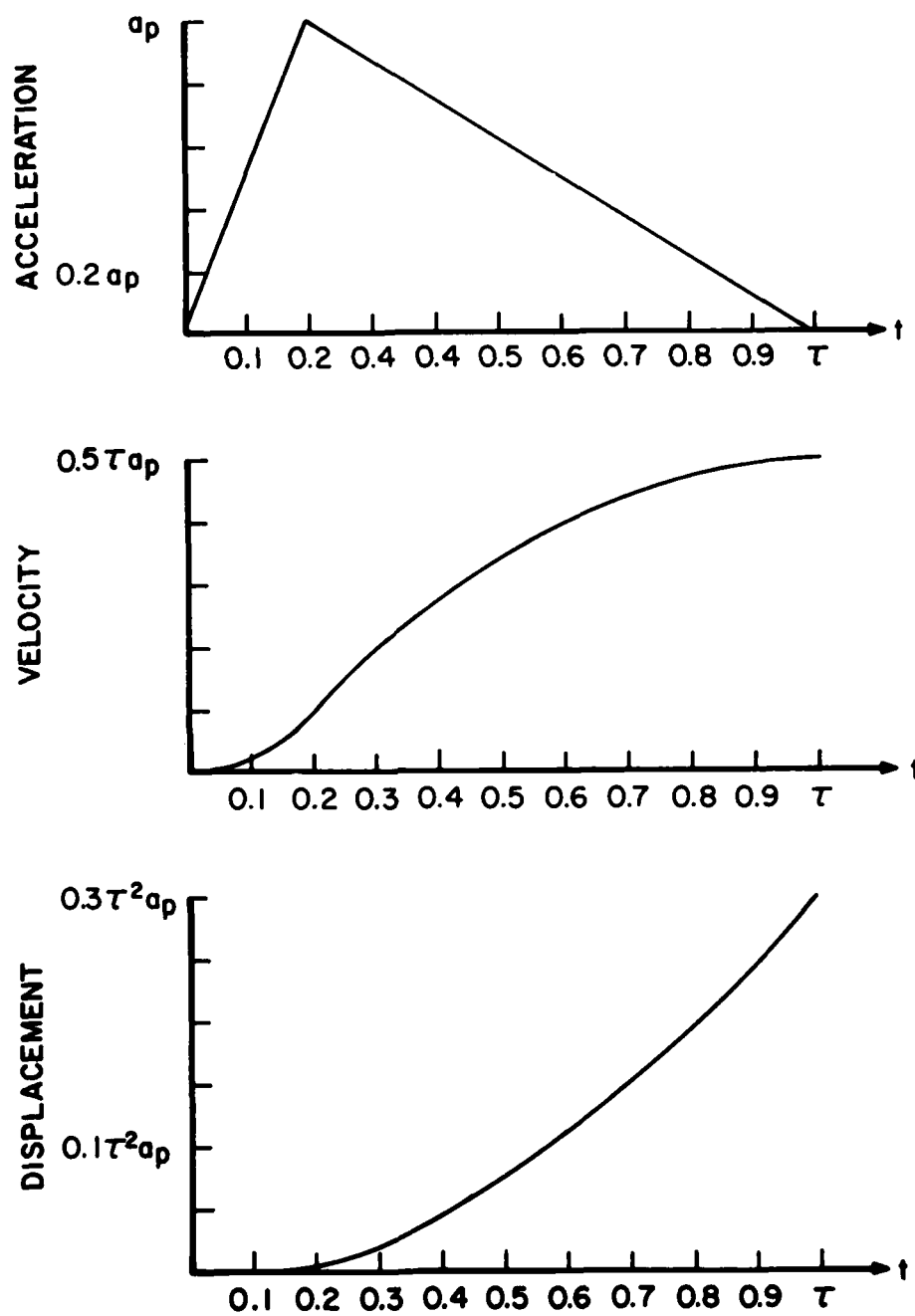


Figure 18. Generalized Triangular Kinematics.

that the canopy is accelerated and creates a velocity input which must be dissipated. From Figure 19, it appears that the canopy does respond in a transient manner as though impacted upon impulsively. If the half-sine pulse is assumed to be the transient response, then the period of the response is 0.038 seconds and the maximum displacement is 6.75 inches. This implies an impulsive velocity of 1110 inches per second normal to the surface. This must then be the final velocity of the bird impact kinematics. Having a value for the final velocity, all other parameters were established as functions of time.

Using the equations

$$F = \rho A (V \sin \phi - v_p)^2 / \sin \phi, \text{ and}$$

$$\frac{s}{l} = \frac{vt}{l} - \int_0^t \frac{v_p}{l \sin \phi} dt$$

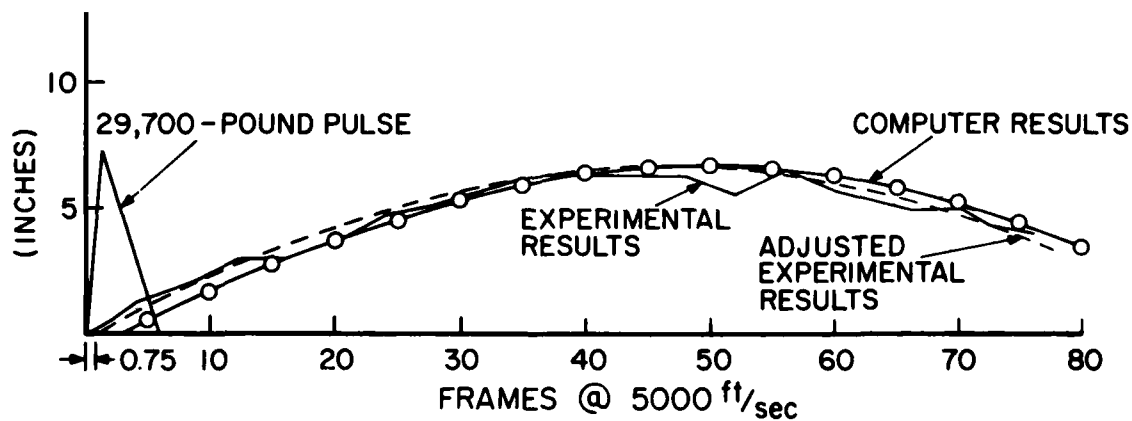


Figure 19. Model Fit of Experimental Data.

with appropriate plots from UDRI-TR-77-17, it is possible to calculate the theoretical force-time pulse for a bird impacting a "locally rigid" windshield by accounting for the motion of the windshield. The resulting plot is shown in Figure 20.

The complete picture is then one of a bird impacting a surface and creating a triangular acceleration pulse at the impact point. A velocity of 1110 inches per second is stored in the canopy in 1.185 milliseconds while a force of 29,700 pounds is being developed. The local deformation during the pulse reaches 0.79 inches normal to the surface. Following the pulse, the canopy responds by deforming a maximum of 6.75 inches at 26.3 Hz in order to reach the 1110 inches per second impulsively applied. The difference between the approximate 33,600 pounds shown in Figure 20 and the more exact 29,700 pounds makes it questionable whether or not accounting for the local deformation is necessary.

The next step was to relate the now-known input to the observed output in order to approximate the canopy stiffness. It was assumed that the canopy could be modeled as shown in Figure 21.

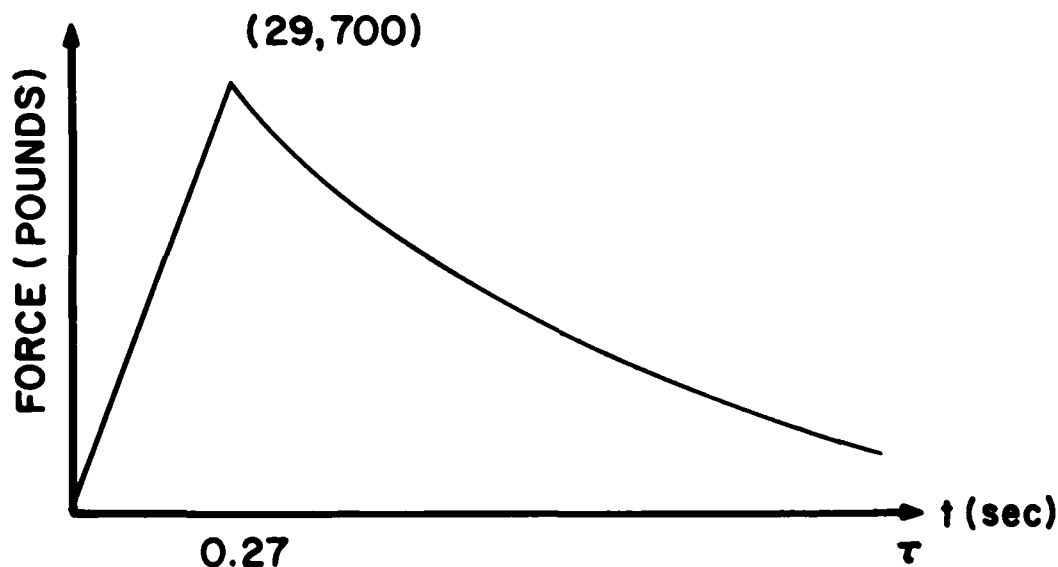


Figure 20. Force-Time Profile of Local Deforming Canopy.

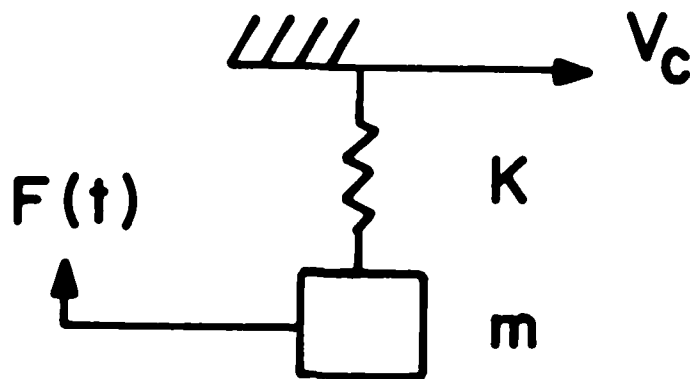


Figure 21. Canopy Stiffness Model.

The force-time profile known acts upon an unknown mass supported by an unknown stiffness. The system travels along the canopy mold line at the speed of the wave and displaces according to the mass and stiffness present. The equations used were taken from the Shock and Vibration Handbook^[15] and were simply the equations for transient response of an undamped single-degree-of-freedom system responding to a triangular force-time pulse. The results are shown in Figure 19.

For a pulse peak of 29,700 pounds at two-tenths of 1.185 milliseconds, a stiffness of 426.2 pounds per inch and a mass of 0.01562 (about 6 pounds) generates the curve shown. Hence, for the 0.500-inch-thick canopy, the bird impact creates a response similar to that of a 6-pound weight supported by a 426 pound-per-inch spring. A similar procedure was followed in analyzing Test 4657, a 4-pound bird impacting at 363 knots. The peak force was found and applied to the model to duplicate deformation and time to peak. The 5/8-inch-thick canopy required a stiffness input of 1326.5 pounds/inch and a mass input equivalent to 9.64 pounds, to duplicate the observed wave motion of the canopy.

The final step necessary to generate a bird/canopy element was to establish a physical size and orientation of the bump. Waveforms of several tests were plotted on half-scale layout drawings of previously described eye-analysis points. A typical plot is shown in Figure 22. The waveforms available were subdivided by linear extrapolation and the intersections between

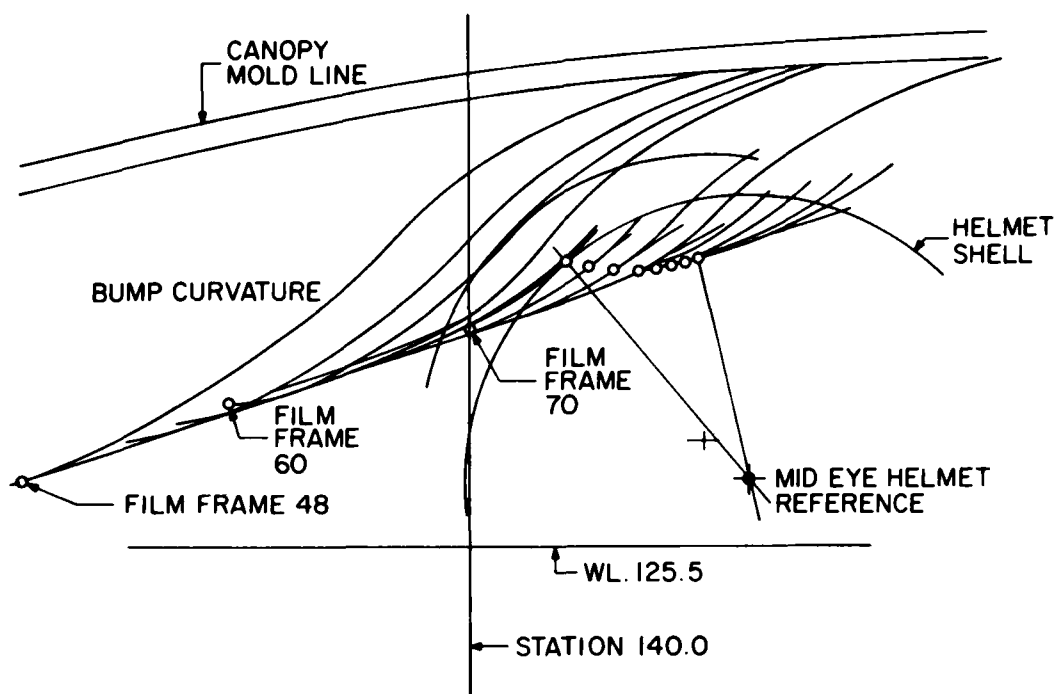


Figure 22. Bird/Helmet Impact Points for Mid-Eye Analysis Point.

helmet and wave were located. Although the wave changed with time, the envelope of the motion is bounded by a line of about 19° from the horizontal. Eleven different large-deformation waveforms were examined to determine the motion of the bump. From these it was found that the impact angle varied from 11.4° to 23.4° above the horizontal with the mean being about 19° .

Additionally, the curves of canopy curvature were reviewed based upon the times of intersection between bump and helmet. For the same tests, the mean radius of curvature was about 10 inches with less variation than seen in the attitude angle above.

In summary, the bird/canopy element for the ATBM can be represented by a 10-inch-radius sphere, traveling at the wave-speed appropriate for the initial conditions, hitting the helmet with a velocity of V traveling along an axis of 19° from the horizontal, and having a mass and stiffness dependent upon the

canopy thickness. For a 0.500-inch thickness, the canopy "weighs" 6 pounds and has a surface stiffness of 426 pounds per inch. For the 0.625-inch thick canopy, the canopy "weighs" 9.64 pounds and has a surface stiffness of 1326.5 pounds per inch. All of the developed results are, of course, applicable only to the F-16 configuration.

HELMET CONFIGURATION

The helmet idealization consists of a shell and a liner. Both can be represented by ellipsoids located at specified points necessary to create the necessary thickness of liner at the brow and the crown. The original concept was to have the crushability of the helmet upon the skull duplicated by a crushing stiffness and forces generated by elastic elements.

The Calspan CAL3D model creates forces between bodies by having forcing functions specified in terms of the interference between the two bodies. If two spheres intersect, the force generated is either a functional relationship of the intersection depth, or it is found from a table look-up carried within the routine. However, the relationship is fixed and is independent of orientation. If the two spheres intersect at any incidence angle, the force depends only upon the maximum depth of penetration. This is not representative of the helmet shell crushing on the skull because the liner is a varying thickness from brow to crown, and this creates a variable crush strength that depends upon the attitude of the impact.

The initial approach was to "suspend" the shell upon the skull by seven elastic elements. This is as shown in Figure 23. With this type of arrangement the force generated as the shell moves on the skull is dictated by elongation of each elastic element as well as by the interference generated by the shell ellipsoid passing through the liner ellipsoid. The elastic elements possible in Calspan can generate only tensile forces, and hence the need for "springs" on all sides of the skull. As the

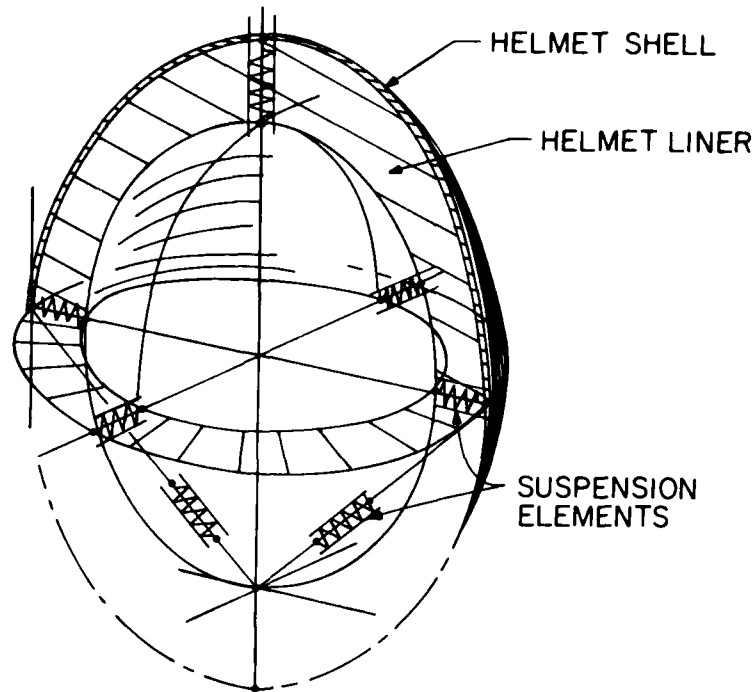


Figure 23. Schematic of "Suspension" System Used in CAL3D Model to Support Helmet and Liner on Skull.

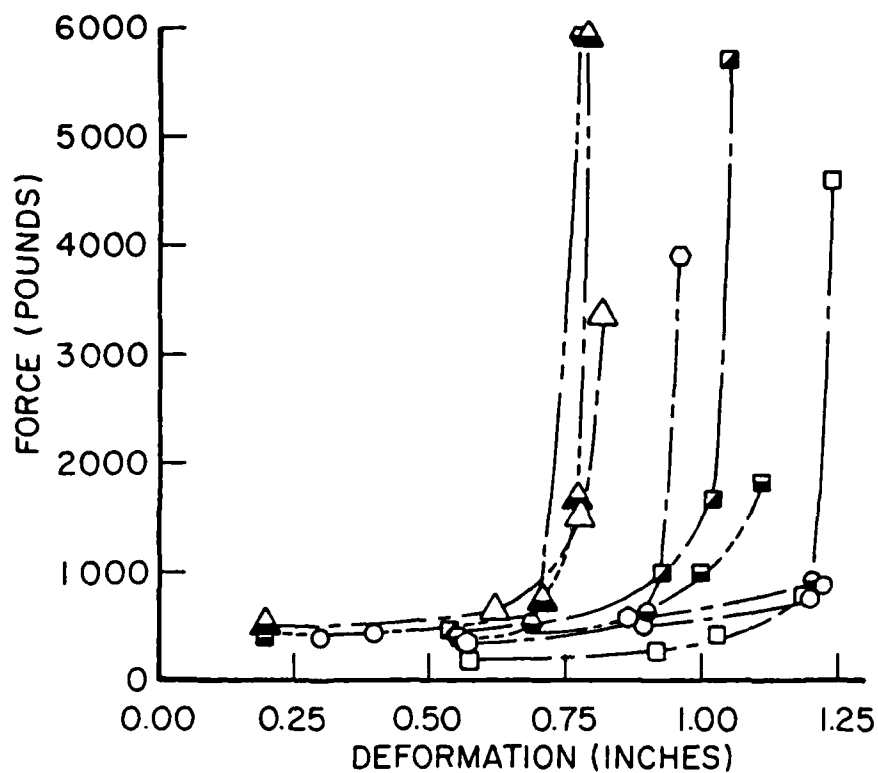
shell is crushed onto the skull, the interference generates a "crush stiffness" and the elastic elements create the difference between observed crush stiffness laterally, vertically, and fore and aft.

The characteristics for the force-function between shell and liner, and the elastic element stiffness, were programmed along with appropriate locations of the attachment and the free length of the elastic elements. Several runs were made and none were successful. Based upon the results generated, it appears that the elastic element feature available is based upon forces acting outward from the element. The assumption is made that if an elastic element attaches to another, the force must act outwardly on each body. In the idealization attempted, it is necessary to have forces acting inward on the shell ellipsoid and outward on the skull ellipsoid. Some effort was made to "fool" the routine,

but it was not possible to solve the problem. Consequently, the helmet representation reverted back to the originally intended idealization technique of Calspan in that the intersection of the bird/canopy and the helmet shell would be dictated by the intersection depth of the two.

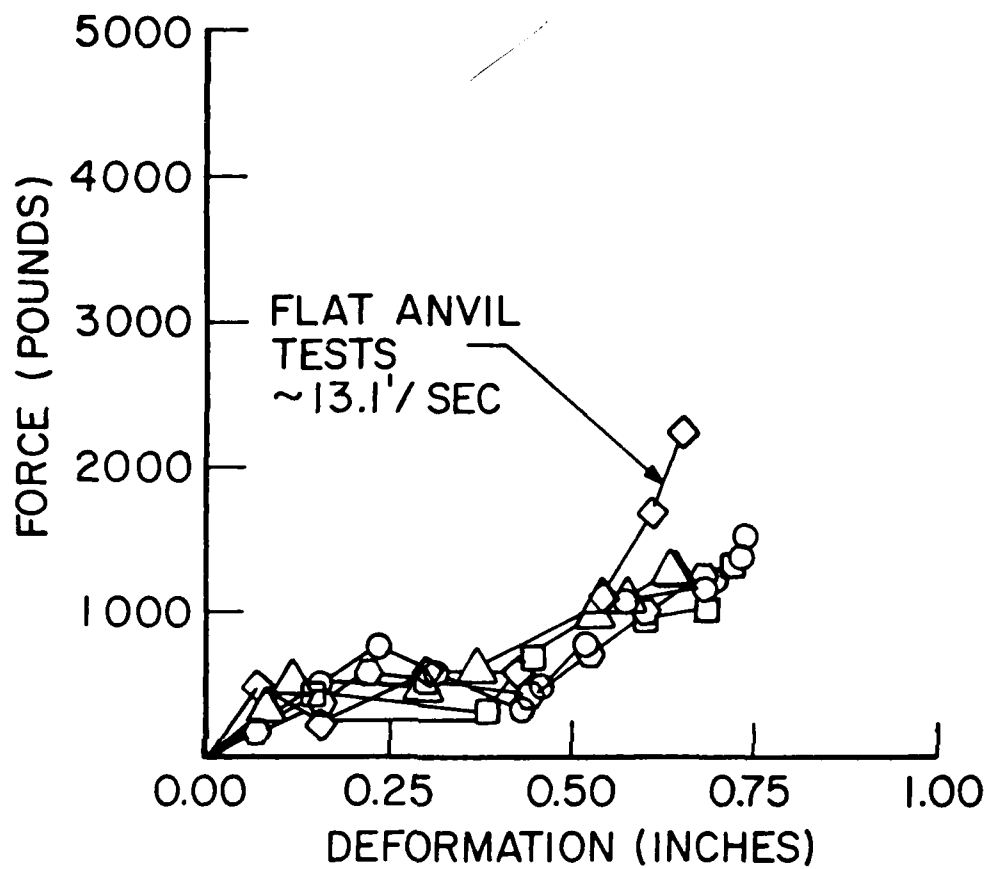
Test data were available from drop tests conducted at AMRL. Oscillograph recordings containing the accelerations of the head forms and forces of impact, for a standard Z90 test were reduced. The acceleration, indicative of head form motion, was doubly integrated to provide displacement versus time plots for the drops. These were cross-plotted with the force-time curves to generate force displacement curves for the impacted shell and liner combination. Two sets of data were available. Figure 24 indicates the stiffness generated for tests conducted with styrofoam, insolite, and foam inserts within the shell impacted upon a hemispherical anvil. Figure 25 indicates the results obtained for a similar liner, using a different impact velocity and a flat anvil. The results of the hemispherical anvil impacts are more informative in that they do show the differences that exist due to location of the impact point. Those tests with greater liner thickness have more prolonged plateaus, whereas the thinner liner more quickly generates extremely high forces. The curves are indicative of a crushable foam having a relatively constant force plateau followed by a rapid rise in resistance as the foam "bottoms." The curve approximated for preliminary use was that of Drop Number 16, as impact into a liner having a measured liner thickness of 1.19 inches at the impact point. Therefore, in duplicating the interaction between canopy and helmet, the stiffness was created by summing the displacements for given forces.

The helmet shell and liner were represented in the ATBM by ellipsoids. The shell is an outer ellipsoid having the curvature required to match the dimensions of AFSC, RTD Drawing No. 65F 1578. The true helmet is not a pure ellipsoid, but viewed laterally the shell does have a constant radius over the majority of upper



SYMBOL	TEST NO.	LOCATION OF IMPACT	THICKNESS OF LINER (INCHES)
○	8	CROWN	1.59
●	13	CROWN	1.30
△	9	LEFT FRONT	1.19
▲	14	LEFT FRONT	1.03
□	10	RIGHT FRONT	0.78
■	11	RIGHT REAR	1.63
▣	16	RIGHT REAR	1.13
○	12	LEFT REAR	NOT AVAILABLE
●	17	LEFT REAR	1.06

Figure 24. Force-Deformation Curves from Drop Test Data on HGU-22/P Styrofoam, Insolite, and Foam Helmets at Impact Velocities of 16.23 and 16.9 ft/sec Against Hemispherical Anvil.



□	23	REAR	NOT AVAILABLE
⬡	24	LEFT SIDE	
△	25	RIGHT SIDE	
◇	26	FRONT	
○	27	CROWN	NOT AVAILABLE

Figure 25. Force-Deformation Curves from Drop Tests on HGU-22/P Helmet with Fitting Pads, at Impact Velocity of 13.08 ft/sec Against Flat Anvil.

surface. In a frontal view the shell does have curvature to reflect the need for earphones, but still has a constant curvature over the crown. The liner is another ellipsoid concentric with the outer shell. In locating the elements it was necessary to find a location for the intersection of the axes that satisfies the liner thickness requirements over the skull.

The weight of the helmet was available but inertial properties were not. Therefore, the helmet was idealized as a hemispherical shell of known weight and radius, and the inertial properties were calculated for the idealized shell. With the inertial characteristics available, all necessary parameters to idealize the helmet were established.

ANTHROPOMETRIC DATA AND SEAT CONFIGURATION

The ATBM program that was made available through AMRL came with anthropometric information that was considered most representative of the aircrewman. The data were for a 95th percentile aircrewman having head, neck; upper, middle, and lower torso; and extremities. Coefficients of joint stiffness and damping joint stops and inertial properties for all segments used are included in Appendix A. The body was established in a seated position for the F-16 cockpit. Torso segments are at a 30-degree back angle, the neck is vertical, and the head and helmet are tilted back at 6 degrees. The upper legs are at 119.0 degrees from the vertical for a seat pan angle of 29 degrees from horizontal.

Seat back and seat cushion elasticity were also available with the ATBM. A previous study had required the model to reflect realistic values of seat cushion and seat back stiffnesses. These are also listed in Appendix A.

This concludes the development of segment characteristics required for the model. The following discusses the use of the model in calculating birdstrike responses.

CALCULATION OF SELECTED IMPACTS

Several initial runs were made for purposes of checking the output data. These were made to simulate the birdstrike of an F-16 with the 95th percentile aircrewman seated at the upper eye analysis point for an impact similar to Test 4607. The interference that would theoretically exist if the canopy deformation passed through the envelope of the helmet was calculated and the bird located to create this interference with the correct attitude and velocity. In subsequent discussions, theoretical interference is the maximum depth of the intersection between the canopy envelope and helmet envelope which occurs as though there were no interaction between the two bodies. This is shown as Δ in Figure 58. At the same time, calibration data were available from AEDC. For loads applied normal to the canopy at the point of impact, the measured stiffness was 2200 pounds per inch for the 0.500-inch thick material. This is significantly "stiffer" than 429 pounds per inch found in the modeling of canopy response. However, the measured stiffness at a point does not necessarily define the compliance of the entire canopy. Consequently, two of the initial runs used both a "stiff" and a "soft" canopy to calculate the response. The results were:

	$\ddot{\theta}$	$\dot{\theta}$	\ddot{X}	\ddot{Z}	Neck Force X	Neck Force Z
Soft	16.7	4704	45.7	4.85	175 pounds	234 pounds
Stiff	40.8	17,442	166	52.1	437 pounds	516 pounds

The angular values are in radians per second and radians per second squared. The translational accelerations are in G's. Neck forces are shear and axial at the base of the skull.

The results clearly indicate that there is a significant difference in the response. The interference for both was a theoretical value of 1.75 inches. For the "soft" canopy two thirds of the interference is taken by the canopy and one third by the helmet. For the "stiff" canopy, just the reverse is true. The compliance of the canopy has a significant effect.

It was originally assumed that computer runs would be made to study F-16 configurations. However, with the first runs it became apparent that it would be more worthwhile to conduct runs for various levels of interference. In this manner anyone wanting to evaluate a particular F-16 configuration could first establish the location of the helmet and then determine the interference. This could then be related to computed outputs. This also has the advantage of providing data relative to interference regardless of the absolute location of the head. Consequently, regardless of where the helmet exists, if the interference is a given number, the output would be available. Unfortunately, because of the compliant canopy, interference can be difficult to establish.

Several computer runs were made for the F-16 seating configuration using the force displacement curve generated by a static calibration curve and the helmet shell test data previously used. For this curve, Figure 26, the canopy stiffness is 6250 pounds per inch for a 0.625-inch-thick canopy, and the resulting curve is significantly closer to the helmet-alone characteristics than the previous 0.500-inch-thick canopy data. Using this curve, a 9.6-pound bird, and a wave speed of 1400 inches per second, the relation between a theoretical interference and the calculated is shown in Figure 27. The theoretical displacement δ is the

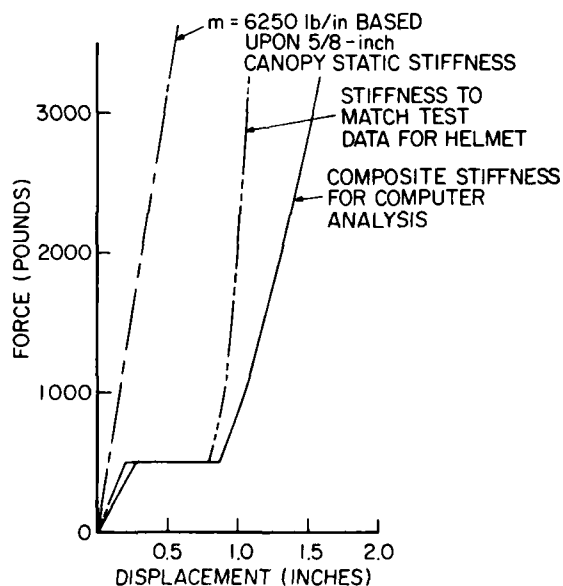


Figure 26. Force-Displacement Curves for Canopy Helmet Interference.

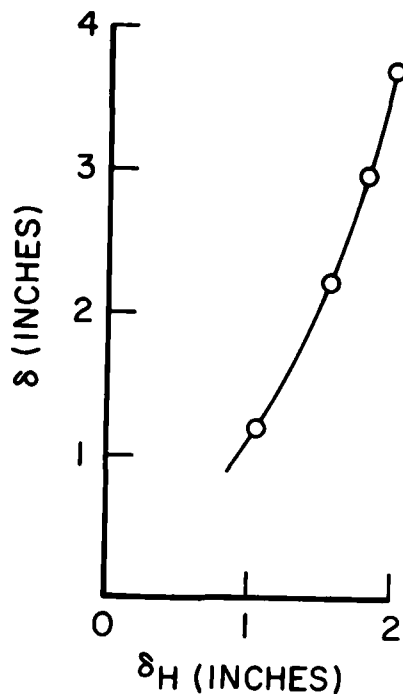


Figure 27. Theoretical Displacement δ versus Computed Displacement δ_H .

maximum interference that would exist if the bird ellipsoid were to pass through the helmet ellipsoid without any mutual response. The computed displacement δ_H is the interference between bump and helmet that is generated during the interaction of forces at the helmet, bird, head, neck, etc. and reflects the inertial response of all components of the system. That is, the computed displacement is the result of the system response to the birdstrike phenomena.

From the curve it is apparent that at displacements greater than unity, the two values quickly diverge. At a theoretical interference of 3.7 inches, only 2.0 inches of deformation exist at the bird/shell interface. At large deformations, the forces become so large the head is rotated away from the bird, and the bird is ejected from the shell. At the lower displacements, the forces are smaller and they do not cause significant motion.

Several injury criteria parameters are tabulated, and fore and aft translational accelerations are plotted for selected runs on Figure 28. The high peak value is really invalid in that a 2.0-inch computed displacement is more indicative of a crushed skull than the extrapolated helmet/liner force shown.

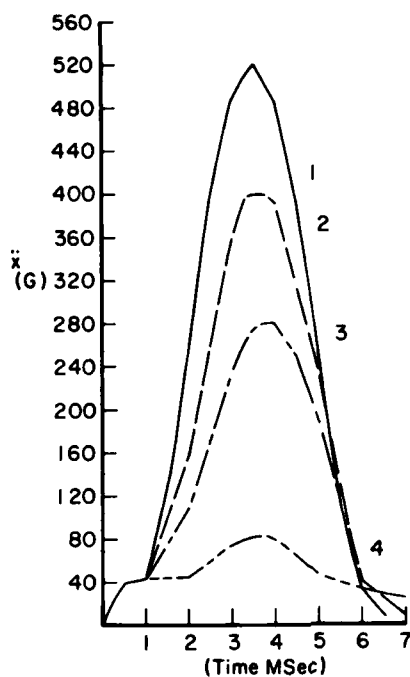
In order to appreciate the magnitude of the variables, they have been individually plotted with full-scale computed displacement as the abscissa. Half-scale reproductions of the plots are presented in Figures 29, 30, and 31. In the following sections there will be more discussions as to how specific injury criteria will be established. However, at the time the computer results were produced, several injury criteria limits had been established as indicative of concussion. These are shown in Table 2.

TABLE 2. LIMITS OF INJURY RESULTING IN CONCUSSION.

	Limit	δ_H (inches)
Head Fore and Aft Translational Acceleration (\ddot{X})	38 G	0.90
Head Translational Velocity (\dot{X})	7.5 ft/sec	0.90
Head Angular Acceleration ($\ddot{\theta}$)	1800 rad/sec ²	< 0.875
Head Angular Velocity ($\dot{\theta}$)	30 rad/sec ²	1.25
Skull Force (pounds)	900 pounds	1.02
Neck Axial Force (pounds)	440 pounds	1.07
Neck Shear Force (pounds)	200 pounds	0.97
Neck Moment	420 inch-pounds	< 0.875

The selected parameters will be explained in detail later and indeed expanded upon, and are presented here as values which are indicative and should be at least recognized as such by those familiar with biomechanical data currently available.

Although the angular acceleration generated is "intolerable", examination of the tolerance curve which is the source of this number indicates that the head angular rotation of 25,300 rad/sec² and 52.9 rad/sec is nearly on the tolerance curve and therefore the angular motion criterion that is applicable is only the angular velocity which is exceeded at about 1.54 inches of interference between bump and helmet (δ_H).



	Curve Number			
	1	2	3	4
Theoretical Interference δ In Inches	3.70	2.95	2.20	1.20
Generated Interference δ In Inches	2.00	1.80	1.55	1.05
Head Acceleration in G's	521	404	280.8	82.9
Head Velocity Peak in ft/sec	48.8	40.8	29.6	11.8
Head Angular Acceleration in Rad/Sec ²	49,700	36,900	25,300	8,880
Head Angular Velocity in Rad/Sec	119.0	76.4	52.9	19.8
Skull Force in Pounds	5,624	4,560	3,192	1,000
Neck Force Axial in Pounds	1,219	771	803	435
Neck Force Shear in Pounds	796	872	654	226
Neck Moment in Inch Pounds	9,347	4,701	3,279	1,208

Figure 28. Fore-and-Aft Head Acceleration versus Time with Other Tabulated Output Variables.

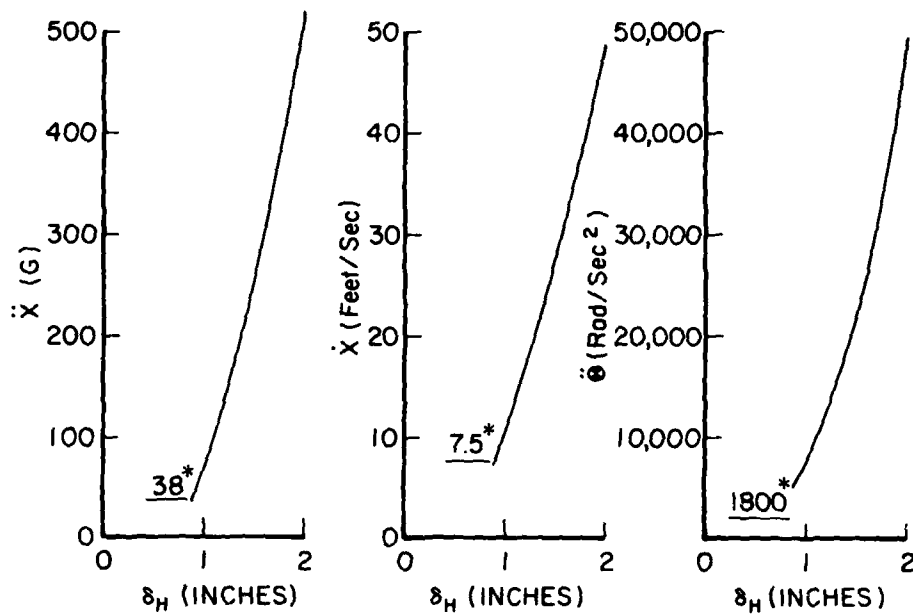


Figure 29. Injury Parameters versus Displacement for Head Fore-and-Aft Translational Acceleration \ddot{x} , Head Translational Velocity \dot{x} , and Head Angular Acceleration, $\ddot{\theta}$. *Criteria correspond with criteria shown in Table 2.

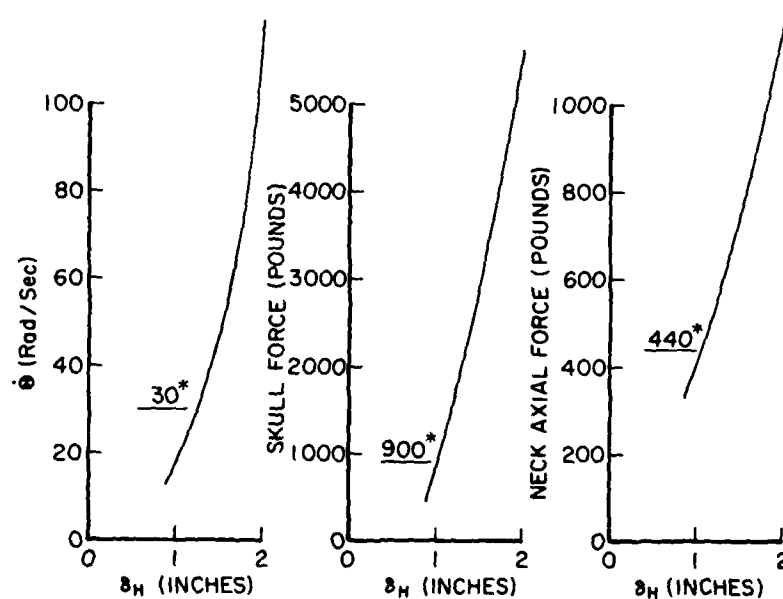


Figure 30. Injury Parameters versus Displacement for Head Angular Velocity $\dot{\theta}$, Skull Force, and Neck Axial Force. *Criteria correspond with criteria shown in Table 2.

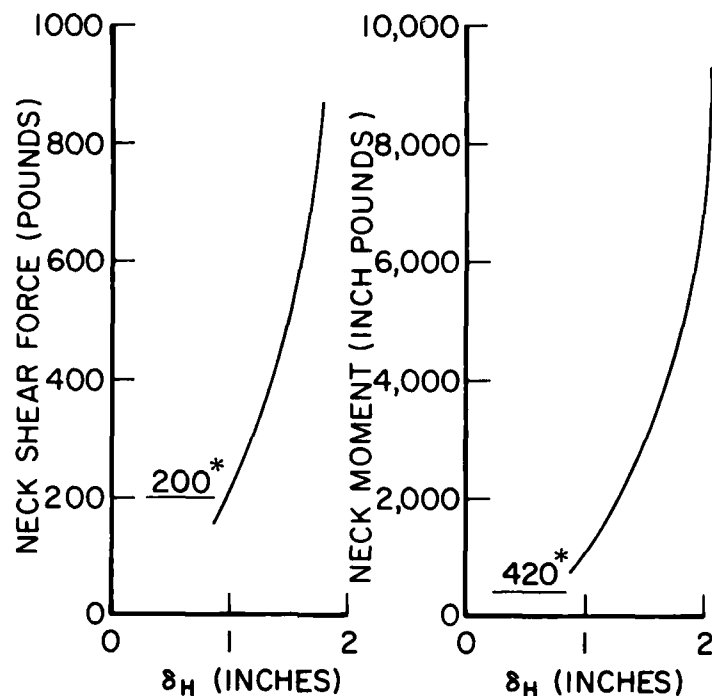


Figure 31. Injury Parameters versus Displacement for Neck Shear Force and Neck Moment. *Criteria correspond with criteria shown in Table 2.

Another method of presenting the data is to present number of injury criteria exceeded, versus displacement as shown in Figure 32.

The lowest tolerance limit exceeded is that of neck moment which is a predicted value and therefore suspect. However, even if the limit were doubled, the result would be the same. The head translational velocity and acceleration are better supported by measured and theoretical data.

The curves presented clearly indicate that there may be arguments about the "exact" level of injury, but a doubling of the value selected does not significantly alter the results. All parameters are generated more because of the crushing force of the helmet at larger displacements than anything else. At

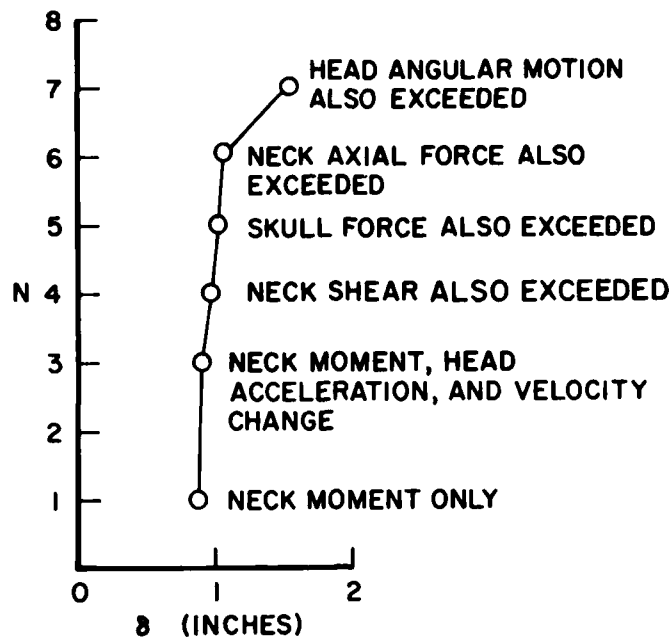


Figure 32. Number of Injury Criteria Exceeded versus Displacement.

large displacements the foam helmet liner "bottoms out" and extremely high forces result. Once the computer displacement exceeds 0.875 inches the response is dictated by a liner that has compressed about as far as it can go, and the stiffness is more a function of the canopy than the helmet.

Assuming that the plot shown in Figure 32 is reasonably correct, the difference between one injury criterion being exceeded, and six exceeded is 0.20 inches. For the molded-in-place foam liner, the thickness at the crown is "approximately 1-1/4 inches" according to MIL-P-83379 which suggests a 1/4-inch tolerance. The severity of the impact beyond the "plateau" level of the foam makes it questionable whether or not rigorous determination of the injury limit is necessary.

Since it was apparent that at higher levels of head impact force the response was more dictated by the canopy, additional runs were made using a "soft" canopy. As mentioned previously,

a canopy stiffness of 1326 pounds/inch was found to duplicate the observed wave motion of the canopy. This stiffness was used and resulting changes in displacement are shown in Figure 33. The "soft" curve indicates that for theoretical interference of 2.2 inches, 1.84 inches of crush is calculated. For the 1.2-inch interference, 1.11 inch of crush is calculated. When compared with the values of crush for the "hard" canopy, for the same interferences, it is apparent that there is really a small difference. At the smallest crush the difference is less than 1/16th of an inch. However, the true difference is seen in the amount of crush in canopy and helmet.

By referring back to the stiffness curves discussed it can be seen that for the stiff canopy and 1.1 inches of crush for Figure 26, 0.92 inches is helmet crush and 0.19 inches is canopy deformation. For the "soft" canopy, 0.70 inches is helmet crush and 0.40 inches is canopy deformation. Since the helmet and liner are only capable of about 0.8 inches of crush before "bottoming," the "soft" canopy does permit the helmet to stay at the lower force level.

Figures 34, 35, and 36 indicate the changes in injury parameters versus displacement due to the softer canopy. In all data presented, the effect is the same. The tolerable crush has been increased by a small amount. Picking the criteria requiring the greatest crush dictates a crush of about 1.5 inches. From the plot of interference versus crush, this implies a theoretical interference of 1.7 inches. Therefore, even for the soft canopy, in the range of tolerability, the theoretical interference and calculated crush are not too different. The question is then one of establishing whether or not the canopy is "soft" or "hard".

Fortunately, one test with an instrumented dummy was available. This test will be discussed later in developing a test apparatus. However, the results of the photographic reduction are necessary for the conclusion of this section. A test labeled FW-017 provided high-speed film data for a 4-pound bird at a kinetic energy level of 21,000 foot pounds. For a 5/8-inch-thick canopy

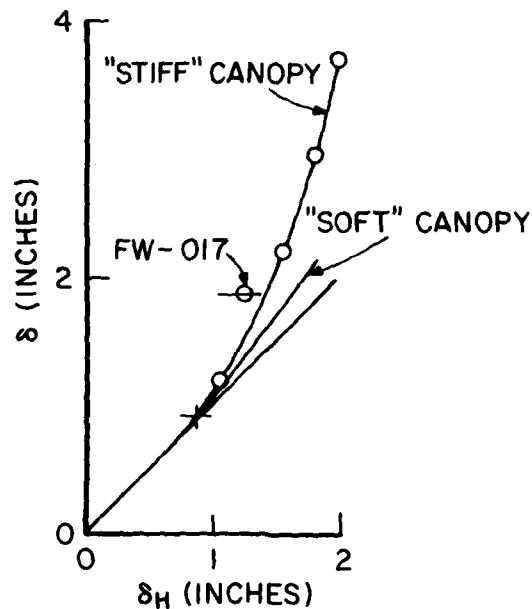


Figure 33. Theoretical Displacement δ versus Computed Displacement δ_H with Comparison of "Stiff" and "Soft" Canopy.

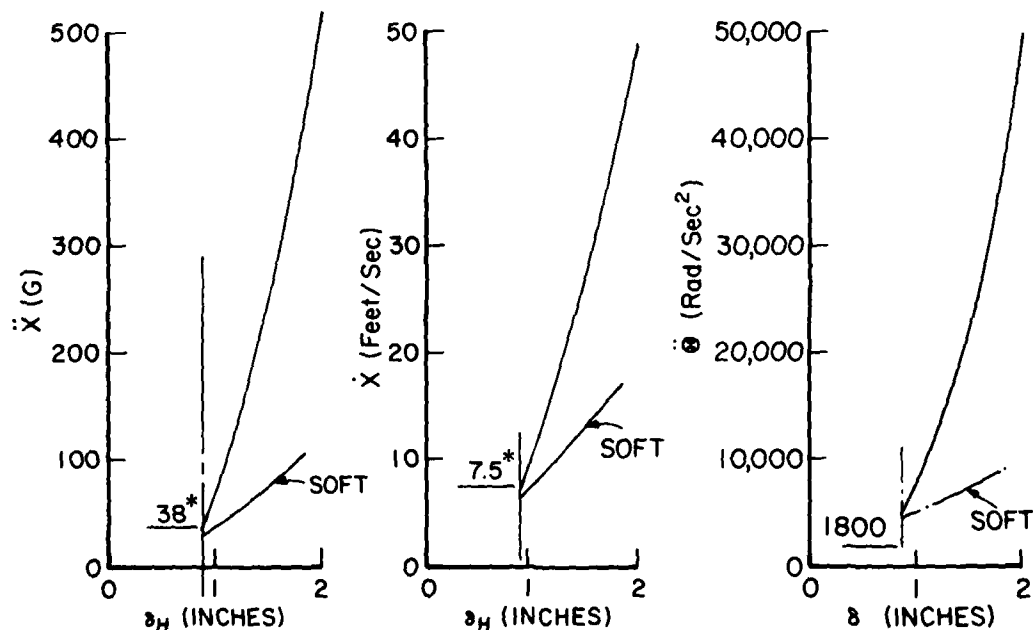


Figure 34. Comparison of Injury Parameters versus Displacement for Stiff and Soft Canopies for Head Fore-and-Aft Translational Acceleration \dot{x} , and Head Angular Acceleration $\ddot{\theta}$. *Criteria correspond with criteria shown in Table 2.

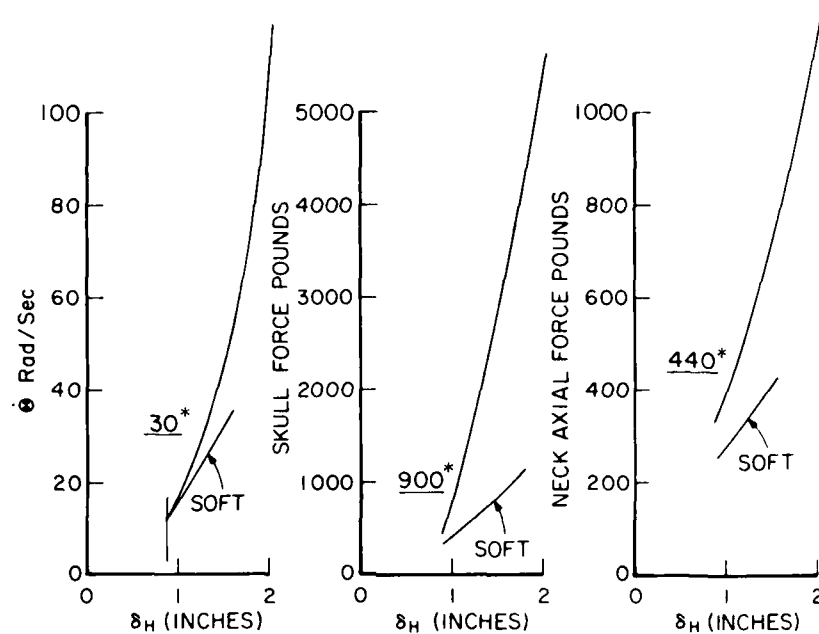


Figure 35. Comparison of Injury Parameters versus Displacement for Stiff and Soft Canopies for Head Angular Velocity θ , Skull Force and Neck Axial Force. *Criteria correspond with criteria shown in Table 2.

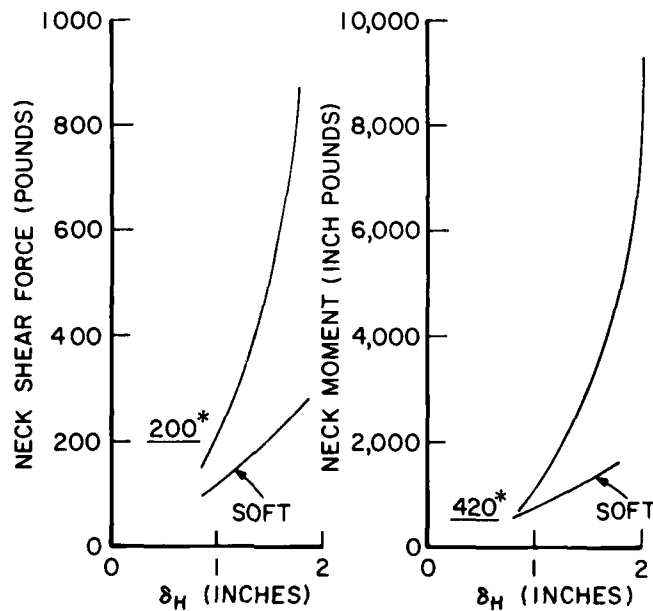


Figure 36. Comparison of Injury Parameters versus Displacement for Stiff and Soft Canopies for Neck Shear Force and Neck Moment. *Criteria correspond with criteria shown in Table 2.

the predicted maximum normal deformation would be about 5 inches, the observed deformation just ahead of a helmeted head was 4.38 inches. The interference that would have been generated if this had passed through the helmet envelope would have been 1.88 inches. The observed "crush" (assuming that the motion was all helmet and there was not head motion beneath it) was 1.25 inches. The maximum force acting on the skull was computed to be 1455 pounds. Plotting these values (FW-017) on Figure 33 indicates that the calculated responses infer a "stiff" system response.

Emphasis is placed upon system response since it is important to remember that the force-displacement curve that is used in calculating head/neck response is a composite of canopy, shell, and liner stiffness. The curve is not uniquely defined and hence it is possible to have a stiffer helmet coupled with a softer canopy which would generate a similar response.

Assuming that the stiff canopy is representative of the F-16 configuration, the limit of crush would then be about 7/8-inch in order to not exceed the "plateau" of the helmet liner. At that displacement the theoretical and computed interference are nearly equal. Therefore, 7/8-inch is the permissible interference which can be placed on the helmet in calculating permissible clearance for the helmeted head. Based upon this, and using the "analysis" eye points, for the 5/8-inch-thick canopy, the tolerable clearances are:

- 1-7/8 inch for the upper eye position,
- 2-7/8 inch for the design eye position, and
- 4-1/8 inch for the lower eye position.

These ignore the visor knob since there were no data available on the stiffness of the knob, and it does not exist for the "ram's horn" visor configuration. However, the visor was accounted for dimensionally and assumed to be a "rigid" body between bird and helmet shell.

COMPUTER ANALYSIS OF VISOR EFFECT

From the beginning of the research, the question of the effect of the visor had been discussed. Testing to evaluate

the impact protective capabilities of a helmet is never conducted with a visor, yet it is physically present and it was obvious that it should not be ignored.

A helmet shell and visor were tested using test headforms that were contoured to the inside of the shell. The unlined shell was tested in several configurations of visor shade positions, and several deformation pattern curves were generated as shown in Figure 38. At the upper loading points near the beaded edge, the curve is nearly linear up to about 70 percent of the ultimate deformation possible. With the visor stiffness available, a composite force displacement curve for the stiff canopy and visor/helmet combination was generated. The ATBM model was adjusted to reflect the new helmet radius, and the "bird" repositioned to provide the same interference values used before. That is, the bird passes through the same clearance depth and must crush through additional visor material.

The effect of the visor on translational fore and aft acceleration is shown in Figure 39. The impact is one due to an interference of 1.20 inches. The presence of the visor softens the system response and reduces the peak acceleration. This is

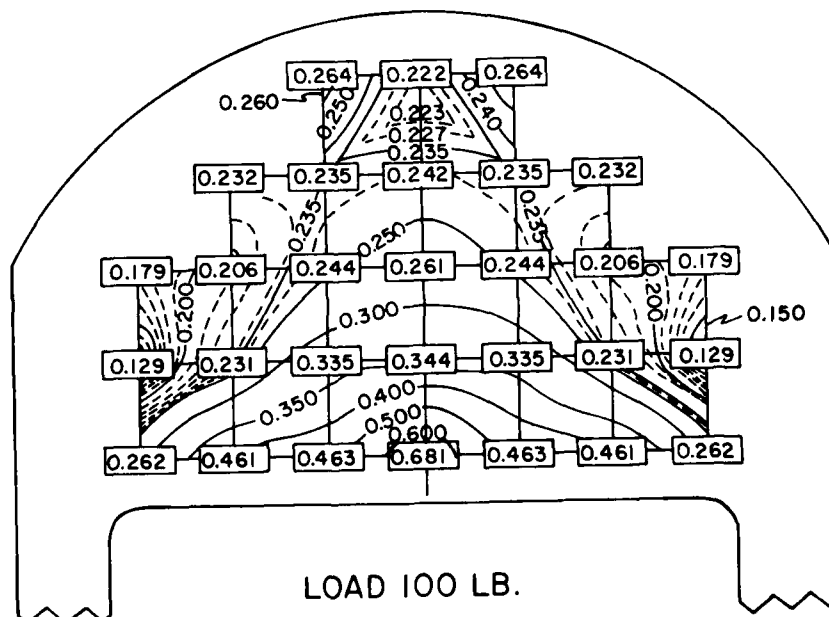


Figure 37. Deformation Patterns for Helmet Visor with Both Shades in the Up Position.

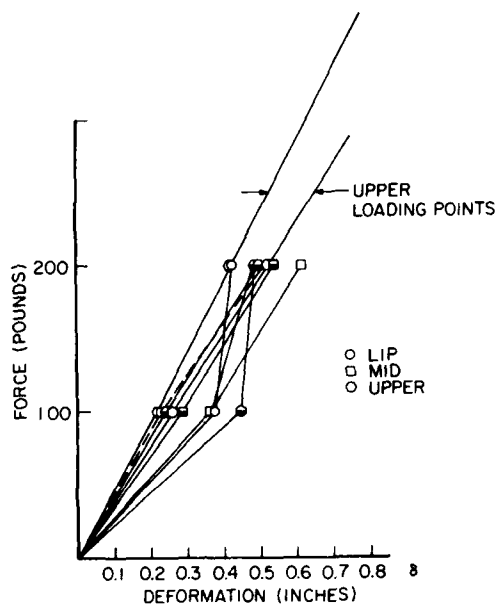


Figure 38. Visor Force-Displacement Curves.

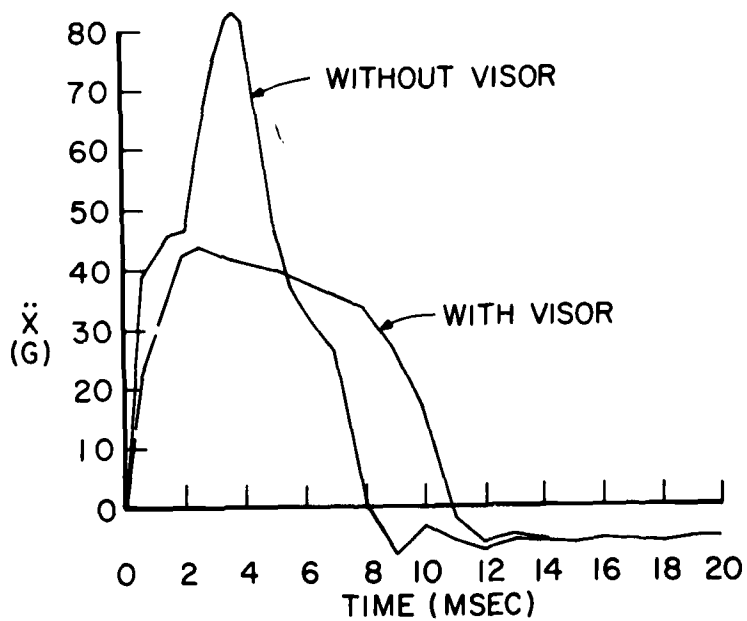


Figure 39. Head Acceleration Generated With and Without Visor.

because of the greater stroke needed to exceed the plateau force of the liner. For shell alone the liner crush exceeds the plateau level by 0.2 inches. For the "with visor" crush, the stroke is 0.012 inches short of the end of the plateau. Hence, tolerable responses are dictated by crushing to within the plateau limit by values less than the fabrication tolerances of the liner.

Figure 40 indicates the changes that occur in neck forces. Notice that the visor reduces the peak axial force by 30 percent and the peak shear force by 50 percent. Both are indicative of the differences in peak force on the helmet developed with and without visor. Both plots are similar in waveform to the acceleration curves up to maximum acceleration.

The angular responses are shown in Figure 41. Both are well below the established tolerance levels, and the peak angular acceleration of shell plus visor is significantly reduced.

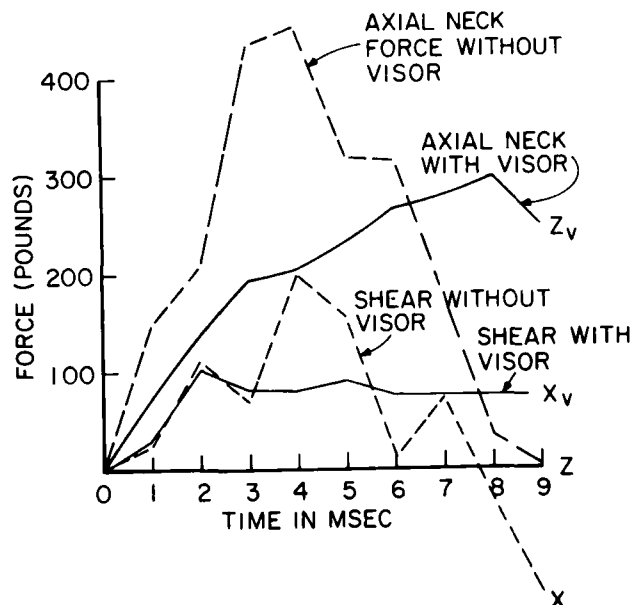


Figure 40. Neck Forces as Functions of Helmet Shell Without Visor.

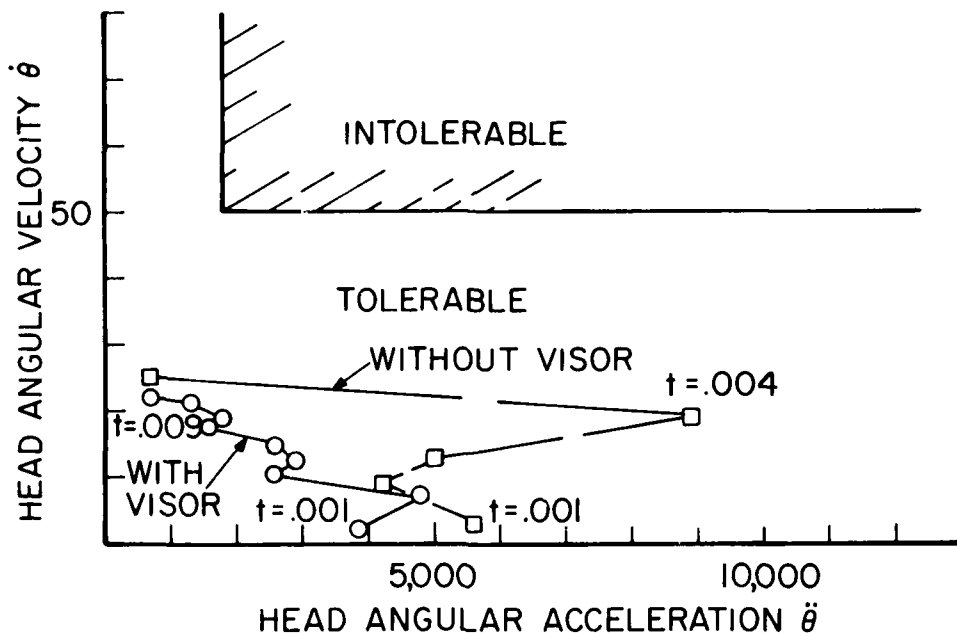


Figure 41. Head Angular Motion Due to Shell With and Without Visor.

The force displacement curves of both configurations indicate similar energy absorption up to peak force or maximum crush. The maximum absorbed energy is 42.8 foot pounds with the visor and 43.7 foot pounds without the visor. From the force-time plot, impulse to maximum force is calculated to be 2.145 pound seconds without and 2.005 pound seconds with visor.

The above values indicate that the presence of a visor for what was a "tolerable" impact, has not created a more severe environment for the crewman, but has reduced the maximum value for several of the injury parameters. Therefore, the added softness of the visor has offset the increased interference.

Lastly, it was reasonable to investigate whether or not the model agreed with the real world when comparing the intersection of idealized shell and canopy with that of the physical visor. The impact point is below the point where the visor stiffness measurements were taken, but maximum displacement does occur at a point where the computer stiffness should be indicative

of measured data. The bump separates from the model visor at a point where it should leave the real visor. The points of interest are shown on Figure 42. It is important to check the idealization, in that the visor idealization is a complete ellipsoid over the head and consequently the bump could have generated an intersection well over the top of the head. However, due to the attitude of the bump, the theoretical intersection of the two seems to be a reasonable approximation to the real world.

The data discussed are for an aircrewman seated with head tilted back at 6° and impacted by a canopy bump traveling at 19° from the horizontal. For this condition, the presence of the visor does not increase the severity of the impact. The most significant reduction is the decrease of the skull force from 1000 to 500 pounds.

If the impact were higher on the crown, the response would be dictated more by the characteristics of the shell alone, since the visor becomes stiffer. Additionally, at the higher impacts

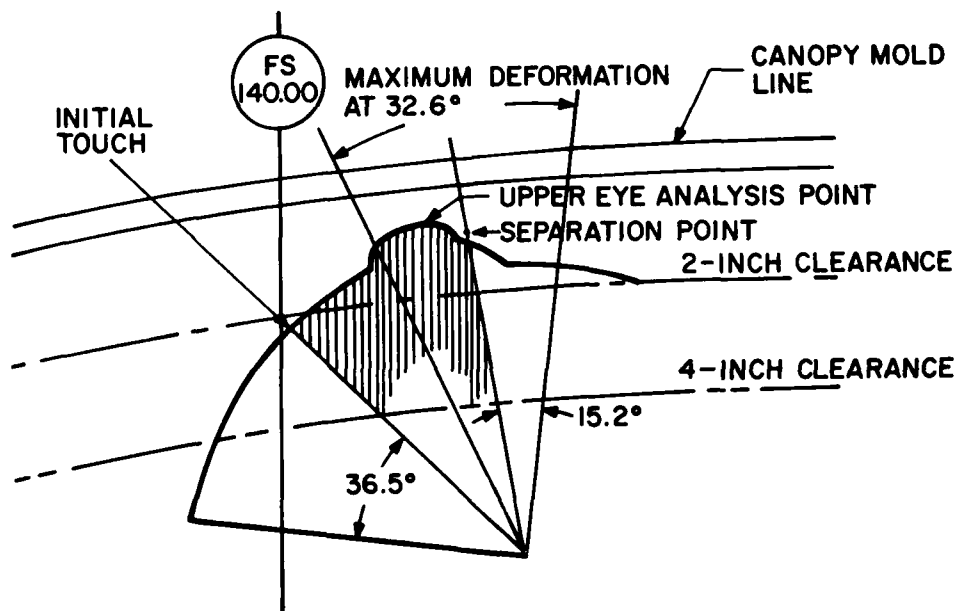


Figure 42. Visor Impact Area.

the presence of a knob must be considered. The above analysis assumed no knob or a "ram's horn" configuration. If the visor has a centerline knob this is extremely dangerous. The knob is probably a solid part made of plastic with its "stiffness" dictated by its elasticity. Therefore, the part is essentially "rigid" relative to the stiffness of the liner. If this is true, one inch is added to the interferences between canopy and shell. By referring back to Figure 32 it is apparent that in going from 1.20 to 2.20 inches of interference, you have exceeded every injury criterion listed. When a centerline knob configuration visor is available, it should be tested to determine the stiffness to failure. If the knob fails at 500 pounds, the liner stiffness will still dominate. If the knob can carry 1000 pounds, then the presence of the knob does create a potentially injurious condition from one which was tolerable.

COMPUTER ANALYSIS OF HEADREST RESPONSE

Another series of runs was made to investigate the effects of the presence of a headrest: If a headrest were present, where should it be located, and what should the stiffness be?

The first analysis was an analytical representation of the F-16 configuration. Using the one-half scale layout drawings, it was apparent that the headrest is approximately 3-3/8 inches from the rear of the helmet. This was used to establish a contact plane in the ATBM. From a report prepared by Beta Industries Inc., [16] for the Budd Company, a force displacement curve for an Insolite headrest was available. This was used with the helmet/liner stiffness curve to generate an appropriate stiffness for the intersection of helmet and headrest. The composite curve is shown in Figure 43. Note that the liner still dominates because of the greater stiffness of the headrest.

The impact condition used for visor analysis was also used for the headrest study. The response curve for the impact is shown in Figure 44. The initial deceleration is that previously

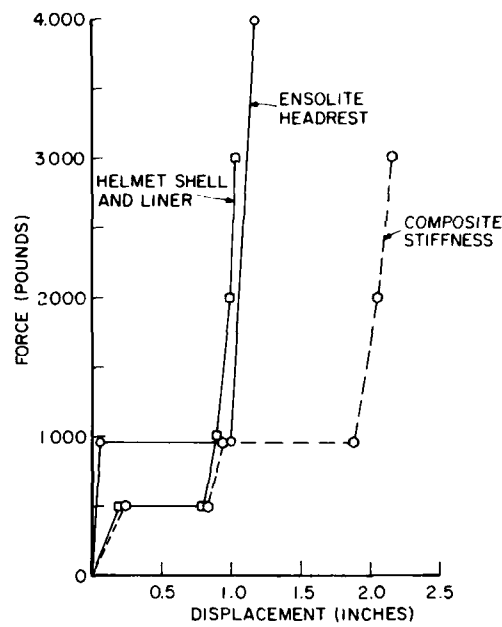


Figure 43. Helmet and Headrest Stiffness.

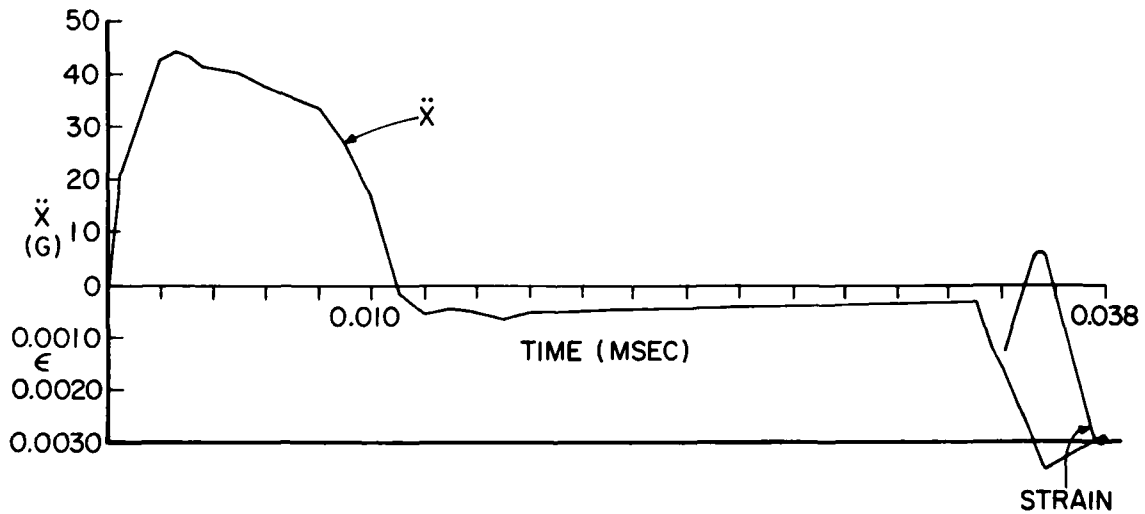


Figure 44. Head Acceleration and Strain for Birdstrike and Headrest Impact.

shown, followed by the head being decelerated by the viscous and elastic elements of the head and neck. Impact with the headrest occurs at about 33 m/sec and generates a 35 g peak. The system response is dominated by a long period of deceleration due to the characteristics of the aircrewman. During this time some of the energy of the birdstrike is dissipated and this reduces the impact velocity into the headrest. At headrest impact, the response is dictated by liner stiffness and hence the maximum force generated is only 500 pounds. All of the acceleration, velocities, and displacements are within tolerable limits. Therefore, if the birdstrike impact is tolerable, the second impact into the headrest will also be tolerable, if a lag is provided between birdstrike response and headrest impact.

A second condition examined was that of headrest impact at maximum impact velocity. The headrest plane was relocated to a position where maximum "rebound" of the head would exist. The response is shown in Figure 45. In this instance the head and

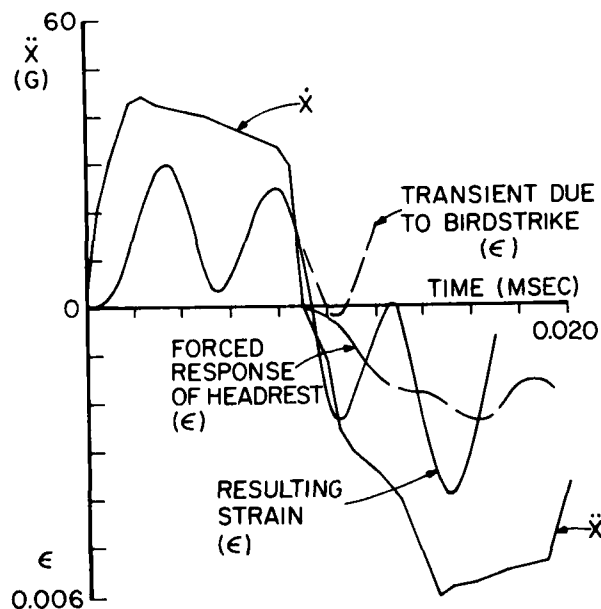


Figure 45. Head Response with Headrest Located at Point of Maximum Velocity.

neck system cannot dissipate energy between impacts and the resulting headrest impact creates a greater acceleration with a peak force of 968 pounds. The response is therefore very similar to the original birdstrike response.

Another condition studied was that of having the headrest touch the helmet at bird impact. The response is shown in Figure 46. The location was off slightly so that head acceleration reached 42 g before the headrest began to act. The headrest response is significantly reduced in magnitude but prolonged in time. This suggests that the headrest could be used to create a lower deceleration level by making use of the prolonged "plateau" crush. However, the practicality of locating the headrest in such a manner for operational usage would be a problem.

The use of the current model to study the helmet and headrest "touching" situation is questionable. In developing the model it was necessary to have the helmet shell interact with the canopy,

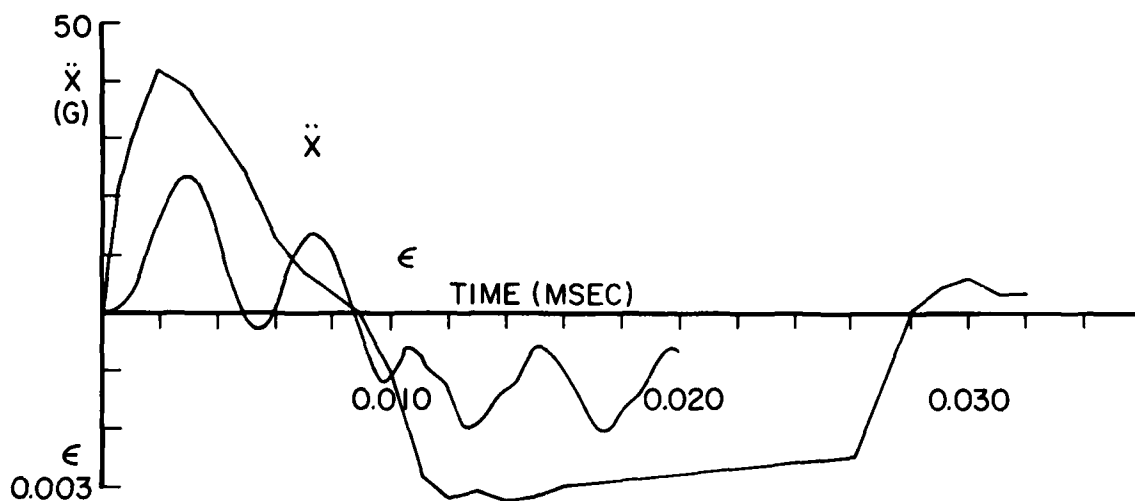


Figure 46. Head Response with Headrest Touching Helmet Shell at Impact.

and the liner interact with the headrest. This means that the head is crushed between canopy and headrest and that the shell stiffness across a diameter is an unknown and was assumed to be small in relation to the known stiffness of liner and headrest.

CREWMAN SIMULATION RESULTS

The results of the investigation into the use of a computer model of the aircrewman are many. Several are related to the overall usage of the model and some are specifically oriented toward the F-16 configuration.

The primary result is that the ATBM used is compatible with the needs of a birdstrike simulation. The nature of the model with elements that can be related to one another through joints, provides sufficient flexibility to simulate the body, helmet, shell, liner, headrest, and bird/canopy. Additionally, the concept of a force-displacement function to indicate the nature of the interaction between two bodies can be utilized with test data to idealize their interaction. The elements can be positioned in space to meet the realistic cockpit conditions, and the initial conditions of the body can be specified to duplicate any necessary relative velocities.

The model's ability to specify permissible contacts is another desirable feature. This permitted, for example, the study of headrest response when the headrest was touching the helmet. The shell was permitted to contact the bump, but not the headrest. The liner could interact with the headrest but not the bump. Therefore, the two reactions could occur. If the shell could not have been "ignored" by the liner, the response would have been that of a "rigid" helmet with the head bouncing around inside.

There was one instance of the ATBM not being able to satisfy a desired representation. In idealizing the suspension system of the helmet, it was not possible to use elastic elements as elements internal to a body. However, this was circumvented.

In general, the ATBM provided sufficient flexibility to provide modeling capability to every situation examined. The idealization may require some ingenuity, but the representation does permit realistic simulation of the input, and the output kinetics are sufficient for comparison with existing injury criteria.

For the specific application of the ATBM to the birdstrike phenomena acting on the F-16 configuraton, several other results are indicated.

- (1) Based upon very limited test data the canopy interaction with the helmet can be characterized "stiff" more than soft. That is, the stiffness is greater than that of the liner and is better approximated by the static calibration data measured at the impact point, than by the inertial response model used (Figure 21). The simplified model yields a value of stiffness which is of the same order of magnitude, thousands of pounds per inch, but it is too small by a factor of about 5.
- (2) The variation of injury parameters with interference is such that any deformation beyond the plateau force level of the liner creates an intolerable response. Even with variations of canopy stiffness the results are similar.
- (3) The variation of crushing deformation with interference becomes small at tolerable response levels. As the interference is reduced, the forces at the interface of the bird and shell are reduced and hence the relative motion between bird and head is reduced. Therefore, the interference approaches the crush depth. This implies that if clearance between canopy interior mold line and helmet is desired, the crush depth permitted by the helmet liner can be used to determine the interference permitted.

- (4) The visor assembly does not increase the injury potential of the birdstrike, assuming a centerline knob is not present. Given that the bird will sweep through a given clearance, the presence of the visor, although adding additional interference, will not amplify the head response.
- (5) The position of the headrest is such that time is available for the head to decelerate naturally prior to headrest impact. The material properties used for the headrest were "stiffer" than those of the helmet and therefore the helmet dictates the response. Placing the helmet against the headrest permits the headrest to assist in reducing the head acceleration but at the expense of possibly crushing the skull. Additionally, the bird translational acceleration criterion is for a freely responding head and not for one responding between two forces. Hence, there are really no criteria currently available for this specific condition.

SECTION 5

ESTABLISHMENT OF INJURY CRITERIA

INTRODUCTION

One of the primary objectives of the research was to provide methods for assessing the biomedical effects of direct impact to an aircrewman's helmeted head. From previous sections it is apparent that there are numerous parameters that provide kinetic and kinematic information about the response of the aircrewman. From the previous computer analyses, motions are available for both translational and rotational response of all segments, and forces and moments are available at all points between body segments. The question is one of determining the level for each that is injurious. Further, even the degree of the injury has to be quantitatively described. This is necessary because the response of the aircrewman must be restricted to a short-period disruption of the psychomotor performance; concussion, not long-term recoverable injury. The aircrewman must be able to perform properly. If a blow is survivable but results in long term disability, it must be classified as unacceptable for the current study. Biomechanical data that exist and are related to linear skull fracture, or injurious but survivable, must be quantitative related to the noninjurious criteria for this effort. Consequently, the following paragraphs attempt to relate all data to levels which would be indicative of a nonconcussive response.

DATA SEARCH

Two literature searches were performed. One search was run through NTIS looking for head injury, helmet testing, and head protection, and a second was run through COMPENDEX for the same subject headings. Data from these sources were collected. In addition, searches were conducted through literature available at the University of Dayton. This included an examination of all related technical journals as well as available proceedings such as the Stapp Car Crash Conferences. From these sources, and

references within them, data considered relevant were compiled into those parameters best related to the kinetic response of the ATBM. Angular motions, translational motions, forces, and moments of selected body segments are listed with those criteria considered pertinent.

Angular Displacements

Torso motions are defined in two documents. AFSC DH-1-3(DN 2B11)^[17] indicates a range of possible motion of 70° flexion and 30° hyperextension for the lower spine. Voluntary limits taken from DOT HS-800 499^[18], Injury Criteria Model for Restraint System Effectiveness Evaluation, yield 20° flexion and 30° hyperextension for the upper spine and 20° and 45° respectively for the lower. For the purposes of this program it is not necessary to worry about the lower spine since back support would always be available. Indeed, probably even an upper spine limit will probably not be necessary. However, the angle between the upper torso element and center torso, which defines the axis of the spine, will be compared with the angles of 30° and 20° as suggested above. Although these are from a DOT publication they are also from an SAE J963 specification.

Neck motion has several references. The design handbook indicates 50° hyperextension and 40° flexion in the sagittal plane about a point at the base of the skull. Comparable angles from the injury criteria model are both 60° at the base of the neck. The latest and most comprehensive data are contained in "A Prediction of Response of the Head and Neck of the U.S. Adult Military Population to Dynamic Impact Accelerations from Selected Dynamic Test Subjects," UM-HSRI-76-10.^[19] The angles are maximums achieved by voluntary effort and are shown in Figure 47.

These are related to points specified as the neck joint at the occipital condyles and the lower neck at C₇ - T₁. Notice that these angles provide a measure of both head and neck angular displacement. The neck pivot angles are very similar to the SAE

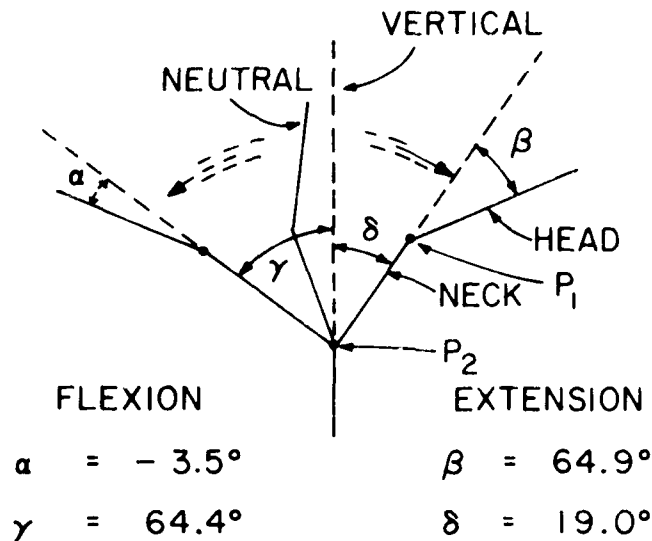


Figure 47. Maximum Angular Rotation of Head and Neck in the Sagittal Plane about the Base of the Skull. (P_1 : Neck Joint at Occipital Condyles; P_2 : Joint at $C_7 - T_1$.)

angles, and the occipital angles have no source of comparison. By virtue of the completeness of the HSRI report and the agreement seen between their measured and computer data, the above representation will be used with the ATBM in estimating tolerable head and neck angular motion.

Angular Velocity

There are no known tolerance specifications on the angular velocity capability of the torso. Neither are there specifications for the neck as a separate entity. However, there are limits hypothesized for the angular velocity of the head.

The latest estimate of concussion-producing angular head velocity by Ommaya as contained in "Injury Criteria and Human Tolerance for the Neck,"^[20] by C.L. Ewing, in Aircraft worthiness indicates a tolerable velocity of 50 rad/sec.

AD-A087 737

DAYTON UNIV OH SCHOOL OF ENGINEERING

F/G 6/5

ANALYSIS AND MEASUREMENT OF HELMETED AIRCREWMAN RESPONSE RESULT--ETC(U)

JAN 80 N S PHILLIPS

F33615-77-C-0534

UNCLASSIFIED

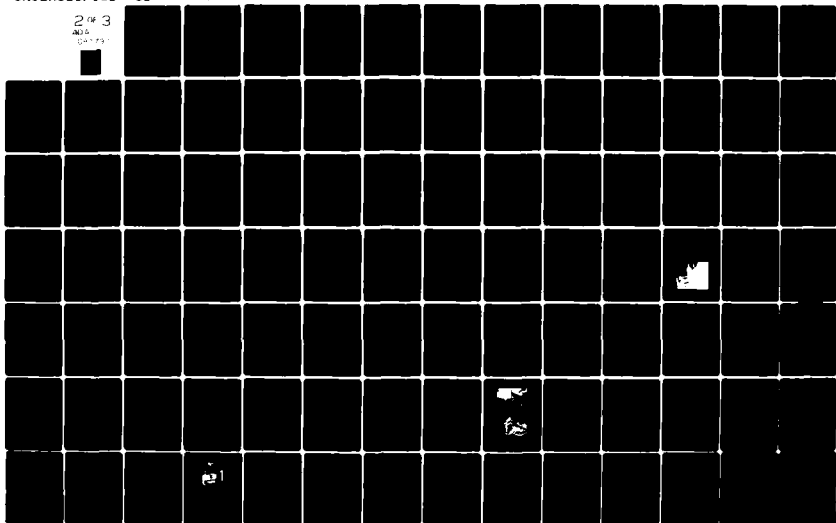
UDR-TR-79-56

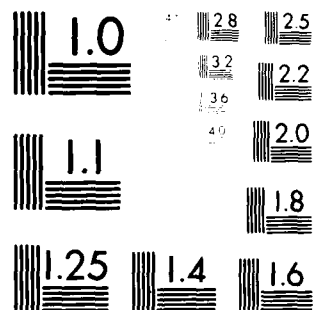
AMRL-TR-79-75

NL

2 OF 3

AD-A087 737





MICROCOPY RESOLUTION TEST CHART
 NATIONAL BUREAU OF STANDARDS-1963-A

in his own article indicates angular velocities of 38 rad/sec have been achieved without adverse effects. The theoretical work of Bycroft, "Mathematical Model of a Head Subjected to an Angular Acceleration," Journal of Biomechanics, September 1973,^[21] yields an angular velocity at the tolerable angular acceleration of 90 rad/sec. Therefore, we have limited measured data indicating 38 rad/sec, extrapolated animal data indicating 50 rad/sec, and theoretical calculations based upon brain material properties indicating 90 rad/sec.

The first number indicates the test was tolerable, the second predicts a 50 percent probability of concussion, and the last one indicates that a rigorous viscoelastic model does not follow the Holburn scaling law exactly as used in calculating the second number. Additionally, the 50 rad/sec number was originally 30 rad/sec prior to a revision. And finally, the Bycroft article^[21] indicates that while concussion is dictated by strain at a particular brain location, large shear strains are possible at the outer surface of the brain which may cause damage at less than a concussive level.

Parker's "Angular Acceleration of the Head"^[22] studied boxing, skating, dancing, and head-turning data and concluded that the following parameter relations were tolerable:

$$\begin{aligned} &15 \text{ rad/sec and } 2700 \text{ rad/sec}^2 \\ &40 \text{ rad/sec and } 180 \text{ rad/sec}^2. \end{aligned}$$

Considering the various aspects presented it is felt that 50 rad/sec is a reasonable estimate of tolerable angular velocity. There have been measurements made on humans indicating no adverse effects in the 30 to 40 rad/sec regime, and the upper limit of 90 rad/sec is evolved even suggesting possible brain damage whether concussed or not. Hence, the angular velocity should be greater than 30 and less than 90, and it has some verification or authenticity at 50 rad/sec.

Angular Acceleration

Angular acceleration of the head is examined by the same authors mentioned in the previous paragraph on angular velocity. Bycroft^[21], using strain data from Ommaya^[23] and Unterharnscheidt^[24], calculated the threshold of concussion for man assuming a certain shear strain (0.05) would occur in the region of the upper reticular formation. The curve evolved by Bycroft^[21] is shown in Figure 48.

The minimum angular acceleration occurs at a value of 3500 rad/sec^2 at 20 msec pulse duration. The pulse used was a half-sine pulse.

Ommaya and Hirsch^[25] established by scaling that the probable onset of cerebral concussion for man would be 1800 rad/sec^2 .

Ewing in his "Injury Criteria and Human Tolerance for the Neck,"^[20] refers to unpublished data indicating volunteer exposures

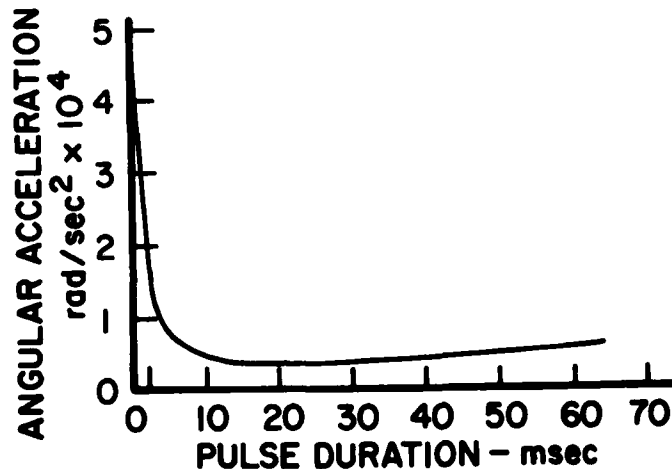


Figure 48. Theoretical Threshold of Concussion; Man.

have reached 2675 rad/sec^2 without adverse effects. Unfortunately, it is not stated whether or not this occurred with a 38 rad/sec angular velocity mentioned, or what the pulse duration may have been.

Parker, as mentioned previously, [22] indicated 2700 rad/sec^2 were tolerable at 15 rad/sec . The plot of Figure 49 presents the results of all four authors. If Ewing's two numbers are indicative of a single test condition, then the acceleration and velocity dictate a point outside of Ommaya's tolerance curve and would indicate a tolerable condition. Bycroft's work plots well outside Ommaya's tolerance curve and would be judged intolerable. The data point plotted at 1660 rad/sec^2 is a calculated point contained in Ommaya's article. The point is the mathematical calculation of the angular acceleration that may have existed in an auto collision which generated observable subdural hematoma.

Based upon the curves of Figure 49, it is believed that Ommaya's tolerance curve is still a reasonable estimate of the relations between angular velocity and acceleration for probably concussion. Therefore, the 1800 rad/sec^2 angular acceleration, above 50 rad/sec will be used as the head angular acceleration criterion.

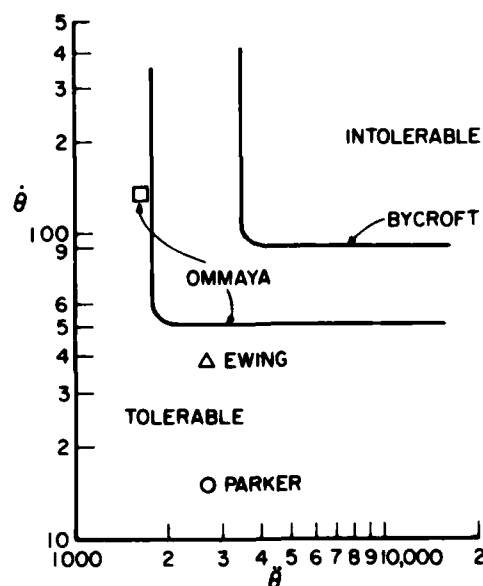


Figure 49. Head Angular Velocity $\dot{\theta}$ versus Angular Acceleration $\ddot{\theta}$.

Translational Displacement

There are no translational displacement criteria known to be available. Relative displacements between body segments that have been injured have not been found.

Translational Velocity

There are many sources of data for tolerable translational velocity. Several will be listed to indicate the differences that exist between authors for various approaches to establishing the proper level.

Patrick and Sato in "Methods of Establishing Human Tolerance Levels," contained in Impact Injury and Crash Protection,^[26] tabulate three points for frontal impact on the forehead in the A-P direction. The tabulated data and derived impulse and velocity changes are:

<u>Force Peak</u>	<u>Time Pulse</u>	<u>Impulse</u>	<u>Velocity Change</u>
400 pounds	5 msec	1.00 pound sec	3 ft/sec
285 pounds	32 msec	4.56 pound sec	14.6 ft/sec
2000 pounds	4 msec	4.60 pound sec	12.9 ft/sec

The first was for a human volunteer and lists no injury. The second was also for a human volunteer with no injury. The third was measured on a cadaver and is recorded as the threshold for skull fracture. Therefore, for impulsive response, 3 ft/sec is tolerable, and 12.9 ft/sec is near fracture. The middle point is a sustained acceleration which if plotted on an Eiband acceleration tolerance plot would be listed as uninjured, undebilitated.

Hirsch, "Current Problems in Head Protection,"^[27] in Head Injury Conference Proceedings, selects 4.8 pound-seconds for a tolerable, without damage, impulse. Using the 50 g and 5 msec values he discusses, a triangular pulse would require a 4 ft/sec velocity change. The approach refers to the original Wayne State^[28] Curve and therefore the velocity may or may not be related to concussion or fracture.

Hodgson and Thomas "Head Injury Tolerance"^[29] in Aircraft Crashworthiness, lists several impact tests to establish tolerance to linear fracture for frontal impacts and several surfaces. The average value for input velocity is 10.7 ft/sec. Against cylindrical surfaces, the value is 9.7 ft/sec, "Fracture Behavior of the Skull Frontal Bone to Cylindrical Surfaces,"^[30] Proceedings of the 14th Stapp Car Crash Conference, Hodgson et al. The pulse durations for all points were less than 5 msec.

"Structural Modeling of Human Head" by Advani and Owings,^[31] in the Journal of Engineering Mechanics Division, ASCE, discusses the development of a model used to calculate internal pressure and strains within the skull. The tolerance level established is an acceleration of 150 g at 5 msec. Using these and assuming a triangular waveform, a 12.1 ft/sec velocity change would cause theoretical shear strains to approximate measured shear failure values.

Robert Hickling and Michael Wenner in "Mathematical Model of a Head Subjected to an Axisymmetric Impact,"^[32] Journal of Biomechanics, March 1973, establish a theoretical relation between a triangular pressure pulse and brain negative pressure. For a 4 msec pulse the velocity change required is 8.3 ft/sec. The 4 msec was used as a point where impulsive response ends as shown in the figure contained in the referenced text,^[32]

"Effects of Pulse Duration on Head Injury,"^[33] Journal of Engineering Mechanics Division, by N. Akkas provides another model to theoretically establish both fracture and brain injury criteria. For a rectangular pulse two curves are evolved. One is based upon a fracture stress and another is for brain internal pressure at the impact point. By relating the pressure intensity values to applied force, and using the critical 0.57 milliseconds pulse duration, the critical velocity changes for fracture and internal pressure are 4.5 and 5.7 ft/sec respectively.

Previous development of scaled primate data led to the determination that an approximately 20 g triangular pulse of 7.5 msec

would be representative of a no-injury impact. This would generate a 2.4 ft/sec velocity change. Using the same Maximum Strain Criterion (MSC) model approach, and looking at tolerable deceleration as evolved from the Eiband point, "A Mechanical Impedance Model for Head Injury Due to Linear Impacts," by Stalnaker et al., from AMRL-TR-71-29,^[34] indicates that the minimum acceleration peak corresponds to a velocity change of 4.8 ft/sec.

The previously referenced work of Parker^[22] contained translational data derived from the rotational data. Tolerable limits were 7.5 ft/sec for 5 msec and 20 ft/sec for 200 msec.

"Package Cushioning for the Human Head" by Y.K. Liu and K.B. Chandron^[35] presents a combined lumped parameter and continuous media model. The final relation evolved is to calculate cavitation pressure to velocity change of the head. The critical value found, and listed as conservative, is 1.27 m/sec (4.18 ft/sec).

All of the above works can be collected in one group as shown in Figure 50. The figure is adapted from the MSC curve of Stalnaker and is used to combine MSC, the Wayne State Curve (WSC),

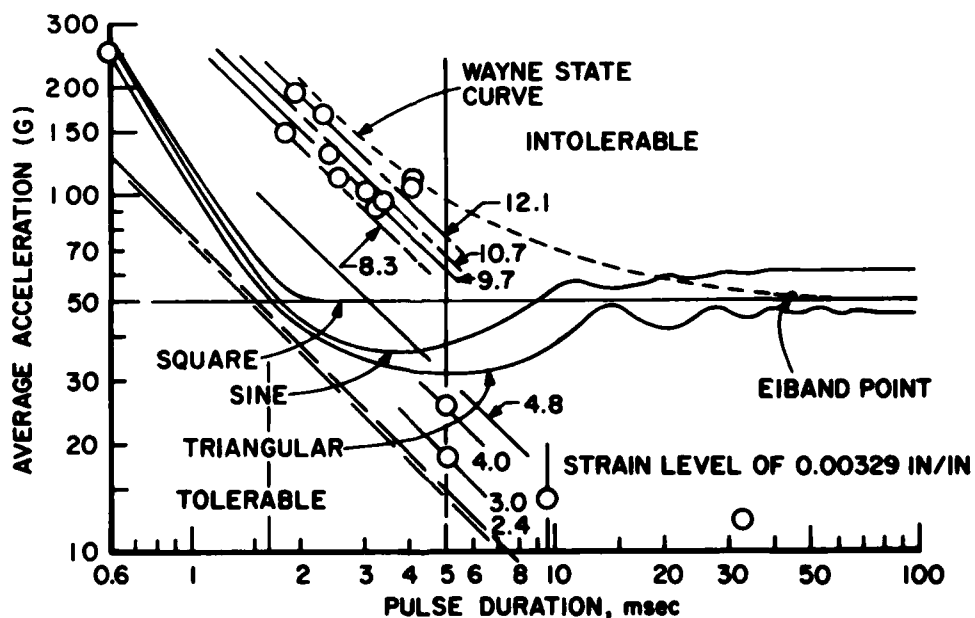


Figure 50. Compilation of Translational Velocity.

and the acceleration, velocity, and time duration together. Note that lines of constant velocity are superimposed on the graph. The lowest value of velocity plotted is that of 2.4 ft/sec, the value indicative of "no injury" extrapolated from animal data. For the triangular pulse strain response, this value nearly touches the tolerance curve based upon the Eiband points. The Patrick data point of 3 ft/sec is plotted at 5 m/sec and is obviously between the constant no-injury velocity and "tolerable" MSC of 0.032 in/in. Hirsch's point is plotted just over it as indicative of "tolerable." Other referenced data are presented and the only one of significance is that of Akkas^[33] at 0.6 milliseconds. These are at only 4.5 ft/sec, but they are also at very small time durations as was the intent of the model. It was evolved for use in the microsecond regime, not milliseconds.

Based upon the examination of the data available, and considering only linear velocity, it appears that the value of 2.4 ft/sec is a reasonable estimate of a "noninjurious" impact. The fact that MSC and the Wayne State curves are curved in this area indicates that the velocity is not the total picture, but does at least indicate that in the region of impulsive response, 2.4 ft/sec is a reasonable number for complete absence of injury. If, however, we use the same approach as for the rotational kinematics, and look for a number above no injury and yet beneath measured injury, a more reasonable velocity would be approximately 7.5 ft/sec.

All velocity points beneath 7.5 ft/sec are based upon "tolerable" conditions except for the theoretical and conservative point of Liu.^[35] Just above the 7.5 ft/sec line is a point theoretically related to concussion and just above that is a fracture due to a cylindrical impactor. Hence, for guaranteed "no injury" 2.4 ft/sec satisfies all data, and for a realistic or pragmatic value, 7.5 ft/sec is reasonable.

Translational Acceleration

Translational acceleration has been examined for many years by many authors. The original work of Gurdjian, Lissner, and Patrick^[28] led to the development of the WSC Cerebral Concussion

Tolerance Curve using skull fracture in frontal impacts at short pulse durations, and an acceleration value of 45 g for long durations. The Gadd Severity Index^[36] was used to fit the measured acceleration/pulse duration variations seen for "tolerable" impacts. Therefore, the acceleration value by itself has significance only for longer pulse durations.

Stapp, in his summary "Voluntary Human Tolerance Levels"^[37] in Impact Injury and Crash Protection provides some related data. Backward-facing seat tests generated brief occipital headaches beyond 15 g and "the aftereffects of a few good blows to the chin" at beyond 20 g peaks. The data presented indicate that for one run, backward at 35.0 g, the helmet responded at 40 g with a triangular pulse of about 40 msec. At this level "confusion and depression" existed afterward along with a brief headache. The data point was collected for the unsupported head and neck system which could be driven into a head support. The head and neck system is a low frequency system as indicated by "Preliminary Discussion of an Approach to Modeling Living Human Head and Neck to $-G_x$ Impact Acceleration,"^[38] by E.B. Becker. The measured response indicates a natural frequency of approximately one cycle per second, certainly no greater than two. This implies that the impulsive regime for the head and neck would apply for durations as great as 250 msec. Therefore, the head and neck, for the data presented, was responding to the velocity change. From the figure depicting the measured data, the head experienced a 40 g peak value and an effective plateau of approximately 52 msec to generate 67 ft/sec. This point is plotted on Figure 51.

If it is assumed that we are attempting to find a tolerable acceleration level which produces no adverse effects we must revert to the 15 g test level and scale up to an equivalent 17.1 head acceleration. This is a square wave and therefore the average value for a triangular pulse. Therefore, a 34.2 peak triangular pulse generating 28.7 ft/sec is plotted as shown on Figure 51 with the 52 msec pulse duration required.

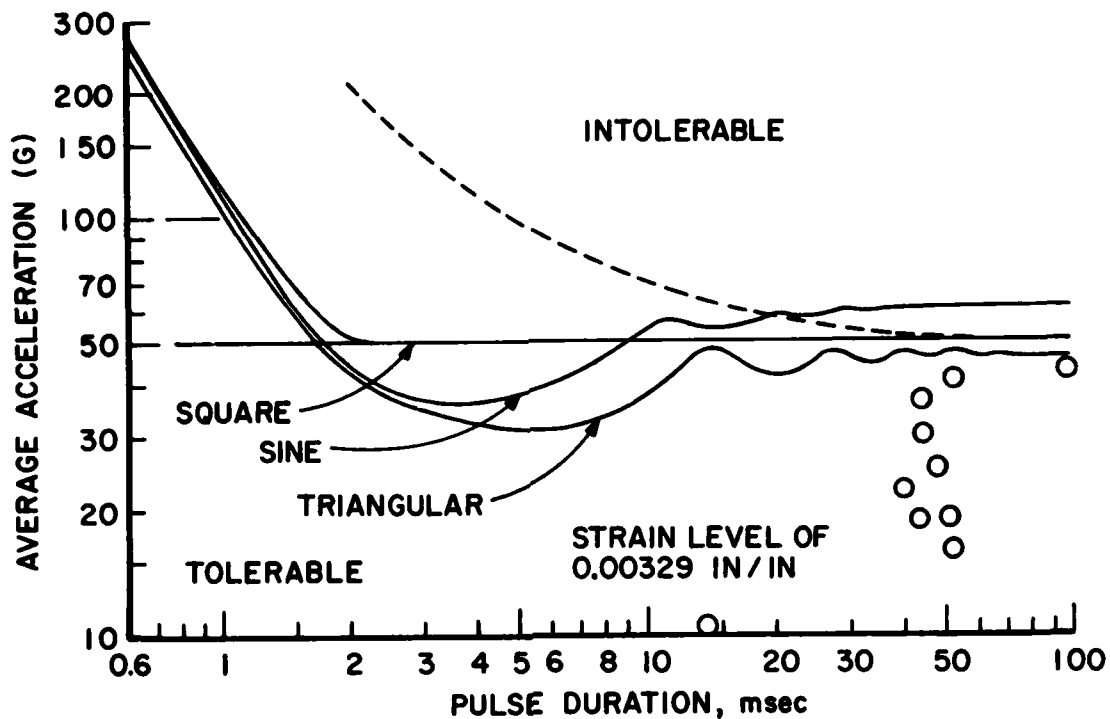


Figure 51. Compilation of Acceleration Data.

There are additional data available as referenced in AMRL-TR-71-101, An Investigation of Automatic Restraint and Body Positioning Techniques,^[39] where head impact tests were voluntarily stopped at peak accelerations of 22 g with velocity changes of 5 ft/sec. This is also referenced in "Voluntary Tolerance of the Human to Impact Accelerations of the Head," by C. F. Lombard.^[40] This same document indicates the need for protection at or above 7 ft/sec.

Previous paragraphs have already inferred the variations of acceleration levels that can be deemed tolerable as a function of brain motion, internal pressure, skull fracture, and concussion. These have to be examined in the context of the time duration of the pulse as discussed. However, in pursuit of one acceleration value, it appears that the average acceleration of about 19 g is a tolerable long time limit. Another way of putting it is to say

that if the average acceleration is less than 19 g no injury or concussion is possible. If the average acceleration is greater, then more rigorous examination is required.

Joint Forces

Forces generated between the torso and the neck can be used as estimates of injury. From Some Aspects of Biodynamic Modeling for Aircraft Escape Systems by P. R. Payne^[41] in AMRL-TR-71-29, the average failure load in compression for C3 is 200 Kg. From "Human Vertebral Centrum" by Kazarian and Graves, Spine, Vol. 2, March 1977,^[42] the average ultimate load is significantly influenced by loading rate. By examining computed data for neck force versus time it is apparent that the impact phenomena of concern are at approximately 30 ft/sec which permits comparison with data collected at 2100 in/min (35 ft/sec). For the highest spinal position of Kazarian's work, ultimate load is approximately double the "static." However, we do not want failure, rather nonfailure. By examining a typical load versus displacement plot, it appears that the linear portion of the curve is at approximately one-half the ultimate. Assuming that linearity and reversibility infer non-injury, the effect of strain rate and the desire for noninjury, establishes the tolerable axial compression force at 440 pounds.

The head/neck junction is better defined in terms of measured or calculated forces. M. J. Mertz and T. M. Patrick, "Investigation of the Kinematics and Kinetic of Whiplash," Proceedings of the Eleventh Stapp Car Crash Conference,^[43] have generated the following maximums for human volunteers in a hanging position: maximum shear force of 192 pounds and maximum tensile force of 254. Critz et al., "Determination of Human Tolerance to Negative Impact Acceleration"^[44] measured 28.6 g peak acceleration without incapacitating symptoms or injuries. This would infer at least the 254 pounds mentioned above.

Tentatively, we will have to consider 440 pounds axial force at the torso/neck junction, and 200 and 250 pounds, shear and axial force at the occipital condyles, as being tolerable.

Joint Torques

All of the references of the previous section also contained some data relative to tolerable torques at the head/neck and neck/torso junction. Patrick and Grime^[45] calculated static torque values at the condyles of 10 to 15 foot-pounds for volunteers. Mertz and Patrick^[43] proposed 35 foot-pounds as the noninjurious dynamic torque level. Schneider et al. calculated values of 20.5 and 26.4 foot-pounds at head and neck as indicative of that capable due to neck muscles. Ewing and Thomas^[46] have observed torques at the condyles of 22.5 foot-pounds in the reduction of their sled data. All of these indicate that the proposed limit of 35 foot-pounds may indeed be reasonable since values not too much smaller have been observed (calculated) from experimental work.

Contact Forces

The contact force of concern is that of the force generated at the head. Patrick and Sato^[26] tabulated two tests having peak forces of 285 and 400 pounds on the forehead of volunteers with no injury. Nahum et al., "Impact Tolerances of the Skull and Face," Proceedings of the 12th Stapp Car Crash Conference, 1968, pp 303-316,^[47] tabulate tolerance thresholds for clinically significant fractures when impacted with a one-square-inch impactor. For the frontal bone, the value is 1100 pounds and the minimum tolerance level is 900 pounds. Hodgson et al.,^[30] in a similar publication, found threshold tolerance of about 1275 pounds for the frontal bone using cylinders of 5/16-inch and 1-inch diameters. Hodgson and Thomas, Breaking Strength of the Human Skull Versus Impact Surface Curvature, DOT-HS 801 002^[48] tabulate peak force for tolerance to linear fracture in front sagittal impacts at 8.9 to 13.8 ft/sec. The forces are a low of 1280 at a 1.8-inch radius, and a maximum of 2800 pounds for a flat 60-durometer rubber surface. Additionally, the work of Melvin et al., "Human Head and Knee Tolerance to Localized Pressure," International Automobile Safety Conference Compendium, Paper 690477,^[49] indicates that penetration forces for a one-square-inch penetrator are comparable to those of fracture. Hence, for our applications the force will dictate, not the penetration pressure.

The collected data infer that 900 pounds will be a reasonable level to begin with as tolerable. We have data of 300 to 400 pounds as no injury, 900 pounds as minimum value for fracture, and 1100 to 1280 pounds as threshold for fracture. It is important to note that the pulse durations for these tests are on the order of 2 to 4 msec, which is near our range of interest.

SUMMARY OF INJURY CRITERIA

The purpose of the previous paragraphs in this section was to establish levels for comparison with computer output. This is not the ultimate goal in that it is desirable to tie all parameters together if possible. This may be possible through the use of derived parameters such as Severity Index of MSC. Wherever velocity and accelerations or forces are used as the only indicators, they cannot do the job over the complete time scale for all pulse waveforms. Therefore, derived parameters are needed.

DATA CORRELATION AND COMPILATION

The means of evaluating the effects of an acceleration waveform is to use it as the input to a simplified model which can generate a quantitative output indicative of injury. The Severity Index is one such means and is based upon a weighted integral of the acceleration.^[36] Originally the concept was based upon points plotted on an acceleration-time coordinate system referred to as the Wayne State Curve. This approach has led others to a similar approach in that data, plotted upon a particular coordinate system, is used to infer the response of a particular model that will match the data by a particular output parameter of the model.

From the translational data velocity available, a plot of measured acceleration versus time was evolved (see Figure 52). The dark data points indicate "injurious" response either because of fracture, intracranial pressure, or excessive shear stress. The fully darkened points are measured data points and those partially filled in are theoretically injurious. The open data

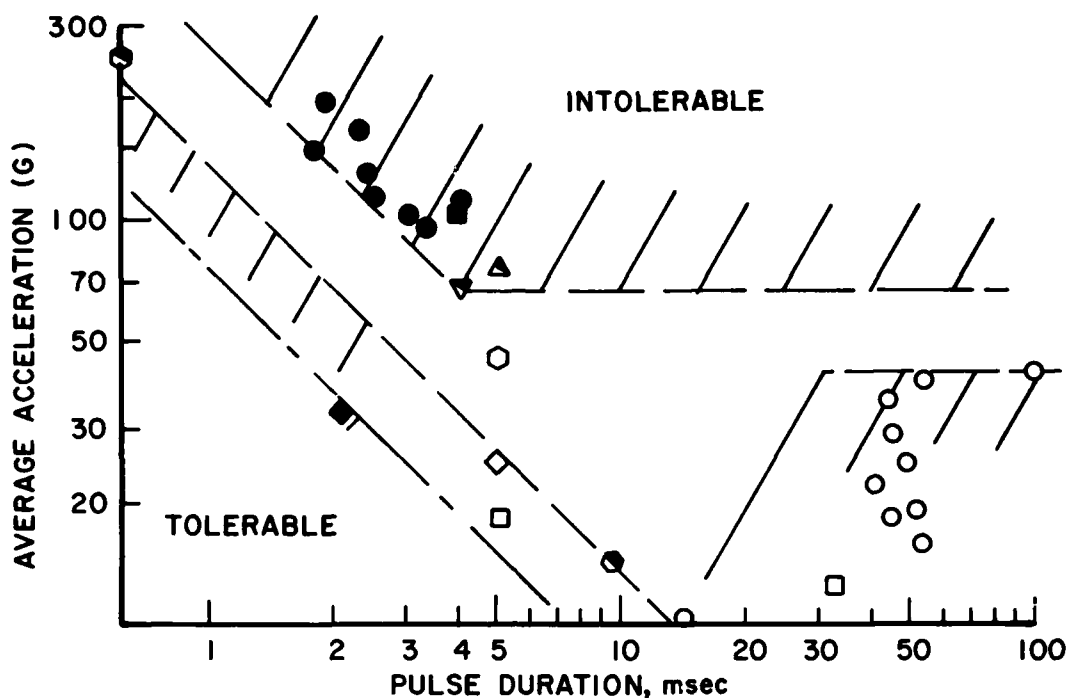


Figure 52. Compilation of Translational Data with Approximate Boundaries for Tolerable Response.

points are theoretical calculations of acceleration on humans subjected to tolerable and nonconcussive environments. These indicate intolerable accelerations that lie above a constant velocity change of about 8.3 feet per second. At the lower limit of theoretical concussion, a velocity change of 2.4 feet per second is predicted.

Similarly, translational acceleration data calculated or measured from noninjurious conditions are plotted in Figure 53. Both are then compiled in Figure 54 with approximate boundaries of tolerable, or nonconcussive response. These do, of course, fit the envelopes suggested several years ago by Kornhauser^[50] and others, in that they suggest the response of a single degree of freedom model to time dependent inputs. One such model is the MSC model originally presented by Stalnaker and McElhaney.^[51] The model is specifically for head response and uses strain as the

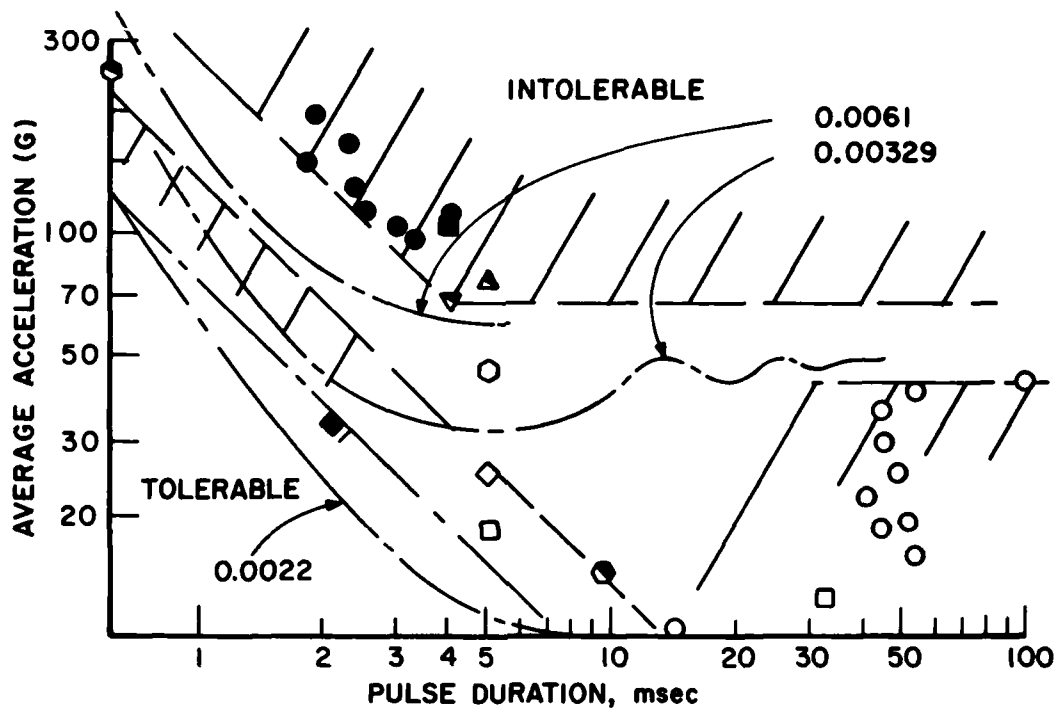


Figure 53. Translational Acceleration Data with Maximum Strain Criteria Variations.

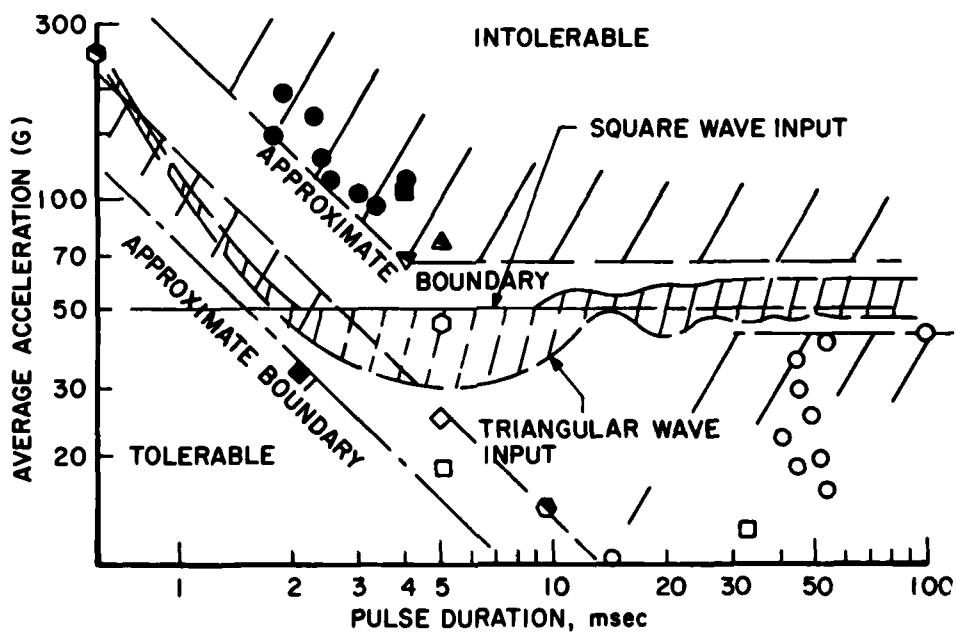


Figure 54. Translational Data with Maximum Strain Criteria of 0.00329.

quantitative output for evaluation of injury severity. The evolution of the MSC model is well documented^[52] and will not be reviewed here. However, it is necessary to briefly describe the model. The analytical model is as shown in Figure 55.

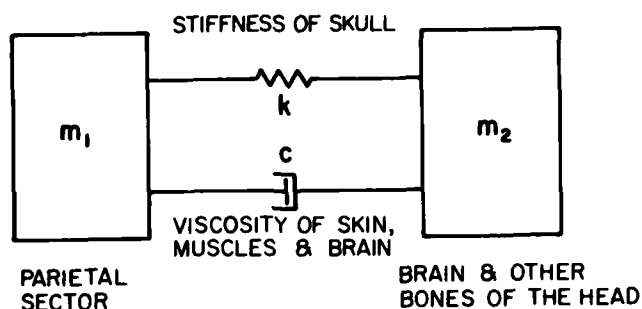


Figure 55. Maximum Strain Criterion Head Model.

The masses are assumed to be indicative of masses of the skull and brain and are quantitatively established from impedance data. The values necessary are tabulated below in Table 3.

TABLE 3. HEAD MODEL PARAMETERS

	L (inches)	x_{max} (inches)	c in/in	m_1 (lbs)	m_2 (lbs)	c (lb-sec/in)	K (lb/in)	Anti- Reson- ance Hz	Reson- ance Hz
1. R.L. Stalnaker Squirrel Monkey Lateral	1.293	0.1131	0.088	0.05	0.20	0.25	4,000	443	987
2. R.L. Stalnaker Rhesus Monkey Lateral	2.18	0.2143	0.098	0.06	1.20	1.00	10,000	283	1305
3. R.L. Stalnaker Baboon Lateral	2.758	--	--	0.08	3.46	1.60	30,000	289	1926
4. R.L. Stalnaker Chimpanzee Lateral	3.504	--	--	0.08	4.75	2.40	35,000	265	2070
5. R.L. Stalnaker Human Lateral	4.718	0.0155	0.0033	0.40	9.00	2.40	26,000	167	812
6. V.R. Hodgson Human Longitudinal	5.78	0.0190	0.0033	0.60	10.00	2.00	50,000	207	923
7. Vienna Inst. of Tech. Human Longitudinal	--	--	--	--	10.00	33.00	10,400	102	--

The acceleration input to the skull mass creates several response parameters. The one of interest is the relative displacement between the two masses divided by the initial displacement or strain. If the model is subjected to triangular input accelerations and selected strains are plotted, the curves can be placed upon the previously compiled data as shown in Figure 53. The least strain curve, $\epsilon = 0.0022$, is indicative of the strain corresponding to a no-injury impact. The number was obtained by referring back to the original data of Stalnaker as contained in Reference [51] and determining a strain compatible with the test data evaluated as noninjurious and nonconcussive. Note that the intercepts of the constant strain are at approximately those of the 2.4 foot per second velocity change line. Hence the MSC of 0.0022 infers that a velocity change of 2.4 feet per second would be nonconcussive.

The upper curve of $\epsilon = 0.0061$ is indicative of a level "3", or a "marginal as to whether injury is irreversible," tolerance level. This is the level originally established using primates and scaling laws to determine the compatible strain. The curve is just beneath data indicative of intolerable response due to skull fracture. Consequently, it appears that the strain of 0.0061 inches/inches is consistent with the higher impact velocities of 8 and 9 feet per second at the pulse duration of interest.

Finally, the intermediate curve, $\epsilon = 0.00329$, is the strain dictated by having tolerability defined by the Eiband point.^[53] If it is assumed that a 50 g and 45 m sec plateau separates "uninjured and undeliberated" from "area of severe injury", then a strain of 0.00329 for the MSC model defines the boundary.

The boundaries defined by a strain of 0.00329 for both a triangular pulse and a rectangular pulse are plotted with the compiled data on Figure 54. The curves when compared with the data points suggest that the strain level of 0.00329 is a reasonable value to be used in predicting the tolerability of a birdstrike impact. There are no measured intolerable data points within the

strain envelopes and there are no tolerable points outside the envelopes. The lesser value of 0.0022 was evaluated for all points on primates known to be noninjurious-nonconcussive, and the upper limit of 0.0061 was for points known to be injurious. Should the strain level be totally nonconcussive? Should the concussion be permitted for 30 seconds or less than one minute? These are questions that cannot be answered because of the limited amount of data available, as well as uncertainties inherent in relating quantitative kinetics to qualitative injury.

The data indicate that a velocity change of 7.5 feet per second may indeed be acceptable at impulsive time durations. This suggests a strain curve having a less severe slope at short time durations. At longer pulse durations it appears that the 40 to 50 g limit is realistic. These both suggest that the coefficients of the model should be modified to reflect a lower frequency model. Since the MSC model is based upon driving point impedance of the skull, it does not reflect any flexibility of the neck. If the MSC model were "mounted" upon a flexible neck, the natural frequency of the system would be reduced, shifting the peak response of the model toward a longer pulse duration. In this manner, a revised model would probably better fit both impulsive and long duration responses.

The advantage in specifying a tolerable longitudinal strain is that it provides the mechanism to evaluate lateral impacts also. The concept of tolerable strain was originally based upon the assumption that the brain is equally vulnerable to strain in all directions. If this is valid, then the values of the model presented previously for lateral response can be used to calculate another tolerance curve. A curve of lateral tolerance for a strain of 0.00329 is presented in Figure 56.

The lateral tolerance curve is significantly lower than that for longitudinal tolerance and reflects the differences in mass distribution and the significantly lower stiffness.

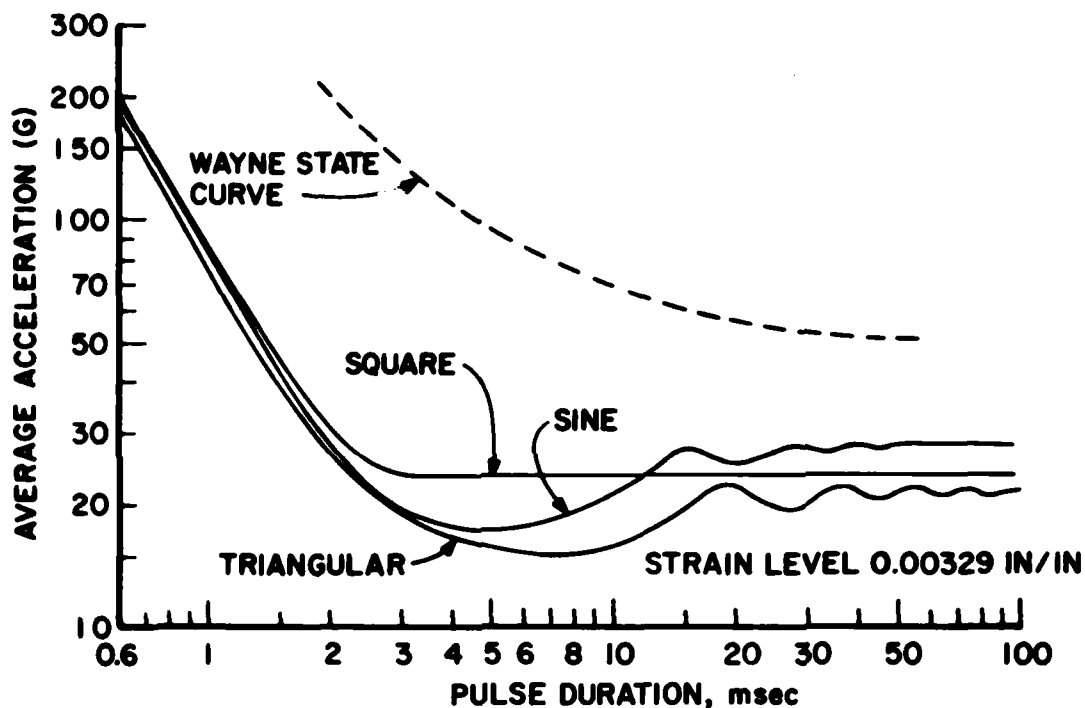


Figure 56. Maximum Strain Criterion Curves for Human Lateral Head Impact.

There are no data available concerning strain criteria for vertically applied impacts, hence the MSC approach cannot be applied to the determination of vertical tolerance criteria. Consequently, a different approach is necessary. In the vertical direction, the only parameters suggested by the data are skull force and neck axial force. The skull force permitted is in the range of 900 to 1000 pounds, and the neck tolerable axial force is estimated to be 440 pounds. These can be correlated by using a model suggested originally by Von Gierke^[54] and used recently by Schneider.^[19]

From Schneider's work, a 17.67-pound head and neck are assumed to be supported by an elastic neck of light damping. If the skull is subjected to a triangular pulse, it is easily possible to calculate the velocity and displacement between skull and shoulder and determine the necessary skull force and resulting neck force. Using 1000 pounds as the limiting skull force and 440

pounds as the maximum axial force, the triangular acceleration pulses that are limiting are plotted on Figure 57. The curves reflect the bimodal nature of the response and are shown with the effects of coupling with a torso element. The long-term steady state limit is determined assuming a three pound helmet.

The approach used in establishing a correlation between forces and accelerations is covered more fully in a later section. However, the simplified approach does demonstrate that the simplest biomechanical model can be used with selected empirical data to infer injury modes which are significantly different than those seen using MSC representations. The criteria for injury are still forces, but if the input acceleration waveform at the skull is known, then some meaningful relations can be evolved between the forces and the kinematics.

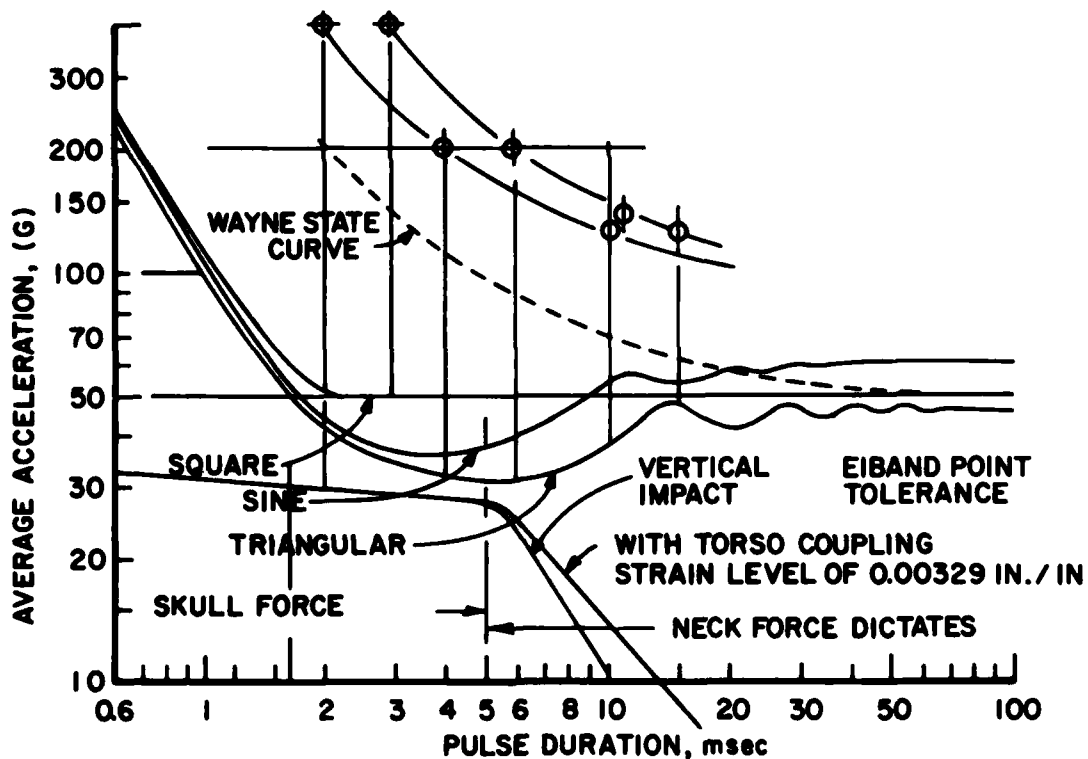


Figure 57. Vertical Impact Tolerance Curve Based Upon 1000-Pound Skull Force and 440-Pound Neck Axial Force Limits.

SELECTION OF CRITERIA

The purpose of this chapter was to ultimately specify quantitative values of particular parameters that could be used as criteria for nonconcussive impacts. Establishing a particular number as a go-no-go criterion is always difficult when the system being studied is the human body. This is true not just because of the nature of the system, but because of the lack of statistically defined data. Seldom are there injury or biomechanical data with many data points, standard deviations, variances, or confidence limits. Consequently, the numbers arrived at are a function of the judgment of the evaluator in relating the criteria he finds to the practical problem at hand. For these reasons, the numbers given in Table 4 are thought to be reasonable estimates which should be investigated more fully by any particular investigator. The numbers are in general taken from or related to referenced work and it is advisable that the "first source" be consulted if the use of the number is critical.

TABLE 4. SUGGESTED REASONABLE CRITERIA FOR NONCONCUSSIVE IMPACTS

<u>Parameter</u>	<u>Comments</u>
Skull force < 900 pounds.	Force applied to the skull should not exceed this value regardless of time duration. It is assumed that since this is for helmeted head applications, the force is distributed over a finite area such that pressure is not critical. If the threshold for fracture can be shown to be related to concussion, this can be raised at least to 1000 pounds, since current threshold values are 1100 pounds.
Neck axial force < 440 pounds.	This is based upon compression strength of cervical vertebra with an attempt to include the effects of high strain rate, and relates linearity to concussion.

TABLE 4. SUGGESTED REASONABLE CRITERIA FOR NONCONCUSSIVE IMPACTS
(Continued)

<u>Parameter</u>	<u>Comments</u>
Neck shear force < 250 pounds	This is based upon calculated measurements for volunteers tested at subinjurious levels. This is probably conservative but "upper" limits data are nonexistent.
Neck moment < 35 foot-pounds	This is a proposed value which was estimated for static volunteer data.
Longitudinal velocity, Change < 7 feet/second	This is considered to be a realistic value for impulsive longitudinal response of the skull. It is based primarily upon the fact that it fell below all "injurious" data on the acceleration time plot, is related to boxing and skating data, and reflects the limit established by energy considerations measured on volunteers.
Lateral velocity change < 5 feet/second	This is based upon examination of the lateral MSC curve which assumes a strain limit of 0.00329. This corresponds to the restriction of 7 feet/second longitudinally. It is for impulsive response.
Longitudinal acceleration < 40 g	The long term, steady state acceleration level is suggested by sled data available using volunteers, and by the Eiband point used with the strain value of 0.00329.
Lateral acceleration < 22 g	This is a steady state value based upon the lateral MSC curve and reduced by the same ratio as was used longitudinally.
Maximum strain criteria < 0.00329 in/in	If the skull acceleration waveform can be predicted, the response of the MSC model, either longitudinal or lateral, to that waveform should generate a strain of less than 0.00329 in/in. From the curves shown it is apparent that this is a more restrictive criterion to be placed upon the acceleration waveform. Hence, for a conservative (less injurious) environment, the MSC approach could be used.

TABLE 4. SUGGESTED REASONABLE CRITERIA FOR NONCONCUSSIVE IMPACTS
(Concluded)

<u>Parameter</u>	<u>Comments</u>
Rotational accelerations and velocities < 50 rad/sec and 1800 rad/sec ²	The values proposed are those of Ommaya and Hirsch ^[25] .

The parameters listed are those of significance. Additional values are available in the previous sections but are not those that will dictate tolerability.

SUMMARY

Injury criteria parameters relative to the response of a head and neck system impacted by a bird have been established based upon all data readily available. The plotted points are combinations of theoretical, measured, and derived information that has been interpreted in terms of concussive or nonconcussive results. The original goal was to quantitatively describe the degree of injury and this has been accomplished to some extent by use of the MSC model. Some data are available which can be used to dictate specific levels of strain for specific levels of injury. However, the value selected was based more upon its relation to the existing human data rather than scaled primate data as was the original approach.

SECTION 6

DEVELOPMENT OF A SIMPLIFIED ANALOG MODEL

INTRODUCTION

The analysis of the birdstrike phenomena has been modeled by use of the ATBM. All primary parameters of the phenomena can be included in the analysis because of the extensive capability of the routine. Body segment inertial characteristics, joint stiffness, bird kinematics, helmet and seat properties, and varied input conditions can be quantitatively described and then utilized by the routine to produce a variety of output kinetics for any selected segment. The capability available can create astonishment, admiration, or intimidation depending upon the familiarity of the output user with large digital routines. Consequently, it was desirable to determine whether or not the birdstrike phenomena could be represented by a simplified model that would be more easily used by a designer, or engineering analyst, to provide acceptable results. Could the phenomena because of inherent characteristics be reduced to a simplified analog which would permit algebraic solutions? For the research analyst the ATBM provides the tool for birdstrike analysis. For the engineer "on the boards" it was desirable to provide a less sophisticated tool. However, the "algebraic" tool would have to duplicate the ATBM results for those parameters selected as critical injury parameters, and would have to do so within reasonable engineering accuracy.

MODEL DEVELOPMENT

Results of the ATBM birdstrike analyses were examined to establish qualitatively how the helmeted head-neck system responded. It was first noted that at interference levels where injury would theoretically occur, the forces of interaction between canopy and helmet were small relative to the maximum force sustained at bird impact, and to the maximum force capability of the helmet shell and liner. For approximately one inch of interference, the force generated is about 1000 pounds. Additionally, the impact between canopy and helmet is impulsive. The head response is a transient response that takes place after the bird has passed. Hence, the

head and neck cannot respond while the canopy bump passes over the helmet. Since the impulse is too small to cause significant canopy or helmet motion away from the impact point, the crush developed is essentially equal to the interference that exists for two intersecting spheres crossing without mutual response. The two intersecting bodies act as though the bird crushes the helmet onto the head while the head does not move. If this were a valid approximation, then it could be assumed that the forces generated at the skull could be found by merely calculating the deformation, as a function of time, between two intersecting spheres.

A curve representing the force displacement relation for a canopy and helmet is shown in Figure 26. If two spheres intersect, the configuration can be described as shown in Figure 58. For a given radius "bird" (canopy bump), and shell, the equations relating depth or crush to maximum deformation are

$$\cos \beta = \frac{(R_H + R_B - \Delta)}{(R_H + R_B - \delta)}$$

and

$$d = (R_H + R_B - \delta) \sin \beta,$$

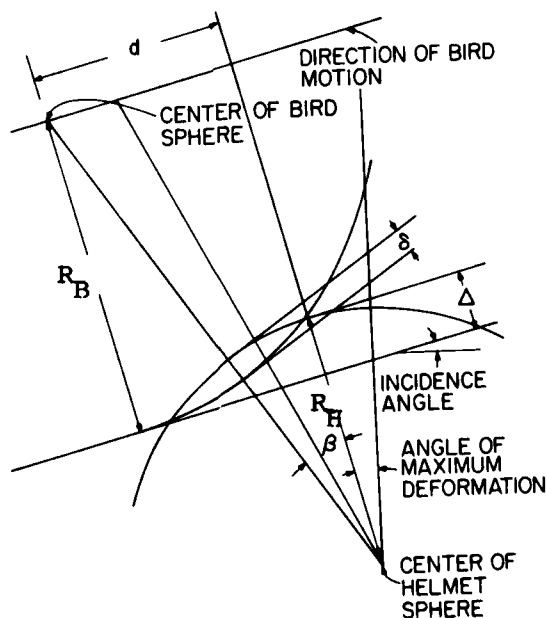


Figure 58. Deformation Configuration for Two Intersecting Spheres.

where R_H is the radius of the helmet
 R_B is the radius of the bird
 Δ is the maximum theoretical interference
 δ is the deformation at the angle β .

Once the maximum interference is selected, and the radii are established, there is an angle β for any desired deformation. Knowing the angle β , the distance to maximum deformation can be established and hence the time to maximum deformation can be calculated using the velocity of the bird.

For example, assuming a 10-inch-radius canopy bump and 5.375-inch-radius helmet shell, a maximum deformation of 2 inches will generate a 30-degree angle between touch and maximum deformation. During that motion, the bump will traverse 7.69 inches (d) which requires 0.00547 seconds at 1400 inches per second. For one inch of crush, β is 21° and the bump has traversed 4.78 inches. This implies 0.00341 seconds from the peak or 0.00206 seconds from touch.

The procedures outlined can be used to calculate a profile showing the depth of crush versus time for any selected set of impact conditions. Since the ultimate goal is to establish the forcing function of the impact to be applied to a simplified head model, force should be calculated for the significant points on the force-deformation curve of Figure 26. That is, the force-time profile should be established by selecting the deformation where the force slope changes significantly. From the force-displacement curve there are significant changes at 0.28 inches and 0.88 inches. These are then deformations to be used in calculating the time from touch. Once the times for given deformations are calculated, the force-time profile is obtained from the force-displacement curve.

The forces found are forces normal to the curvature of the shell and can be resolved into components in an inertial reference. Relative to an axis system through the maximum deformation, the vertical and horizontal force components are

$$V = N \cos \beta + N \sin \beta$$

$$H = N \sin \beta + N \cos \beta$$

and can be calculated for each time of interest. The vertical and horizontal forces can then be related to the inertial reference by accounting for the angle of incidence of the bump. For the example chosen:

$$Z = V \cos 19^\circ - H \sin 19^\circ$$

$$X = V \sin 19^\circ + H \cos 19^\circ.$$

The results of the manual computation of the steps outlined are shown in Figure 59. The moment curve included reflects the moment generated about a pivot point at the base of the neck. Since the force components are known, and the point of impact is known, the moment arm between applied force and pivot point can be easily established for any selected geometry. The moment shown was calculated for the dimensions used in the ATBM representation.

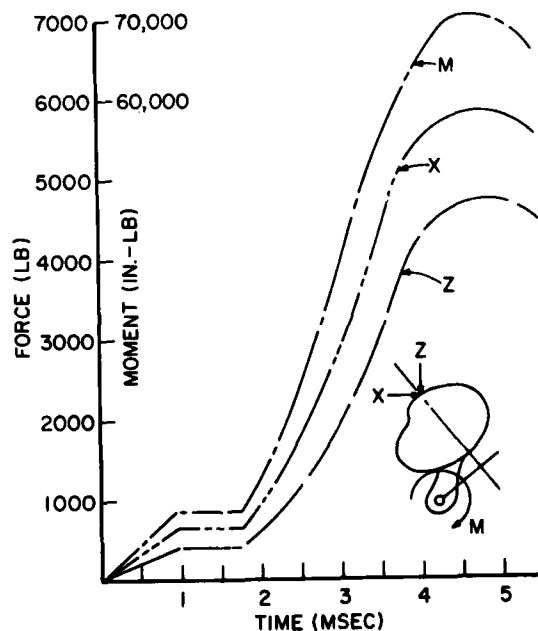


Figure 59. Applied Force and Moment versus Time for 2-Inch Interference of 10-Inch Radius Bird (Bump) and Extra-Large Helmet Shell at 1400 Inches per Second; Impact Path 19° from Horizontal.

The above paragraphs indicate that the forcing function to the head of the aircrewman can be calculated manually if the force displacement curve is available, and if it is assumed that the head does not move a significant amount during impact. This reduces one aspect of the total response problem to a statics problem rather than a dynamics problem. The interface between bird/canopy and helmet/head has been reduced to the intersection of two spheres.

The equations for the interface forces were then programmed to permit the study of many parameter variations. The initial studies assumed that the head and neck system pivots about the neck shoulder joint and that the response would be duplicated by various assumed dynamic models. Examination of the initial ATBM computer runs indicated that the neck motion was very small and that the head rotated primarily about the skull-neck joint (the occipital condyles). Consequently, the moment arm for the rigid body being considered was reduced to reflect the distance between head center of gravity and the skull-neck attachment.

The simplest model possible is that of a rigid head rotating about the skull-neck joint with no vibrational response. That is, a body rotating about a joint with no joint resistance and the acceleration dictated by the applied torque and the rotational inertia of the body. The ATBM output for an interference of 1.05 inches indicates an angular acceleration of 8880 radians per second squared. The acceleration generated by a pivoted head of moment of inertia 0.642 inch-pounds/sec² is 11,700 rad/sec², indicating that there is additional resistance to motion supplied by the joint.

The moment generated at the pivot point is:

$$M_p = C\ddot{\theta} + K\dot{\theta}$$

$$M_p = 1.745\ddot{\theta} + 21.293\dot{\theta}$$

for the ATBM coefficients used. For angular motion integrated using the pivoted body acceleration, the values of the terms are

$$M_p = 1.745 (1450) + 21.293 (2.37)$$

$$= 2,580 \text{ inch-pounds.}$$

This indicates that the resistance of the joint at the peak applied moment is a significant amount generated primarily by the resistance of the angular velocity. The contribution due to angular displacement is less than two percent of the total. Therefore, the response is better approximated by considering the joint as having a viscous damper. The differential equation of motion for a pivoted head with viscous damping is

$$\Sigma M(t) = I\ddot{\theta} + C\dot{\theta},$$

and the solution is

$$\ddot{\theta} = \frac{-K}{C} \{e^{-\frac{C}{I}t} - 1\}$$

for a linear input $M(t) = kt$.

The solution is in the form that permits calculations of the response by reducing the moment curve to a series of linear slopes. The moment curve for a 1.05-inch interference is approximated as shown in Figure 60.

The response of the head at any instant is then the summation of the responses to each segment. Therefore, the angular acceleration is

$$\ddot{\theta} = \Sigma - \frac{K_i}{C} \left\{ \frac{1}{e^{\frac{C}{I}(t - \tau_i)}} - 1 \right\},$$

where K_i is the slope of the i^{th} segment, and

τ_i is the time delay for the i^{th} segment.

Using the one-millisecond approximation and summing the contributions to the peak angular acceleration yields a value of

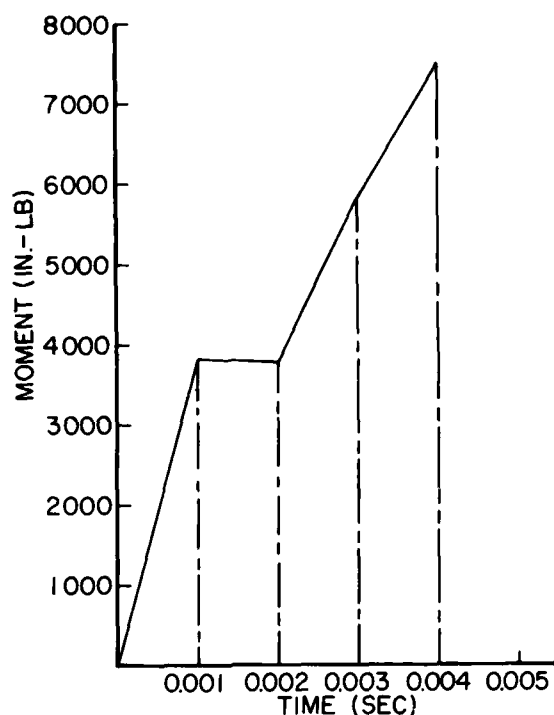


Figure 60. Approximation of Moment Curve for Intersection of Helmet with 10-Inch Radius Bird for Interference of 1.05 Inches.

8394 rad/sec^2 for an error of 5.5 percent. The same equation integrated for velocity and displacement yields values of less than nine percent error.

The equations above were also programmed for use in studying parameter variations. This was necessary since the number of parameters that could be changed, and the tedious nature of the calculations, made it desirable. The program was written to examine the response of one- and also one-half-millisecond approximations to the applied moment curve.

The first impact studied was the 2.20-inch interference in order to examine the response at large values of force and acceleration. If the large values could be well approximated it was assumed that "fit" for the smaller values would follow. For the 2.20-inch interference the values are as follows:

	θ	$\dot{\theta}$	$\ddot{\theta}$
ATBM	3.5°	52.8	25,336
Simplified Model	3.56°	48.5	25,226
Percent Error	1.5	8.2	0.4

Therefore, if it is assumed that the ATBM is represented by a body pivoted about a fixed point with the same inertial and dimensional characteristics as the helmeted head, and that the applied moment is only a function of an interference between two nondisplaced bodies, then the peak angular motions are correct within less than 10 percent, with the acceleration incorrect within less than one percent.

The computer-generated results are values calculated for the peak value of input moment and not necessarily for the peak that could be calculated. Therefore, the simplified model values for velocity and displacement should be low since they are the values at peak moment and not the peak value that would exist had integration been carried on. The model duplicates peak values of ATBM results, but does not have the same time-to-peak.

In order to use the simplified model it is necessary to calculate the head angular motions, as shown, but it is also necessary to demonstrate that translational motions and forces can also be reasonably approximated. For a fixed pivot motion the normal and tangential accelerations can be found from the angular motion. The normal acceleration is the familiar $r\omega^2$ and the tangential acceleration is $r\alpha$. Since the ATBM distance between pivot and center of gravity is 3.07 inches, the peak values of normal and tangential acceleration can be calculated as 9,299 and 99,643 inches per second squared respectively. Comparison with ATBM output indicate that these are within less than 6 percent error when compared with accelerations in the inertial reference systems. The accelerations in the program are transformed into the inertial reference by accounting for the incidence angle and the tilt angle of the head. In the data to be represented it is assumed that the head is tilted back at a 6-degree angle. Additionally, the incidence angle is 19° and the dimensions used are shown in Figure 61.

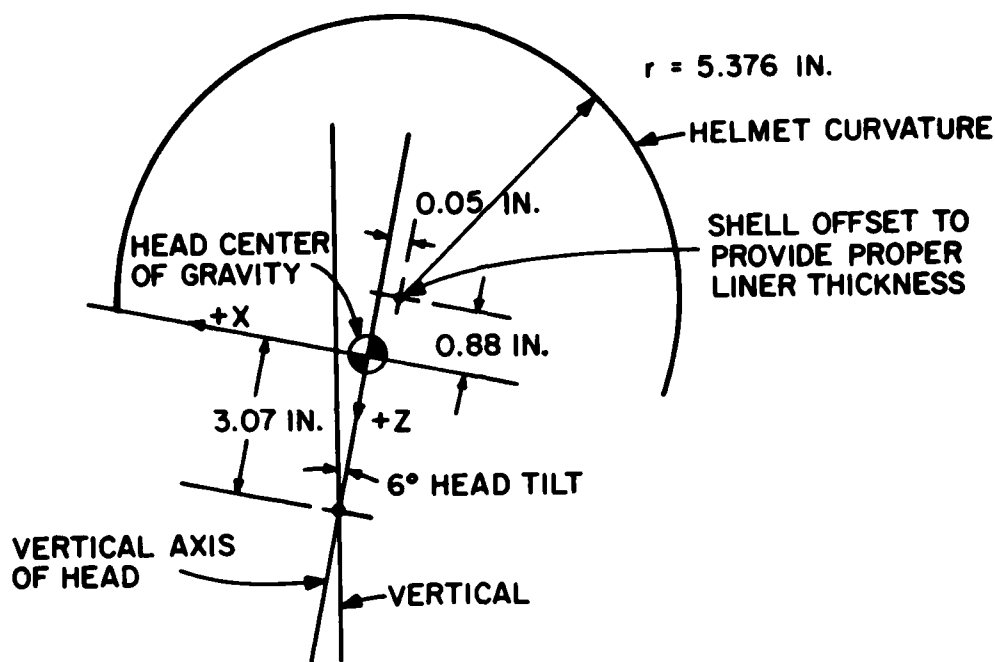


Figure 61. Dimensional Data Necessary for Simplified Model.

For the data shown, and calculating the kinetic parameters from the diagrams and the equations of motion, the values of neck forces and moments required are

	<u>Axial</u>	<u>Shear</u>	<u>Moment</u>
Simplified Model	1520	1063	6540
ATBM	803	654	3279
Percent Error	89.2	62.5	99.4

The kinematics of the simplified model at the highest impact levels are in reasonable agreement, but the kinetics are in very poor agreement. The values are in the right direction, intolerable, and hence are correct if the only criterion is tolerability.

By repeating the same procedure for the low level impact which is known to be tolerable based upon MSC, the following values are found:

	<u>Axial</u>	<u>Shear</u>	<u>Moment</u>
Simplified Model	374	630	2108
ATBM	226	435	1280
Percent Error	65.4	44.8	64.7

The percent error is still large, but again all values are conservative in that they predict a larger response than the more "exact" calculation. Additionally, the absolute error may not be unreasonable in that the variables examined are probably those with the least reliable injury criteria. The axial force allowable is a predicted number derived from compression testing of a vertebral element. Is the 440-pound level indicative of a true value that could be 660 pounds? Similarly, could the shear allowable be 500 pounds rather than 250? Based upon available biomechanics data, the moment allowable is probably the most suspect.

Another aspect that reduces the necessity of having exact kinetic matching is that the curve of number of injury tolerance variables exceeded, versus displacement, indicates that the first variables to be exceeded with increased displacement are neck moment, head acceleration, and head velocity. Hence, considering those parameters that are the best substantiated, and most critical, the duplication of head kinematics is more important.

The previous sections have shown that the head velocity and acceleration are well matched. This is further substantiated by using the curves of head fore-and-aft accelerations for both impact levels in calculating for MSC strain. Using the approximations shown in Figures 62 and 63, the MSC strain values are

	\ddot{X}	ϵ	\ddot{X}	ϵ
Simplified Model	34,600 in/sec ²	0.00319	99,319	0.00726
ATBM	31,800 in/sec ²	0.00297	105,900	0.00641
Percent Error	8.8	7.4	6.2	13.2
	Low Level		High Level	

The peak acceleration and maximum strains at the lower level are reasonably close together. The peak acceleration predicted is greater than the "exact", and the strain is greater. Both imply that the simplified model has generated conservative values at the levels where it is assumed that a "tolerable" response exists. At the upper level the simplified model does not predict a conservative acceleration peak, but does indicate a conservative

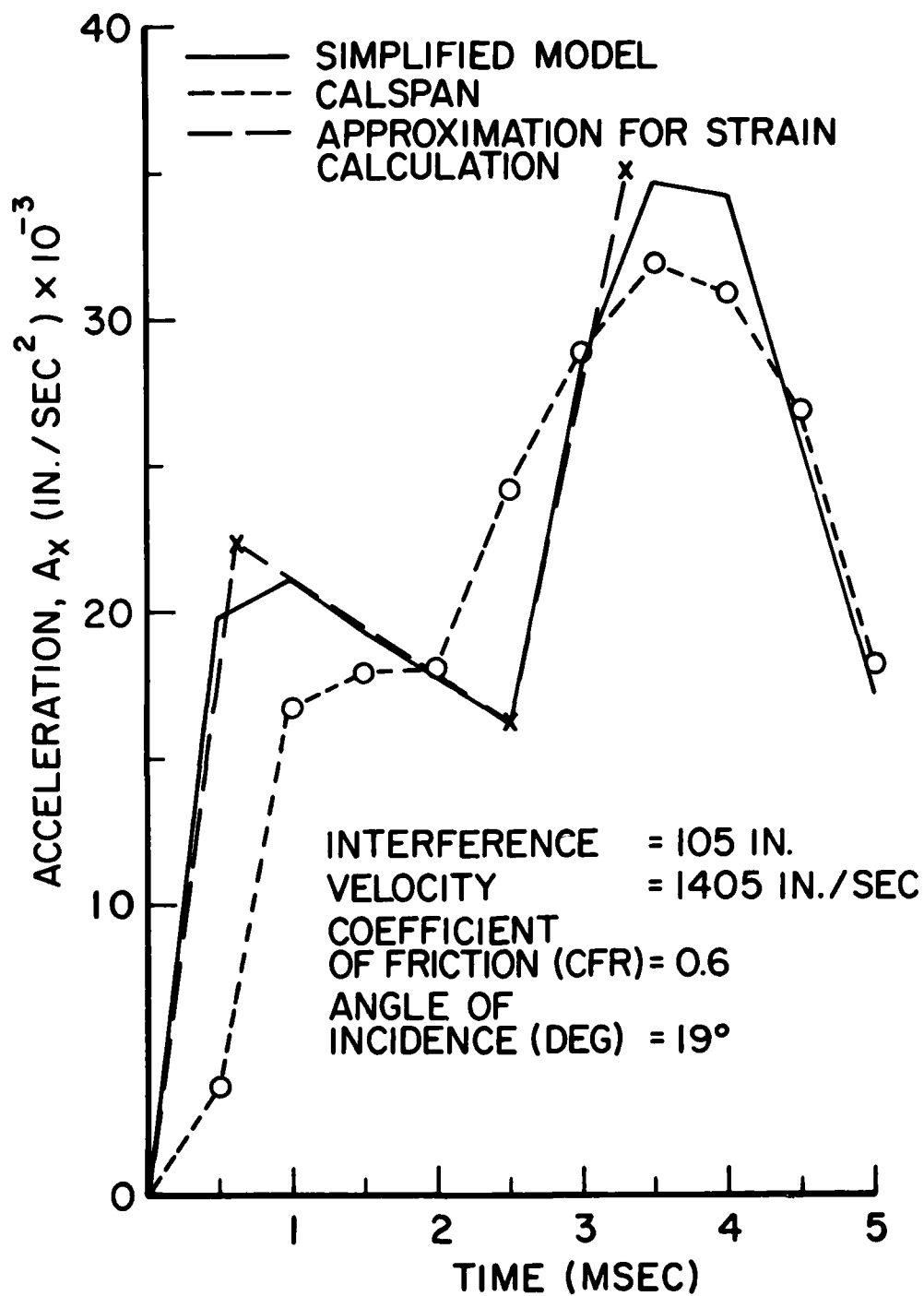


Figure 62. Waveforms for Low-Level Birdstrikes.

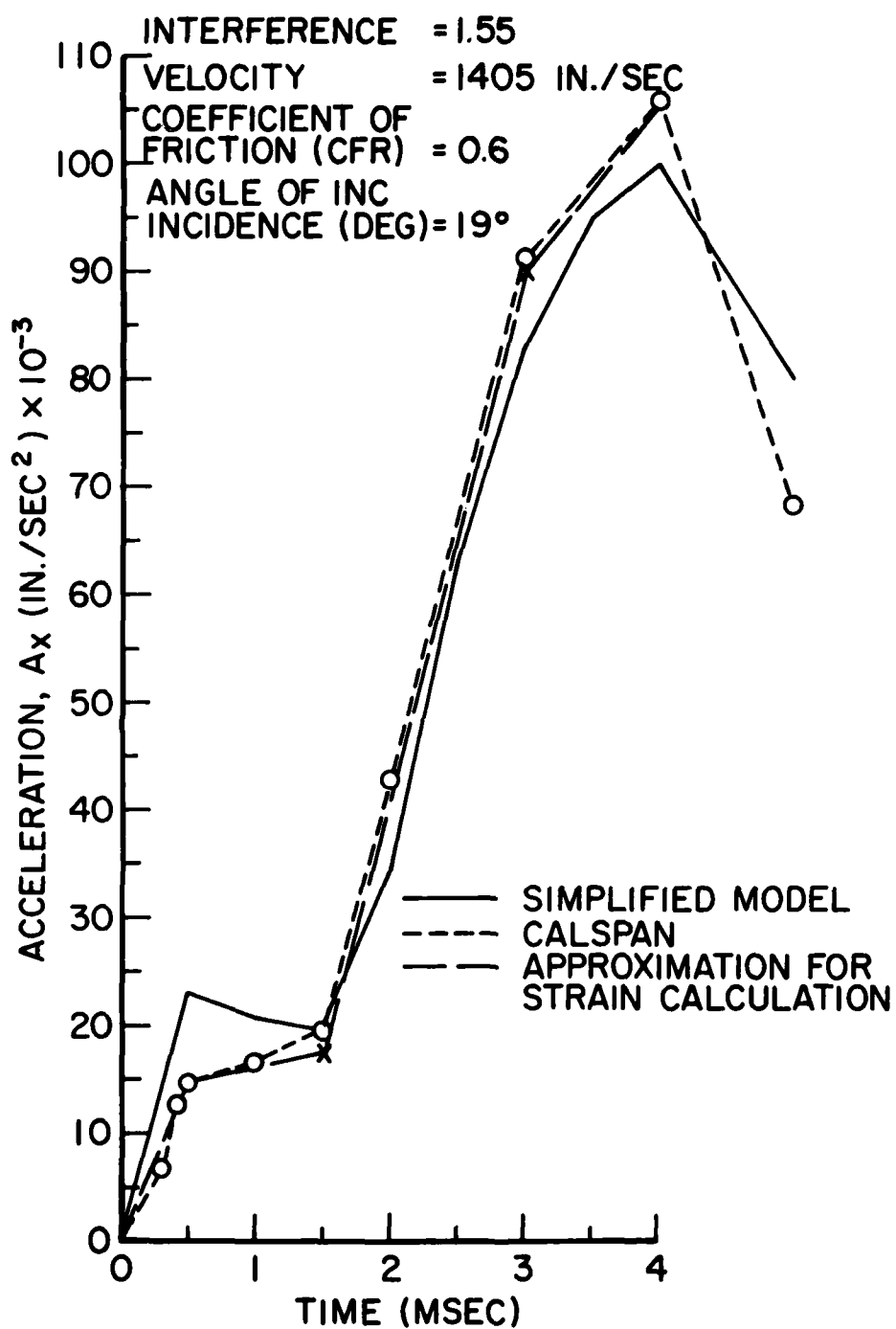


Figure 63. Waveforms for High-Level Birdstrikes.

strain. This occurs because the calculation of strain reflects an integration process which accounts for the effect of waveform.

The results presented are interpreted as justifying the use of the simplified model in conducting further studies. The angular and translational kinematics of the simplified model compare favorably with the results of the ATBM representation at interference levels indicative of tolerable impacts. Additionally, the MSC model, when used with calculated head acceleration, yields maximum strains that are also acceptable. Use of the model at greater interference levels yields maximum strain values that are still conservative.

The calculation of forces and moments at the neck produces values that are considerably higher, in terms of percent error, than exact computation would indicate. However, the values are conservative and the criteria used are those of least reliability.

Efforts were made to revise the model and force it to better "fit" the exact. Variations in mass, mass moment of inertia, and geometry were attempted without success. These suggest that the refinement must entail additional complexity. Since the kinematics are dictated by the skull force, its applied moment, the geometry of the shell, the mass and mass moment of inertia of the helmeted head, and an assumed pivot location relative to the center of gravity and these match without having neck forces match; it is difficult to change any parameter for force fitting that does not destroy the fit of the motion. This indicates that the model must be altered if greater kinetic matching is required. One means of recognizing this is the equation for angular acceleration of a rigid body. This equation is:

$$\Sigma \vec{M}_0 = I_0 \dot{\omega} + \vec{r}_c \times \overline{M \vec{R}_0}.$$

If the pivot point is at the center of gravity, or if the pivot point is not accelerating, we have the familiar

$$\Sigma \bar{M}_0 = I_0 \times \bar{\alpha}.$$

This is the assumption made in using the simplified model. However, if the pivot point does accelerate, there is a second term which must be accounted for. The simplified model does not have a means for achieving this. Is the acceleration of the neck appreciable? From ATBM data for the lower level impact, neck translational acceleration at peak head acceleration is 13.8 g with a peak of 19.86 g one-half millisecond sooner. Should the neck acceleration be accounted for? The only possible way would be to include another body pivoted at both the head and shoulder.

At this point it appears that a more refined model should not be developed. One of the primary goals of the research was to find a simplified model that could be used manually, if necessary, to generate outputs with meaning relative to selected injury criteria. The model selected has reduced the dynamics problem to a series of algebraic equations starting with a force displacement curve and resulting in the calculation of maximum strain. If the model were to have the added complexity of another degree of freedom it is doubtful if the algebraic simplicity could be retained.

If the ultimate goal becomes one of creating an "intermediate" model used with a computer routine, then the addition of another connected body will probably satisfy both kinematic and kinetics requirements. The intermediate model should also be constrained to reflect current geometric and inertial properties of the human. It would still be desirable to have input data that relates to anthropometric measurements. A model evolved just to "fit" may create another set of input data not easily related to the real world.

PARAMETER VARIATION STUDY

One of the primary objectives of the research was the development of the simplified model for future usage. In addition, a

more immediate goal was usage of the model to calculate many parameter variations that would have taken considerable time using the ATBM.

The birdstrike phenomena involve several easily identifiable parameters that are within the capability of the simplified model to analyze. The "bird" (represented by the bump on the inner surface of the canopy) is assumed to have a particular radius of curvature that intersects a constant-radius helmet shell. The bird travels at a velocity having variable magnitude and direction. The impact angle can vary depending upon the shape of the canopy and the depth of the deformation. The speed of the bump varies between a "slow" wave speed and the impact speed of the bird. Additionally, the interference varies and the friction at the intersection is a variable. Finally, the damping coefficient at the "neck" is a variable in that its magnitude depends upon the source of the biomechanical data used.

In conducting the parametric study, the variables were given the values shown in Table 5.

It is important to realize that the combinations of bump size and velocity, as well as surface friction, are only idealizations of the true impact phenomena. The wave motion that sweeps over the helmet shell has a curvature that varies with time. Also, the depth varies with time, which is partially accounted for by specifying the direction of the bump. Additionally, the intersection of bump and shell is assumed to have some longitudinal velocity that creates the need for a frictional force. It is possible that the bump is better characterized by wave phenomena where motion is normal to the surface and not along the surface. Hence the parameters used are idealizations which may or may not adequately represent the true impact. These cannot be evaluated fully without test data.

The initial runs were for the conditions found to be "tolerable" using the ATBM. Variation in impact angle as shown in

TABLE 5. VALUES USED IN PARAMETRIC STUDY

<u>Parameter</u>	<u>Comment</u>
<u>Velocity</u>	
Magnitude 1000, 1405, 2000, 2500, and 3500 in/sec	The speeds were selected to cover the magnitude seen in wave speed analysis.
<u>Angle of Incidence</u>	
Direction 10, 15, 19, 25, and 30°	The direction is indicative of the angle from the horizontal that the bird travels across the helmet.
<u>Interference</u>	
Magnitude 1.05 and 1.55 inches	Based upon ATBM results these were the only values that would possibly result in tolerable responses.
<u>Coefficient of Friction</u>	
Magnitude 0.2 and 0.6 inches	Measured data for phenolic on phenolic span this approximate range.
<u>Radius of Bird</u>	
Magnitudes of 10 and 20 inches	F-16 photographic data indicated radii of these values were seen at locations of impact.
<u>Neck Damping Coefficients</u>	
Magnitudes of 25.3, 77.5, and 100	These span the biomedical damping coefficients of Schneider, et al., and those indicative of a Sierra dummy.

Figure 64 shows a 16 percent change exists in going from a 5-degree to a 30-degree angle of incidence. Variations due to changes in wavespeed are shown in Figure 65. As higher speeds are encountered for a fixed interference, the peak acceleration increases by 20 percent. Hence a change of incidence by a factor of 6 changes the peak acceleration by approximately the same percentage change as a velocity change of three and one-half times. The same variation was examined in terms of strain as shown in Figure 66. Using the approximations shown in Figure 66, the strain increases from 0.00319 to 0.00497. This demonstrates that if a particular clearance is selected to create a tolerable impact,

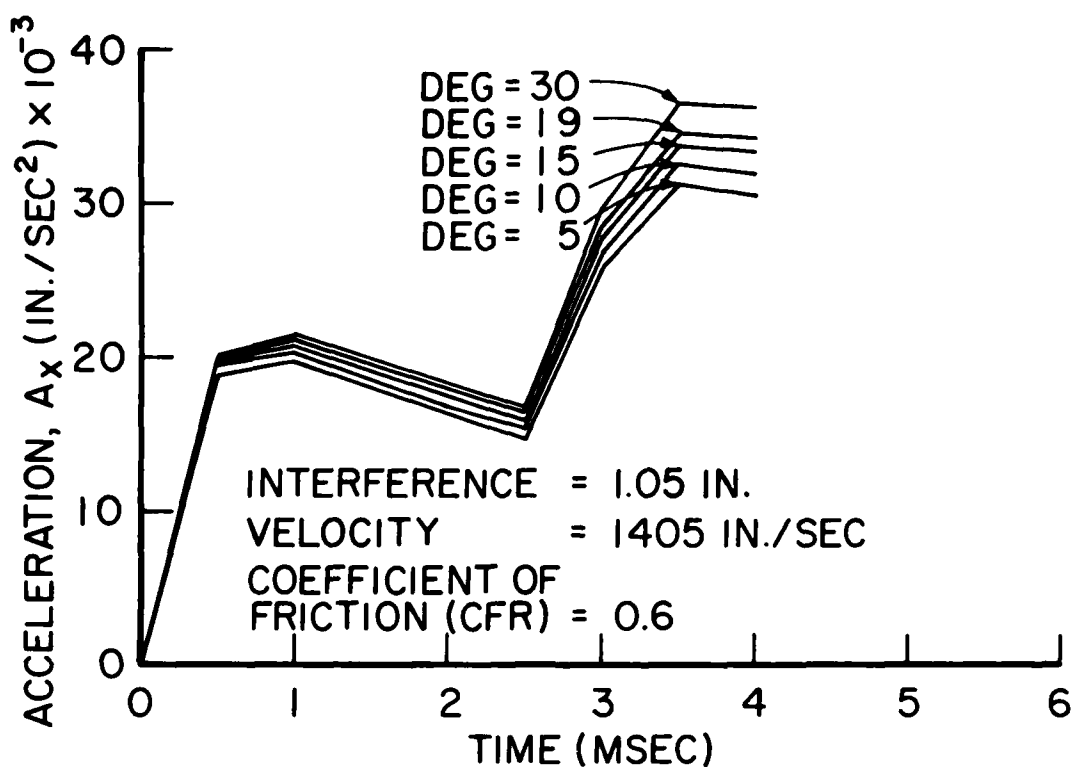


Figure 64. Variations in Acceleration Due to Different Angles of Incidence for 1.05-Inch Interference.

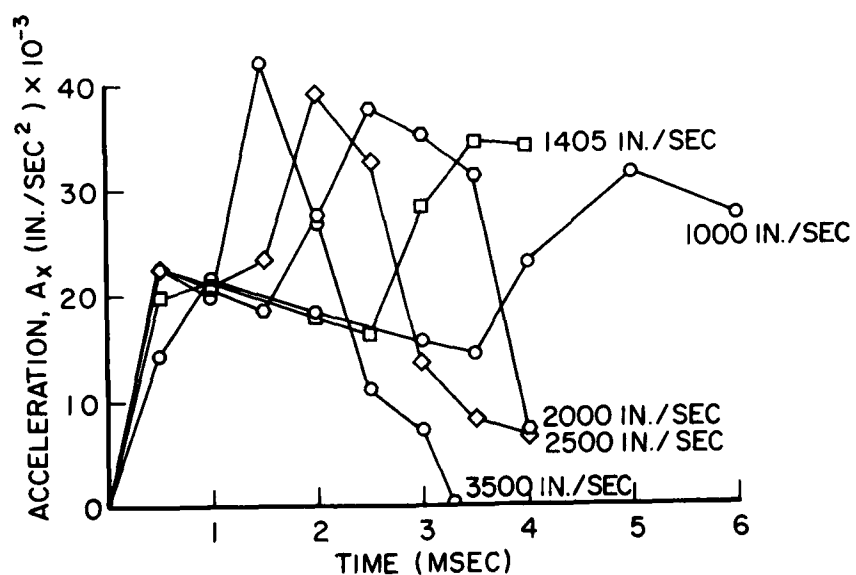


Figure 65. Variations in Acceleration Due to Different Wave Speeds for 1.05-Inch Interference.

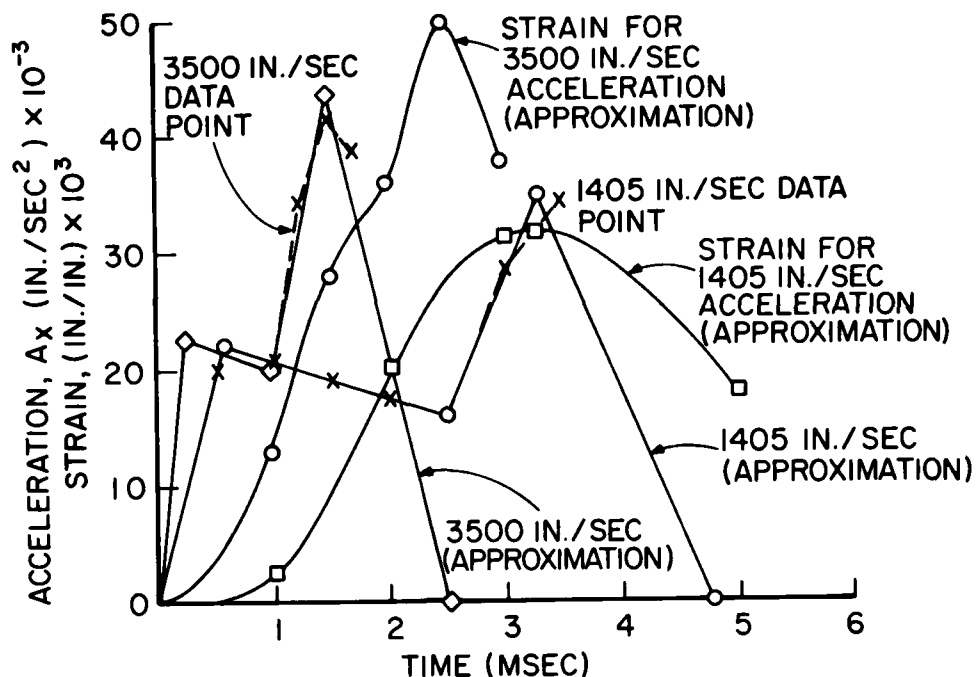


Figure 66. Effects of Wave Speed Upon Maximum Strain for 1.05-Inch Interference.

an increase in wave speed (which could be caused by a slower bird), would create an intolerable condition. However, in order to have the "slower" bird create the assumed bump depth, the head would have to be positioned more closely to the impact point of the bird with the canopy.

Similar variations for the 1.55-inch interference are shown in Figure 67 and 68. For the baseline velocity, changes in incidence angle create a maximum 15 percent increase in acceleration. The change in going from 1405 in/sec to 3000 in/sec creates an increase of 23 percent. These indicate that for the conditions and models assumed, the changes due to incidence and wave speed are approximately the same at both interference levels.

Variations due to changes in frictional coefficient are shown in Figures 69 and 70. The percent change due to incidence at the reference velocity is 35 percent which indicates that at low coefficients of friction, the acceleration response is more

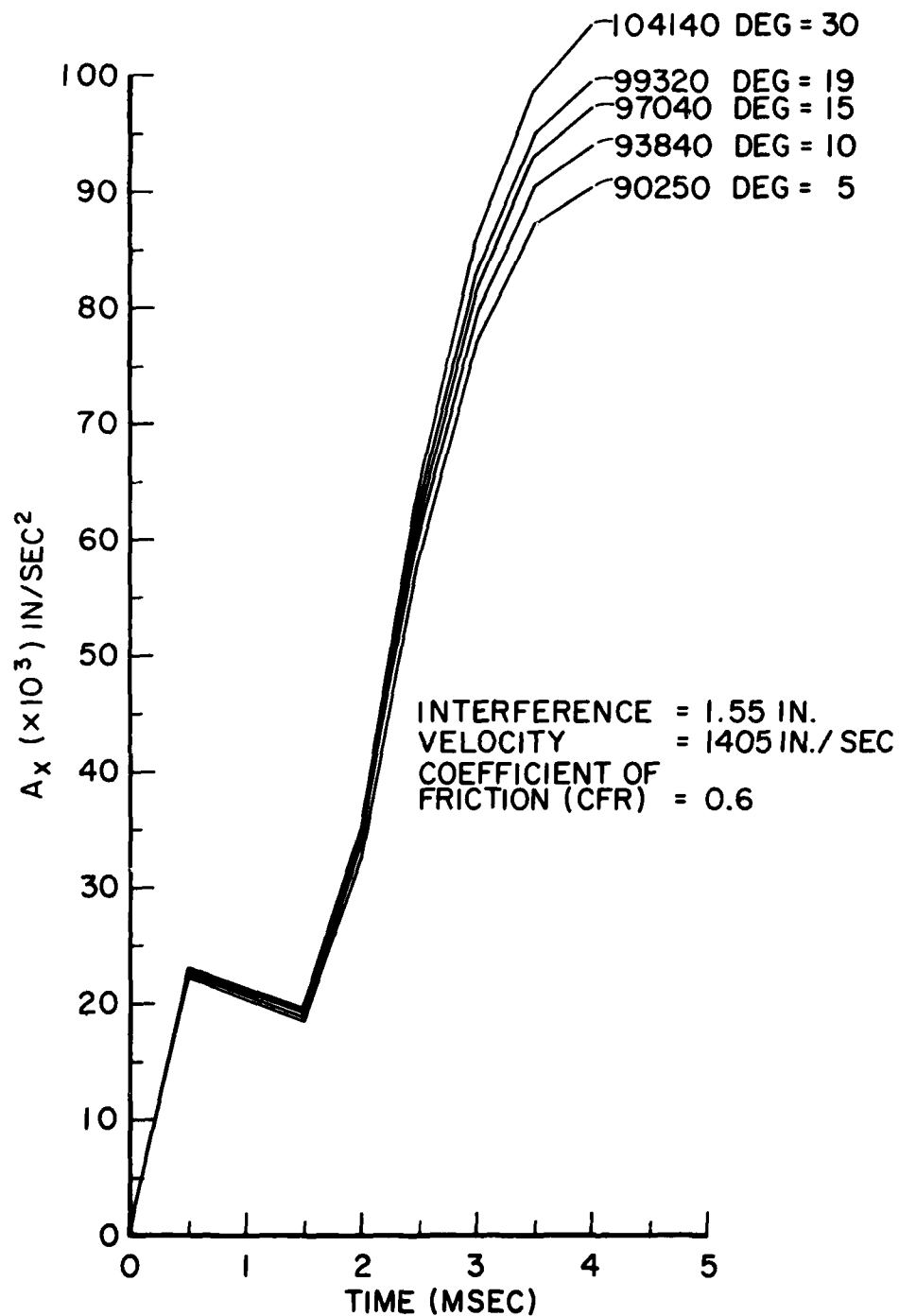


Figure 67. Variations in Acceleration Due to Different Angles of Incidence for 1.55-Inch Interference.

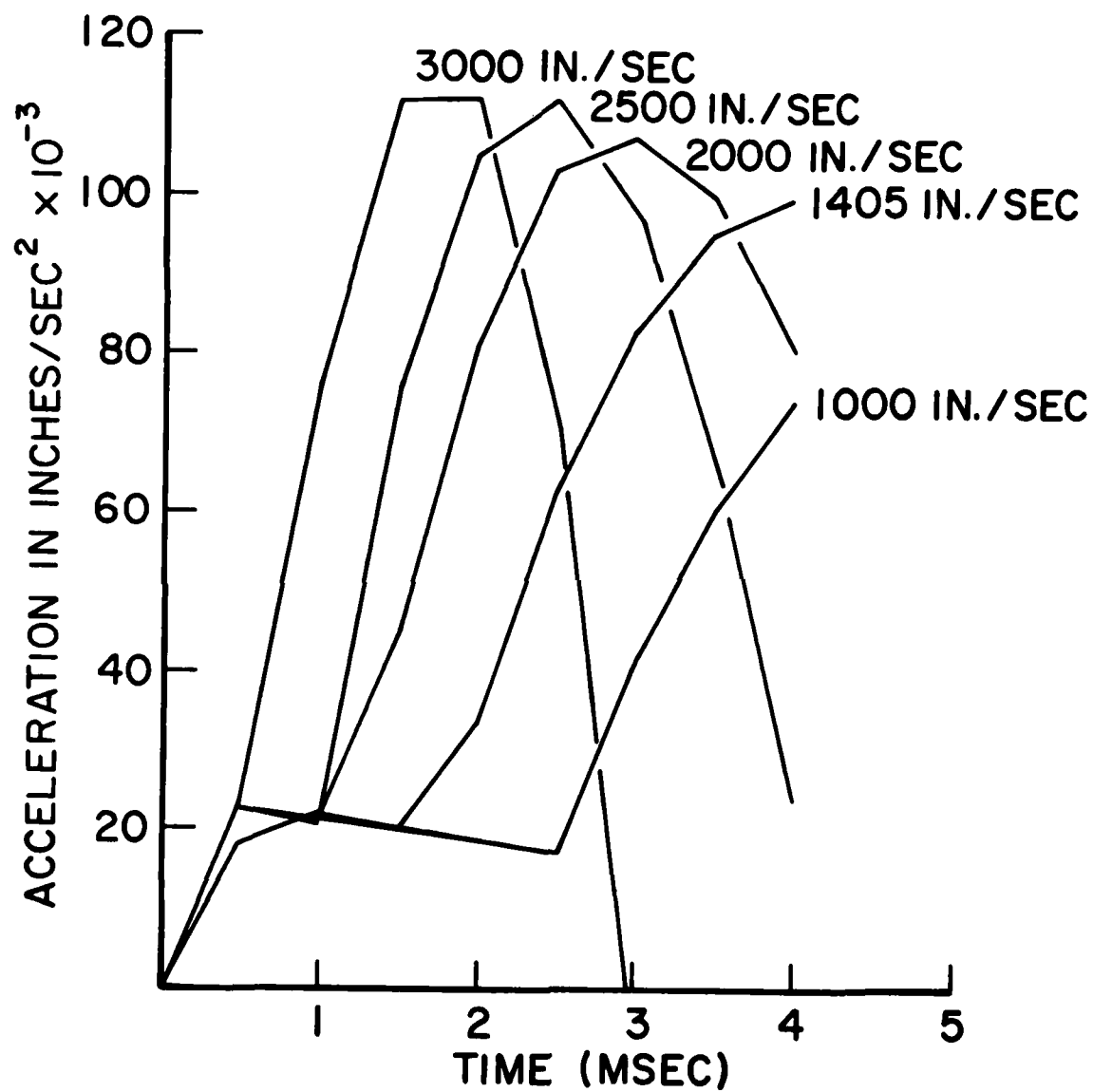


Figure 68. Variations in Acceleration Due to Different Wave Speeds for 1.55-Inch Interference.

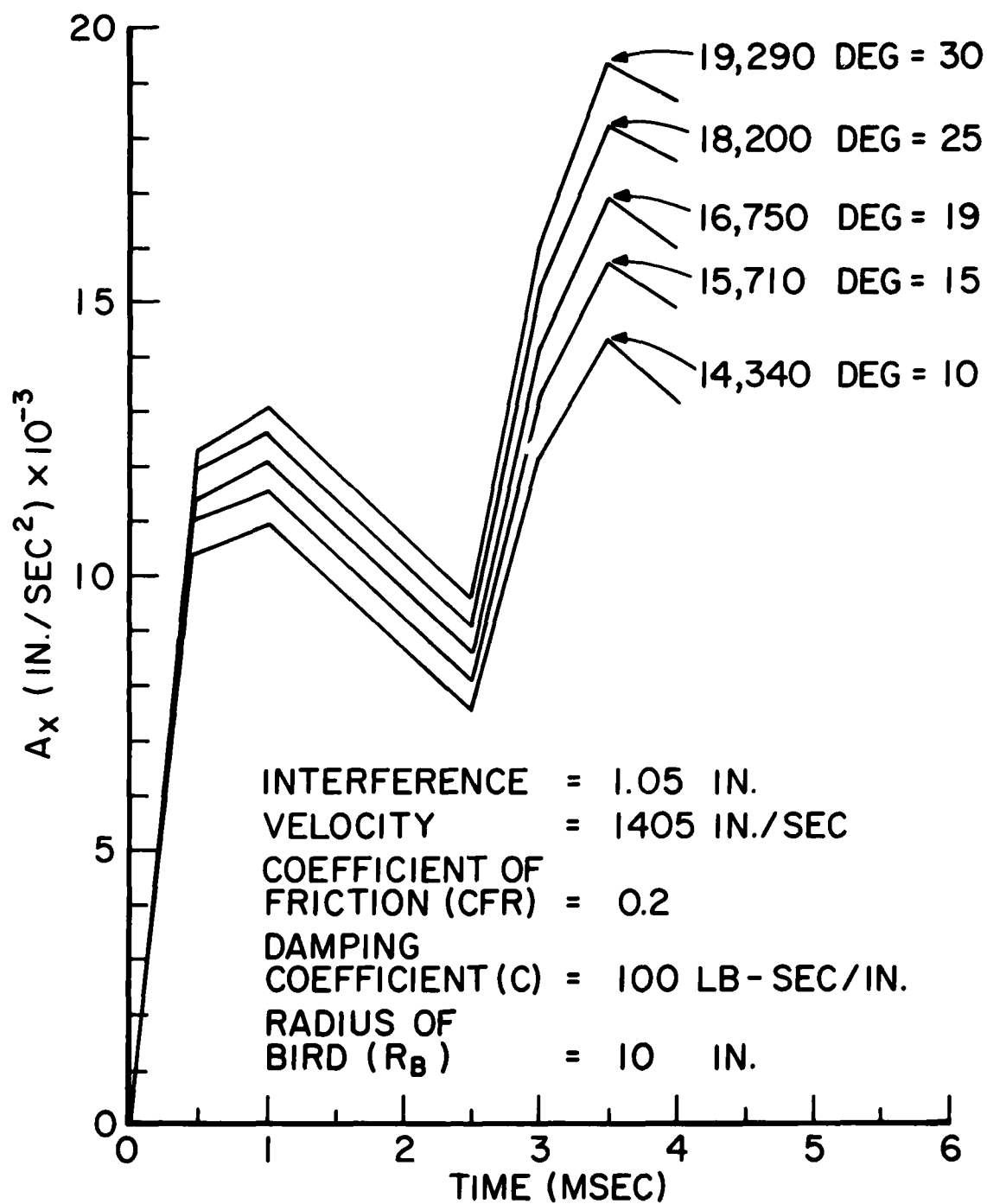


Figure 69. Variations in Acceleration Due to Different Friction Coefficients for 1.05-Inch Interference.

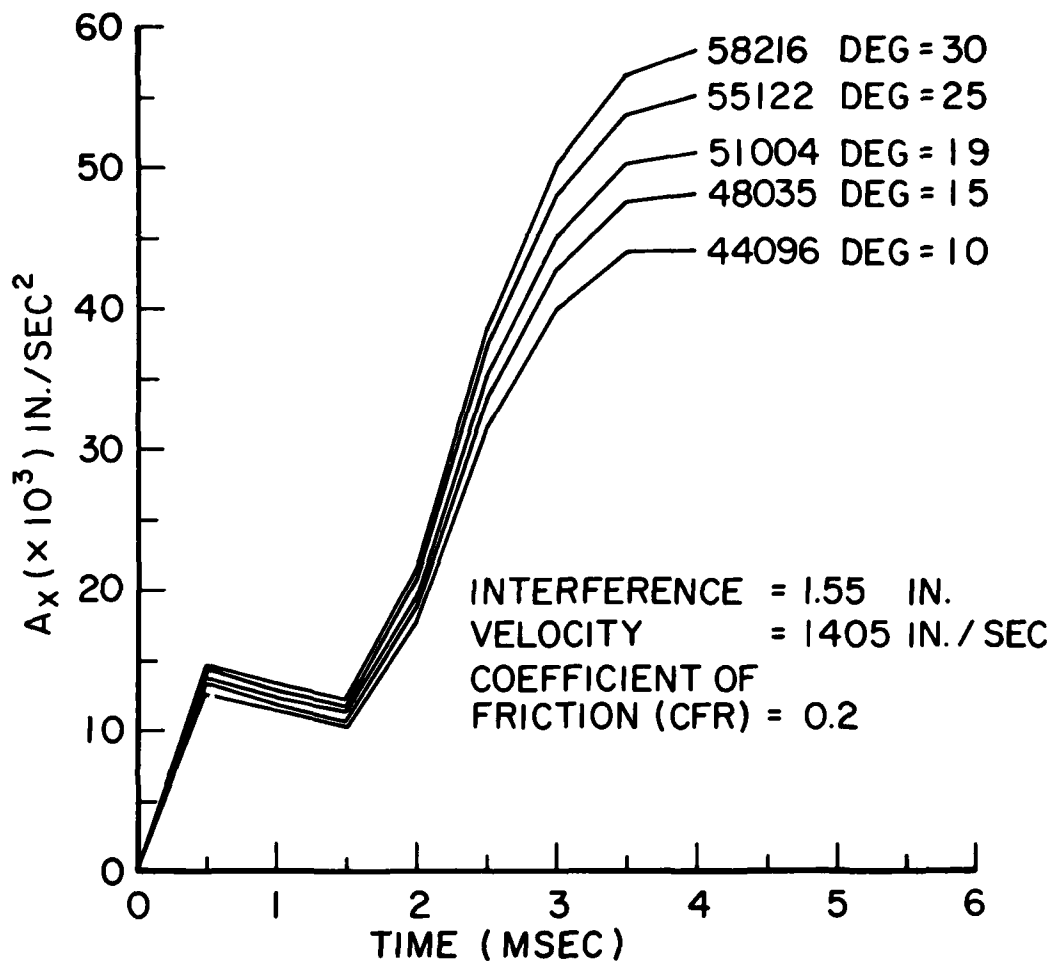


Figure 70. Variations in Acceleration Due to Different Friction Coefficients for 1.55-Inch Interference.

sensitive to changes in incidence angle. This is true at the higher velocity also. Of greater interest is the fact that the reduction of the friction coefficient by a factor of three reduces the baseline condition acceleration by 52 percent.

If the wave speed is increased to the maximum of 3500 in/sec, a peak acceleration of 25,394 does not create an intolerable condition. However, if the interference is 1.55 inches and the coefficient of friction is 0.2, even the lowest wave speed is

intolerable. Hence a decrease in acceleration caused by a reduction in the coefficient of friction by a factor of three, can be offset by an interference increase of one-half-inch.

Figure 71 indicates the effect of increasing the bird radius by a factor of two. The large radius increases the duration of the acceleration pulse, but the peak acceleration is decreased by only 6 percent. These are indicative of the effects of bird radius at other conditions also.

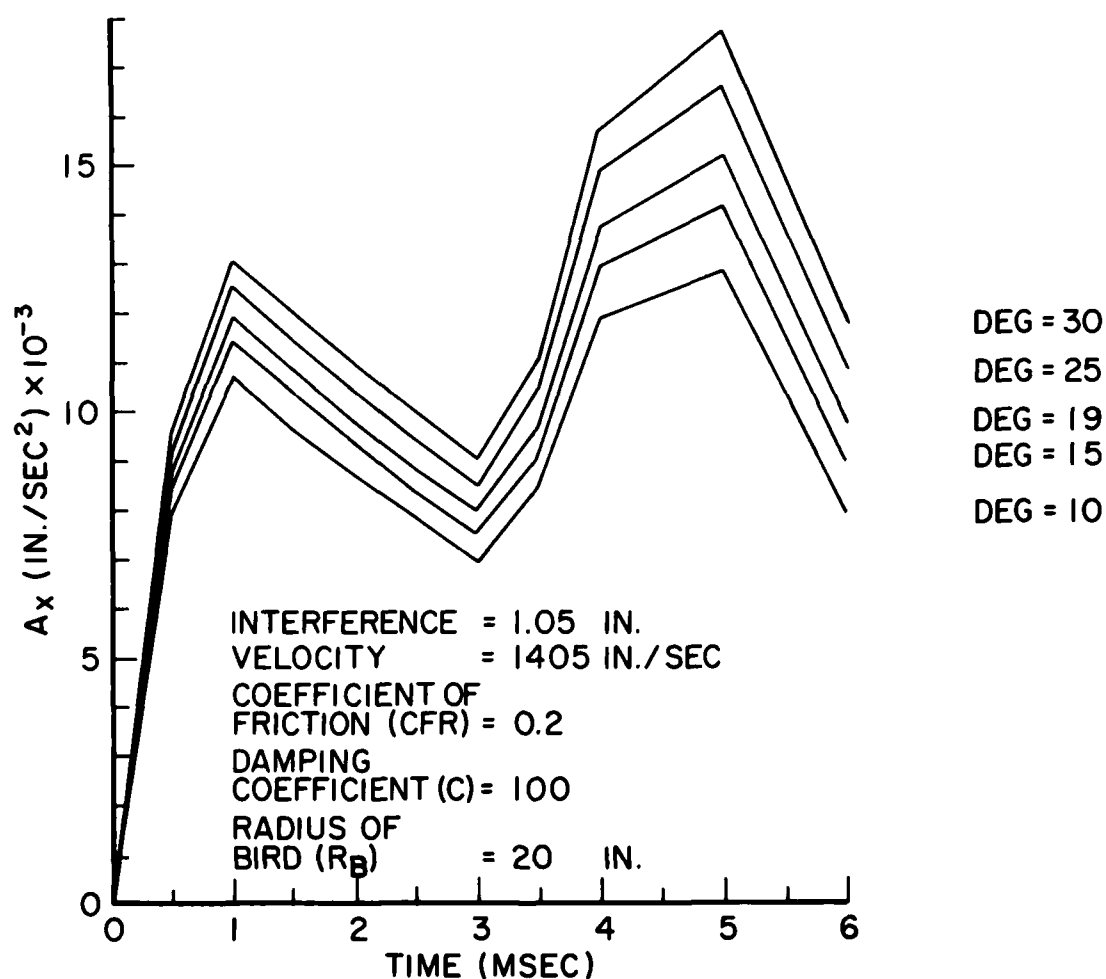


Figure 71. Effect on Duration of Acceleration Pulse and on Peak Acceleration of Increasing Bird Radius by a Factor of Two (to 20-Inch Radius of Canopy Bump).

The final parameter of interest was the neck damping coefficient. Variations are shown in Figure 72. A change in neck damping of minus 25 percent creates a plus 6 percent change in peak acceleration, and a damping change of minus 75 percent creates a peak acceleration change of plus 24 percent.

In summarizing the results of the parametric study, the variables and the percent change are given in Table 6.

TABLE 6. PERCENT CHANGE OF PEAK ACCELERATION
DUE TO VARIATION IN PARAMETERS

<u>Variation in Parameters</u>	<u>Peak Acceleration Change</u>
<u>Velocity</u>	<u>Approximate</u>
Magnitude change from 1000 to 3500 in/sec	+20 to +23 percent
Direction range from 5° to 30°	+10 to +35 percent
<u>Interference</u>	
Magnitude change from 1.05 to 1.55 in.	+175 to +205 percent
<u>Coefficient of Friction (CFR)</u>	
Magnitude change from 0.2 to 0.6 in.	+52 percent
<u>Radius of Bird</u>	
Magnitude change from 10 to 20 in.	-6 percent
<u>Neck Damping Coefficient</u>	
Magnitude change from 25 to 100 in-lb/sec.	-24 percent

The tabulated results indicate that an increase in any variable generally creates an increased peak acceleration, which is intolerable. The only exception is the neck damping coefficient, which indicates that if the coefficient is reduced there is less resistance to motion for a given applied moment, which results in an increased acceleration. The results are indicative of a

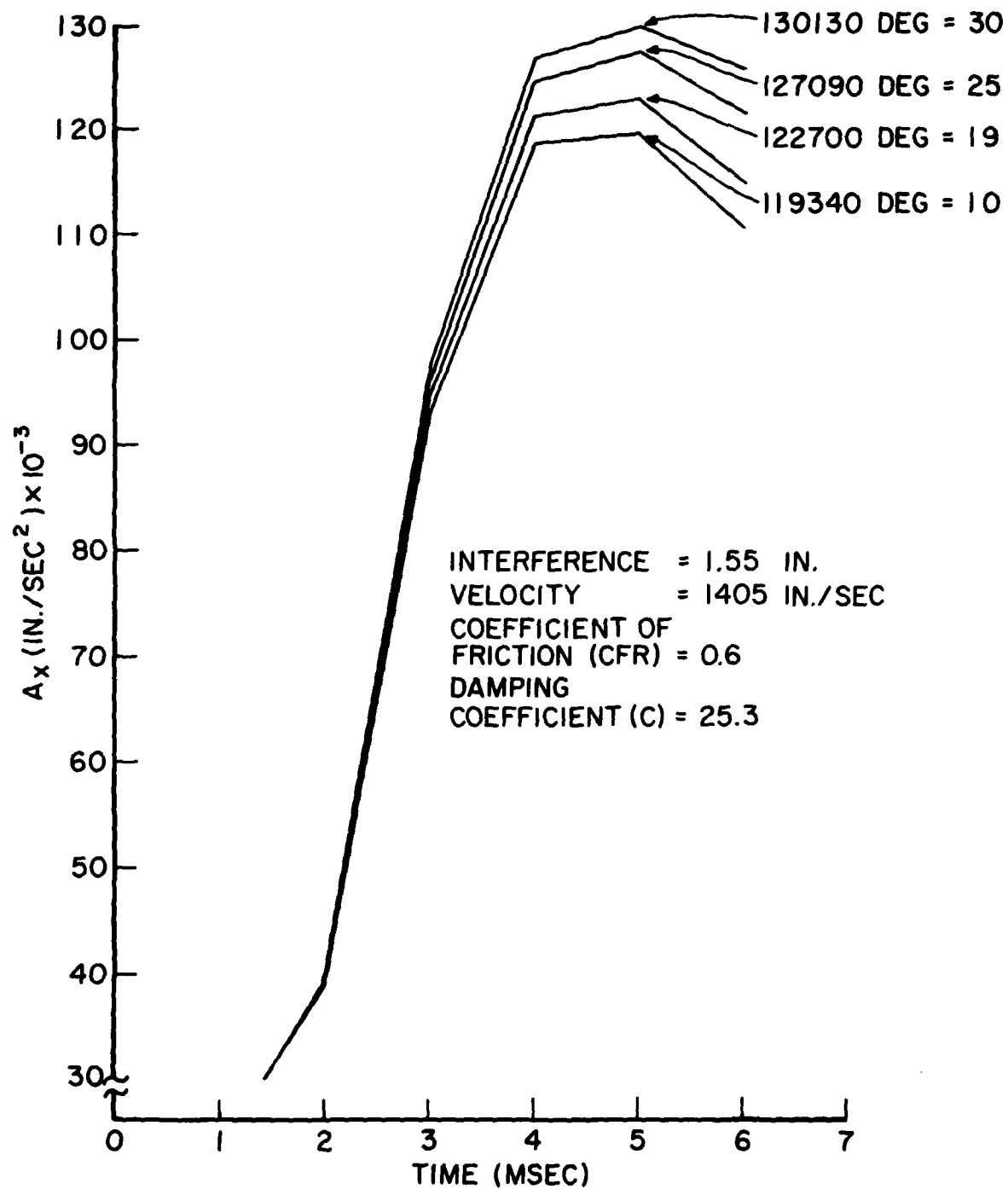


Figure 72. Effect of Changing Neck Damping Coefficient on Peak Acceleration.

selected range of each variable, for the related data available on the F-16 from phenolic data, and from biomechanics and dummy data. Absolute changes of one-half inch in interference create responses that are unequivocally intolerable regardless of the criterion of evaluation.

SECTION 7

DEVELOPMENT OF AIRCREWMAN SIMULATION FOR TESTING

INTRODUCTION

Another goal of the research was to develop an apparatus that could be used in impact tests of aircraft canopies to measure the forces acting upon the crewman during helmet impact. Much of the work accomplished had analytically provided a better understanding of the impact phenomena, but some means of measurement was required to validate or refute the assumptions inherent in the models used.

The problem is not unique in that many other experiments have been conducted where it was desirable to measure directly an impact force without influencing the experiment. In this particular environment, the canopy impacts the helmet and it is desired to measure the impact force for direct comparison with the injury criteria. Similarly, that would be desirable for the neck. Hence, what is needed is an instrumented helmeted head which could generate the same inertial response as the human, while providing adequate kinetic data to completely define the response. This is equivalent to requiring the measurement of impact force, skull acceleration, and neck force, without knowing exactly where the impact will occur.

From the anthropometric study and the bird impact films, it is apparent that the location of the impact between canopy and helmet can vary, and the specific location on the helmet can vary. Hence the impact point location on the canopy or helmet is not a fixed location. A transducer location cannot be specified even if we had a flexible, wireless, large-area sensor to apply to either canopy or helmet. Consequently, the direct measurement of the impact force seems to be a difficult task.

Another measurement desired is that of skull acceleration. This fortunately can be obtained from using anthropometric dummies which have accelerometer mounts provided within the "skull." If the anthropometric head and neck system provides realistic response, the accelerations are reasonable approximations to those the human

would experience. This provides a step in the right direction in that if neck forces can be measured, the combination of neck force and inertial response implies the impact force required. If the skull responds as a rigid body acted upon by an impact force, and reacted upon by a neck force, then the difference is the inertial response vector of head mass times acceleration.

The discussion above establishes the philosophy of the design of the test apparatus. It is assumed that direct measurement of the impact forces is virtually impossible. Therefore, measurements must be made which can establish indirectly what the force had to be. This, along with the neck force and head accelerations, can then be compared with injury criteria.

PRELIMINARY TEST HARDWARE DESIGNS

A test device was required for tests conducted prior to complete analysis of the films of birdstrike data. Based upon the philosophy established, a test device was designed to measure forces and moments at the neck of an anthropometric dummy. Accelerations at the skull and neck were also measured. The device schematically is as shown in Figure 73.

Six load cells pin-connected to a rigid plate provide the means of calculating the forces and moments at the neck attachment point. The design criteria were established by examining the then-existing test and analytical data. From drop test data of helmets, peak forces of 6000 pounds had been calculated. Additionally, from F-111 information it was anticipated that the motion of the head was dominated by rotational response about the neck/shoulder pivot point. By assuming a forcing function of 600-pound plateau force for 0.0025 seconds followed by an 0.007-second rise to 6000 pounds, the response for a pivoted helmeted head was calculated. The response at the 6000 pound force is shown in Figure 74.

The accelerations calculated are approximately 114 g which compared favorably with the measured head accelerations of one F-111 test.

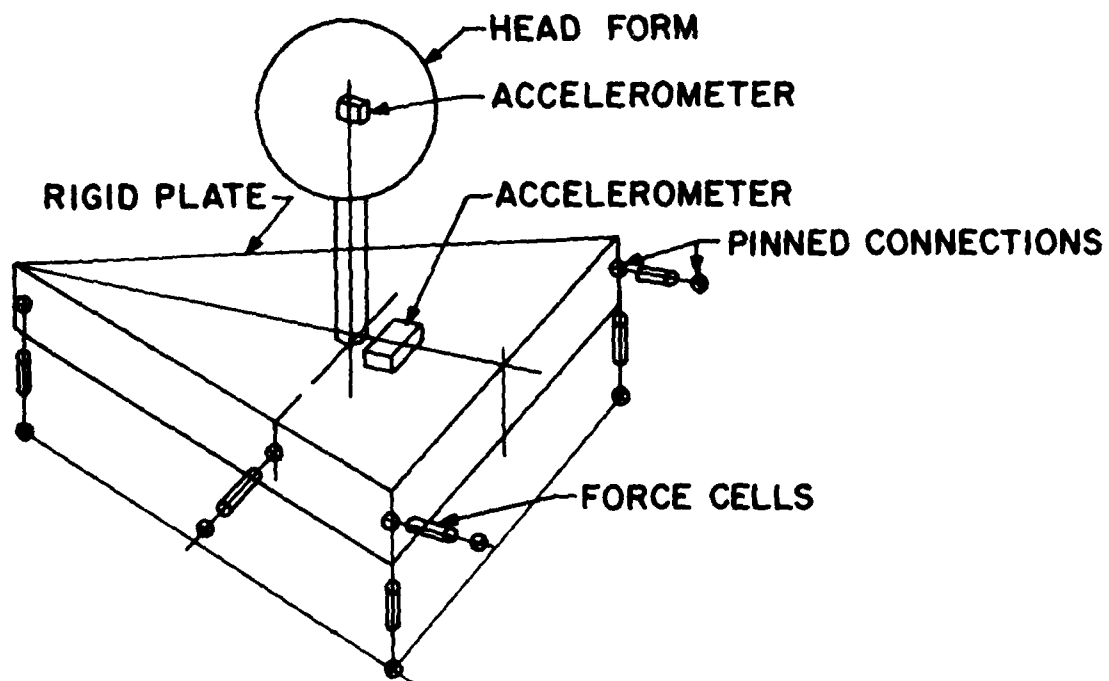


Figure 73. Schematic of Head-Neck Test Device.

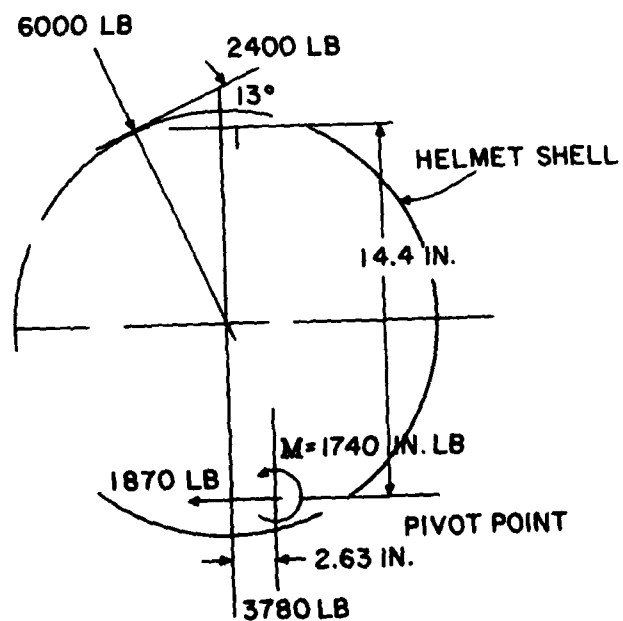


Figure 74. Calculated Head Response to 6000-Pound Impact Normal to Surface of Helmet.

Using the forces and moments found it was easily possible to develop a plate supported by pin-connected load cells. The original concept was based upon the use of 1000-pound load cells but 2500 and 5000-pound cells were available which provided a greater margin of safety. The final design, shown in Figure 75, was completed and fabricated by Air Force personnel. After fabrication, the system was calibrated by applying 1000 pounds along each of the axes of the plate as well as through a fixed point 8 inches above the surface of the plate. In this manner, load cell outputs were collected for all pure axial forces as well as axial force plus moment. By examining the outputs for pure axial load first and calculating the linear coefficients for forces alone, it was then possible to extract the force effects from the combined loads data and evaluate the coefficients for pure couples about each axis. The results of the analysis are shown in the following in matrix form.



Figure 75.

$$\begin{bmatrix} D_1 \\ D_2 \\ V_1 \\ V_2 \\ V_3 \\ S \end{bmatrix} = \begin{bmatrix} +0.462 & -0.299 & -0.023 & -0.003 & +0.000 & +0.047 \\ +0.474 & +0.350 & -0.015 & -0.002 & +0.000 & -0.047 \\ -0.002 & +0.001 & -0.384 & +0.047 & -0.047 & +0.000 \\ -0.013 & +0.001 & -0.413 & -0.048 & -0.044 & +0.000 \\ -0.011 & +0.002 & -0.197 & +0.006 & +0.100 & +0.000 \\ +0.007 & 0.937 & -0.001 & +0.000 & +0.000 & +0.000 \end{bmatrix} \cdot \begin{bmatrix} X \\ Y \\ Z \\ M_X \\ M_Y \\ M_Z \end{bmatrix}$$

This indicates that the load cell outputs are possible functions of each applied force and couple. By inverting the matrix and eliminating insignificant terms, the relations desired are shown in the following matrix. Hence for any given time that all cells are read, the axial force and couple that exist at the plate surface are found by summing the appropriate terms. The terms that are near unity should theoretically be unity. Those near ten, should be ten; and the values -1.830 and +8.34 should (theoretically) be -2.55 and +6.70. However, the values tabulated reflect all aspects of the misalignments, tolerances, and reading errors inherent in the system.

$$\begin{bmatrix} X \\ Y \\ Z \\ M_X \\ M_Y \\ M_Z \end{bmatrix} = \begin{bmatrix} 1.071 & 1.071 & 0 & 0 & 0 & -0.059 \\ 0 & 0 & 0 & 0 & 0 & 1.067 \\ 0 & 0 & -0.929 & -0.929 & -0.843 & 0 \\ 0 & 0 & 10.757 & -10.295 & +0.526 & 0 \\ 0 & 0 & -1.830 & -1.830 & +0.834 & 0 \\ 10.465 & -10.319 & 0 & 0 & 0 & 7.362 \end{bmatrix} \begin{bmatrix} D_1 \\ D_2 \\ V_1 \\ V_2 \\ V_3 \\ S \end{bmatrix}$$

TEST RESULTS USING FIRST GENERATION DEVICE

Data from four impact tests conducted by General Dynamics, Fort Worth, were available for analysis. The tests were conducted using a 5/8-inch-thick coated canopy, and a 4-pound bird.

Only two tests, conducted at 319 and 365 knots, were reduced because only these two produced appreciable measured response. Data channels available were accelerations in three axes at the head and support plate, and all six force cells. Unfortunately, the exact location of the helmet relative to the canopy, and the type of helmet and liner were not available.

From the record it is apparent that the response of the head was dictated not just by the birdstrike, but by the structural response of the entire test system. The bird impact causes a structural response in the head/neck test device well before the canopy bump hits the helmet. For analysis the point of maximum acceleration was examined. The data were as shown in Tables 7 and 8 where (C) signifies compression; (T) tension; and the cells

TABLE 7. COMPUTATION OF LOAD CELL FORCE MAGNITUDES

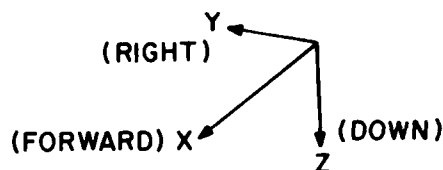
<u>Load Cells</u>	<u>Measurement</u>	<u>Calibration</u>	<u>Magnitude</u>
No. 1	0.20 cm (C)	393.7 lb/cm ($\times \frac{0.60}{0.58}$)	- 81.46 lb
No. 2	0.05 cm (T)	1968.5 lb/cm ($\times \frac{0.56}{0.58}$)	+103.99 lb
No. 3	0	6	0
No. 4	0.25 cm (C)	985.3 lb/cm ($\times \frac{0.27}{0.56}$)	-118.76 lb
No. 5	0.25 cm (C)	985.3 lb/cm ($\times \frac{0.58}{0.56}$)	-255.122 lb
No. 6	0	0	0

TABLE 8. COMPUTATION OF ACCELERATION MAGNITUDES

<u>Head Acceleration</u>	<u>Measurement</u>	<u>Calibration</u>	<u>Magnitude</u>
X	0		0
Z	1.40 cm (D)	73.22/0.3x($\frac{1}{254}$)	134.53 g
Y	0.20 cm (R)	71.57/1.28x($\frac{1}{254}$)	20.13 g
<u>Plate Acceleration</u>			
X	0.1 cm (A)	90.78/0.29x($\frac{1}{254}$)	12.32 g
Z	0.2 cm (U)	85.25/0.20x($\frac{1}{254}$)	22.37 g
Y	0		0

are S , V_3 , V_1 , X_1 , X_2 , and V_2 to correspond to the matrix values. The calibration values are those provided by a calibration pulse and corrected by the millivolt/millivolt correction factor. Using the matrix evolved from calibration data, the forces and moments at the neck are:

$X = -395.5$ pounds
 $Y = -86.9$ pounds
 $Z = -87.7$ pounds
 $M_X = 54.7$ inch-pounds
 $M_Y = 867.3$ inch-pounds
 $M_Z = 757.5$ inch-pounds



Therefore, since the plate acceleration is dictated by the above forces and the neck forces, $\Sigma \bar{F} = m\bar{a}$, the forces due to the neck are:

$X = -735$
 $Y = +87$ (Based upon a 27.6-pound plate.)
 $Z = +694.$

Assuming a 16-pound head, and using the head accelerations;

$X_{HEAD} = -735$ pounds
 $Y_{HEAD} = +233$ pounds
 $Z_{HEAD} = +1455$ pounds.

The head is being acted upon by the canopy with forces of -735 pounds, 233 pounds, and 1455 pounds. The forces X and Z indicate a resultant force generated by visor and liner crush. The film data indicated a 1-1/4-inch interference and although the exact force displacement curve of the visor and liner was not known, previous work had indicated that if crush exceeded about 3/4 inch, force levels would be greater than the 500-pound plateau level. The exact force would depend upon the thickness of the liner at impact, and the strength capability of the visor.

This test is interesting in that the neck is in tension. It is being pulled downward by the motion of the plate which is responding to the initial bird impact on the canopy. However, the tensile force is not sufficient to pull the head down fast enough to create the measured acceleration. Therefore, additional forces must be generated by the canopy/helmet impact. This leads to the question of whether or not the test device should be isolated from the canopy test hardware, or is the response seen indicative of the true impact environment. The plate responds to a relatively high frequency input, whereas the true head and neck is supported by a low frequency torso on a seat cushion. Therefore, the revised design isolates the head from the plate by having sufficient elasticity to create a 10-Hz fundamental. This then duplicates data which indicates the torso response to be around 6 to 10 Hz depending upon the vibrational or transient reference used.

As a means of comparison, the same run was examined using a theoretical calibration matrix. The results are:

<u>Theoretical</u>	<u>Measured Calibrations</u>
Head Forces (pounds)	(pounds)
X - 714	-735
Y + 238	+233
Z + 1429	+1455

The test conducted at 319 knots generated forces of -949 pounds, -821 pounds, and +390.5 pounds for X, Y, and Z, respectively. This implies that the flow was on the other side of the head and that the resultant force was about two-thirds that of the more severe test. Additionally, both runs generated forces in excess of that required to fracture a skull, with neck forces that are excessive, and accelerations that exceed "tolerable" based upon average acceleration and a pulse duration of 2 msec. Film data for this shot were not available.

ADDITIONAL MEASUREMENT TECHNIQUE

During the development of the head/neck device additional attempts were made to develop "passive" sensors. One approach was that of using the head/neck system as a sensor. Could the translational and rotational motion of the head be used to determine the forces and moments generated at the neck attachment point? Could the head and neck be calibrated to infer neck loads? The following was conducted prior to the availability of an exact description of the test environment. It was assumed that photographic equipment would be available, and that space in the test environment would permit the cameras to be located as ideally required. This assumption never did become realized and hence the technique was never used. However, the approach and the results are presented for future consideration.

If forces are applied to the head it translates and rotates depending upon the stiffness about three axes. It may translate laterally and rotate about one or several axes. Consequently, if one point on the head were observed from the front or top, it might appear to remain fixed while in fact it had translated sideways and then rotated in such a manner to return the point to its original position as viewed from the front or top. Additionally, we would like to be able to apply forces and moments in such a manner that we could eventually relate displacements seen photographically to unknown applied forces and moments.

A head is shown in Figure 76 in its original position and some displaced position. Two coordinate systems exist as shown by the coordinate vectors \bar{i} , \bar{j} , \bar{k} , as originally, and as displaced \bar{i}^1 , \bar{j}^1 , \bar{k}^1 . The classical way to relate these is through Euler angles. In other words, in order to locate the body after displacement there are translations Δx , Δy , Δz , and rotations ψ , θ , and ϕ about the original x , y , z coordinates.

If some point "A" is followed from one position to the next it can be shown that the distances A_x , A_y , and A_z seen photographically are as follows.

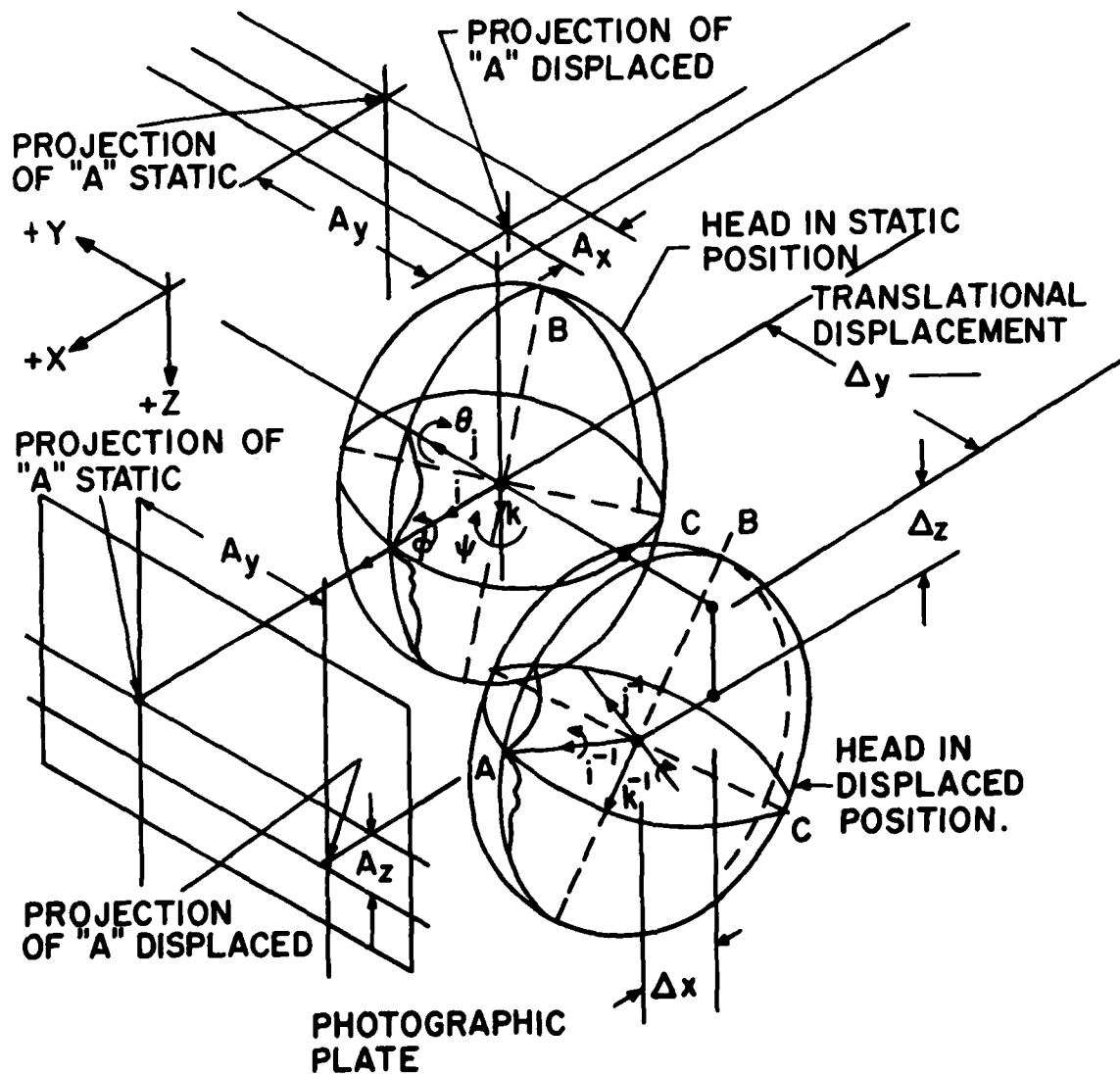


Figure 76. Motion of Fixed Points Due to Translational and Rotational Motion of the Head.

$$\begin{aligned}
A_x &= \Delta x + A \cos \theta \cos \psi \\
A_y &= \Delta y + A \cos \theta \sin \psi \\
A_z &= \Delta z - A \sin \theta
\end{aligned}$$

where Δx , Δy , Δz , are translations of the center of gravity, ψ , θ , ϕ , are rotations about the original axes. If the center of gravity travels down, Δz , but rotates upward, $A \sin \theta$, it is possible there would be no apparent motion of the point A.

The photograph of one point A would give you A_x , A_y , and A_z , to solve for six unknowns, Δx , Δy , Δz , ψ , θ , ϕ . Therefore, two points are a minimum. The other could be at the top of the head, B, and its components would be:

$$\begin{aligned}
\beta_x &= \Delta x + \beta (\cos \phi \sin \theta \cos \psi + \sin \phi \sin \psi) \\
\beta_y &= \Delta y + \beta (\cos \phi \sin \theta \sin \psi - \sin \phi \cos \psi) \\
\beta_z &= \Delta z + \beta \cos \phi \cos \theta.
\end{aligned}$$

This would theoretically do it, but practically, some of the angles are very small and difficult to evaluate. Consequently, another point is desired. If a point were located on the ear at "C", then the last set of equations would be:

$$\begin{aligned}
C_x &= \Delta x + C (\sin \theta \sin \phi \cos \psi - \cos \psi \sin \psi) \\
C_y &= \Delta y + C (\sin \phi \sin \theta \sin \psi + \cos \phi \cos \psi) \\
C_z &= \Delta z + C \sin \psi \cos \theta.
\end{aligned}$$

All values A_x , B_x . . . B_z , C_z , are values taken off of the photograph and are the horizontal and vertical distances from the original references. By using these where appropriate, or in all equations for a check, the unknown displacements and rotations are found. Three points on the head, all orthogonal to one another, are necessary.

As a known force, or moment, is applied to the head, the head moves from its initial reference position as dictated by the stiffness of the neck and the location and magnitude of the force. Applied forces of up to 50 pounds were applied to the system shown in Figure 75 in order to evaluate the response. Photographs were taken from three orthogonal planes and the necessary measurements of reference point motion measured. Because of the small angles involved it is possible to manually iterate through the nonlinear equation and find an approximate solution.

To improve the solution calculation procedure, a digital program was written to minimize the total error associated with the equations at each reference point being considered. That is, an error function was established capable of utilizing 18 nonlinear equations depending upon those desired by the analyst. A typical output is shown in Figure 77. The top of the figure indicates the 18 possible observable dimensions. If 13 points seemed to be reasonably measurable, then 13 are entered for optimization. The routines then calculate the displacements and rotations necessary to minimize the "error" for the equations of motion for two observed positions.

Two test series of static calibrations were run with loads of 10, 20, and 50 pounds applied rearward and sideways with replicates. The results indicated that the selection of the number of equations did influence the calculated response, but that the variation was small, less than 6 percent. Also, the deformation was approximately linear with applied load and generated a neck stiffness of 13.1 inch-pounds per degree versus 17.2 for the Calspan representation, and 17.6 from Schneider.

No further testing was conducted on the head/neck segment since the use of the approach was abandoned. It was realized that the practical considerations of the test environments would not permit the required photographic test setup to be used. If the procedure should be pursued, calibration tests should be conducted to measure the stiffness dynamically under controlled

LIST OF EQUATIONS					
1-A1X	2-A1Y	3-A1Z	4-B1X	5-B1Y	6-B1Z
7-C1X	8-C1Y	9-C1Z	10-B2X	11-B2Y	12-B2Z
13-A2X	14-A2Y	15-A2Z	16-C2X	17-C2Y	18-C2Z
ENTER THE NUMBER OF EQUATIONS TO BE USED-----:			13		
ENTER THE CODE OF EACH EQUATION TO BE USED-----:			1,2,3,4,5,6,7,9,10,11,12,13,14		
ENTER THE MEASURED VALUE OF A1X-----:			3.27		
ENTER THE MEASURED VALUE OF A1Y-----:			0.386		
ENTER THE MEASURED VALUE OF A1Z-----:			-0.486		
ENTER THE MEASURED VALUE OF B1X-----:			-1.108		
ENTER THE MEASURED VALUE OF B1Y-----:			0.048		
ENTER THE MEASURED VALUE OF B1Z-----:			-4.595		
ENTER THE MEASURED VALUE OF C1X-----:			-0.324		
ENTER THE MEASURED VALUE OF C1Z-----:			-0.027		
ENTER THE MEASURED VALUE OF B2X-----:			-1.081		
ENTER THE MEASURED VALUE OF B2Y-----:			-1.253		
ENTER THE MEASURED VALUE OF B2Z-----:			-4.486		
ENTER THE MEASURED VALUE OF A2X-----:			0.0		
ENTER THE MEASURED VALUE OF A2Y-----:			0.145		
ENTER THE VALUE OF AA-----:			3.75		
ENTER THE VALUE OF BB-----:			-4.5		
ENTER THE VALUE OF CC-----:			-2.5		
ENTER THE VALUE OF AX-----:			2.07		
ENTER THE VALUE OF AZ-----:			-2.97		
ENTER THE VALUE OF BY-----:			-1.417		
ENTER THE VALUE OF BZ-----:			-4.417		
ENTER THE INITIAL VALUES OF X,Y,AND Z-----:			0,0,0		
ENTER THE INITIAL VALUES OF THETA, PHI,AND PSI----			0,0,0		
THE VALUE OF X IS-----:			-0.723086		
THE VALUE OF Y IS-----:			-0.160714		
THE VALUE OF Z IS-----:			0.003988		
THE VALUE OF THETA IS-----:			8.635952		
THE VALUE OF PHI IS-----:			3.690138		
THE VALUE OF PSI IS-----:			8.864789		

Figure 77. Facsimile of Typical Output of Dummy Head Motion Program.

conditions which would permit separation of force and couple responses. The developed computer routine will establish the kinematic response; calibrations are necessary to relate the motions to generated forces and moments.

DEVELOPMENT OF DESIGN CRITERIA

There were three sources of test design criteria: (1) measured test data, (2) computer generated numbers, and (3) human tolerance data. For example:

	X	Y	Z
Skull Forces Tolerable	900 lb	900 lb	900 lb
Test at 319 kt	976	837	293
Test at 345 kt	735	233	1455

The "tolerable" level was that specified in Section 3. The test data was that reduced from the head/neck apparatus tests conducted and reported earlier in this section. From the above it is apparent that if we use 900 pounds as the maximum expected, or limit force, and use a factor of safety of 2, we will design for 1800 pounds, which would exceed the maximum measured (1455 pounds) by 25 percent.

	X	Y	Z
Neck Forces Tolerable	200	200	400
Test at 319 kt	735	87	694
Test at 345 kt	1446	1165	1122

	X	Y	Z
Neck Moments Tolerable	-	425 in/lb	-
Test at 318 kt	812	2250	299
Test at 345 kt	0	695	866

Data available indicate that the forces and moments generated at the neck-shoulder pivot are far greater than tolerable levels. Since we may encounter unusual environments, as was generated during the tests, we should consider the 1446 pounds as a limit value and consider 2800 pounds as an ultimate. This implies that if the skull has the 1800-pound ultimate, the head could generate

1000 pounds of inertial force. If the helmeted head and neck weigh 20 pounds, this means a head acceleration of 50 g's which is not unreasonable.

The maximum measured moment of 2250 in. lb generates a 4500 in. lb ultimate, using the factor of safety of 2.0. It is assumed that this value will be equally probable about all axes until additional data are available.

	X	Y	Z
Head Accelerations Tolerable	22 g	22 g	40 g
Test at 319 kt	29	14	103
Test at 345 kt	22	20	144
Torso Accelerations Tolerable	50	50	20
Test at 319 kt	32	29	67
Test at 345 kt	36	22	57

The above data indicate that for preliminary design we should use 1800 pounds for head impact force, 2800 pounds axial force at the base of the neck, and an ultimate applied moment of 4500 in.lb at the base of the neck. Design moments of 4500 in.lb will be used about the Y axis and 1800 in.lb about the other axes. Accelerometers for the testing will have to be of 50 g range laterally and 150 g vertically for both head and base plate.

TEST DEVICE PRELIMINARY DESIGN

The first approach was that of revising the concept being used. With the new design criteria, how would the six-load-cell test platform be altered? Three design conditions were examined.

Condition 1, force applied in the plane of symmetry:

$$\begin{aligned}
 X &= 1800 \text{ lb} \\
 Z &= 1800 \text{ lb} \\
 M_Y &= 4500 \text{ in. lb} \\
 \ddot{X}_p &= 50 \text{ g (1250 lb)} \\
 \ddot{Z}_p &= 50 \text{ g (1250 lb)}
 \end{aligned}$$

where X and Z are forces, M_Y is the moment about the Y axis, and the \ddot{X}_p and \ddot{Z}_p accelerations are those of the plate.

Condition 2, force applied laterally,

$$Y = 1800 \text{ lb}$$

$$Z = 1800 \text{ lb}$$

$$M_x = 4500 \text{ in.lb}$$

$$Y_p = 50 \text{ g}$$

$$Z_p = 50 \text{ g.}$$

Condition 3, asymmetric loading,

$$X = 1273 \text{ lb}$$

$$Y = 1273 \text{ lb}$$

$$M_x = 3150 \text{ in.lb}$$

$$M_y = 3150 \text{ in.lb}$$

$$Z = 1800 \text{ lb}$$

$$M_z = 4500 \text{ in.lb.}$$

All three conditions were examined for a rigid plate as shown in Figure 78.

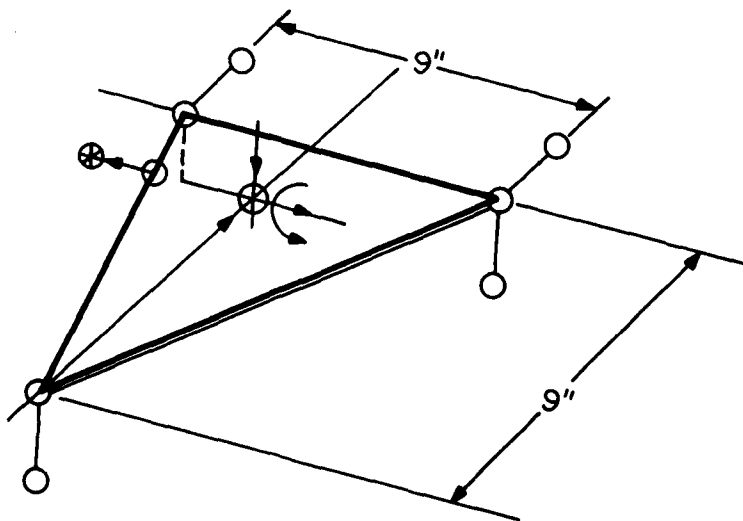


Figure 78. Schematic Showing Three Design Conditions Applied to a Rigid Plate.

The maximum forces were:

FORCES	CONDITIONS		
	1	2	3
Rear Drag	1525	0	1300
Rear Vertical	1267	1517	1300
Side	0	3050	1273
Forward Vertical	517	1517	600

These were then used to calculate stresses within the plate by assuming beam elements between points of load application and load cell attachment points. A typical figure is Figure 79, which shows Condition 2.

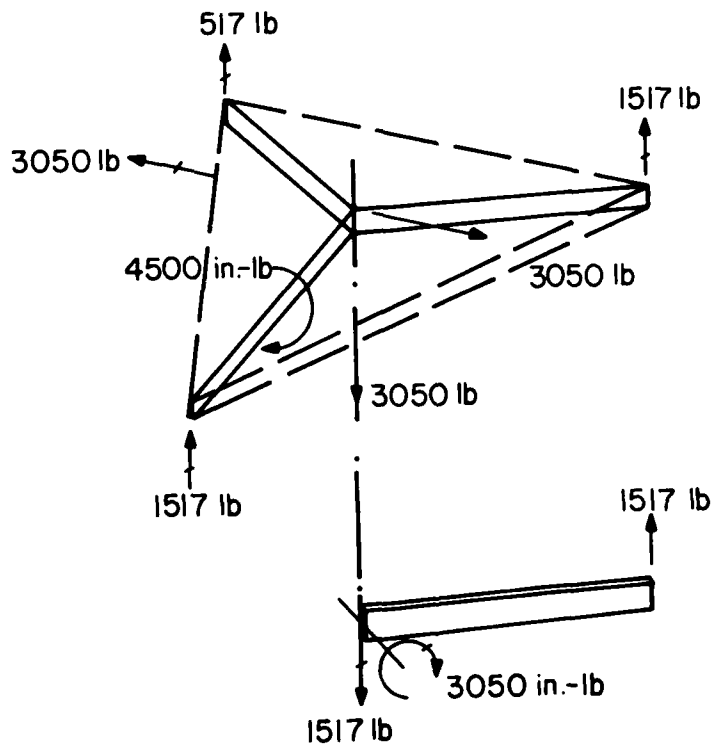


Figure 79. Assumed Beam Elements for Condition 2.

Assume a 1-inch by 1-inch beam;

$$f_b = \frac{mY}{I} = \frac{8350 (1/2)}{1/12} = 50, 100 \text{ psi and}$$

$$f_s = \frac{VQ}{Ib} = \frac{3}{2} \frac{(1517)}{1} = 2,275 \text{ psi,}$$

which would require a high-strength aluminum plate.

The above steps were repeated for all conditions and assumed beams. Stresses were calculated and combined to evaluate the principal stresses. After this, a revised drawing was made to establish total weight in order to select a foam pad to be placed between the load cell support plate and an attachment plate. At this stage, with an estimated weight of 100 pounds, without a mounting plate, it was decided to reexamine another concept.

A tube supporting the head and neck structure and strain-gaged at four points located 90 degrees from one another would appear as shown in Figure 80.

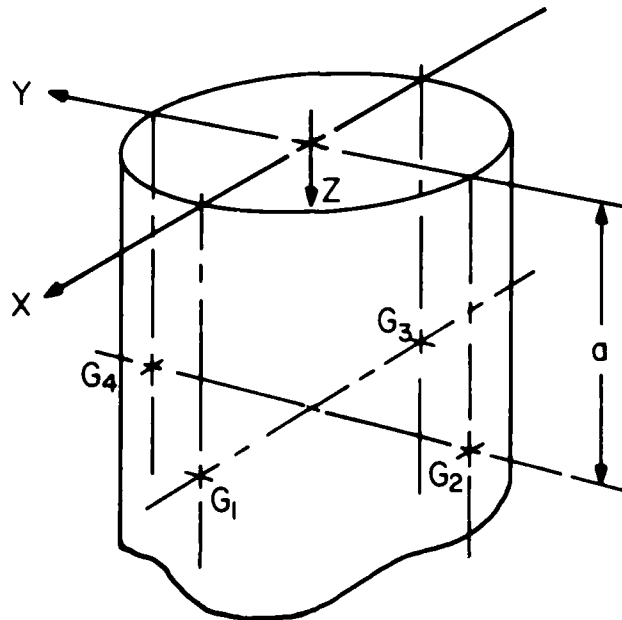


Figure 80. Strain Gage Locations on Tube Supporting Head and Neck Structures.

The gages (G) are subjected to the following stresses:

$$G_1 = \left(\frac{V_x a r}{I} + \frac{V_z}{A} - \frac{M_y r}{I} \right) \bar{k} + \left(\frac{V_y Q}{Ib} + \frac{M_z C}{J} \right) \bar{j}$$

$$G_2 = \left(\frac{-V_x a r}{I} + \frac{V_z}{A} - \frac{M_y r}{I} \right) \bar{k} + \left(\frac{V_x Q}{Ib} + \frac{M_z C}{J} \right) \bar{i}$$

$$G_3 = \left(\frac{-V_x a r}{I} + \frac{V_z}{A} + \frac{M_y r}{I} \right) \bar{k} + \left(\frac{V_y Q}{Ib} - \frac{M_z C}{J} \right) \bar{j}$$

$$G_4 = \left(\frac{V_y a r}{I} + \frac{V_z}{A} + \frac{M_x r}{I} \right) \bar{k} + \left(\frac{V_x Q}{Ib} - \frac{M_z C}{J} \right) \bar{i}$$

where V_x , V_y , and V_z are the applied shear forces; M_x , M_y , and M_z are the applied moments; "a" is the distance vertically from point of load application to strain gage; "r" is the radius of the tube; A is the cross-sectional area; I is the moment of inertia; J is the polar moment of inertia; and \bar{i} , \bar{j} , and \bar{k} are unit vectors in the direction of x, y, and z respectively. The stresses are grouped as normal (\bar{k}) and shearing stresses (\bar{i} , \bar{j}).

If each gage is a rosette, the normal and shearing stresses in the \bar{k} , \bar{i} , and \bar{j} directions can be found from strain gage outputs. Therefore, each bracketed term can be evaluated. Adding the stresses of gages 1 and 3,

$$\left(\frac{2V_z}{A} \right) \bar{k} + \left(\frac{2V_y Q}{Ib} \right) \bar{j} = (\sigma_1 + \sigma_3) \bar{k} + (\tau_1 + \tau_3) \bar{j}.$$

The right hand side is known and the properties of the tube are known. Hence V_z and V_y can be found. Adding the stresses of gages 2 and 4 yields a second solution for V_z , and a solution for V_x . Any gage reading can then be used to evaluate the applied moment.

Four rosettes provide redundant information in that 12 outputs are being used for 6 unknowns. However, the 12 are necessary for 8 strains and hence the redundancy is really the least possible.

Several configurations of tube size were examined. Standard tube sizes were used in order to be sure that any size found to be structurally acceptable would be commercially available. The tube had to be checked to ensure that it would not fail as a beam column nor would it cripple locally. Additionally, it was desirable to get the applied stresses as large as possible. Although the gages will read values of 100 μ strain, an order of magnitude higher output was desired.

The tube selected has a 3-inch OD with a thickness of 0.063 inch at the gage. This is based upon placing the gages 3 inches below the plane of load application in order to get away from end effects. Refer to Figure 81. The tube has a length of 6 inches to a fixed base. Therefore:

$$\frac{L'}{\rho} = \frac{2(6)}{1.039} = 10.6, \text{ a short column}$$

$$\frac{r}{t} = \frac{1.5}{1/16} = 24,$$

$$F_{cc} = \frac{0.3(10.10^6)}{24} = 125,000 \text{ psi for cripple.}$$

Thus, the column will neither buckle or cripple within the elastic range.

At the gages:

$$\sigma_1 = \frac{7250_{1000}}{0.6224} \pm \frac{1740_{1000}}{0.5768} \pm \frac{6020_{1000}}{0.6224} = 14,010 \text{ psi max.}$$

$$\tau_1 = \frac{2(1800)}{0.5768} \pm \frac{4500(1.5)}{2\pi(1.5)^3(0.063)} = 11,320 \text{ psi max.}$$

The principal stresses would be $\sigma_m = 30,100$ psi and $\tau_m = 17,600$ psi. For 6061-T6 drawn tube, the allowables are 42,000 psi and 27,000 psi. Hence the design forces and moments can generate stresses that are approximately 70 percent of the ultimate. Compared with yield, the values are 85 percent of the allowable.

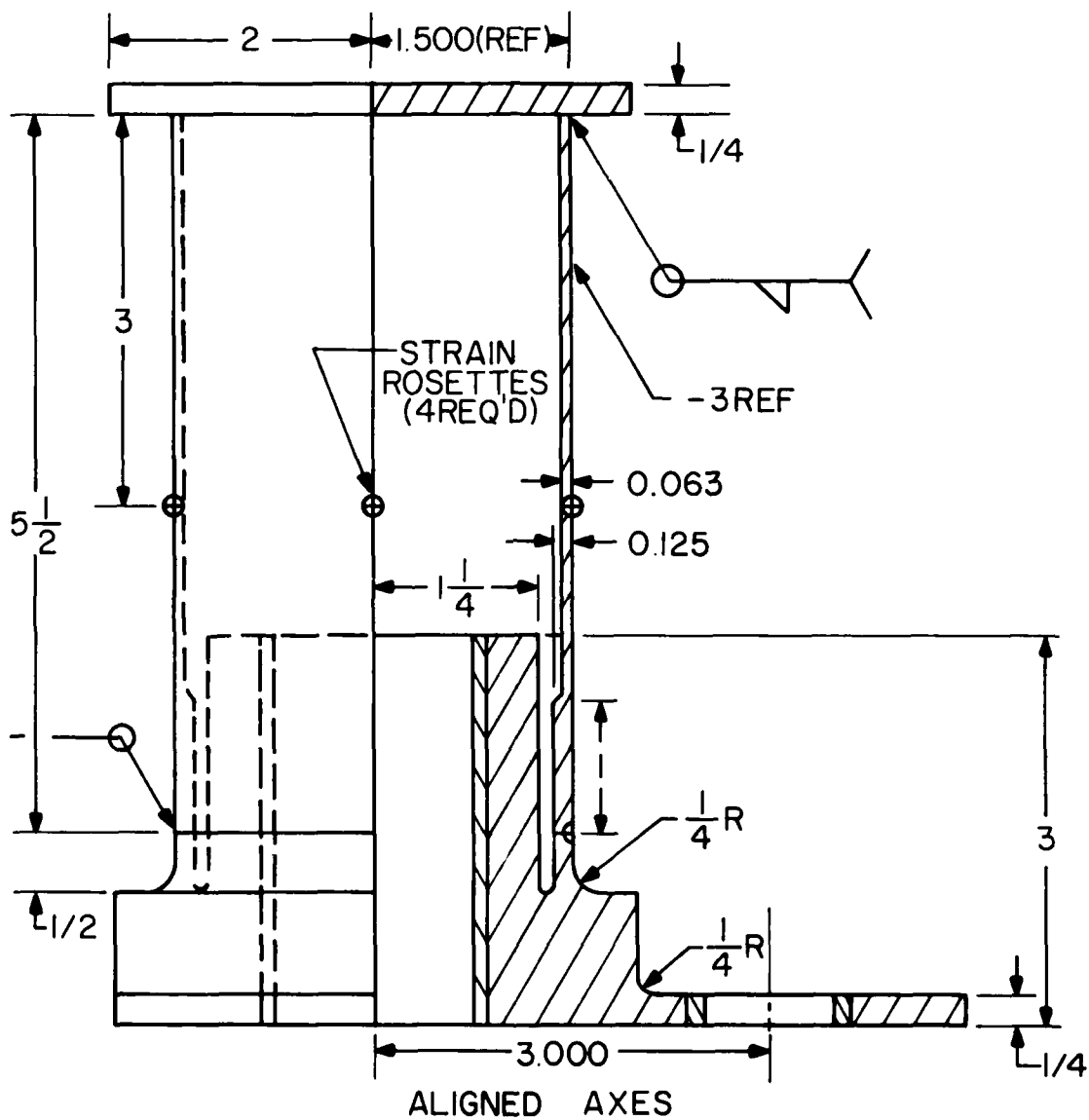


Figure 81. Supporting Tube Assembly for Test Device, Preliminary Design.

At the base of the tube it is easiest to weld the tube to the base material. A stepped sleeve is provided to create a 0.125-inch-thick welding surface. The material properties at the weld are 24,000 psi and 15,000 psi for normal and shearing stress. Using a wall thickness of 0.125 inch, the maximum applied stresses are 19,700 and 6,050 psi.

The tube slides vertically on one post. A post of 1.50-inch diameter will generate 56,000 psi at the base requiring a high strength aluminum. The 1-1/2-inch diameter of the guide is dictated by the bending carried in transferring the moment from the tube into the post. The stresses are relatively low.

The applied forces and moments go from upper base plate, through the tube as a beam column, into the base of the column through the welds, into the "bushing" and out the post. This is true for everything except the applied torque about the post. The torque is taken out through the secondary post which is loaded by a thin tab. The tab is designed to carry a shearing force into the post without providing any appreciable stiffness to any other load. Hence, all forces and moments should be carried by the primary post except for the applied torque. With the 1/4-inch-thick tab, the bearing stress is low, and the tab bending stress is very low. The one-inch diameter post will carry only 33,750 psi at ultimate load (see Figure 82).

The entire sensing head rests upon a 2-inch thick piece of Ethafoam, a Dow Chemical product. If the circular 4-inch diameter collar is used, a static stress of 3.25 psi is generated. This will cause the isolated head to have a natural frequency, when base excited, of about 8 Hz. If a 4-by-4-inch square is used, the static stress is reduced to 2.25 psi and the system natural frequency is about 10 Hz (see Figure 83).

The static displacement of the sensing head due an applied 1000 pounds at the upper edge of the tube is about 0.072-inch based upon the deflection of a 5-1/2-inch-high tube and a 3-inch post. This implies a natural frequency of 18.8 Hz. Using a

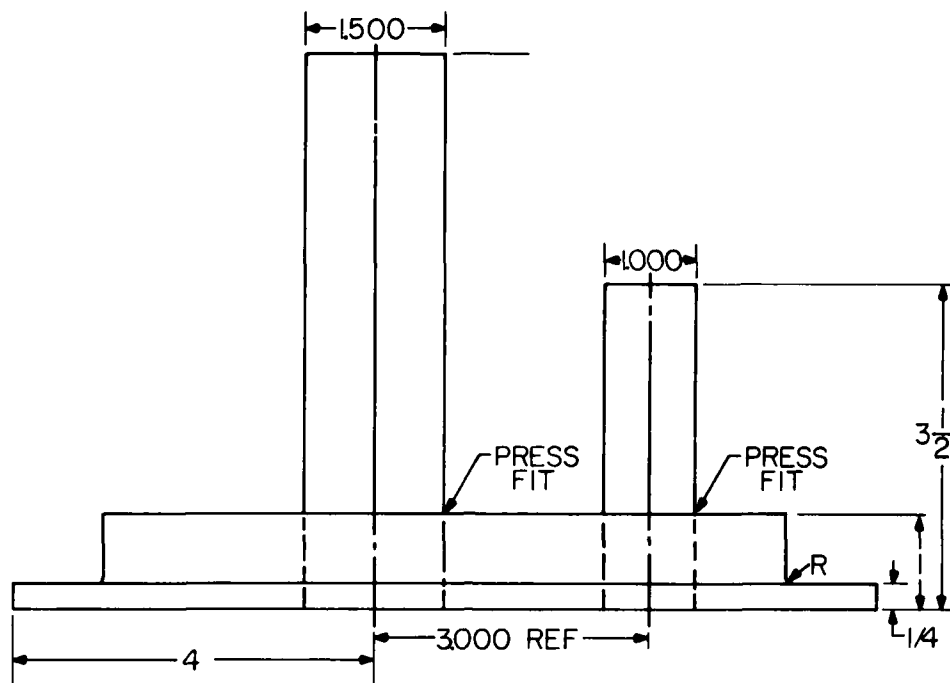


Figure 82. Base Assembly for Test Device, Preliminary Design.
(Dimensions in inches.)

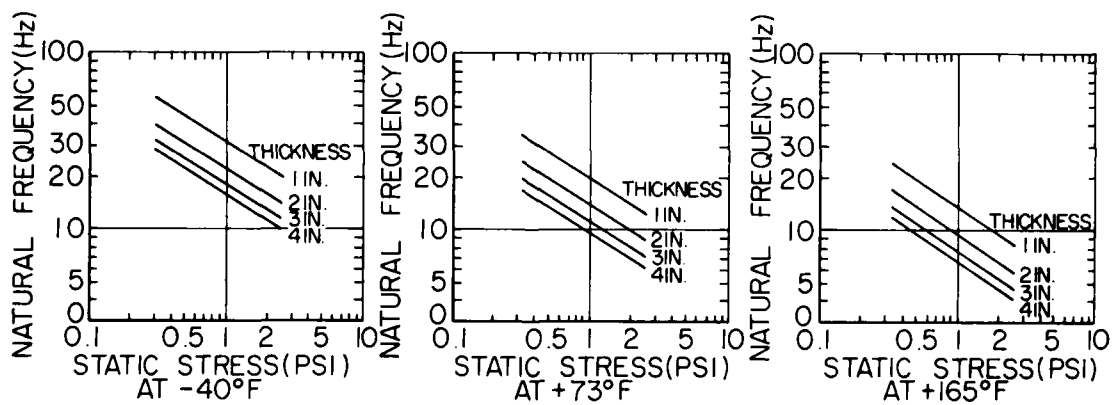


Figure 83. Natural Frequency versus Static Strength of Ethafoam.
(Reproduction of Data from Reference 55.)

similar approach for torsional response, the natural frequency is over 300 Hz dictated by the bending of the secondary post.

The assembly drawing, Figure 84, shows that a tubular, two-piece shield is added to protect the strain gages. This is simply a shield attached by four screws to cover the gages and provide an access hole to the leads. The attachments are rotated 45 degrees from the plane of symmetry to avoid any interference problems. The secondary post retains the head with a pin and washer. All components were commercially available and the fabrication did not require any unique hardware. The weights listed were calculated assuming aluminum with a density of 0.1 pound per cubic inch. The total weight of the assembly is about 9-1/2 pounds.

The sensing head is a feasible means of measuring three forces and moments at a particular location and is really nothing more unusual than a wind tunnel sting or a multifore load cell. The advantages of the design are: (1) it is light in weight, (2) it is easily adaptable to different frequency response characteristics, and (3) it is self contained. The disadvantages are: (1) more data channels are required and therefore, (2) more calibration is required.

Additional aspects to be mentioned are: (1) by changing the type of foam and thickness it is possible to adjust the vertical natural frequency to any reasonably "low" frequency indicative of spinal response over a complete temperature range of -40°F to 165°F, as indicated by available test data; (2) by adding mass and by adjusting its location, the fore-and-aft frequency response can be altered to better fit any desired frequency; and (3) if additional data channels are available, another ring of four rosettes could be added for even greater redundancy at a lower level, say one inch below the initial ring. This would provide outputs indicative of greater normal stresses with improved accuracy at lower force inputs.

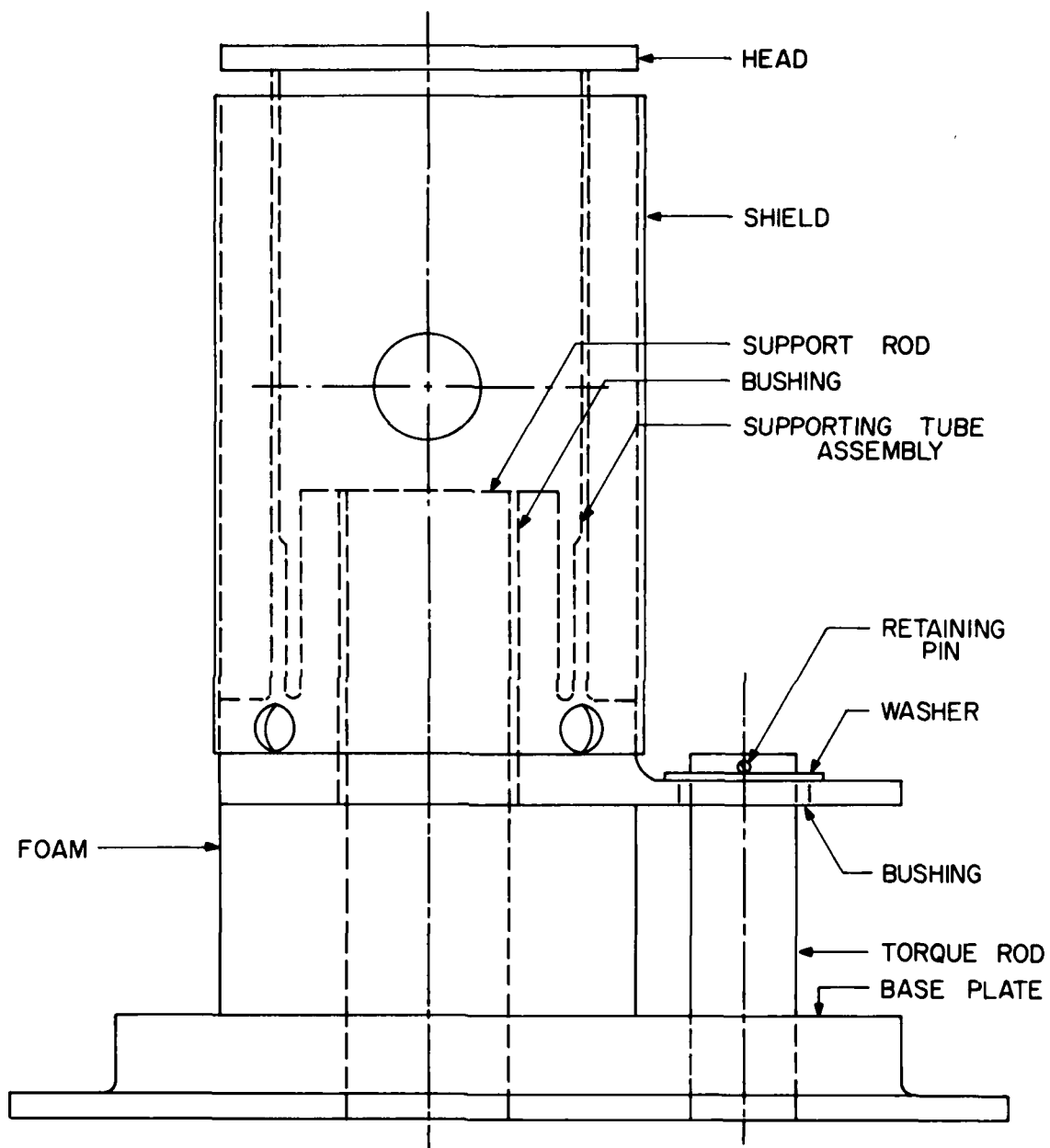


Figure 84. Assembly, Preliminary Design of Test Device.

FINALIZED DEVICE DESIGN

The drawings for the test device preliminary design were reviewed by the Engineering Development Group of the University of Dayton Research Institute. Comments from detail design and model shop personnel suggested several ways to make the design simpler to fabricate and at less cost. Suggestions incorporated were:

- (a) The upper plate used to attach to the dummy neck should have a machined groove to fit the diameter of the sensing tube. This will prevent an unnecessary warpage due to welding.
- (b) The diameter change in the tube to increase wall thickness should be done externally instead of internally to eliminate internal boring.
- (c) The lower welding of the tube can be eliminated by going to a press fit of cylindrical clamps.
- (d) The lower segment of the tube having increased thickness can be a tubular segment all turned on a lathe and eliminate the square tab for the second support column.
- (e) The second column, which was necessary to resist torque, can be replaced by an arm, tapped into the cylindrical base, which would be positioned between two vertical guides. The protruding arm, like the spoke on a wheel, would slide freely between two vertical blocks, but would not permit rotation. This eliminates the need for two "perfectly" aligned shaft and bearing combinations.
- (f) The primary shaft should be stainless steel for wear and life consideration.
- (g) The base plate design can have a thicker mounting flange to reduce machining time and cost. The thickness is reasonably arbitrary since we really don't know where and how the plate will be attached.

The final design is shown in Figure 85.

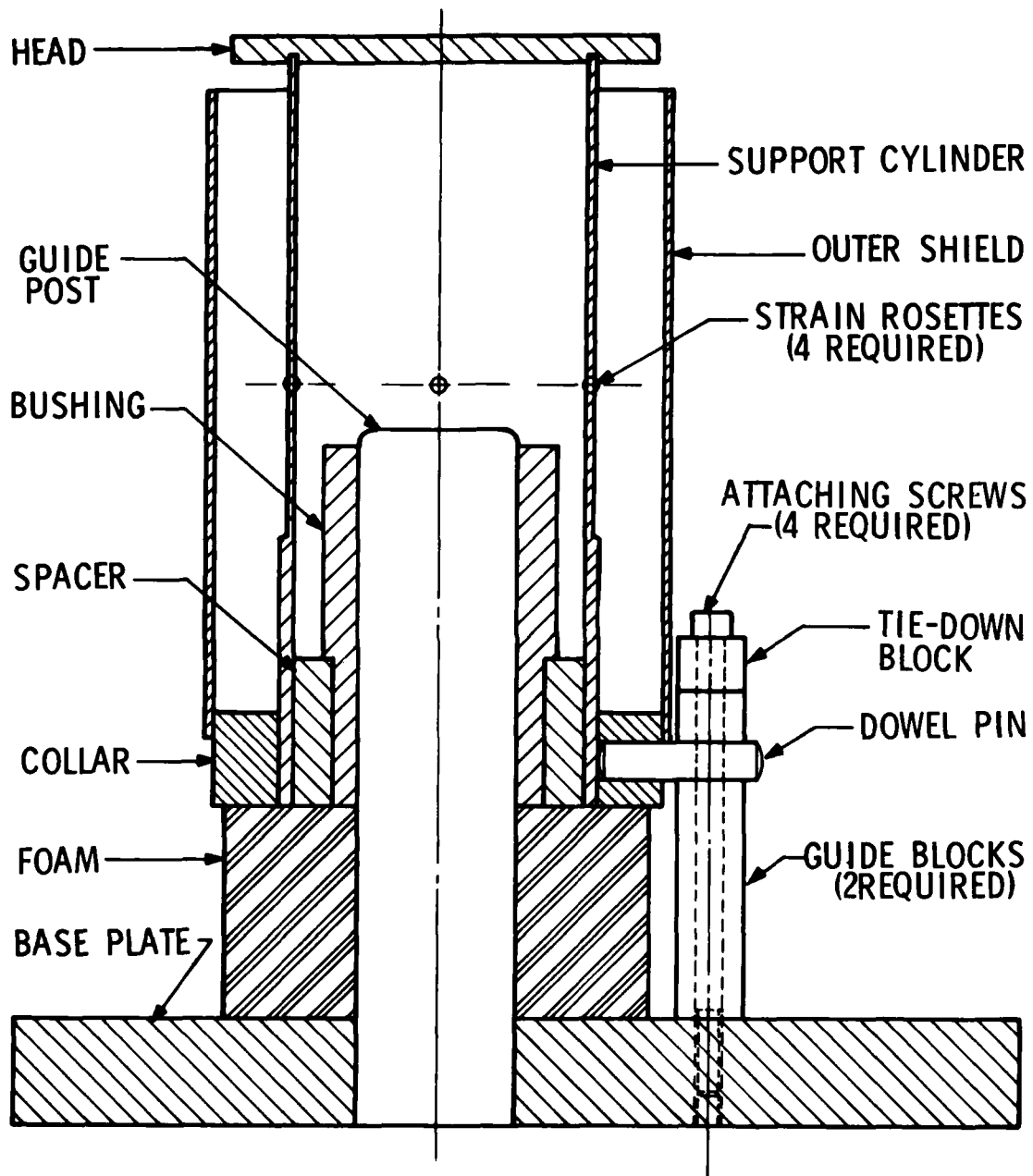


Figure 85. Assembly, Finalized Design of Test Device.

In addition to the structural changes, more strain gages were included. A complete set of four rosettes were added one inch above the primary gages. This was done to ensure adequate measurement capability for future usage. Although one set of rosettes is adequate to calculate applied forces and couples, it was decided that it would be worthwhile to install another set and have them calibrated, in view of the uncertainty associated with the testing environment. Although probably not all gages would ever be simultaneously recorded, the set of redundant gages provides a source of immediately usable calibrated data collection at the test site should it be necessary. Failure of a gage need not delay a test. However, in the final data analysis, the strain-to-load matrix would have to be modified to reflect the calibrations for the newly selected gage.

TEST DEVICE CALIBRATION

The test device was calibrated using a test fixture designed to support an MTS series 204 actuator as shown in Figure 86. The actuator was in series with a Baldwin SR-4 load cell as shown in Figure 87. The test device was anchored beneath two angles which permitted the device to be slid laterally relative to the actuator.

The protocol developed for the testing required 24 tests consisting of 200-pound increments from no-load to 1000 pounds and return. Loads were applied in the +X direction first, followed by adjustment of the device to produce a positive M_z and then negative M_z moment about the Z axis. In Figure 87 detents can be seen in the loading head. These were of greater radius than the loading stud and hence generated a point contact of 2.5 inches either side of the centerline. The loading series was followed by a positive Y loading series, and then both were replicated for calibration of the spare, or redundant, gages. The shear loading and shear and couple loading of both directions and both signs require 16 tests. Axial loading tests were conducted on an Instron testing machine. An axial force was applied down the centerline, and then at 2.5 inches from the centerline at four orthogonal points on the loading head. These were replicated for the redundant gages.

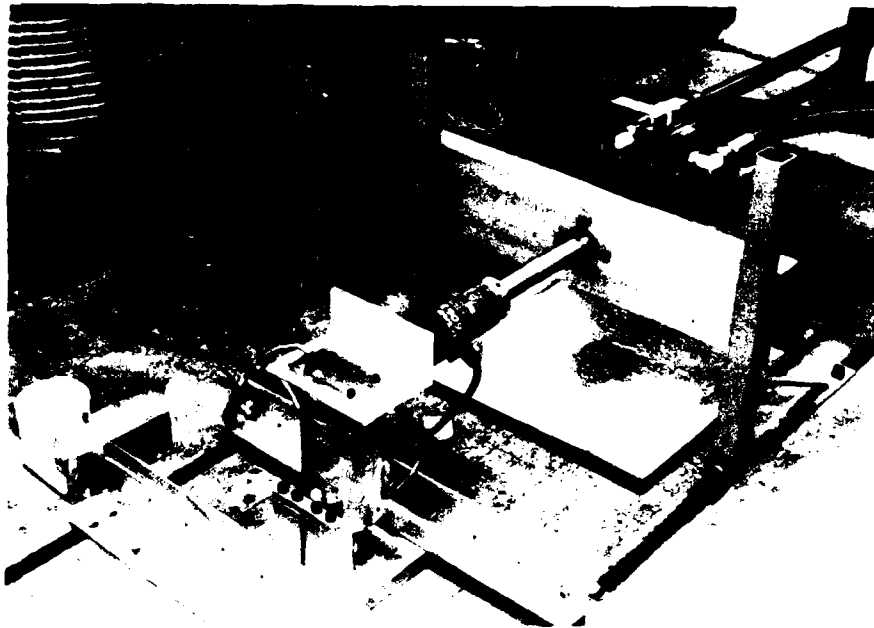


Figure 86. Calibration Fixture for Test Device.

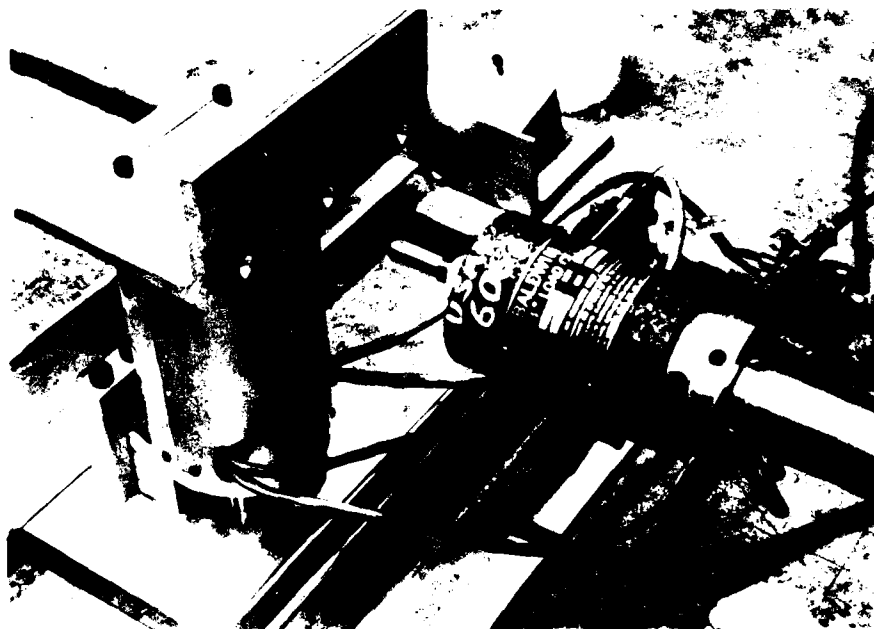


Figure 87. Closeup of Test Device Calibration Fixture, Showing Load Cell.

The recorded data were read and digitized. The mean values for the ascending and descending load pairs were calculated and printed out for analysis. The mean values plotted are shown in the typical plot of Figure 88. The abscissa is the load applied and the ordinate is the strain measured. From these it is apparent that the outputs are, as expected, not perfectly linear, nor do some of the gages indicate absolute zero as would be theoretically predicted. From these curves it was possible to pick out those gages having the greatest output for any specific applied load. For example, in the Y direction gage 2-2, the axial strain gage element at location 2, provides the greatest output and should be most indicative of the applied force. The strain readings for the force applied in the opposite direction are used with those of positive force to calculate a least squares fit for the linear calibration curve that is forced to pass through the origin. In this manner the best calibration is established for use in a calibration matrix relating applied force to strain.

Various sets of gages were examined to determine how well the shear and normal stresses compared with theoretical values. Using the relations that exist for stress and strain of rosette elements, it was possible to select gages which generated the strains most indicated of those which should exist. That is, the shear strain should be a maximum at the neutral axis for an applied shear force and a minimum along the axis of force application. Several sets of gages were selected and the relation between strain gage output in microstrain related to applied force and moment in pounds and inch-pound respectively. The relation is shown in matrix form where ϵ_{101} indicates the rosette at location one, and the number one element.

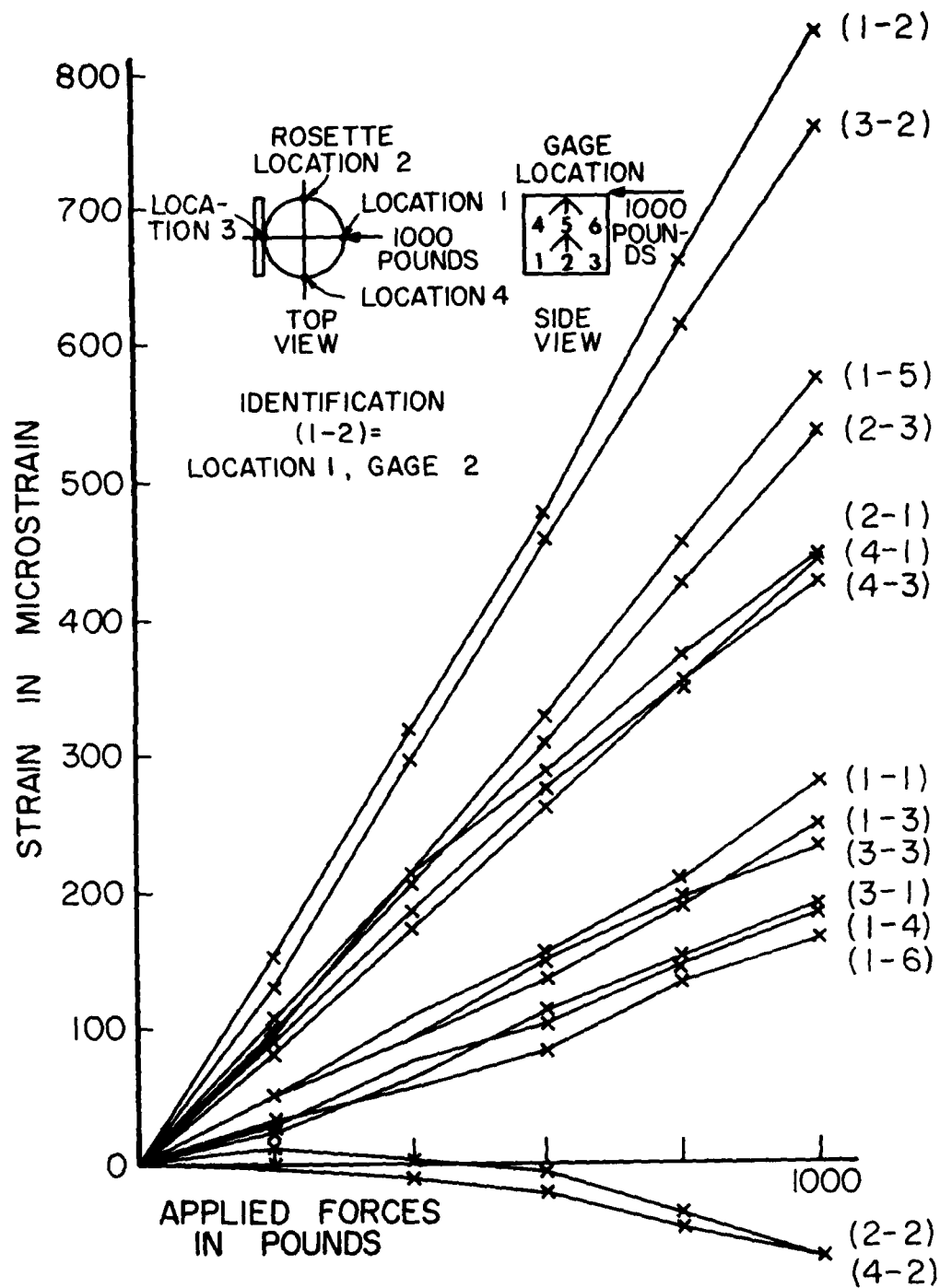


Figure 88. Typical Strain versus Calibration Force for Minus-X Loading.

$$\begin{bmatrix} \epsilon_{101} \\ \epsilon_{102} \\ \epsilon_{201} \\ \epsilon_{202} \\ \epsilon_{401} \\ \epsilon_{402} \end{bmatrix} = \begin{bmatrix} -0.245 & -0.505 & -0.090 & +0.004 & 0.172 & +0.150 \\ -0.920 & -0.510 & -0.180 & +0.004 & 0.396 & +0.003 \\ -0.500 & +0.250 & -0.090 & +0.132 & 0.012 & +0.178 \\ 0.010 & +0.810 & -0.180 & +0.252 & 0.100 & -0.016 \\ 0.420 & -0.150 & -0.090 & -0.126 & -0.024 & +0.156 \\ -0.050 & -0.740 & -0.180 & -0.252 & +0.004 & 0.028 \end{bmatrix} \begin{bmatrix} X \\ Y \\ Z \\ M_x \\ M_y \\ M_z \end{bmatrix}$$

By finding the inverse of the matrix the relation between applied forces and moments as functions of strain output are established.

$$\begin{bmatrix} X \\ Y \\ Z \\ M_x \\ M_y \\ M_z \end{bmatrix} = \begin{bmatrix} 1.125 & -0.582 & -1.160 & 0.599 & 0.345 & -0.172 \\ -2.639 & 1.335 & 0.595 & -0.302 & 1.981 & -1.001 \\ -1.012 & 1.365 & -0.272 & -3.071 & 1.668 & -4.042 \\ 8.262 & -4.677 & -1.097 & 2.790 & -6.605 & 1.607 \\ -1.330 & 3.556 & -2.059 & -0.409 & 4.151 & -3.528 \\ +0.318 & 0.408 & 2.337 & -1.486 & 3.651 & -2.075 \end{bmatrix} \begin{bmatrix} \epsilon_{101} \\ \epsilon_{102} \\ \epsilon_{201} \\ \epsilon_{202} \\ \epsilon_{401} \\ \epsilon_{402} \end{bmatrix}$$

With measured data from six selected gages, the applied forces and moments that exist at the base of the device can be calculated.

SUMMARY

Moving from a condition of very little information, a prototype piece of test hardware was designed and fabricated. Using limited measured data from this device and existing human tolerance criteria, a new test device was designed. The new test device was smaller, lighter, and more reliable because of both the simplicity of its design and the additional redundant gages. The redundant gages of the simplified design were calibrated for all possible forces and loads at the same time as the primary gages. The calibration data were reduced and load strain matrices were generated for future use.

SECTION 8

FLIGHT HELMET STUDY

INTRODUCTION

One aspect of the research was an investigation into the influence of the USAF pilot's flight helmet upon the injury potential of a birdstrike. This was required because it was realized that theoretical investigations into helmet shell and liner configurations do not necessarily adequately describe the response of a hardware item. The theoretical models used have idealized the helmet into an ellipsoid being crushed upon the head. The shell did not deform, and the liner crush followed a particular force-displacement curve. The investigation required was to consider the fact that the helmet shell does deform, and has compound curvature and finite stiffness. Additionally, the liner is of variable thickness, is not a continuous element within the shell, and has finite fabrication tolerances. The helmet used by the aircrewman is a shell of complex curvature, having a large segment of its ellipsoidal shape removed for access of the head, has many holes drilled into it for attachments, and is coupled with a visor assembly. Similarly the liner, whether pads or foamed-in-place segments, is a manufactured material with a leather covering, segmented for installation, and not necessarily located at a fixed position in the shell. Hence, neither shell nor liner is a well defined symmetrical, isotropic element as is sometimes idealized for finite element analysis.

The primary questions of concern in investigating the standard flight helmet response were: How does the shell contribute to protection and how does the liner add to the protection? Can the effects of both be separated in order to infer how future designs should be modified? Is there a mutual response between the two in addition to their individual effects? How can the effects be isolated?

SELECTION OF PROTOCOL AND TEST PROCEDURES

As the shell is impacted by the canopy, a localized force acts upon the shell. Depending upon shell stiffness, the shell may buckle locally while transmitting the force into the liner beneath. The local effect becomes more diffuse as the shell crushes the liner onto the skull and a state of equilibrium is created by the distributed pressures of the liner acting on skull and shell. Consequently, the response depends upon the shell material, thickness, curvature, and configuration as well as the same characteristics for the liner. However, idealization is always necessary and has not always permitted exact duplication of the hardware item.

In isolating the effects of shell and liner, and since the investigation was particularly for an Air Force helmet which could be tested, a test protocol was developed to empirically investigate the effects of each element. If the shell configuration were fixed (curvature and size) then the effect of stiffness dictated by material strength could be measured. The shell is compressed against the liner and locally deforms to achieve some equilibrium state. If the liner were very soft, no appreciable resistance would come from the liner to balance the external stresses. If the liner were very stiff, the shell could not deform.

The approach established in testing shells and liners makes use of the idea of testing limiting conditions of both. A liner may have no shell or a completely rigid shell. The shell may be supported by a soft liner or a rigid liner. Somewhere in between will be the helmet as it exists. Therefore, the approach was to test three combinations of shell stiffness for two different liners. For current military standard helmets there are two liners, the foamed-in-place liner and the expanded polystyrene and pad type. These reflect a soft and stiff liner, respectively. Both can be tested within a completely rigid shell, with no shell at all; or as

they exist within a regulation shell. By testing in this manner, test data are generated which reflect the extremes of variability for the configuration selected.

Before testing to particular shell and liner stiffness, a test protocol was necessary to determine specific testing conditions. The variables involved were: helmet type, size, and material; liner type, size, and material; location of impact sites; impact speed; and "bird" radius. These are variables in addition to the use of the rigid shell and no-shell control tests. Clearly the number of variables does not permit complete testing of all combinations with any statistical validity without an enormous amount of testing. Consequently, some reasonable steps had to be taken to reduce the number of variables.

The helmet shell configuration was dictated by selecting the standard Air Force flight helmet. The large size was selected, since this is the size in greatest use. Material type and thickness were therefore specified.

Two liner types were required. Foamed-in-place liners and the expanded polystyrene padded type would be used. Hence the material types were fixed. The thickness of the foamed-in-place liner is dictated by having the liner foamed within the shell while placed upon an HCL4 standard anthropometric headform.^[56] Hence liner thickness variations over the surface of the head are also fixed.

Impact sites were selected by assuming that tests would be conducted at 30-degree increments to the right and left of the shell centerline, and at every 30 degrees of pitch. This generates a need for 16 tests for one shell.

In summary, the variables are:

Helmet Shell Configuration	1
Helmet Liner Configuration	2
Test Sites	16

Hence, 32 tests are required to test the standard flight helmet without examining variations created by "stiff" and soft shells.

The final test protocol to measure the effects of shell and liner stiffnesses must reflect testing of three shell stiffnesses and two liner stiffnesses. Beginning with a rigid epoxy shell, both liners are tested over the 16 points selected. This provides a measure of the variation due to liner types alone. Next a series is conducted using a soft shell, or no shell, to determine the response of unrestrained liners. Finally, tests are conducted to observe the stiffness of the standard flight helmet. In this manner we have a measure of how the response of soft and stiffer liners are influenced by the presence of, or absence of, a shell. An additional question concerns whether the current shell is more closely related to the response of a rigid shell or to no shell at all. In this manner, even though we cannot quantitatively establish relations between shell and liner material properties and configurations, we can qualitatively see the effect of the shell.

Although a detailed protocol can be evolved, the detail required was minimized by the number of test items available. At the time of the testing, three helmets, two with foamed-in-place liners and one with fitting pads, were available for testing. This reduces the testing possible because of the failures that occur.

In order to have data at levels compatible with injury, testing must be at force levels of at least 1000 pounds. At this level, the liner will certainly have failed in that the elastic limit will have been exceeded. Hence, the same site cannot be retested. Indeed, several sites cannot be tested since the crushing involves an area considerably greater than that directly beneath the impact point. Therefore, the test protocol was reexamined to determine those tests of critical importance.

From the analyses conducted it was apparent that the impact site most probably is high on the crown of the helmet. The crew station study and canopy film data indicate that impacts at 30° from the crown are realistic. This reflects the head tilt as well as incidence angle of the canopy. Consequently, data concerning the crush of shell and liner at that point was most desirable.

Given that the site is selected, what configuration is tested? The configuration of greatest desirability is that of the flight helmet as it exists with the liners, which are conventionally used. If each liner is tested, there can be one test only, and therefore only one test with a fitting pad liner and only two with the foamed-in-place liner. For the foamed-in-place liner the choice was to test with and without shell to examine the effects of the "flexible" shell.

The protocol alluded to is that necessary to empirically evaluate the effects of shell and liner. By looking at the extremes of rigid shell and no shell, the influence of the shell upon two types of liners can be found for any number of helmet types and sizes. However, the quantity of test items used becomes prohibitive. Each test, at the force level desired, is a failure and can not be repeated. Consequently for the number of test items that were available, the testing conducted was limited to those tests of critical importance.

FABRICATION OF TEST HARDWARE

All tests were conducted using an Instron model TM-S testing machine. The machine is a relatively low speed machine capable of the 1000 pounds required. The lower speeds were satisfactory since although it was originally anticipated that impact tests for additional helmets would be conducted, neither additional helmets nor sufficient time was available.

Test hardware was designed and constructed to permit testing of up to 1000 pounds with the flexibility of permitting any yawing angle of the head at every ten degrees of pitch. Such a device was designed and fabricated and is shown in Figure 89.

The head form was made using an epoxy material poured into a plaster mold of the HCL-4 head form. The form is molded around a baseplate which may be removed from the test device for replacement. The slender rod arm is clamped within a locking block that permits the rod to be rotated a full 360 degrees. The locking

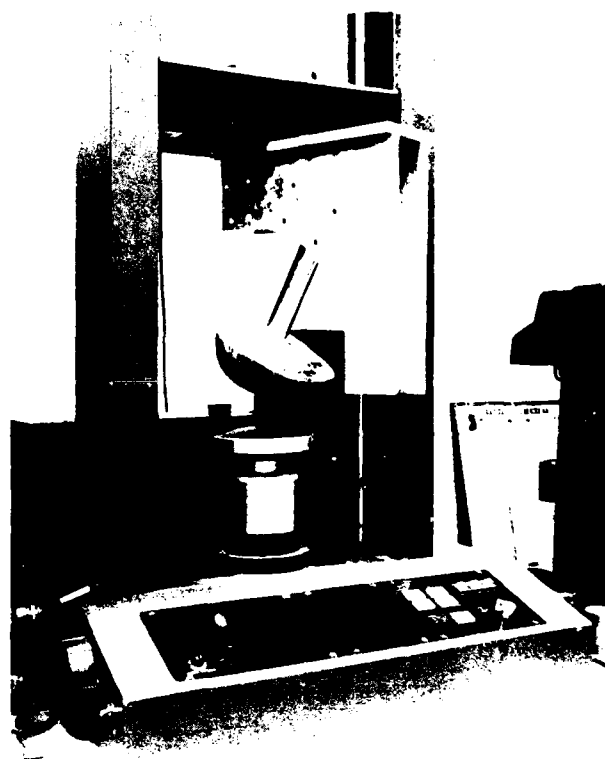


Figure 89. Helmet Testing Device, Showing HCL-4 Head Form (Skull Cap) and Anvil Representing Bird.

block is attached to the support frame by a series of bolt attachments which can be placed along every ten degrees of arc. The design was based upon a large helmet shell and use of a foamed-in-place liner. That is, the location of the loading point on the helmet dictates the center of curvature for the support frame attachment points. If the helmet size, the liner thickness, or the head form changes, the point of load application may vary slightly. During testing it was found this was not a significant problem. The point of load application was established visually by seating the helmet on the head form at the desired point.

TEST PROGRAM

Impact test results from Air Force drop tests had shown that the thickness of the liner at the impact point did significantly influence the response. The amount of crushable material

would greatly influence the stroke available prior to development of excessive force at the skull. Measurements of the liner thickness were made at selected points prior to any testing.

The measurement of liner thickness quickly pointed out some of the problems in quantitatively describing the liners. For the foamed-in-place liner, there are two segments which do not necessarily remain fixed in the shell. In fact, relative motion within the shell is easily achieved. The two segments are not loose within the shell, and are difficult to remove, but are not fixed. Neither is the thickness easily established. The foam liner has a leather covering on the inside surface and is inherently crushable. This makes it somewhat arbitrary in defining the thickness at a static condition. What amount of compression exists during static compression on the head?

Liner thicknesses were established by examining the two provided at 11 different sites as shown schematically in Figure 90. The figure represents a top view of the helmet showing the crown (B) and measurement sites at 30 degrees of yaw and pitch. Measurements at the brow of the helmet were not possible since the liner does not go that far down within the shell. Three different sets of observations were made using a caliper and vernier scale. The measurements were made with the liner in the shell and the values tabulated in Table 9 reflect liner and shell thickness.

The readings are averages of at least two as measured by three individuals. The mean difference between the readings and the average at that location were examined and it was found that the average differences for all values of 0.045 inches, or less than one sixteenth of an inch. Also, the differences were compared with the average thickness at the same location and found to correlate very weakly ($r = 0.16$) indicated that measurement error was not directly related to the magnitude of the measurement.

The data indicates that the liner thickness decreases from the crown to the brow in all vertical planes. However, due to the shape of the selected headforms within the shell, the thickness

TABLE 9. LINER AND SHELL THICKNESS FOR POINTS DESCRIBED IN FIGURE 90.

Location	Thickness			\bar{X}
	1	2	3	
B	1.000	1.398	1.484	1.461
D	1.125	1.156	1.258	1.181
E	1.047	1.133	1.164	1.115
F	1.281	1.273	1.289	1.281
G	0.883	0.906	0.070	0.953
H	1.348	1.375	1.422	1.398
I	1.039	1.070	1.086	1.065
J	1.336	1.266	1.383	1.328
K	0.938	0.945	1.070	0.984
L	1.219	1.164	1.250	1.211
M	1.141	1.156	1.172	1.156

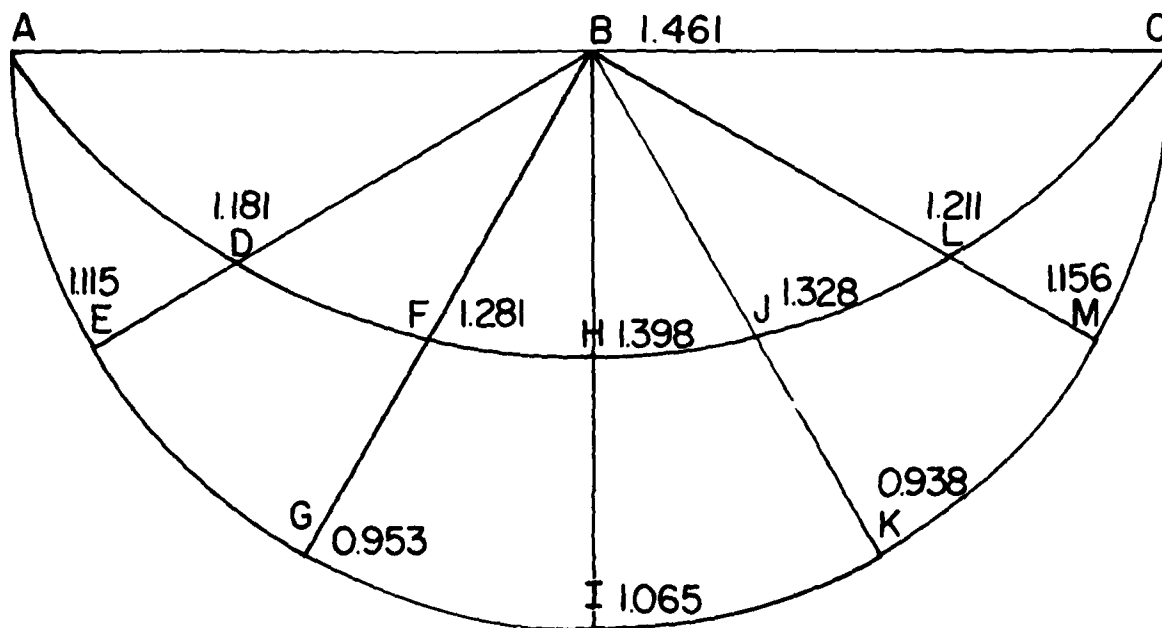


Figure 90. Sites for Measurement of Liner Thickness, Standard Large-Size Air Force Helmet with HCL-4 Head Form.

at 60 degrees of pitch does not decrease monotonically from front to side. Additionally, the previously assumed dimensions of one and one quarter inch at the crown and one inch at the brow appear to be reasonable estimates for the headform and helmet selected.

The initial tests were conducted with the flight helmet mounted at 30° of pitch, with a loading speed of two inches per minute. The loading head had a 10-inch radius. The foam and shell and fitting pads and shell are shown in Figure 91. The curves are normalized by using strain rather than displacement. The displacement values shown on the figures are those measured on the particular shell used. From the figure it is apparent that the curves have the same general shape except for a slight depression in the fitting pad curve.

The liners were tested in the same configuration at the same strain rate. The curves, shown in Figure 92, indicate that there is a greater difference seen in liner response than in the liner and shell.

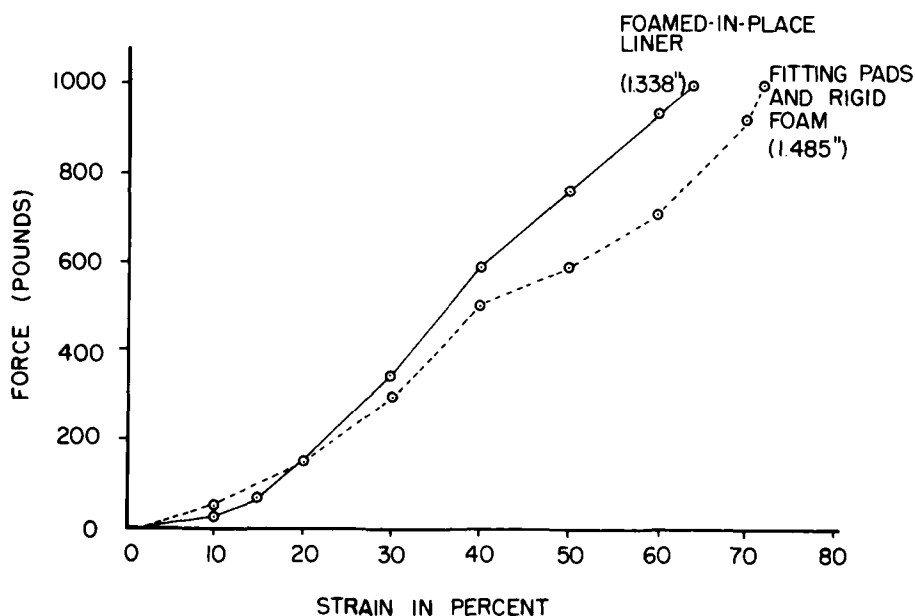


Figure 91. Force-Strain Curves for Standard Flight Helmet Tested with HCL-4 Head Form and 10-Inch Radius Loading Head Positioned 30° Forward of Crown.

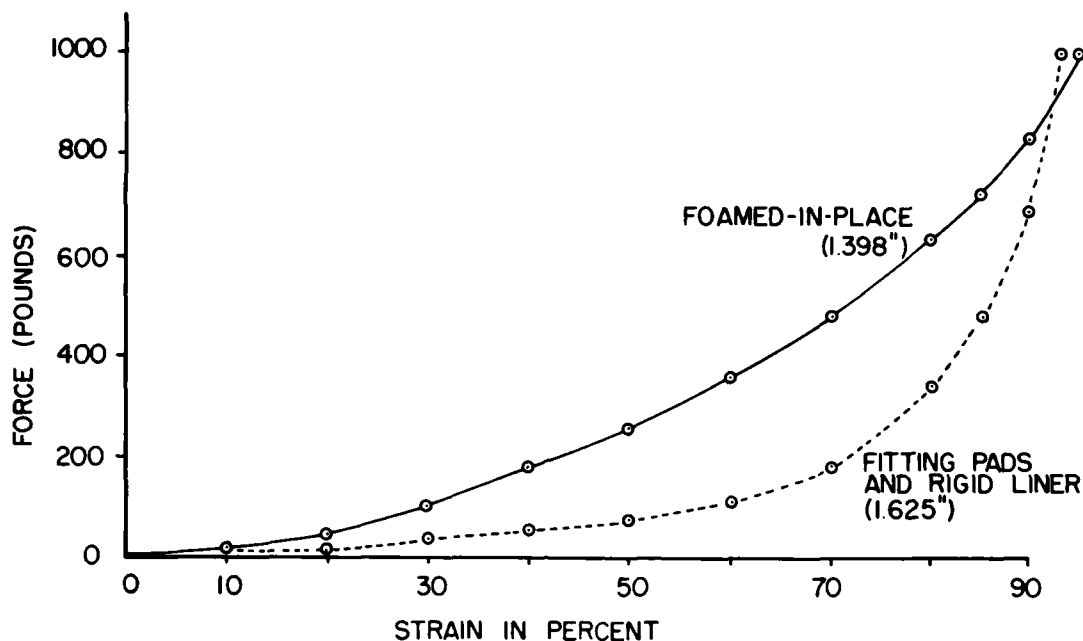


Figure 92. Force-Strain Curves for Helmet Liners Alone.

Using the curves developed, the difference between liner-and-shell and liner-alone responses was found and plotted in Figure 93. The curves indicate that the interaction between shell and liner is quite similar up to 400 pounds of interaction force. The total force at that level is about 500 to 600 pounds. Beyond the 48 percent strain level, the shell and fitting pad response is more flat than curved upward.

Both shells were failed based upon separation of the laminates of the shell. It is not possible to indicate the force level where failure occurred although it is apparent during testing that the shell does buckle locally during loading. The unloading curve of the tests indicates an increase in force with decrease in crush at about the 100-pound force levels. This is interpreted as the buckle in the shell elastically returning to its undeformed shape.

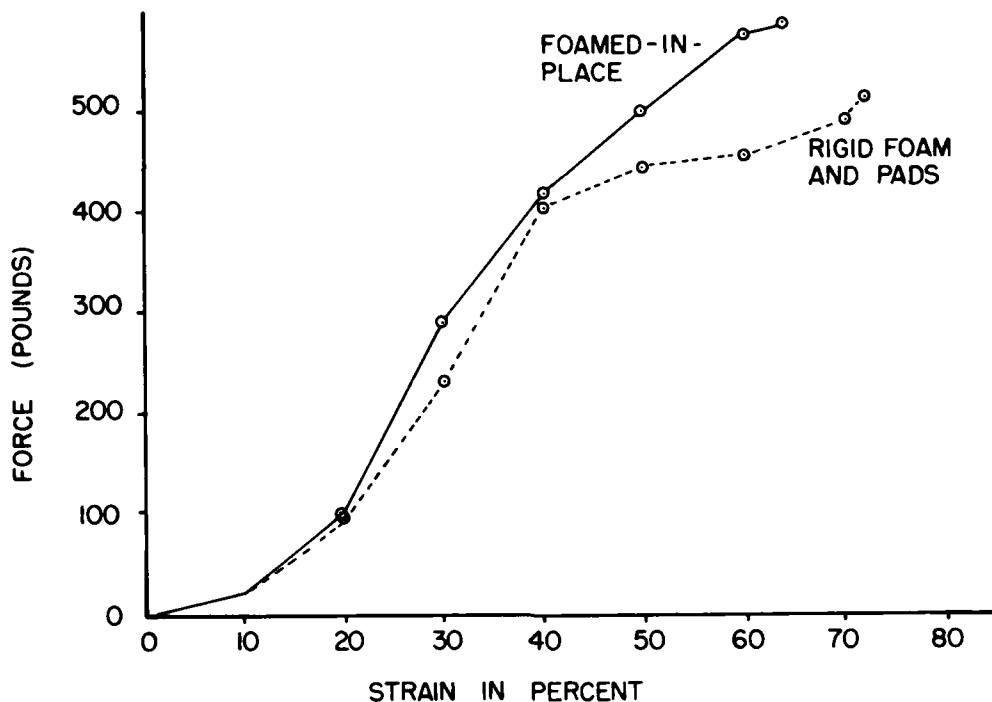


Figure 93. Force Differences Between Shell with Liner and Liner Alone (or "No-Shell") Conditions.

The curve for fitting pad and shell is plotted in Figure 94 on the curves for a similar configuration determined from impact tests. The curve is similar to all others and follows closely that for a liner of similar thickness. The one area of particular difference is that of initial displacement. The curves indicate that the difference between static and dynamic response is in the initial deformation.

The next tests were conducted to determine which helmet would be tested with a "rigid" shell. With a limited number of shells and liners, and knowing that each test could not be repeated, or the liner and shell retested; it was imperative to test a critical point that would yield data. Tests were conducted by rotating the head form so that loads would be applied at 30 degrees aft of the crown in the longitudinal plane. The data collected are shown in

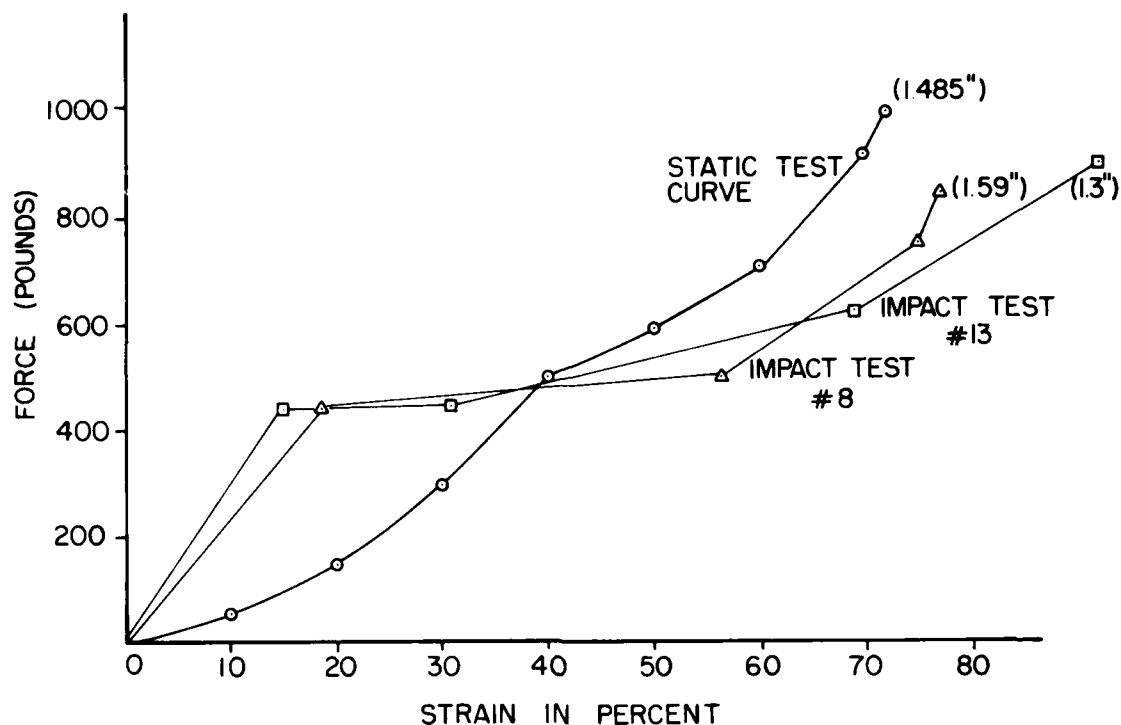


Figure 94. Comparison of Static and Dynamic Force-Strain Curves for Similar Thickness Liner Locations.

Figure 95. Notice that the results for the foamed-in-place liner are more closely related to the previous results than those of the fitting pad liner. From this it was concluded that testing with the foamed-in-place liner and helmet, and a rigid shell, would provide data that could be compared with the previous helmet and no-shell data. Tests for the "rigid" shell condition were conducted using a stainless steel shell of the correct inside diameter to fit the liner. All conditions were identical with previous tests. The results of all three related tests are shown in Figure 96. The curves for forces due to the interactions between shells and liners are shown in Figure 97.

DATA INTERPRETATION

The curves presented can be interpreted with some additional discussion of the mechanism of deformation during testing. For

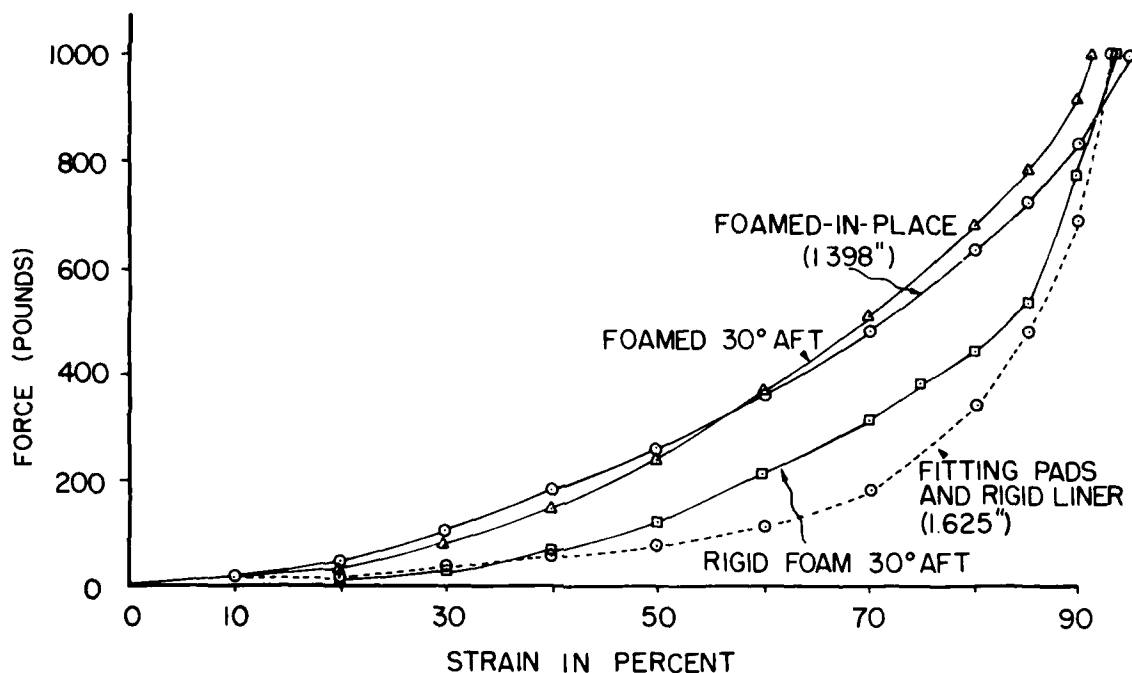


Figure 95. Force-Strain Curves for Impact Sites 30° Forward and 30° Aft of Crown.

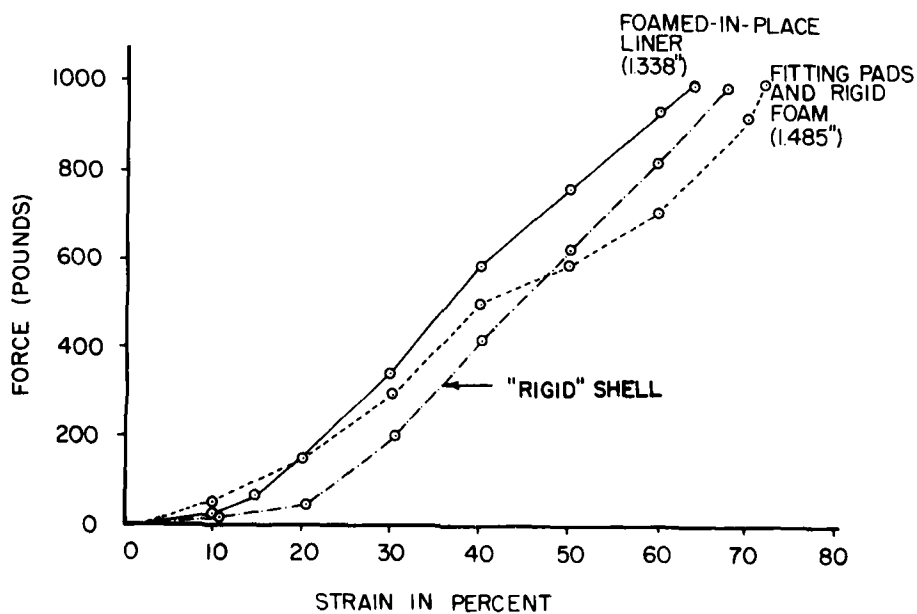


Figure 96. Force-Strain Curves for Standard Flight Helmet Configuration and "Rigid" Shell with Foamed-in-Place Liner.

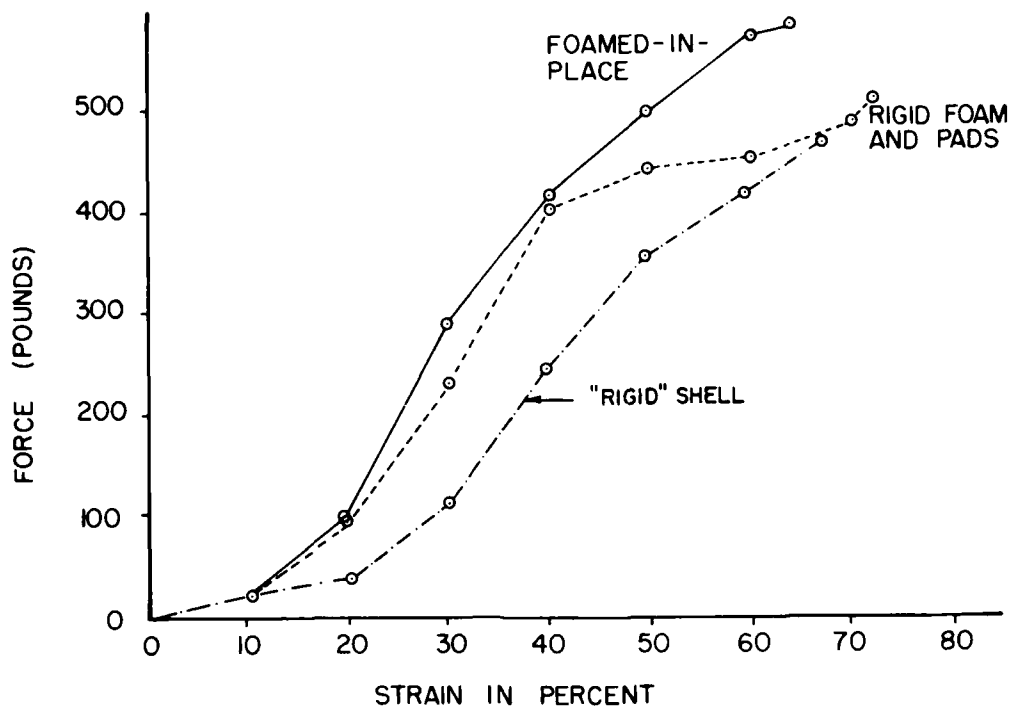
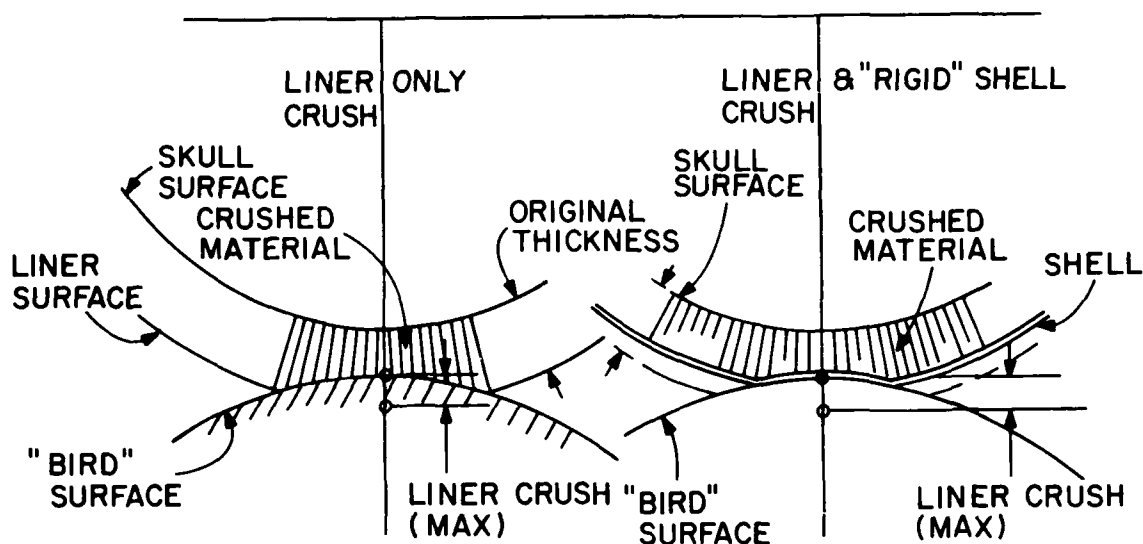


Figure 97. Force-Strain Curves for Interaction Forces for Two Standard Air Force Flight Helmets and one "Rigid" Shell with Foamed-in-Place Liner.

example, if only the liner is compressed between head form and "bird" form, the configuration is as shown in Figure 98.

The foam is crushed locally to conform to the contour of the "bird" and only a small portion of the liner acts to resist the deformation. If a "rigid" shell is added to the liner, the deformation due to "bird" curvature is quite small and the headform acts to crush a far greater amount of liner depending upon the radii of curvature of headform and shells. In order for the headform to crush into the liner the same amount as measured during crush of liner alone, a significantly large amount of liner would have to be crushed. Also, since the greater the crush depth, the greater the stress, it would appear that with more liner crushed, the rigid shell configuration would generate more force for a given crush depth. However, this is not seen in



SCHEMATIC OF COMPARATIVE LINER CRUSH MECHANISM FOR COMMON MAXIMUM CRUSH.

Figure 98. Schematic Comparing Liner Crush Mechanisms for Common Maximum Crush, for Liner-Only and Liner with "Rigid" Shell Configurations.

the data. The force-strain curve for the standard helmet shell and foamed-in-place liner is above that of the "rigid" shell configuration. Since it is greater, and yet the force developed by liner alone has to be less, the increased force must be due to the deformation of the shell.

The curves of Figures 91 and 92 indicate that the standard Air Force helmet responds more as "shelled" liner than one of no shell. This suggests that the shell has more effect than was originally anticipated. Previous impact data provided for force-displacement curves believed to be created primarily by liner material properties. However, the curves for shell and no-shell data are significantly different. Additionally, the forces of interaction indicate that the shell and its interaction can create as much as 80 percent of the total force.

Another interesting aspect is that the curves indicate that the current shell and liner is "better" considering energy absorbed than is the rigid shell or liner alone. This implies that as the shell goes from "rigid" to "flexible", the force of resistance to crush developed passed through some optimum. However, this is an interpretation of only static results.

Interpretation of the data can most easily be explained by going from the least complex system to the most complex. Static tests for liners alone indicate that they provide a very soft head covering. Both liners have similar force-strain curves, the foamed-in-place liner being "stiffer". By adding a shell and testing statically, the shell forces more liner material to compress and raises the force developed for a given strain. The force curve developed statically did not have the "plateau" characteristic that was anticipated; however the curve did reflect the elastic dimple of the shell. Dynamic test data indicated the presence of the plateau, yet the elastic deformation of the shell dimple was present. Consequently, if the plateau was not created by the shell, then it must be a function of liner or liner and shell interaction. At the beginning of the impact, the relative velocity across the shell and liner is greatest. If the shell responds elastically, then the increase in force must be due to the viscoelastic response of the liner. If the liner responds in a viscous and elastic manner the force initially after impact would be greater than the static for a given strain, and the curve would approach the static as the relative velocity is dissipated. This is what is seen in the limited amount of data available.

TEST DATA SUMMARY

The following results are extracted from the data.

- (1) The liner, when loaded by a standard head form and hemispherical loading surface, generates a "soft" force-strain curve reaching 1000 pounds at about 90 percent strain.

AD-A087 737

DAYTON UNIV OH SCHOOL OF ENGINEERING

F/G 6/5

ANALYSIS AND MEASUREMENT OF HELMETED AIRCREWMAN RESPONSE RESULT--ETC(U)

JAN 80 N S PHILLIPS

F33615-77-C-0534

UNCLASSIFIED

UDR-TR-79-56

AMRL-TR-79-75

NL

3 OF 3

0814

000000

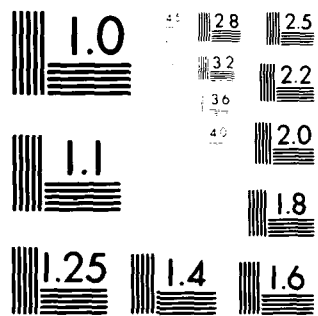
END

DATE

FILED

0-80

DTIC



MICROCOPY RESOLUTION TEST CHART
 NATIONAL BUREAU OF STANDARDS-1963-A

- (2) The liner and shell, when loaded in a similar manner, generate a stiffer force-strain curve. The shell forces more liner material to crush than would have crushed as just a liner. The shell does create additional force over and above that due to crush of the liner as seen with a "rigid" shell. Deformation of the shell creates a resistance to be added to that of the crushed liner. The added force is relatively constant over the range of strain tested and amounts to about 8 to 10 percent of the 1000-pound force.
- (3) Dynamic test data indicate that the force-strain curves have a greater stiffness in the lower strain levels. This is thought to be due to the viscoelastic nature of the liner material and not due to the shell.

From these observations two comments can be made about the role of shell and liner in providing protection for an aircrewman. First, the shell can provide some elastic resistance to deformation. The hemispherical configuration when loaded by a "point" load which is reacted by a liner pressure load, does resist deformation. However, the effect of the shell stiffness is relatively small. The shell does however cause a large amount of liner to be compressed and resist deformation. Second, the liner in addition to creating a pressure distribution between shell and skull, also generates a viscoelastic response which is significant in changing the force-strain profile at the impact velocity used. This implies that more energy can be dissipated by the shell and liner for a given strain without exceeding the tolerable force limit, than can be dissipated by the liner alone or the shell and liner at lesser impact velocities.

It is interesting to note that for the theoretical models used, the impact velocity at the point of impact is approximately 50 to 60 feet per second. This is the velocity of the interface between bird and shell calculated from interface depth versus time and calculated for shell motion only. That is, the interference reflects crush of bird and helmet. For a given change

in interference over a finite time, only a portion of the interference is that of shell. Hence, locally the shell deforms at 50 to 60 feet per second at the impact point while shell center of gravity and head velocity are only about 12 feet per second. Consequently, the test data used in evolving the force-displacement curves was collected at about one-third the velocity developed at the impact point. Yet the velocity change of the head is approximately equal to the velocity change desired to duplicate head response.

If the viscoelastic response of the locally deforming shell and liner is to be evaluated accurately in order to calculate the liner force-displacement curve, testing will have to be conducted by a technique other than a drop test. The impact velocity at the shell surface does not equal eventual head velocity change. This suggests the use of a unique device rather than a drop test device.

SECTION 9

PROPOSED STANDARD

INTRODUCTION

A standard is developed to provide a written "general agreement among makers, sellers, and user groups as to the best current practice with regard to some specific problem." The statement is paraphrased from The American National Standards Institute description of the standards booklet for ANSI Z90.1. This reflects the fact that the standard is a compromise among several individuals concerned with the safety of the user. The specific standard mentioned is the specification for protective headgear for vehicular users. This was initiated as a road user's helmet specification and was oriented primarily toward automobile drivers engaged in high hazard activities, and for motorcyclists. The standard mentions that protective headgear has many users requiring significantly different design criteria, and this is particularly true in that this specification also applies to Army and Air Force helmets. Consequently, the specification for an impacted aircrewman helmet is currently the same as for the motorcyclist.

The purpose of developing a proposed standard for the aircrewman's helmet was to establish the fact that there is a difference between the aircrewman's environment, a difference in the helmet configuration, and a difference in a unique environment, the helmet visor is a permanent attachment to the helmet, and tolerable injury in an aircraft and in an automobile are different. There are, of course, many parts of a standard that will be similar, or the same. Testing procedures, test equipment, definitions, sampling, and labeling may be identical. Therefore, the proposed standard will reflect acceptable portions of the current standard along with the necessary revisions.

The development of the standard must reflect the nature of the helmet as it is currently acceptable. If a proposed standard were to be evolved without considering the criteria currently

applied to it, it is quite possible that the new standard could make the previous impossible to satisfy. If a helmet is to protect the aircrewman from a birdstrike, what birdstrike environment should be selected? For a severe environment, protection is provided by increased liner thickness with a low plateau force. Yet, this is incompatible with the currently acceptable design. The thicker-shell helmet may prevent injury due to a severe birdstrike but would not be worn by the aircrewman. This then establishes that the acceptable configuration is the one that currently satisfies both the user and the generator of the standard. If the configuration is relatively fixed in size and weight, then the protection provided against a birdstrike is dictated by injury criteria and the helmet properties. For a particular helmet there is only a certain amount of protection capability available against a birdstrike impact. The force waveform generated by surface deformation passes on to the skull as a force-time profile which creates an acceleration pulse. The acceleration pulse depends upon the "crushability" of the helmet. Therefore, given that the helmet characteristics are defined (they are defined in order to satisfy the high level impact testing) the "tolerable" acceleration or maximum strain places a restriction upon the environment that is permitted. The "Acceptable" helmet dictates the level of impact testing for birdstrike evaluation.

It would be ideal if a standard could be written that would evaluate the product for the most extreme condition it would encounter. However, some environments that exist are so severe that protection cannot be reasonably achieved. In these instances a compromise is necessary. Standard Z90 is such a compromise in that it reflects a product that will be worn and has provided protection that is acceptable for the wearer. If the worst birdstrike impact were used as the environment to be protected against, there is some justification in selecting a three-inch-deep bump. It could be reasoned that anything greater would imply canopy failure, and hence, a completely new environment. Unfortunately,

if a three-inch-thick liner is required for protection, the helmet will be unacceptable by the user regardless of wording of the specification. In this manner, the reasonable or realistic helmet size has been established and the generation of a standard that fails to recognize this is unnecessary. Therefore, the standard proposed in this Section reflects the assumption that helmet testing to satisfy birdstrike requirements must be evolved from current data on helmet characteristics.

REVIEW OF CURRENT STANDARDS

Several sources of information are available that are directly related to the evaluation of helmet performance. These are:

- (1) Standardization of Impact Testing of Protective Helmets, AGARD-R-629.^[57]
- (2) Considerations in Establishing Performance Criteria for Structural Firefighters' Helmets, NBSTR-77-1251.^[58]
- (3) Riot Helmets, NILECJ-STD-0104.00.^[59]
- (4) Industrial Safety Helmets, ISO 3873.^[60]
- (5) Specifications for Protective Headgear for Vehicular Users, ANSI Z90.1 - 1971.^[61]
- (6) American National Standard Safety Requirements for Industrial Head Protection, ANSI Z89.1 - 1969.^[62]
- (7) Motorcycle Helmets, Federal Motor Vehicle Safety Standard FMVSC 218, NHTSA Federal Register 38.F.F. 22390.^[63]

This is not an exhaustive list but is sufficient to establish the state of the art in protective helmet evaluation.

Regardless of the reference selected, there are several characteristic features that are present in most standards. The method of impact testing can be either by a dropped headform or by a swing-away headform impacted by a striker. If the headform is dropped, an anvil of flat or hemispherical form is used.

The site of the impact is specified to reflect front, back, crown, and sides; and the number of impacts at a particular site may be indicated.

The severity of the impact is established by the mass of the impactor, by the drop height, or by direct specification of the impact energy required. The response to the impact is established by accelerometer and/or force cell outputs. It is the last item that is most pertinent.

One of the primary aspects of interest was that of establishing acceptance relative to biological effects. For the standards reviewed, acceptance implies evaluation of the headform accelerometer response. Figure 99 indicates current acceptance criteria. For example, Z90 requires that an impacted headform not exceed 400G, 200G for more than 3 msecs, or 150G for more than 6 msec. These are the revised values as of 30 March 1973. Previous revisions restricted the acceleration peaks to 2 and 4 msec. The triangular curves shown are those which do not exceed the specifications

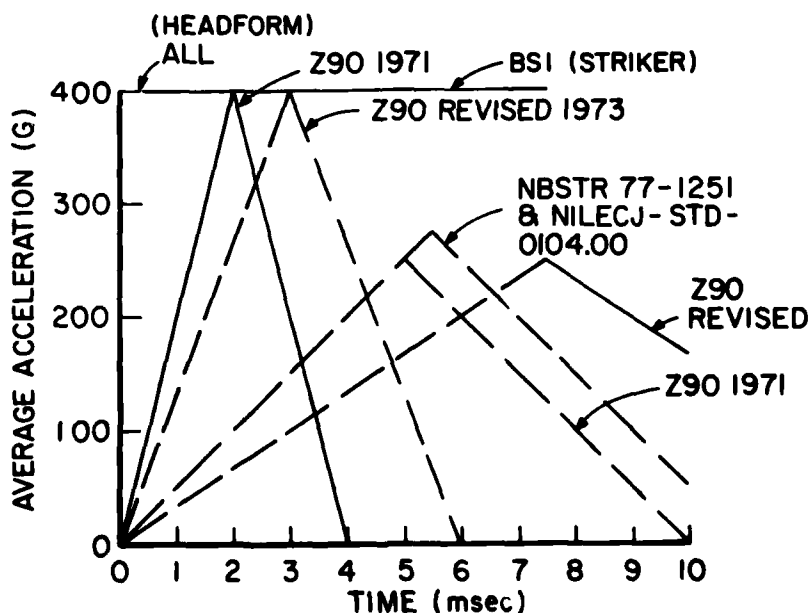


Figure 99. Triangular Waveforms Satisfying Particular Criteria.

listed. These can be replotted on the familiar MSC plot if the triangular pulses are reduced to average acceleration and pulse durations as shown on Figure 100. Hence, the 400G peak triangular waveform that does not exceed 200G for more than 2 msec is plotted at 200G and 4 msec duration. The curves are rather surprising in that they are well above the Wayne State curve. This would indicate that the response of the headform is more severe than what would be considered "tolerable." Additionally, the specification of G levels is usually not related to the orientation of the blow. The only standard listed which reflects a difference in acceptability due to orientation is the fire fighters standard which lists 150G as the maximum for an impact on the top of the helmet.

Another pass criterion for shock absorption is that of transmitted force. Values of 5000 pounds, 4400 pounds, and 1125 pounds are in the literature. The first two numbers are interpreted as implying force limits to insure structural integrity, and only the third is related to tolerance.

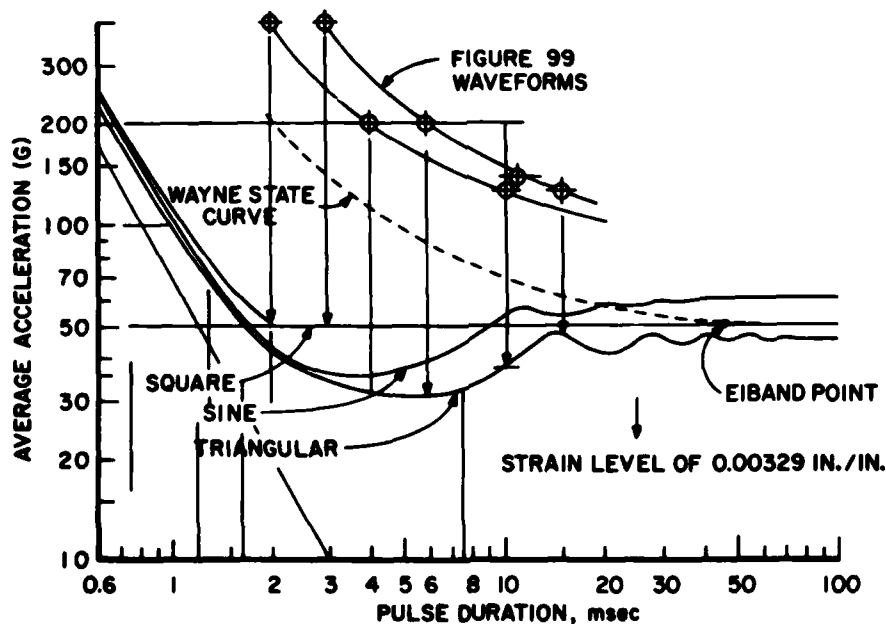


Figure 100. Location of Waveform Pulses from Figure 99 on MSC Plot.

The standards available are more similar than dissimilar, and the levels of accelerations and forces that are acceptable indicate a desire to have a helmet which survives an impact without failure rather than one which restricts injury. Consequently, the standard may be written as a severe test that the helmet must meet if it is to provide protection at a reduced, more realistic level. The forces and accelerations that are acceptable are appreciably greater than values thought to be tolerable. Additionally, the pass criterion are usually independent of the orientation of the helmet, as is the impact energy. This implies that the same impact is equally probable from any direction and that the response of the head is independent of the point of load application. The proposed standard reflects the differences that exist due to the impact location.

DEVELOPMENT OF NEW CRITERIA

The existing Z90 standard establishes acceptance in terms of a peak acceleration of the impacting headform. This same approach can be taken to establish acceptable impacts for lower level impacts. The curves presented in Figure 100 can be used as guidelines. In order to satisfy the strain of 0.00329 inch per inch, triangular acceleration pulses can be assumed in the same manner as the current standard. If the triangular pulse never exceeds 76G, never exceeds 48G for more than 1 millisecond, and never exceeds 35G for more than 2 milliseconds, then the plotted acceleration closely approximates the proper strain for tolerable response. However, by comparing the criteria with the acceleration pulse of the nonvisored helmet, it can be seen that all accelerations were exceeded, yet the pulse did not generate intolerable response. Hence, the use of a "standard" waveform leads to a conservative criterion. This approach can be used if it is desired to be compatible with current specification. The reason for the difference is, of course, that MSC is generated as a function of the waveform and the natural response of the skull/brain model. The waveform generated by the helmet cannot be

easily approximated by a triangular waveform, and it is the rise time that creates the acceptable response.

The same approach can be used laterally in that there are tolerance curves available for lateral human response, again based upon the MSC model. Figure 56 indicates that if triangular pulse waveforms are to be used to compare with measured lateral response, the peak acceleration at 5 milliseconds is only about 30G. The acceptable lateral pulse is significantly less than that of the longitudinal. The acceptable strain is the same, but the mass, stiffness, and damping of the model for lateral impact requires a lesser input to achieve the same strain output.

The triangular pulse approach can be continued for studying the response of the head to a blow to the crown. We have assumed that about 1000 pounds is the maximum permissible force on the skull. We have also assumed from the vertebral column data that about 440 pounds of axial force is indicative of the limits of elastic deformation at large strain rates. These, along with currently acceptable models of the axial response of the head and neck permit us to investigate the force response of the model to determine tolerable limits.

The head and neck have a natural frequency response axially of about 30 Hz. This was recently used with angular motion kinematics to duplicate the response of the head-neck system to inertial accelerations. A rigid head supported by an elastic neck is the model used by Schneider in duplicating axial response. The coefficients for the model were:

Weight of Head	14.3 pounds
Weight of Neck	3.37 pounds
Natural Frequency	30 Hz

and from these:

Total Mass	0.04 pounds sec ² /inch
Stiffness	940 pounds/inch
Damping	6.04 pounds sec/inch
Damping Ratio	0.5

If it is assumed that the skull is driven by a triangular acceleration pulse, the velocity and displacement can be found and the equation of motion

$$M\ddot{X} + C\dot{X} + Kx = F(t)$$

can be used to calculate the kinetic response.

A triangular pulse of 50G peak with duration of 5 milliseconds will generate a force of 900 pounds at peak acceleration, and 400 pounds at zero acceleration or maximum velocity. The forces generated are shown in Figure 101. Since the forces are linearly related to the peak acceleration, an increase in the peak value up to 55G reaches the 440-pound neck limiting force before the 1000-pound skull limit is reached. Using this simplified approach it is possible to examine the effects of a triangular waveform in terms of skull and neck force.

By decreasing the pulse duration to 4 milliseconds, the applied force peak is 890 pounds with a maximum neck force of 128

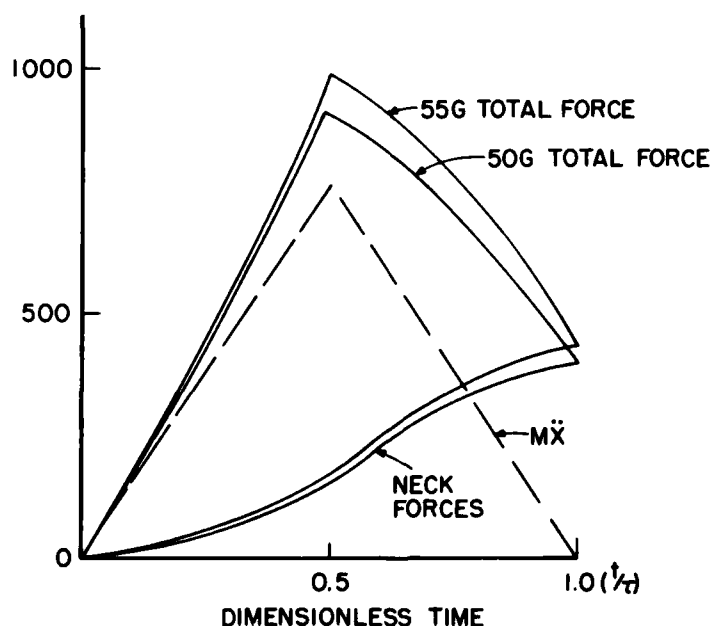


Figure 101. Skull and Neck Forces Required to Generate Triangular Pulse.

pounds. By increasing the peak acceleration the allowable skull force is reached at 56G while the neck forces reaches only one-third of "tolerable." Hence, at about 5 milliseconds, tolerable response shifts from skull force limiting to neck force limiting for a triangular acceleration pulse. At the other side of 0.005 seconds, 0.010 seconds, the neck force for a 50G peak is 1037 pounds which requires a reduction of peak G to 21.2 to keep neck force to the permissible 440 pounds. The steady state acceleration for the neck force limit is 28.5G. The acceleration for impulsive response approaches 65G.

A second approach taken was that of assuming the skull acted upon by a 1000-pound half-sine pulse of 0.005 seconds duration. For the previously assumed model coefficients, the response spectra curve indicates that the ratio between maximum displacement and peak force over stiffness is:

$$\frac{v}{\epsilon_p} = \frac{x_{\max}}{F_{\text{peak}}/K} = 0.4$$

or

$$0.4 = \frac{x_{\max}}{1000/940} \quad , \quad x_{\max} = 0.426 \text{ inches,}$$

and therefore, the maximum neck force is $0.426 \times (940) = 400$ pounds. Hence, although a different input wave form is assumed and force is the driving parameter, the results are nearly identical to those of the 5-millisecond acceleration pulse.

The curve of limiting acceleration for a crown impact is shown in Figure 102. The curve is completely different from that of the MSC curve because of the completely different nature of the model. The MSC curve assumes a brain that responds at a relatively high frequency to an acceleration input. The "crown" limit is based upon forces calculated for a relatively low frequency system connected to a lower frequency torso.

The effect of the lower torso frequency was evaluated by idealizing the head and torso as a coupled system with the head and neck as idealized above, and the lower torso as a 10-Hz

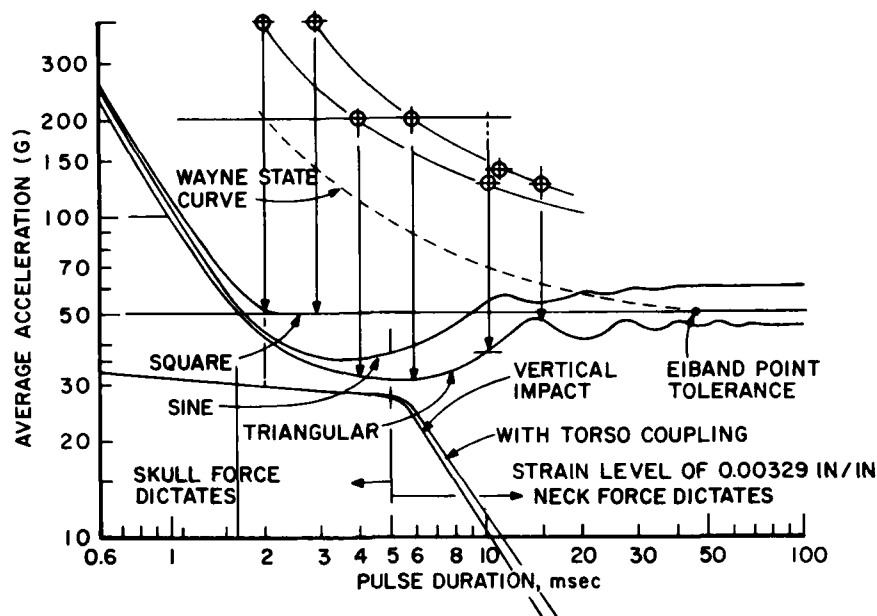


Figure 102. Vertical Impact Tolerance Curve Based Upon 1000-Pound Skull Force and 440-Pound Neck Axial Force Limits.

system of two tenths critical damping. Solving the differential equations and calculating the response due to a triangular pulse of 0.010-second duration yields a 997-pound neck force for the 50G peak. The 440-pound limit restricts the acceleration to 22.1G or an average of 14.1G on Figure 102. As shown, the effects of torso coupling are reduced with decreased pulse duration.

The injury criteria for head protection have been established for each of the three axes. The criteria are in terms of maximum strain for two axes where some experimental data are available, and are in terms of force response for the other. All are established as being indicative of injury below the concussive level. The data are now used to calculate standards data.

DEVELOPMENT OF IMPACT TESTING REQUIREMENTS

The introduction of this chapter established the need to relate any helmet standard development to the current Z90 standard.

The "acceptable" helmet is one which has passed Z90 and therefore possesses certain characteristics which must be reflected in any revisions. An examination of Z90 indicates that most of the requirements will not be changed. The only areas requiring revisions are those related to impact attenuation and for those, a new low-level test series must be generated. For a given "acceptable" helmet, what drop heights are compatible with the injury levels evolved?

The first area investigated is that of a blow to the crown of the helmet. This will be examined first in relation to the birdstrike environment and then for an arbitrary blow to the crown. Several curves had previously been presented to indicate the effects of having the birdstrike impact at a more horizontal attitude. As the impact angle becomes more shallow, the fore-and-aft head acceleration incidence is reduced slightly over the entire pulse. The curve shown for a 5° incidence angle on Figure 64 reflects a "tolerable" environment as predicted by the MSC. For this condition the vertical response is calculated to determine the severity at the least impact angle. The acceleration time pulse selected generates a peak force of 1000 pounds vertically and 600 pounds of frictional force. By calculating the angular kinematics at the peak force; $\alpha = 10,000 \text{ rad/sec}^2$, $\omega = 28.8 \text{ rad/sec}$, and $\theta = 3.4^\circ$; it is possible to calculate the forces carried at the neck. From a free body diagram with head tilted back at 6° , dynamic equilibrium requires 800 pounds of axial force, and 233 pounds of shear force at the skull/neck joint. The vertical acceleration is 6.6G which explains why the applied vertical force and neck axial force are nearly the same. These indicate that the neck axial force is too great and a less severe pulse must be examined.

By reducing the interference to 0.85 inches, the response is reduced significantly. The maximum kinematic values are: $\alpha = 6500$, $\omega = 18.1$, and $\theta = 2.7^\circ$. Using these and calculating the forces generated at the neck, the maximum axial force is 438 pounds, and maximum shear force is 328 pounds. The maximum vertical acceleration becomes 2.6G.

The analysis indicates that the head vertical response to a birdstrike input is dominated by the force response. The accelerations are small, the velocities are reasonable, and the angular motion very small. The parameter of concern is the force developed whether at the skull or the neck/skull attachment.

With the nature of the response known, it is possible to reexamine head/neck vertical response more carefully. The head and neck are modeled by a mass upon a spring and damper as previously discussed. The system's damped natural frequency is 22.6 Hz and the duration of the pulse is about 0.004 seconds. Therefore, the ratio of pulse duration to system period is 0.004/0.042, or less than one-tenth. This is impulsive response. Vertically the head cannot respond until after the pulse has passed. For such a condition, the displacement of the head relative to the shoulders is analytically expressed

$$x = \frac{F_o}{M} \left(\frac{e^{-\alpha t}}{\beta} \right) \sin \beta t$$

where: X is the displacement
 F_o is the impulse
 M is the mass
 α is the damping term $C/2m$, and
 β is the damped natural frequency.

Assuming that a 500-pound crush force acts over 0.003 seconds, the response can be calculated in terms of both displacement and velocity. Since the stiffness and damping coefficients are known, the force developed at the neck is then calculated. The maximum axial force possible is only 226 pounds which is directly proportional to impulse. The velocity generated by the impulse is $F_o/m = 37.5$ inches per second and the average acceleration is 32.5G. These would plot between the strain limits for longitudinal and lateral head impact. By calculating the velocity out to 20 milliseconds the maximum upward velocity is found, at about 16 milliseconds, to be 11.8 inches per second. Therefore, the total velocity change is 49.3 inches per second.

If the magnitude of the impulse is raised as a result of increased interference, to develop a 1000-pound peak skull force, the impulse becomes 2.5 pounds seconds raising the impulsive velocity to 62.5 inches per second and the neck axial force to 377 pounds. Correspondingly, the velocity change becomes 82.2 inches per second, and the average acceleration is 36G. The average acceleration over a 0.0045-second duration again plots within the strain limits of longitudinal and lateral response. Hence, the purely vertical impact having a force input dictated by crush characteristics indicative of helmet crushing force and displacement, and related to time by a "slow" bird velocity yields a response that is limited by the force developed at the skull. The acceleration and velocity changes are similar to those of longitudinal and lateral tolerability, but there is no basis for comparing vertical response to them. Therefore, the drop test required should attempt to match the impact conditions, but the response has no means of establishing tolerability, or acceptability, other than force at the impact site.

In order to better evaluate the response of an impact on the crown, a particular impact test was reexamined. Outputs from a Z90 impact test conducted on a helmet having fitting pads, insolite and foam inserts, and a thickness prior to test of 1.3 inches at the crown, were developed into a force-displacement curve as shown in Figure 103. The curve indicates an elastic portion of about 0.11 inches followed by a slowly increasing force up to a maximum of about 900 pounds. For a test device dropped with this crush characteristic, the response in the elastic range is calculated from the equation:

$$\ddot{X} = \frac{-V_0}{\omega} \sin \omega t,$$

where

- \ddot{X} is the acceleration
- V_0 is the impact velocity and
- ω is the natural frequency.

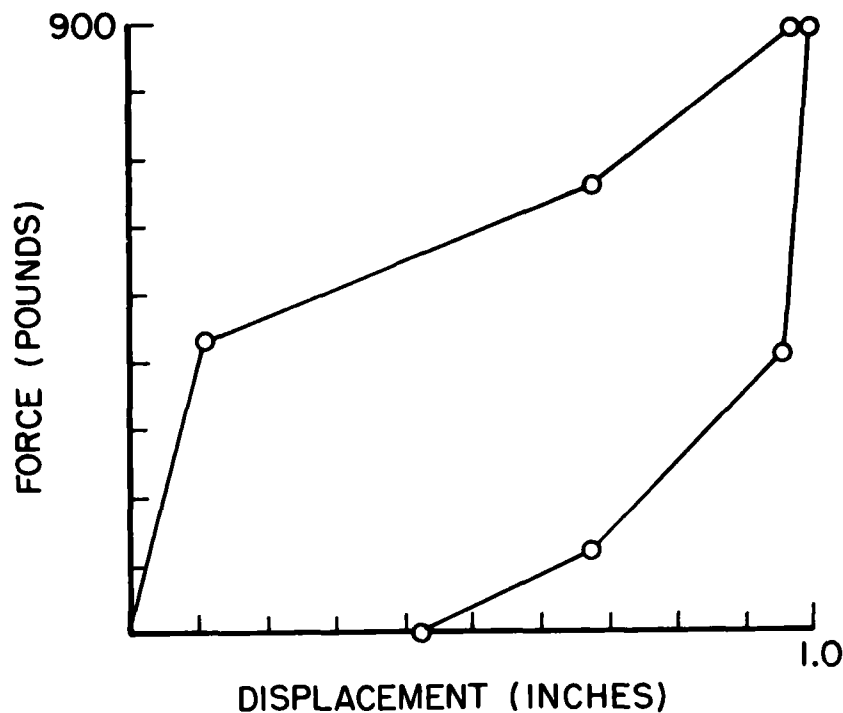


Figure 103. Force-Displacement Curve for Drop No. 13 of HGU-22/P Helmet (Drop on Crown).

For the curve assumed, if the maximum elastic displacement is 0.11 inches for 440 pounds, and the mass of the headform is 0.0292 (11.2 pounds); the natural frequency is then about 59 Hz. The maximum permissible impact velocity is then 40.6 inches per second. Since the response is in the elastic range, the velocity change is therefore 81.2 inches per second. This suggests that a test drop conducted using the existing headform will create the desired velocity change in the elastic range. The peak headform acceleration would be 28.4G, and the impact force at the anvil would be 440 pounds. The acceleration is sinusoidal with a pulse duration of 0.0085 seconds. Even at that duration, the waveform would be impulsive relative to the characteristics of the head/neck system.

During the birdstrike the head is accelerated downwardly by a displacement at the helmet shell. The shell liner creates a force that accelerates the head and creates a velocity change

that must be dissipated by the body. In the impact test environment, a deceleration pulse acts to dissipate an impact velocity and creates a "rebound" velocity depending upon the elasticity of the liner. The significant difference between the two is the integrated displacement. In the birdstrike environment the displacement between skull and neck continually increases since the velocity continually increases. In the drop test the displacement, if it is an elastic range, returns to zero. In the birdstrike environment the "neck" force dictated by velocity and displacement would be quite large. In the drop test the "neck" force would be attributed to only relative velocity. Consequently, the previous impulse analysis was conducted to indicate that in order for the neck force to exceed the allowable, for a given velocity change, the skull force would have been exceeded first. Or, conversely, if we restrict the response of the skull force (anvil force) to 1000 pounds, and only permit a velocity change of 82.2 inches per second, we have established a bound upon the response of a test condition which relates to the only tolerance criteria available.

From the above, the test condition for low level impact to be included with the current Z90 standard would have the following added.

<u>Impact Site</u>	<u>Head Form Drop Height</u>	<u>Pass Criterion</u>
Crown	2.2 inches	< 1000 pounds (anvil)

Calculation of the test conditions required for a longitudinal or lateral impact were more easily developed. For both cases a limiting MSC had been established. Knowing the strain limit, and having MSC model coefficients available for both directions, it was possible to analytically examine the response of an impacting test device at various drop heights.

A force-displacement curve for a liner of about one-inch thickness was selected for analysis to better represent the liner at the brow. Analyses were then conducted to calculate the

acceleration of a Z90 headform mass impacting at selected impact velocities. The results are shown in Figure 104. These were used to calculate the brain "strain" using the coefficients shown below. The strain curves evolved for longitudinal response are also shown in Figure 104 with a cross plot indicating that for a strain of 0.00329 inches per inch it is necessary to drop the test device from about 2.12 feet, which will generate an impact velocity of 11.7 ft/sec and an impact energy of 23.9 ft pounds assuming a 2.3-pound helmet.

The same approach for the lateral coefficients of the MSC model indicates that the response is totally in the elastic range of the force-displacement curve. The limit strain is reached with an impact velocity of only 2.61 feet per second, which generates a velocity change of 5.52 feet per second.

The results for the longitudinal and lateral response can be tabulated as:

<u>Impact Site</u>	<u>Head Form Drop Height</u>	<u>Pass Criteria</u>
Front Brow	25.5 inches	0.00329 MSC
Lateral	1.27 inches	0.00329 MSC

The values listed for all orientations reflect differences in helmet/liner stiffness due to thickness, differences in head/neck actual frequency in two axes, and differences in tolerance criteria as functions of orientation. However, they also reflect the use of empirical data. If the configuration of helmet and liner does not vary significantly, as partially dictated by the need for acceptability under Z90, it is believed that the test parameters are realistic conditions and criteria for lower level tests.

DEVELOPMENT OF PROPOSED STANDARD

The following paragraphs provide a discussion of the American National Standard, Specifications for Protective Headgear for Vehicular Users, ANSI Z90.1. Each main section of

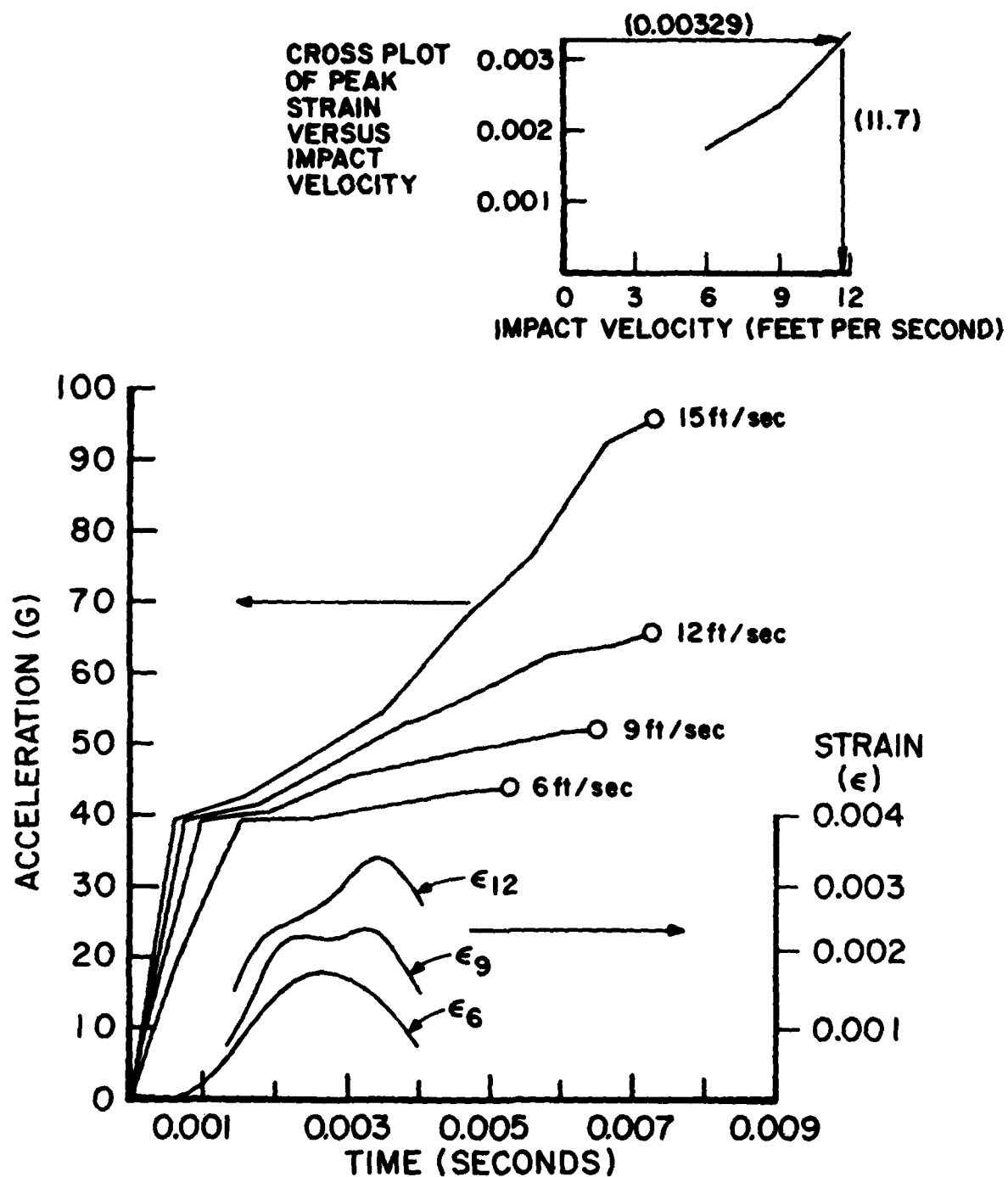


Figure 104. Frontal Acceleration and Strains as Functions of Impact Velocity.

the standard will be discussed to indicate revisions believed to be desirable. (ANSI Standard Z90 is reproduced as Appendix B.)

Scope, Purpose, and Requirements

The standard by virtue of its being used for aircraft should indicate applicability to both surface and flight vehicles. Also, the current description excludes eye and face protection devices, such as a visor, and any future testing should continue to do so. Theoretical results do indicate that the visor does not adversely affect the helmet response, but a full evaluation of the effects of a visor are not known. Any attempts to add testing requirements specifically oriented toward the visor would be based more upon conjecture than upon quantitative prediction.

The purpose of the standard is still to provide minimum performance criteria...to mitigate...adverse effects of a blow. The basis for the criteria is not explained and there is some question as to the large accelerations acceptable although these may be related to "survivability," not injury. The addition of lower level testing is required to mitigate injury in the sense of establishing nonconcussive performance criteria.

The requirements are not changed in that the primary goal is still impact attenuation as well as penetration resistance and strength of the retention system.

Definitions

To the list of definitions should be added: Maximum Strain Criteria: a parameter indicative of injury to the brain computed using the acceleration waveform of the headform, and coefficients related to the strength of the skull and brain.

Construction

Inasmuch as the visor has been excluded from the scope, there is no change required. If the visor is later considered, it would have to be mentioned as an optional device and would influence the definition of external projections.

Materials and Labeling

No changes are necessary.

Extent of Protection and Sample for Testing

Visor components may eventually be considered as detachable components with separate testing requirements.

Conditions for Testing

No changes are required in that the order of testing is established in a later section. All other aspects are not influenced.

Tests for Protective Headgear

Tests shall be conducted at two different impact levels. The first series of tests are conducted to determine the capability of the headgear to provide low level noncussive response to high speed, nonfatal impacts. The second set of tests are those to establish the acceptable performance of the headgear for maximum protection.

Under a new subsection, Acceptable Low Level Performance, the acceleration waveforms are used as input to the MSC model and the peak strain is calculated as indicated in the appendices. Should the strain for either the longitudinal or lateral drop exceed 0.00329, the test will be considered a failure. Should the peak measured force of anvil load cell exceed 1,000 pounds for the crown drop, the test is also a failure. The accelerations shall be measured with an instrumentation system whose accuracy, including reading error, shall be $\pm 28G$ maximum. Readings shall not be corrected for instrumentation accuracy. The impact force shall be measured by a force cell mounted firmly to the anvil. The force measurement system used shall measure forces of up to 10,000 pounds with a flat response within 5 percent between 5 Hz and 1000 Hz.

Low Level Impact Condition

Each protective headgear shall be impacted in not less than three sites. The drop sites are:

Crown No more than one (1) inch from the intersection of the helmet shell, mid-sagittal plane, and the coronal plane.

Side No more than one (1) inch vertically from the intersection of the helmet shell, reference plane, and the coronal plane.

Front No more than one (1) inch vertically from the intersection of the helmet shell, reference plane, and mid-sagittal plane.

Impacts shall occur using a flat steel anvil at an energy level dictated by the following drop heights.

Crown 2.2 inches ± 0.1 inch
Side 1.3 inches ± 0.1 inch
Front 25.4 inches ± 0.1 inch

Acceptable High Level Performance

The high level test is that previously described in the standard. All references to peak acceleration levels, accelerometer capabilities, drop heights, etc. are unchanged.

Impact Description, Headform, Placement of Protective Headgear, and Backing of Anvil; are all unchanged.

Sections describing Penetration Tests and Retention Tests are unchanged. All sections of Preparation of Test Equipment are unchanged.

Calculation of MSC

A new section, A.5, must be added. The new section is as follows.

The acceleration time trace is divided into straight line segments at one-millisecond intervals or at lesser time intervals if necessary to better approximate the curve. The straight line approximation is then reduced to a series of linear slopes which represent the figure. The total response of the MSC model is then the summation of the responses to the individual slopes. The basic equation is:

$$\epsilon = \frac{\ddot{u} (386)}{l_o \omega_n^2} \left[\frac{t}{\tau} - \frac{1}{\omega_n \tau} \cdot \sin (\omega_n t) \right]$$

where \ddot{u} is the acceleration at τ

τ is the time selected to establish the slope

l_o is the reference length depending upon lateral or longitudinal response

ω_n is the natural frequency for lateral or longitudinal response

t is the time of interest.

As an example, for a 50G peak at 5 msec, as shown on Figure 105, the calculation of strain can be accomplished. For longitudinal response, l_o is 5.78 inches and ω_n is 1300 radians per second. Therefore,

$$\epsilon_1 = \frac{100 (386)}{5.78 (1300)^2} \left[\frac{t}{0.01} - \frac{1}{1300 (0.01)} \sin (1300t) \right]$$

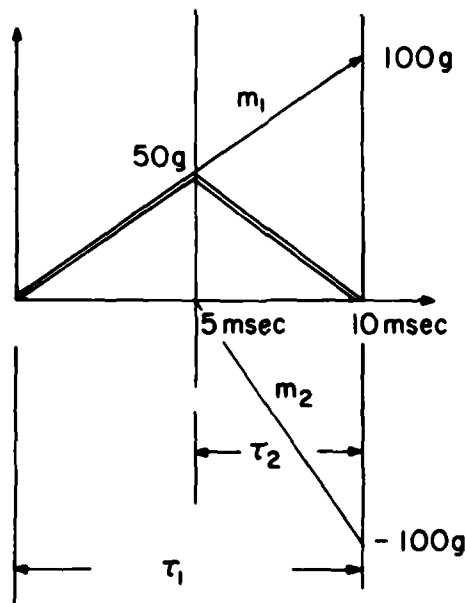


Figure 105. Triangular Acceleration Pulse with Line Approximations.

and similarly

$$\epsilon_2 = \frac{100 (386)}{5.78 (1300)^2} \left[\frac{t}{0.005} - \frac{1}{1300(0.005)} \sin (1300t) \right]$$

These result in:

$$\epsilon_1 = 0.39515t - 0.000304 \sin (1300t)$$

$$\epsilon_2 = 0.7903t - 0.000608 \sin (1300t)$$

By tabulating the values of strain for every millisecond, the resulting curves is as shown in Figure 106. For this the maximum strain is 0.00192, which is tolerable.

The equation used is the response of an undamped single degree of freedom system to a ramp input. The MSC model does have damping, but the damping ratio of 0.028 makes the approximation over a small number of milliseconds acceptable. Note also that maximum strain is influenced by a transient term which peaks at 0.00363 seconds. Hence, the maximum strain will be found without computation of the response for the full pulse duration.

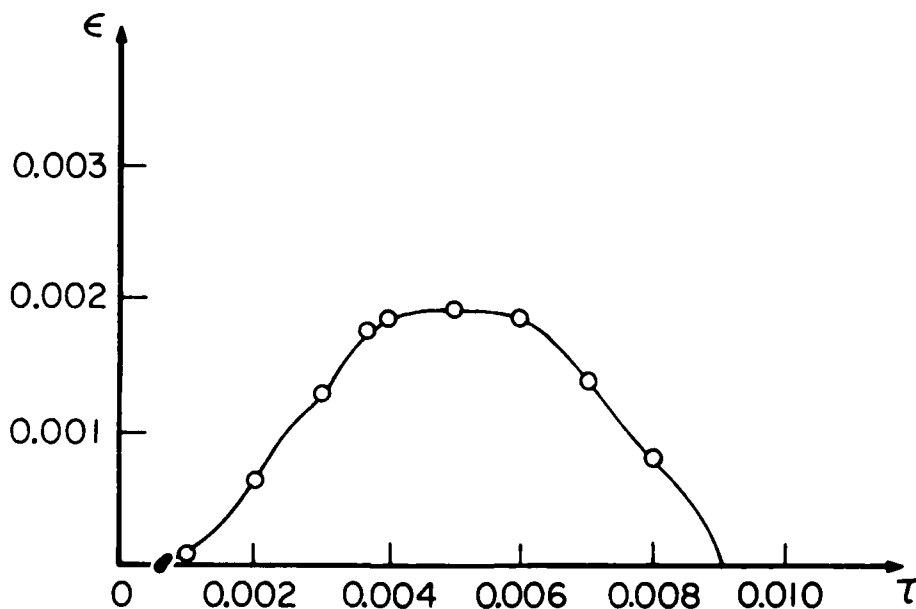


Figure 106. Calculated Strain for 50G Triangular Pulse.

SECTION 10

SUMMARY, CONCLUSIONS, AND RECOMMENDATIONS

SUMMARY

The ultimate goal of all research conducted on this program was to provide the means of assessing the response of a helmeted aircrewman to a birdstrike. Given that a birdstrike occurs, creating a deformation in the canopy that strikes the helmet, what is the response of the aircrewman both kinetically and in terms of injury?

By reviewing biomechanical data indicative of head and neck injury, it was possible to select a level of maximum strain for the MSC model indicative of nonconcussive response. Hence a quantitative evaluation of the head's kinematic response was established.

The kinetic and kinematic response of the helmeted head was established by use of a comprehensive mathematical analog of the human body. From film data of birdstrike tests, impact data from helmet tests, and current biomechanical coefficients, the analog was used to predict aircrewman response. The analyses conducted established the feasibility of using a simplified model which could adequately duplicate the analog's output. Specifically, the parameters with quantitative injury criteria available were duplicated.

Using the analog and limited test data, a test device was designed, fabricated, and calibrated to permit evaluation of the forces transmitted to the crewman's head during bird impact. The device, in conjunction with an anthropometric head form and accelerometers, permits the impact forces to be deduced from the measured parameters.

Static tests of a standard helmet were conducted to evaluate the contributions of shell and liner to helmet stiffness. Unique test hardware was fabricated to permit testing of a helmet or liner at any orientation. A series of tests were conducted under static conditions for comparison with drop test data.

Many conclusions and recommendations can be drawn from the research conducted.

CONCLUSIONS

1. For an aircrewman seated with his eye at the design eye point, the helmet clearance beneath the F-16 canopy interior is small enough to be potentially dangerous at the higher bird impact energy levels.
2. Film data analyzed for the F-16 canopy indicate that the bump depth is approximately a linear function with bird kinetic energy.
3. The speed at which the bump travels down the canopy does not increase with bird speed but is believed to be dictated by the impulsive response of the canopy.
4. By using the ATBM to represent the helmeted aircrewman the following was determined.
 - (a) The head and neck system is low-frequency relative to the bird impact and cannot respond quickly enough to generate significant displacement during the impulse.
 - (b) At impact levels thought to be injurious, there is little difference in head response between an impulse due to a "stiff" canopy or a "soft" canopy.
 - (c) Injury, whether defined by translational motion, MSC, or forces, occurs with helmet crush equal to liner thickness, or about one inch.
 - (d) The visor stiffness and added thickness cause the bird impact to be prolonged at a reduced acceleration and applied peak force. The acceleration and force indicate a reduced probability of injury, but the acceleration waveform integrated within the MSC model indicates no improvement in protection. This excludes the presence of a visor knot at the crown.

- (e) The headrest impact response is no greater than that of the birdstrike causing the motion. This is because of the energy dissipation of the system as well as the fact that even headrest response is dictated by liner characteristics.
5. Biomechanical injury data were reviewed and collated. Human test data, cadaver data, model predictions, scaled animal data, and an engineering appreciation of the problem were used to generate a table of values believed to be "tolerable" and nonconcussive. Several parameters such as translational acceleration, translational velocity, and skull force are compatible with the use of the MSC model. For the model, a strain of 0.00329 was selected as tolerable. This permits evaluation of an impact at other than just frontal blows.
 6. The kinetics of the ATBM helmeted head and neck can be approximated by a rigid head model pivoted at the occipital condyles. Using the same geometric and inertial characteristics as would be used by the ATBM, the bird impact on a damped pivoted head creates fore-and-aft translational accelerations, velocities, and displacements as well as maximum strain which duplicates the ATBM response. The dynamic response between bird and helmet can be duplicated by using two intersecting spheres of known force-displacement characteristics assuming no motion of the head.
 7. Parameter variations conducted using the simplified model indicates that a change of interference of one-half inch creates far more change in head translational acceleration and strain than any of the realistic variations studied for wavespeed, incidence angle, surface friction, or neck damping.
 8. Bird impact response of the helmeted head and neck can be measured by using a test device designed to measure forces and moments at levels indicative of injury. The device measures the force and moments at the base of an anthropometric

dummy head and neck. These, with accelerations of the head and device base plate, can be used to calculate the forces applied to the head.

9. The development of a new impact test standard to reflect the birdstrike environment must be dictated by requirements of the current standard. Acceptance criteria of the standard dictates the environment of a low-level birdstrike test.
10. The shell of a helmet forces more liner material to compress on the skull than would do so with no shell. The shell of a standard Air Force helmet creates a force-displacement curve similar to a "rigid" shell when tested statically. Comparisons between static and dynamic tests indicate that the liner behaves as a viscoelastic medium creating a greater force response at the initial higher relative velocity across the liner than is seen at static levels.

RECOMMENDATIONS

1. A great amount of emphasis was initially placed upon establishing the proper clearance between helmet shell outer surface and canopy inside mold line. For a specific eye point, the shell location is essentially specified for all percentiles of aircrewmembers and consequently some measure of acceptance can be established for a particular canopy bump depth. However, a more critical question would be, where does the bird impact? All test data examined were generated by a bird impacting at or near the waterline of the design eye point. If the impact point were raised, there is the possibility that maximum bump depth would be generated right at the least helmet clearance. This does not mean that the same bump depth energy curves can be used. At impacts higher on the canopy, the greater stiffness would probably reduce the depth for a given kinetic energy. However, this is not known to be true. Consequently, impact tests should be conducted with impact points other than the design eye, or the most

probable locations for impact should be established by those familiar with the statistics of the true nature of the birdstrike phenomena.

2. Test data collected using the developed test device is necessary. The true mechanism of helmet-canopy impact is not well understood although it has been idealized. The wave motion of the bump and its interaction at the helmet shell create an unusual condition idealized by crushing and surface friction between two deformable bodies. Would test data verify the results of a computer-generated response? No data were available where all the variables of a test were accurately known prior to the test.
3. Tests are required using the standard Air Force flight helmet at very high impact velocities. Current test data are indicative of impact with a relative velocity across the liner of about 16 feet per second. Based upon the film data analyzed and computer generated results, the impact velocity should be about 60 feet per second. This rules out testing using a standard drop facility, and implies the use of powered test devices where large velocities can be achieved. Hopefully, testing at higher velocities would verify the visco-elastic nature of the shell and liner combination.

APPENDIX

TYPICAL ARTICULATED TOTAL
BODY MODEL INPUT DATA

SEGMENT			WEIGHT (LB.)	SEGMENT MOMENT OF INERTIA (LB.-SEC.**2- IN.)		
I	SYM	PLOT		X	Y	Z
1	LT	5	25.814	1.01760	.60740	1.00320
2	CT	4	28.089	1.24530	1.04030	.74760
3	UT	3	22.471	.75880	.49770	.79630
4	N	2	5.033	.08050	.08050	.03400
5	H	1	10.805	.19760	.23620	.15150
6	HL	6	.219	.00760	.00760	.01140
7	HS	7	2.188	.07550	.07550	.11700
8	UL	8	34.880	3.24400	1.40600	2.09000
9	B	7	9.600	99999.00000	99999.00000	99999.00000

LT = Lower Torso
 CT = Center Torso
 UT = Upper Torso
 N = Neck
 H = Head
 HL = Helmet Liner
 HS = Helmet Shell
 UL = Upper Legs
 B = Bird and Canopy

SEGMENT CONTACT ELLIPSOID					
SEMIAXES (IN.)			CENTER (IN.)		
X	Y	Z	X	Y	Z
3.80	6.79	3.93	0.00	0.00	0.00
4.03	5.34	6.79	0.00	0.00	0.00
4.00	6.29	4.15	0.00	0.00	0.00
2.33	2.33	4.49	0.00	0.00	0.00
4.14	3.25	4.91	0.00	0.00	0.00
5.26	4.90	5.28	0.00	0.00	0.00
5.38	5.00	5.38	0.00	0.00	0.00
2.99	8.19	12.40	0.00	0.00	-2.60
10.00	10.00	10.00	0.00	0.00	0.00

THIS PAGE IS BEST QUALITY REPRODUCIBLE
 FROM COPY FILM AND TAPES

FUNCTION NO. 10

SEAT CUSHION

D0
0.0000

D1
-5.0000

D2
0.0000

FIRST PART OF FUNCTION - 7 TABULAR POINTS

D	F(D)
0.000000	0.0000
1.000000	40.0000
2.000000	70.0000
3.000000	100.0000
4.000000	170.0000
5.000000	280.0000
6.000000	700.0000

D = Distance in Inches
F(D) = Force in Pounds

FUNCTION NO. 13

HEAD CONTACT STIFFENS

D0
0.0000

D1
-2.6000

D2
0.0000

FIRST PART OF FUNCTION - 7 TABULAR POINTS

D	F(D)
0.000000	0.0000
.280000	500.0000
.080000	500.0000
1.060000	1000.0000
1.320000	2000.0000
1.520000	3000.0000
2.600000	9000.0000

THIS PAGE IS TO BE DELETED
FROM COPY 12-11-1960

APPENDIX B

AMERICAN NATIONAL STANDARD SPECIFICATIONS FOR
PROTECTIVE HEADGEAR FOR VEHICULAR USERS

American National Standard

Specifications for Protective Headgear

for Vehicular Users

1. Scope, Purpose, and Requirements

1.1 Scope. These specifications and test methods apply to protective headgear for wear by drivers and passengers of surface vehicles and specifically exclude eye and face protective devices.

1.2 Purpose. This standard specifies minimum performance criteria and test methods, performed under fixed conditions, for protective headgear designed to mitigate the adverse effects of a blow to the head.

1.3 Requirements. Tests are conducted of the protective headgear assembly to ascertain compliance, under specific environmental conditions, with the following requirements:

- (1) Impact attenuation properties of the protective headgear
- (2) Penetration resistance
- (3) Strength of the retention system and its attachments

2. Definitions

basic plane. A plane laid out on a specific reference headform¹ derived from the anatomic basic plane, or Reid's Baseline. (A plane at the level of the external opening of the ear and the floor of the bony rim of the eye socket.)

mid-sagittal plane. A longitudinal, or fore and aft, plane passing through the vertex of the headform, perpendicular to the basic plane, which geometrically bisects the headform.

projection. Any part that extends beyond the surface in abrupt fashion.

protective headgear. A device worn on the head, designed to mitigate the adverse effects of a blow to the head in the area specified elsewhere herein.

reference plane. A plane 2.36 inches (60 mm) \pm 0.04 inch (1 mm) above and parallel to the basic plane, and which shall be located on each headform.

retention system. (Also referred to as "harness assembly.") The completed assembly by means of which the protective headgear is maintained in position on the wearer's head

3. Construction

3.1 General. A protective headgear will consist of a hard, smooth outer surface containing the necessary means of attenuating impact energy and resisting penetration. Optional devices fitted to the protective headgear shall be so designed that they are unlikely to cause injury to the wearer in the event of an accident.

3.2 Projections. The assembled protective headgear shall have no permanent external projections greater than 3/16 inch (5 mm) in height.

3.3 Retention. The retention system shall be so constructed that when properly fastened, the protective headgear cannot be readily dislodged from its normal position on the wearer's head during impact conditions.

3.4 Peripheral Vision. The protective headgear shall provide peripheral visual clearance of a minimum of 120 degrees to each side of the mid-sagittal plane. This angle shall be measured on the standard headform¹ in the basic plane with its apex at the anterior surface of the headform where the mid-sagittal and basic planes intersect.

Medium and large size protective headgear will be tested on a single headform size. Other sizes of protective headgear of the same type will be approved if visual inspection shows the construction to be identical to those tested.

4. Materials

The materials used in the manufacture of the various parts of the protective headgear should be of durable

¹It was necessary for the purposes of these recommendations and in order to give requirements for the extent of protection to define artificial headforms, both to serve as a basis for instrumentation during tests, and to provide fixed parameters for measurement. It is realized that the variation of human head shape is such that the artificial headform may not conform exactly to the shape of any random sample human head, a considerable amount of anthropological data has been reviewed in order to decide the limiting dimensions, and the headform selected is considered suitable to allow for proper testing of protective headgear which will accurately fit approximately 95 percent of the population of all races.

Information concerning sources of the actual headforms or pattern thereof may be obtained by a request addressed to Cragg Industries, 19007 S. Reyes Avenue, Compton, California 90221.

quality, that is, their characteristics should not undergo appreciable alteration under the influence of aging or of the circumstances of use to which the protective headgear is normally subjected, such as exposure to sun, rain, cold, dust, vibration, contact with skin, perspiration, or products commonly applied to the skin or hair.

5. Labeling

Every protective headgear offered for sale shall have durable labeling which will give the model designation and allow the identification of the manufacturer to be made. The labeling shall include the following:

(1) No protective headgear can protect the wearer against all foreseeable impacts. However, for maximum protection under this standard, the helmet must be of good fit and all retention straps must be securely fastened.

(2) This protective headgear is so constructed that the energy of a severe blow is absorbed through partial destruction of the headgear, though damage may not be visible to the naked eye. If it suffers such an impact, it should either be returned to the manufacturer for competent inspection or destroyed and replaced.

6. Extent of Protection

6.1 The extent of protection shall include all areas above the reference plane. None of the protective components of the headgear shall be inadvertently detachable, or detached under test impact.

6.2 The entire area of the protective headgear above the reference plane shall attenuate impact energy to at least the minimum requirements specified in Section 9.

7. Sampling for Testing

7.1 Condition and Attachments. For all testing, protective headgear shall be taken in the condition as offered for sale, and shall be accompanied by all attachments (other than eye protection devices) normally sold with the protective headgear. Such attachments shall not be installed on the helmet during testing.

7.2 Number of Samples. Four samples are required for testing. Each test sample, following exposure to its respective environmental condition as described in Section 8, shall be subjected to all tests and visual observation set forth herein.

8. Conditioning for Testing

8.1 Order of Testing. The impact attenuation, penetration, and retention system tests set forth in Sections 9, 10, and 11 shall be conducted in ascending numerical order.

8.2 Time. Testing shall begin immediately after removal from the conditioning equipment as indicated in 8.4, 8.5, and 8.6. For actual testing, the maximum time during which the protective headgear may be out of the conditioning environment shall not exceed 5 minutes. It must then be returned to the conditioning environment for a minimum of 15 minutes before again being withdrawn. This process must be continued until a specific item has been put through all necessary testing.

8.3 Testing at Ambient Temperature. The first protective headgear shall be tested at ambient conditions as defined in 12.1 of this standard.

8.4 Low Temperature. The protective headgear shall be conditioned by being exposed to a temperature of -10°C (14°F) $\pm 2^{\circ}\text{C}$ (3.6°F) for not less than 4 hours nor more than 24 hours, in a controlled environmental temperature apparatus.

8.5 High Temperature. A third protective headgear shall be conditioned by being exposed to an air temperature of 50°C (122°F) $\pm 2^{\circ}\text{C}$ (3.6°F) for a period of not less than 4 hours nor more than 24 hours, in a circulating air oven.

8.6 Water Immersion. A fourth protective headgear shall be immersed in water at a temperature of 25°C (77°F) $\pm 5^{\circ}\text{C}$ (9°F) for a period of not less than 4 hours nor more than 24 hours.

9. Tests for Protective Headgear

9.1 Impact Energy Attenuation. Impact attenuation shall be measured by determining imparted acceleration to an appropriately instrumented standard headform (see footnote 1, page 7) dropped in a guided fall vertical within 1/2 inch (13 mm) per 15 feet (4.57 m) height upon a fixed rigid steel anvil base.

9.2 Acceptable Acceleration Levels

9.2.1 Any peak acceleration of the test headform, with any of the four preconditioned protective headgear, exceeding 400 G's shall be cause for failure. Acceleration shall be measured with an instrumentation system whose accuracy including reading error shall be ± 28 G's maximum. Readings shall not be corrected for instrumentation accuracy.

9.2.2 Recorded accelerations in excess of 200 G's shall be cause for failure of the protective headgear if the duration of the acceleration at the 200 G level exceeds 2 ms. The time duration of acceleration will be measured with equipment accurate to ± 0.2 ms maximum and the reading shall not be corrected for instrumentation accuracy.

9.2.3 Accelerations in excess of 150 G's shall be cause for failure of the protective headgear if the duration of acceleration at the 150 G level exceeds 4 ms with instrumentation measuring duration as defined in 9.2.2.

9.3 Impact Description

9.3.1 Each protective headgear shall be impacted with two successive identical impacts (the centers of each paired impacts shall be located not more than 1/4 inch [6 mm] apart) in not less than four sites. At least two of these sites shall be upon a flat steel anvil and two upon a hemispherical steel anvil. The impact sites shall be above the reference plane and separated from each other by a distance not less than one-sixth of the maximum circumference of the protective headgear.

9.3.2 The flat steel anvil shall have a 5 inch (127 mm) minimum diameter and the hemispherical steel anvil shall have a 1.9 inch (48 mm) radius.

9.3.3 The impact energy utilized shall be 50 foot-pounds (6.91 kg meters) with the hemispherical steel anvil (54.5 inches ± 0.2 inch or 1340 mm ± 5 mm drop) and 66 foot-pounds (9.12 kg meters) with the flat steel anvil (72 inches ± 0.2 inch or 1.830 mm ± 5 mm drop).

9.4 Headform. The test headform shall be of low resonance magnesium alloy (K-1A) and shall weigh 11 ± 0.2 , - 0 lb (5 kg ± 0.091 , - 0 kg), which weight shall include the supporting arm.

9.5 Placement of Protective Headgear. The protective headgear shall be placed on the headform so that the reference plane on the headgear is coincident with the reference plane on the headform, prior to each drop. The protective headgear shall be secured to the headform and cross arm by its retention system so as to maintain this position during free fall.

9.6 Backup of Anvil. The steel anvil shall be backed up with a solid mass of at least 300 pounds which shall be faced with a steel plate of 1 inch (25.4 mm) minimum thickness and 1 ft² (0.1 m²) minimum surface area.

10. Penetration Test

10.1 Placement on Headform. The complete protective headgear shall be placed on a rigidly mounted standard headform whose surface shall be electrically conduc-

tive. If the protective headgear contains a "sling" or other adjustable sizing component, this shall be relaxed to its most extendable position.

10.2 Mode of Drop. The penetration test shall be conducted by dropping the penetration test striker onto the outer surface of the protective headgear anywhere above the reference plane, in a direction essentially perpendicular to the outer surface of the protective headgear. At least the tip of the striker shall be electrically conductive.

10.3 Failure Criterion. When tested in the above fashion, the protective headform shall be failed if demonstrable electrical contact is made between the penetrator and the conducting surface of the headform.

10.4 Number and Location of Blows. There shall be no less than two penetration blows applied to each of the preconditioned protective headgear (Section 7). Such blows shall be at least 3 inches (76 mm) apart and shall be located no less than 3 inches (76 mm) from the center of any impact points.

10.5 Conditions of Penetration Tests

10.5.1 The weight of the penetration test striker shall be 6 pounds, 10 oz ± 0.1 , - 0 lb (3.0 kg ± 45 , - 0 g).

10.5.2 The point of the striker shall have an included angle of 60 degrees ± 0.5 degrees and a cone altitude or height of not less than 1.5 inches (38 mm).

10.5.3 The radius of the striking point shall be 0.0197 inch ± 0.004 inch (0.5 mm ± 0.1 mm).

10.5.4 The hardness of the striking tip shall be a minimum of 60 Rockwell (Scale C).

10.5.5 The height of the fall shall be 118.11 inches ± 0.6 inch (3 m ± 15 mm), as measured from the striker point to the outer surface of the mounted protective headgear.

11. Test of Tensile Strength of Retaining System

11.1 Placement. The protective headgear shall be placed upon a test headform with the chin strap fastened over a device approximating the shape of the bony structure of the lower jaw. This shall consist of two metal rollers, each 1/2 inch ± 0.004 inch (12.7 mm ± 0.1 mm) in diameter, at a distance of 3 inches ± 0.04 inch (76.2 mm ± 1 mm) separation on center, which would serve to represent the jaw bone. The protective headgear shall be supported on the headform so that the points of attachment of the chin strap to the headgear will be subject to the same test as the strap itself.

11.2 Preload and Tension. The retaining system shall be tested for ultimate strength and for elongation under tension, as follows. After applying a 50 lb preload ± 1 lb (23 kg ± 0.5 kg) for no less than 30 s, an additional 250 lb $- 0, + 5$ lb (113.6 kg $- 0, + 2.2$ kg) weight or tension equivalent thereto shall be applied to the device retained by the chin strap for no less than 2 minutes. Any parting of the strap or its attachments, or elongation of more than 1 inch (25.4 mm) in the vertical distance of the chin strap from the helmet crown, as measured between preload and 300 lb (136 kg) load, shall result in failure. The retaining system shall be loaded to failure.

12. Preparation of Test Equipment

12.1 Equipment and Environment. All equipment shall be turned on and allowed to warm up for at least 30 minutes or until equilibrium is reached, whichever time is greater prior to testing.

The following environmental conditions shall prevail throughout the period of calibration and testing:

Temperature: 70-85° F

Relative humidity: 30-70 percent (22-30° C)

12.2 Instrumentation Check. The entire instrumentation system shall be checked before and after each series of tests by impacting a standardized calibrating medium² capable of producing an acceleration-time history of 400 G's, and a time duration of at least 1 ms duration at 200 G's. At least three such impacts shall be recorded before and after testing and made part of the test report. If the acceleration-time history is out of predetermined tolerance prior to test, the system shall be adjusted or repaired as necessary. If the post-test average of the three impacts differs from the pre-test average by more than 40 G's, the entire test series shall be discarded.

12.3 Record of Test. A record shall be made of each test impact and retained as a permanent record of the acceleration-time history.

² A calibrating medium found to be suitable is a one-inch Open Blue Modular Elastomer Programmer, available from Monterey Research Laboratories, P.O. Box 72, Monterey, California 93940, or equivalent.

13. Test Equipment

13.1 Headform. Standard headforms shall be used in testing and measurement. (See footnote 1, page 7.)

13.1.1 Center of Gravity of Headform. The center of gravity of the headform, including the cross arm, shall lie within a cone with axis vertical and forming a 10 degree included angle with the apex at the point of impact.

13.1.2 Combined Weight of Cross Arm and Headform. The combined weight of the cross arm and headform shall be $11 \pm 0.2, - 0$ lb (5 kg $\pm 0.091, - 0$ kg).

13.1.3 Acceleration Transducer. The acceleration transducer shall be mounted with the sensitive axis aligned to within five degrees of true vertical when the headform is in the impact position.

13.1.4 Headform Size. Medium and large size protective headgear will be tested on the standard headform size. Small size headgear of the same type will be approved if visual inspection shows the construction to be essentially identical to those tested.

13.2 Low Temperature Box. A controlled, mechanically cooled temperature box of at least 2 X 2 X 2 feet (0.6 X 0.6 X 0.6 m) inside dimensions shall be available with controlled temperature capability of $- 10^{\circ}\text{C}$ (14°F) $\pm 2^{\circ}\text{C}$ (3.6°F). It shall hold the prescribed temperature for a minimum of 24 hours.

13.3 High Temperature Box. A controlled temperature box of at least 2 X 2 X 2 feet (0.6 X 0.6 X 0.6 m) inside dimensions shall be available with controlled temperature capability of 50°C (122°F) $\pm 2^{\circ}\text{C}$ (3.6°F). It shall hold the prescribed temperature for a minimum of 24 hours.

13.4 Acceleration Transducer. The acceleration transducers shall have a natural frequency of 20 000 Hz or greater and be capable of withstanding a 2000 G shock without damage.

13.5 Recording System. The recording system must match the frequency response of the accelerometer and the entire recording system shall be flat ± 1 dB over a minimum frequency band of 5 to 3000 Hz.

13.6 Reference Plane. The standard headform, on which the basic plane is marked, shall be positioned on a flat surface so that the basic plane is parallel to this surface. The reference plane shall be scribed on the helmet after it has been positioned on the test head so that the lowermost part of the leading edge at the front of the helmet is 2.36 inches (60 mm) above the basic plane.

REFERENCES

1. Sanders, E.J., "Measurement of Some Crew Effects as a Result of F-111 Canopy Deflection During Bird Impact," AEDC-DR-75-84, Arnold Engineering Development Center, Arnold Air Force Station, Tennessee, September 1975.
2. "F-16 Canopy Birdstrike," F-16 Special Assistance Team Presentation Notes, April 1977.
3. "Analysis of Bird-Impact Tests on F-16 Canopy," F-16 Canopy Special Assistance Team Notes, May 1977.
4. Lawrence, J.H., "Windshield Technology Demonstrator Program: Canopy Detail Design Optimization Study," AFFDL-TR-78-114, Air Force Flight Dynamics Laboratory, Wright-Patterson Air Force Base, Ohio, 1978.
5. King, A.I. and C.C. Shou, "Mathematical Modeling Simulation and Experimental Testing of Biomechanical Systems Crash Response," AIAA Annual Meeting and Technical Display, Washington, D.C., February 1975.
6. Fleck, J.T., F.E. Butler, and S.L. Vogel, "An Improved Three-Dimensional Computer Simulation of Motor Vehicle Crash Victim," Calspan Technical Report No. ZQ-5180-L-1, July 1974.
7. Huston, R.L., C. Passerello, M.W. Harlow, and J.M. Winget, "The UCIN 3-D Aircraft Occupant," Aircraft Crashworthiness, pp 311-324. Edited by K. Saczalski et al., University Press of Virginia, 1975.
8. Young, R.D., "A Three-Dimensional Mathematical Model of an Automobile Passenger," Texas Transportation Institute Research Report 140-2, August 1970.
9. Robbins, D.H., "Three-Dimensional Simulation of Advanced Automobile Restraint Systems," Paper No. 700421, 1970 International Automotive Safety Conference Compendium, Society of Automotive Engineers, 1970.
10. Furusho, H. and K. Yokoya, "Analysis of Occupant's Movement in Head-On Collision," Transactions of the Society of Automotive Engineers of Japan, No. 1, pp 145-55, 1970.
11. Laananen, D.H., "Simulation of an Aircraft Seat and Occupant in a Crash Environment," Aircraft Crashworthiness, pp 347-363, Edited by K. Saczalski, et al., University Press of Virginia, 1975.

12. Robbins, D.H., R.O. Bennett, and V.L. Roberts, HSRI Three-Dimensional Crash Victim Simulator: Analysis, Verification, and User's Manual, Final Report, U.S. Department of Transportation, Contract No. FM-11-6962, June 1971.
13. Fleck, J.T. and F.E. Butler, Development of an Improved Computer Model of the Human Body and Extremity Dynamics, ARML-TR-75-14, Aerospace Medical Research Laboratory, Wright-Patterson Air Force Base, Ohio, July 1975.
14. Barber, J.P., J.S. Wilbeck, and H.R. Taylor, "Bird Impact Forces and Pressures on Rigid and Compliant Targets," UDRI-TR-77-17, University of Dayton Research Institute, Dayton, Ohio, March 1977.
15. Harris, C.M. and C.E. Crede, Shock and Vibration Handbook, McGraw-Hill Book Company, 1961.
16. Carr, R.W. and W.B. Walcott, "Design Criteria for Energy Absorbers, Restraint Systems, Seat Cushions, and Head Rests for a High Strength Armored Crew Seat," Beta Industries Report BII-220-3, Beta Industries Inc., Dayton, Ohio, August 1971.
17. Design Note 2B11, "Anthropometry and Biomechanics," Design Handbook, AFSC DH 1-3, January 1972.
18. Robbins, D.H., R.G. Snyder, and V.L. Roberts, Injury Criteria Model for Restraint System Effectiveness Evaluation, Department of Transportation, HS-800 499, April 1971.
19. Schneider, L.W. et al., "A Prediction of Response of the Head and Neck of the U.S. Adult Military Population to Dynamic Impact Acceleration from Selected Dynamic Test Subjects," UM-HSRI-76-10, May 1976.
20. Ewing, C.L., "Injury Criteria and Human Tolerance for the Neck," Aircraft Crashworthiness, pp 141-152, Edited by R. Saczalski et al., University Press of Virginia.
21. Bycroft, G.N., "Mathematical Model of a Head Subjected to Angular Acceleration," Journal of Biomechanics, Vol 6, pp 487-496, 1973.
22. Parker, J., "Angular Acceleration of the Head," PTM 163, Hymatic Engineering Co. Ltd., 1962.
23. Ommaya, A.K., F. Fas, and P. Yarnell, "Whiplash Injury and Brain Damage," Journal of American Medical Association, 204 (4), 285, 1968.

24. Unterharnscheidt, F. and L.S. Higgins, "Traumatic Lesions of Brain and Spinal Cord Due to Nondeforming Angular Acceleration of the Head," University of Texas Reports in Biological Medicine, 27 (1), 1969.
25. Ommaya, A.K. and A.E. Hirsch, "Tolerance for Cerebral Concussion from Head Impact and Whiplash in Primates," Journal of Biomechanics, Vol 4, pp 13-23, 1971.
26. Patrick, L.M. and T.B. Sato, "Methods of Establishing Human Tolerance Levels: Cadaver and Animal Research and Clinical Observations," Impact Injury and Crash Protection, pp 259-274, Edited by E.S. Gurdjian, et al., Chales C. Thomas, 1970.
27. Hirsch, A.E., "Current Problems in Head Protection," Head Injury Conference Proceedings, pp 37-40. Edited by W.F. Caveness and A.E. Walker, J.B. Lippincott, 1966.
28. Gurdjian, E.S., H.R. Lissner, and L.M. Patrick, "Protection of the Head and Neck in Sports," JAMA, Vol 182, pp 509-512, November 3, 1962.
29. Hodgson, V.R. and L.M. Thomas, "Head Injury Tolerance," Aircraft Crashworthiness, pp 175-196. Edited by K. Saczalski, et al., University Press of Virginia, 1975.
30. Hodgson, V.R. et al., "Fracture Behavior of the Skull Frontal Bone to Cylindrical Surfaces." Proceedings of the 14th Stapp Car Crash Conference, pp 341-355, Society of Automotive Engineers, New York, 1970.
31. Advani, S.H. and R.P. Owings, "Structural Modeling of Human Head," Journal of Engineering Mechanics Division, American Society of Civil Engineers, Vol 101, pp 257-266, 1975.
32. Hickling, R. and M.L. Wenner, "Mathematical Model of a Head Subjected to an Axisymmetric Impact," Journal of Biomechanics, Vol 6, pp 115-132, 1973.
33. Akkas, N., "Effects of Pulse Duration on Head Injury," Journal of Engineering Mechanics Division, American Society of Civil Engineers, Vol 103, pp 35-50, 1977.
34. Stalnaker, R. et al., "A Mechanical Impedance Model for Head Injury." In Symposium on Biodynamic Models and Their Applications, AMRL-TR-71-29 (AD 739 501), Aerospace Medical Research Laboratory, Wright-Patterson Air Force Base, Ohio, pp 905-931, December 1971.
35. Liu, Y.K. and K.B. Chandran, "Package Cushioning for the Human Head," Journal of Applied Mechanics, September 1975.
36. Gadd, C.W., "Use of a Weighted-Impulse," Proceedings of the 10th Stapp Car Crash Conference, Society of Automotive Engineers, pp 164-174, New York, 1966.

37. Stapp, J.P., "Voluntary Human Tolerance Levels," Impact Injury and Crash Protection, pp 308-349. Edited by E.S. Gurdjian et al., Charles E. Thomas, 1970.
38. Becker, E.B., "Preliminary Discussion of an Approach to Modeling Living Human Head and Neck to -G_x Impact Acceleration," Human Impact Response, pp 321-329.^x Edited by W.F. King and H.J. Mertz, Plenum Publishing Corporation.
39. Phillips, N.S. et al., An Investigation of Automotive Restraint and Body Positioning Techniques, AMRL-TR-71-101, Aerospace Medical Research Laboratory, Wright-Patterson Air Force Base, Ohio, December 1973.
40. Lombard, C.F. et al., "Voluntary Tolerance of the Human to Impact Accelerations of the Head," Journal of Aviation Medicine, 22:109, April 1951.
41. Payne, P.R., Some Aspects of Biodynamic Modeling for Aircraft Escape Systems, In Symposium on Biodynamic Models and Their Applications, AMRL-TR-71-29 (AD 739 501), Aerospace Medical Research Laboratory, Wright-Patterson Air Force Base, Ohio, pp 233-336, December 1971.
42. Kazarian, L.E. and G.A. Graves, "Human Vertebral Centrum," Spine, Vol 2, pp 1-14, March 1977.
43. Mertz, H.J., Jr., and L.M. Patrick, "Investigations of the Kinematics and Kinetics of Whiplash," Proceedings of the Eleventh Stapp Car Crash Conference, Society of Automotive Engineers, pp 175-206, New York 1967.
44. Critz, G.T., F.M. Highley, and E. Hendler, "Determination of Human Tolerance to Negative Impact Acceleration: Phase II," Report to NASA, Air Crew Equipment Laboratory, Naval Air Development Center, Warminster, PA, 1963.
45. Patrick, L.M. and G. Grime, "Applications of Human Tolerance Data to Protective Systems," Impact Injury and Crash Protection, pp 444-473. Edited by E.S. Gurdjian et al., Charles C. Thomas, 1970.
46. Ewing, C.L. and D.J. Thomas, "Torque Versus Angular Displacement Response Human Head to -G_x Impact Acceleration," Proceedings of the Seventeenth Stapp Car Crash Conference, pp 309-342, 1974.
47. Nahum, A.M. et al., "Impact Tolerances of the Skull and Face," Proceedings of the 12th Stapp Car Crash Conference, pp 303-316, 1968.
48. Hodgson, V.R. and L.M. Thomas, Breaking Strength of the Human Skull Versus Impact Surface Curvature, Department of Transportation HS 801 002, November 1973.

49. Melvin, J.W. et al., "Human Head and Knee Tolerance to Localized Pressure," International Automobile Safety Compendium, Society of Automotive Engineers, Paper 690477, p 39, New York, 1970.
50. Kornhauser, M. and A. Gold, "Application of the Impact Sensitivity Method to Animate Structures," Impact Acceleration Stress Symposium, Publication 977, NAS-NRC, November 1961.
51. Stalnaker, R.L. and J.H. McElhaney, "Head Injury Tolerance for Linear Impacts by Mechanical Impedance Methods," ASME Paper 70-WA/BHF-4, October 1971.
52. Stalnaker, R.L. et al., Door Crashworthiness Criteria, Department of Transportation, DOT-HS 800 534, June 1971.
53. Eiband, A.M., "Human Tolerance to Rapidly Applied Accelerations: A Summary of the Literature," NASA Memorandum 5-19-59E, June 1959.
54. Von Gierke, H.E., "Biodynamic Response of the Human Body," Applied Mechanics Review, Vol 17, No. 12, December 1964.
55. Ohno, John, "Effects of Temperature on the Viscoelastic Properties of High Polymer Materials," The Shock and Vibration Bulletin, Part 3, November 1968.
56. Zeigen, Robert S., et al., A Head Circumference Sizing System for Helmet Design, WADD Technical Report 60-631, Wright-Patterson Air Force Base, Ohio, December 1960.
57. Glaister, D.H., Standardization of Impact Testing of Protective Helmets, AGARD Report R-629, February 1975.
58. Calyano, Nicholas J., Considerations in Establishing Performance Criteria for Structural Firefighters Helmets, National Bureau of Standards Report NBSIR-77-1251, May 1977.
59. National Institute of Law Enforcement and Criminal Justice Standards for Riot Helmets, NILECJ-STD-0104.00, October 1974.
60. Industrial Safety Helmets, International Standard 3873, 1977.
61. Specifications for Protective Headgear for Vehicular Users, American National Standards Institute, Standard ANSI Z90.1-1971, August 1971.
62. Safety Requirements for Industrial Head Protection, American National Standards Institute, Standard ANSI Z89.1-1969, 1970.
63. Motorcycle Helmets, Federal Motor Vehicle Safety Standard FMVSC No. 218, Federal Register, Volume 38, No. 160, Chapter V, Part 571, page 22390, August 1973.

